

NRL Report 7014

Digital Receiver Decision Techniques
for Certain Fixed Length Binary Block Codes
Transmitted Through the Gaussian Channel

Noel C. Balthasar and Hugo M. Beck

Radio Communication Systems Branch
Communication Sciences Division

November 20, 1969

This document has been approved for public
release and sale; its distribution is
unlimited

DOCUMENT CONTROL DATA - R & D

(Security classification of title, body of abstract and indexing annotation must be entered when the overall report is classified)

1. ORIGINATING ACTIVITY (Corporate author) Naval Research Laboratory Washington, D.C. 20390		2a. REPORT SECURITY CLASSIFICATION UNCLASSIFIED	
		2b. GROUP --	
3. REPORT TITLE DIGITAL RECEIVER DECISION TECHNIQUES FOR CERTAIN FIXED LENGTH BINARY BLOCK CODES TRANSMITTED THROUGH THE CAUSSIAN CHANNEL			
4. DESCRIPTIVE NOTES (Type of report and inclusive dates) An interim report on the problem.			
5. AUTHOR(S) (First name, middle initial, last name) Noel C. Balthasar and Hugo M. Beck			
6. REPORT DATE November 20, 1969	7a. TOTAL NO. OF PAGES 34	7b. NO. OF REFS 9	
8a. CONTRACT OR GRANT NO. NRL Problem R01-46.201 and .202	8b. ORIGINATOR'S REPORT NUMBER(S) NRL Report 7014		
b. PROJECT NO. X-3213-11698; X-1508, Task H	8c. OTHER REPORT NO(S) (Any other numbers that may be assigned this report)		
c.			
d.			
10. DISTRIBUTION STATEMENT This document has been approved for public release and sale; its distribution is unlimited.			
11. SUPPLEMENTARY NOTES		12. SPONSORING MILITARY ACTIVITY Department of the Navy (Naval Electronics Systems Command), Washington, D.C. 20360	
13. ABSTRACT Various types of fixed length binary block encodings of binary data are presented. Binary signaling is used to transmit the binary encoded data through an additive white gaussian noise channel. Certain block decision techniques are investigated and compared. For certain block encoding schemes, the notion of an intelligent receiver is developed. This study is considered basic in analyzing the use of redundant encoding in digital communications systems.			

14. KEY WORDS	LINK A		LINK B		LINK C	
	ROLE	WT	ROLE	WT	ROLE	WT
Redundancy Binary block code Block encoding scheme Correlation Coherent binary signaling Incoherent binary signaling Gaussian channel Block decision technique Bit by bit detection Post-detection integration Predetection integration Probability of a block error (PeB) Intelligent receiver						

CONTENTS

	Page
Abstract	ii
Problem Status	ii
Authorization	ii
INTRODUCTION	1
ENCODING AND TRANSMISSION	1
Block Encoding Schemes	1
Modulation and the Channel	3
RECEPTION AND DECISION TECHNIQUES	3
The Bit by Bit Block Decision Technique	3
The NC2FSK-Sum Block Decision Technique	4
The NCB2FSK-Add Block Decision Technique	5
The NCB2FSK-Add, Subtract Block Decision Technique	7
The CB2FSK Block Decision Technique	9
The CB2PSK Block Decision Technique	9
A Comparison of Decision Techniques	9
THE INTELLIGENT RECEIVER	11
AREAS FOR FURTHER INVESTIGATION	12
APPENDIX 1	13
APPENDIX 2	15
APPENDIX 3	16
REFERENCES	18
FIGURES 1 - 8	19
DIAGRAMS 1 - 4	27

ABSTRACT

Various types of fixed length binary block encodings of binary data are presented. Binary signaling is used to transmit the binary encoded data through an additive white gaussian noise channel. Certain block decision techniques are investigated and compared. For certain block encoding schemes, the notion of an intelligent receiver is developed.

This study is considered basic in analyzing the use of redundant encoding in digital communications systems.

PROBLEM STATUS

This is an interim report; work on the problem is continuing.

AUTHORIZATION

NAVELECSYSCOM TASK NUMBERS

X-3213-11698
X-1508 Task H

NRL PROBLEM NUMBERS

RO1-46.201
RO1-46.202

Manuscript submitted October 24, 1969.

DIGITAL RECEIVER DECISION TECHNIQUES FOR CERTAIN FIXED LENGTH BINARY BLOCK CODES TRANSMITTED THROUGH THE GAUSSIAN CHANNEL

INTRODUCTION

A study was undertaken to provide some of the background basic to the understanding and intelligent pursuit of problems involving the use of redundant encoding schemes in digital communication systems.

Binary data emitted from a source is encoded into fixed length (N) blocks of bits according to various types of block encoding schemes. By using each of the N bits in the block to be transmitted to binary modulate a carrier in phase or frequency, N bit signals are produced and these are transmitted as the signal for that block. Depending on whether the binary signaling is coherent (C2PSK, C2FSK) or noncoherent (NC2FSK), i.e., depending on the bit coherency, and the availability of coherency over the block, the receiver processes the received bit signals according to various block decision techniques. Diagrams of receiver implementations for these block decision techniques are given. The probability of a block error (P_{eB}) is derived for the various block decision techniques. Using various values of N and E_b/N_0 - the average signal energy per bit divided by the average noise power per unit bandwidth, the P_{eB} curves are plotted for each decision technique as a function of N and E_b/N_0 . The block decision techniques are compared in terms of processing gain per bit for given values of N . For certain types of encodings the notion of an intelligent receiver is developed and some of its uses are discussed. Areas for further investigation are outlined.

ENCODING AND TRANSMISSION

Block Encoding Schemes

We assume that the source emits sequences of binary data elements where these may, for example, represent teletype characters or quantized analog signal samples.

Each data element emitted by the source is encoded into a block of N bits (N even, positive). Due to the binary nature of the data, for each data element the encoder must form a block B_0 which is to be transmitted if the data element is a zero and a block B_1 which is to be transmitted if the data element is a one. We let the sequences $\{b_{0i}\}$ $i = 1, \dots, N$ and $\{b_{1i}\}$ $i = 1, \dots, N$ represent the B_0 and B_1 blocks, respectively where $b_{ji} \in \{0, 1\}$ for all $i = 1, \dots, N$ and $j = 0, 1$.

Next we characterize the important properties of the B_0 and B_1 blocks. In this connection we let $\rho(B_0, B_1)$ denote the un-normalized correlation between the B_0 and B_1 blocks, i.e., $\rho(B_0, B_1)$ equals the number (A) of bits i , such that $b_{0i} = b_{1i}$, minus the number (D) of bits i , such that $b_{0i} \neq b_{1i}$. Clearly $A + D = N$.

We say that the B_0 and B_1 blocks belong to a complementary block encoding scheme if $b_{0i} = b_{1i} \oplus 1$ (where \oplus denotes addition modulo two) or equivalently if $\rho(B_0, B_1) = -N$. For this encoding scheme there are

$$\sum_{K=1}^N \binom{N}{K} = 2^N - 1$$
 distinguishable ways to form B_0 and B_1 . When $N = 8$, $B_0 = 01000101$ and $B_1 = 10111010$ is such a distinguishable complementary encoding.

If the B_0 and B_1 blocks belong to a complementary block encoding scheme and either $b_{0i} = 0$ and $b_{1i} = 1$ or $b_{0i} = 1$ and $b_{1i} = 0$ for all $i = 1, \dots, N$, then we say that the B_0 and B_1 blocks belong to a simple complementary block encoding scheme. For this encoding scheme there is only one distinguishable way to form B_0 and B_1 . When $N = 8$, then $B_0 = 00000000$ and $B_1 = 11111111$ is such a simple complementary encoding.

Let $N_0(B_j)$ and $N_1(B_j)$ denote the number of zeros and ones, respectively in the block B_j .

If the B_0 and B_1 blocks belong to a complementary block encoding scheme and we have $N_0(B_0) = N_1(B_0) = N_0(B_1) = N_1(B_1) = N/2$, then we say that the B_0 and B_1 blocks belong to an equi-distributed complementary block encoding scheme. For this scheme there are $\binom{N}{N/2} = N! / [(N/2)!]^2$ distinguishable ways to form B_0 and B_1 . When $N = 8$, $B_0 = 01101010$ and $B_1 = 10010101$ is such a distinguishable equi-distributed complementary encoding.

Let N_{jk} denote the number of bits i for which $b_{0i} = j$ and $b_{1i} = k$ where $j = 0, 1$ and $k = 0, 1$ and $i = 1, \dots, N$.

Suppose that N is such that $N/4$ is an integer. We say that the B_0 and B_1 blocks belong to an equi-distributed random orthogonal block encoding scheme if:

- (i) $N_0(B_0) = N_1(B_0) = N_0(B_1) = N_1(B_1) = N/2$ and
- (ii) $\rho(B_0, B_1) = 0$.

Clearly for this scheme $A = D = N/2$ and $N_{00} = N_{01} = N_{10} = N_{11} = N/4$.

Also, for this scheme there are $\binom{N}{N/2} \cdot \binom{N/2}{N/4} \cdot \binom{N/2}{N/4} = N! / [(N/4)!]^4$

distinguishable ways to form B_0 and B_1 . When $N = 8$, $B_0 = 01110100$ and $B_1 = 01100011$ is such an equi-distributed random orthogonal encoding.

If the B_0 and B_1 blocks belong to an equi-distributed random orthogonal block encoding scheme and we form blocks \hat{B}_0 and \hat{B}_1 from B_0 and B_1 , respectively by using only the $D = N_{01} + N_{10} = N/2$ bits where B_0 and B_1 disagree, then \hat{B}_0 and \hat{B}_1 will belong to an equi-distributed complementary block encoding scheme of length $\hat{N} = N/2$.

Given a particular block encoding scheme we allow that the B_0 and B_1 blocks chosen from this scheme can be the same for all binary data elements, vary for each data bit according to a deterministic rule, or vary for each data bit according to some discrete probability distribution.

Modulation and the Channel

Now suppose the source emits a data bit which in turn determines through a particular block encoding scheme the block $B_j = \{b_{j,i}\} = 1, \dots, N$ to be transmitted. The bits $b_{j,i}$ of B_j binary modulate a signal $S(t)$ in frequency or phase producing bit signals $X_{j,i}(t)$ where for all i , $X_{j,i}(t)$ belongs to a binary PSK or FSK signal set and each $X_{j,i}(t)$ has average energy E_b .

Hence, the block B_j determines a block signal $X(t) = \{X_{j,i}(t)\} i = 1, \dots, N$ which is transmitted bit signal by bit signal through a channel, which we assume adds white gaussian noise of one-sided spectral density N_0 to each bit signal. If T_b is the bit time and W is the effective receiver bandwidth, then we will assume throughout it follows that $T_b W = 1$.

RECEPTION AND DECISION TECHNIQUES

Now we consider certain block decision techniques for various block encoding schemes and binary signal sets. We assume that the B_0 and B_1 blocks are available at the receiver.

The Bit by Bit Block Decision Technique

In this decision technique we employ for each bit signal $X_{j,i}(t)$ a binary signal detection method the form of which depends on the modulation used and the available bit phase coherency at the receiver. After the detection procedure we make a bit decision on which signal of the binary signal set was transmitted. This decision corresponds to a binary decision d_i on $b_{j,i}$. After completing this for all N bit signals, we have formed a block $D = \{d_i\} i = 1, \dots, N$ which is the receiver's estimate of the transmitted block $B_j = \{b_{j,i}\} i = 1, \dots, N$. We make a block decision by computing $\rho(D, B_0)$ and $\rho(D, B_1)$ and then deciding that B_0 was transmitted if $\rho(D, B_0) > \rho(D, B_1)$ and that B_1 was transmitted if $\rho(D, B_1) > \rho(D, B_0)$. If $\rho(D, B_0) = \rho(D, B_1)$, then we flip an unbiased coin to reach a decision.

Diagram 1 gives an implementation of the bit by bit block decision technique receiver when NC2FSK signaling is employed with logic corresponding to frequency.

Now the probability of a block error, P_{eB} , for a given N and E_b/N_0 using the bit by bit decision technique is:

$$P_{eB} = \begin{cases} \sum_{K=0}^N \binom{N}{K} P_{e,b}^K (1 - P_{e,b})^{N-K}, & N \text{ odd} \\ \sum_{K=0}^{\frac{N}{2}} \binom{N}{K} P_{e,b}^K (1 - P_{e,b})^{N-K} + \frac{1}{2} \binom{N}{\frac{N}{2}} P_{e,b}^{\frac{N}{2}} (1 - P_{e,b})^{\frac{N}{2}}, & N \text{ even} \end{cases}$$

$P_{e,b}$ is the probability of a bit error, i.e., $P(d_i \neq b_{j,i}) = P_{e,b}$ and thus clearly, $P_{e,b}$ depends on the type of signaling employed. It is well known that for white gaussian noise of one-sided spectral density N_0 , $P_{e,b}$ equals $\frac{1}{2}[1 - \text{erf}(\sqrt{E_b/N_0})]$ for C2PSK signaling, $\frac{1}{2}[1 - \text{erf}(\sqrt{E_b/2N_0})]$ for C2FSK signaling and $\frac{1}{2} \exp[-E_b/2N_0]$ for NC2FSK signaling where

$$\text{erf}(X) = \frac{2}{\sqrt{\pi}} \int_0^X \exp[-y^2] dy.$$

For C2FSK and NC2FSK signaling we assume that the modulation index is $m = \frac{1}{2}$ or $m = 1$.

The P_{eB} curves for C2PSK, C2FSK, and NC2FSK signaling are given in Figures 1, 2, and 3, respectively. These curves were computed on NRL's CDC 3800 computer using the fact that for a given signaling type, E_b/N_0 and N odd, $P_{eB}(N) = P_{eB}(N+1)$.

Next we consider for which block encoding schemes these P_{eB} curves hold. Suppose that the B_0 and B_1 blocks are such that $-N < \rho(B_0, B_1) < N$. Clearly a bit error ($d_i \neq b_{j,i}$) will influence P_{eB} only when $b_{0,i} \neq b_{1,i}$, since if ($b_{0,i} = b_{1,i}$) $\neq d_i$, then both $\rho(D, B_0)$ and $\rho(D, B_1)$ have a minus one contribution for that bit. Hence, the P_{eB} curves using the formula given above hold only for complementary, simple complementary, or equi-distributed complementary block encoding schemes. If the B_0 and B_1 blocks (of length N) belong to an equi-distributed random orthogonal block encoding scheme, then we see from the considerations above that the P_{eB} curves for this scheme are given by the curves of Figures 1, 2, and 3 where the redundancy is $\hat{N} = N/2$.

The NC2FSK-Sum Block Decision Technique

For this decision technique we assume that binary FSK modulation is employed with modulation index $m = \frac{1}{2}$ or $m = 1$ such that frequency corresponds to logic and due to a lack of bit phase knowledge, we must for each bit signal $X_{j,i}(t)$ detect the envelopes $E_{0,i}$ and $E_{1,i}$ at the binary signaling frequencies. Then using B_0 and B_1 blocks we form for B_0 and B_1 $\mathcal{E}(B_0)$ and $\mathcal{E}(B_1)$, respectively where $\mathcal{E}(B_k)$ is a sum of bit envelopes $Z_{k,i}$ such that the envelopes $Z_{k,i}$ are those which would contain the signal had the B_k block been transmitted. This summing of appropriate bit envelopes is a method of post-detection integration. We make a block decision by

deciding B_0 was transmitted if $\mathcal{E}(B_0) > \mathcal{E}(B_1)$ and that B_1 was transmitted if $\mathcal{E}(B_1) > \mathcal{E}(B_0)$. If $\mathcal{E}(B_0) = \mathcal{E}(B_1)$, then we flip an unbiased coin to reach a decision. From references 1 and 2, we see that this technique as described above is optimum for high E_b/N_0 ratios and the optimum form of this technique for low E_b/N_0 ratios is obtained by replacing the bit envelopes $E_{0,1}$ and $E_{1,1}$ by $E_{0,1}^2$ and $E_{1,1}^2$.

Diagram 2 gives an implementation of the NC2FSK-Sum Block Decision Technique receiver for low E_b/N_0 .

Given N and E_b/N_0 (low E_b/N_0 ratio) and assuming a complementary, simple complementary or equi-distributed complementary block encoding scheme, we have, from Appendix 1 assuming the B_0 block was transmitted, that $\mathcal{E}(B_0)$ is determined to within a constant C by a non-central Chi-Squared distribution with $2N$ degrees of freedom and non-central parameter $2N E_b/N_0$ and $\mathcal{E}(B_1)$ is determined to within the same constant C by a Chi-Squared distribution with $2N$ degrees of freedom. Using these distributions and the approximations found in reference 3, the P_{eB} curves, given in Figure 4, were computed on NRL's CDC 3800 computer using function subprograms for $\text{erf}(X)$ and the inverse cumulative distribution function of the Chi-Squared distribution with $L \geq 1$ degrees of freedom.

Now suppose the B_0 and B_1 blocks (of length N) belong to an equi-distributed random orthogonal block encoding scheme. Since in this case $Z_{0,i} = Z_{1,i}$ for the bits i where the blocks agree, the bits where the blocks agree do not affect the block decision and hence the P_{eB} curves for this scheme are given by the curves of Figure 4 where the redundancy is $\hat{N} = N/2$.

The NCB2FSK-Add Block Decision Technique

For this decision technique we assume that binary FSK modulation is employed with modulation index $m = 1$, frequency corresponds to logic, and there is phase coherency over the block such that for either frequency the initial phase of all N possible bit signals at that frequency is the same but this value is unknown. Let f_0 and f_1 denote the binary signaling frequencies.

The decision technique forms for each bit, the quadrature components at the binary signaling frequencies; i.e., for the i^{th} bit the receiver forms $X(i, s, f_0)$, $X(i, c, f_0)$, $X(i, s, f_1)$ and $X(i, c, f_1)$. Due to the phase coherency over the block with respect to f_0 and f_1 and since frequency corresponds to logic; i.e., $b_{j,i} = 0$ corresponds to f_0 and $b_{j,i} = 1$ corresponds to f_1 ($j = 0, 1$), we can employ predetection integration and form for block B_j ($j = 0, 1$):

$$Y(B_j, s, f_0) = \sum X(i, s, f_0), Y(B_j, c, f_0) = \sum X(i, c, f_0), \text{ where the summation is over } i \text{ s.t. } b_{j,i} = 0 \text{ with } i = 1, \dots, N; \text{ and}$$

$$Y(B_j, s, f_1) = \sum X(i, s, f_1), Y(B_j, c, f_1) = \sum X(i, c, f_1), \text{ where the summation is over } i \text{ s.t. } b_{j,i} = 1 \text{ with } i = 1, \dots, N.$$

Now since the initial phase of any bit signal at either frequency is unknown, we form for block B_j ($j = 0, 1$) the block type envelopes at each frequency; i.e., we form $E(B_j, f_0) = \sqrt{Y^s(B_j, s, f_0) + Y^c(B_j, c, f_0)}$ and $E(B_j, f_1) = \sqrt{Y^s(B_j, s, f_1) + Y^c(B_j, c, f_1)}$.

Then we form for B_j ($j = 0, 1$), $\mathcal{E}(B_j) = E(B_j, f_0) + E(B_j, f_1)$ and we make a block decision by deciding that B_0 was transmitted if $\mathcal{E}(B_0) > \mathcal{E}(B_1)$ and that B_1 was transmitted if $\mathcal{E}(B_1) > \mathcal{E}(B_0)$. If $\mathcal{E}(B_0) = \mathcal{E}(B_1)$ then we flip an unbiased coin to reach a decision. From References 1 and 2 we see that this technique as described above is optimum for high E_b/N_0 ratios. For low E_b/N_0 ratios, the optimum form of this technique is obtained by replacing the block type envelopes $E(B_j, f_0)$ and $E(B_j, f_1)$ by $E^s(B_j, f_0)$ and $E^c(B_j, f_1)$ ($j = 0, 1$).

Diagram 3 gives an implementation of the NCB2FSK-Add Block Decision Technique receiver for low E_b/N_0 ratios.

Next we consider the P_{eB} curves resulting for the various block encoding schemes assuming low E_b/N_0 ratios. Suppose that the B_0 and B_1 blocks (of length N) belong to a simple complementary block encoding scheme. Let us suppose that for all $i = 1, \dots, N$, $b_{0i} = 0$ and $b_{1i} = 1$. In this case $Y(B_0, s, f_1) = Y(B_0, c, f_1) = Y(B_0, s, f_0) = Y(B_1, c, f_0) = 0$ and hence $\mathcal{E}(B_0) = E^s(B_0, f_0)$ and $\mathcal{E}(B_1) = E^c(B_1, f_1)$. We see that for simple complementary block encoding schemes the decision for high or low E_b/N_0 ratios results in the same P_{eB} curves. From Reference 6 we see that for a given N and E_b/N_0 , the probability of a block error is given by:

$$P_{eB} = \frac{1}{2} \exp[-NE_b/2N_0]$$

These curves are given in Figure 5 and were computed on a Wang 300 Series calculator.

Suppose now that the B_0 and B_1 blocks (of length N) belong to an equi-distributed complementary block encoding scheme. From Appendix 2, assuming the B_0 block was transmitted, we have that $\mathcal{E}(B_0)$ is determined to within a constant C by a non-central Chi-Squared distribution with 4 degrees of freedom and non-central parameter $2NE_b/N_0$ and $\mathcal{E}(B_1)$ is determined to within the same constant C by a Chi-Squared distribution within 4 degrees of freedom. Using these distributions and the approximations found in Reference 3, the P_{eB} curves, given in Figure 6, were computed on NRL's CDC 3800 computer using function subprograms for $\text{erf}(X)$ and the inverse cumulative distribution function of the Chi-Squared distribution with $K \geq 1$ degrees of freedom.

Suppose next that the B_0 and B_1 blocks (of length N) belong to a complementary block encoding scheme. Comparing the P_{eB} curves assuming simple complementary encoding to the P_{eB} curves assuming equi-distributed complementary encoding and noting the nature of complementary encoding in terms of these limiting cases we see that for a given N ,

the P_{eB} curve for complementary encoding lies between the P_{eB} curve for simple complementary encoding at N and the P_{eB} curve for equi-distributed complementary encoding at N . Exactly where the P_{eB} curve for complementary encoding lies depends on the distribution of ones and zeros in either the B_0 or B_1 block. The more nearly uniform this distribution is the closer the P_{eB} curve for complementary encoding approaches to the P_{eB} curve for equi-distributed complementary encoding and the more nearly this distribution resembles the degenerate distribution the closer the P_{eB} curve for complementary encoding approaches to the P_{eB} curve for simple complementary encoding.

Suppose finally that the B_0 and B_1 blocks (of length N) belong to an equi-distributed, random orthogonal block encoding scheme. In this case, we see from the properties of this type of encoding scheme that $Y(B_0, s, f_0)$ and $Y(B_0, c, f_0)$ will have $N/4$ terms in common with $Y(B_1, s, f_0)$ and $Y(B_1, c, f_0)$, respectively and $Y(B_0, s, f_1)$ and $Y(B_0, c, f_1)$ will have $N/4$ terms in common with $Y(B_1, s, f_1)$ and $Y(B_1, c, f_1)$, respectively. Hence, $E^2(B_0, f_0)$ and $E^2(B_1, f_0)$ will each consist of a block type squared envelope term where the quadrature components appearing therein are taken with respect to the complementary bit portions of the blocks plus a term which is the same for both $E^2(B_0, f_0)$ and $E^2(B_1, f_0)$ plus a term consisting of a product of two sums of quadrature components where one sum is the same for both $E^2(B_0, f_0)$ and $E^2(B_1, f_0)$. The same relation exists between $E^2(B_0, f_1)$ and $E^2(B_1, f_1)$. If we regard the block decision as consisting only of a comparison of the sums of the block type squared envelopes, then, since these are formed only with respect to the complementary bit portions of the blocks, the resulting P_{eB} curves would be the same as those for equi-distributed complementary block encoding where the redundancy is $\hat{N} = N/2$. But because of the extra terms, which are just normal random variables appearing in $E^2(B_0, f_0)$ and $E^2(B_1, f_0)$ and $E^2(B_0, f_1)$ and $E^2(B_1, f_1)$, we see that the P_{eB} curves for equi-distributed random orthogonal block encoding schemes (of length N) are slightly to the left of the P_{eB} curves (of length $N/2$) for equi-distributed complementary block encoding schemes.

The NCB2FSK-Add, Subtract Block Decision Technique

For this decision technique we assume that binary FSK modulation is employed with modulation index $m = 1$, frequency corresponds to logic, and there is phase coherency over the block such that for either frequency the initial phase of all N possible bit signals at that frequency is the same but this value is unknown. Let f_0 and f_1 denote the binary signaling frequencies.

The decision technique forms for each bit, the quadrature components at the binary signaling frequencies; i.e., for the i^{th} bit the receiver forms $X(i, s, f_0)$, $X(i, c, f_0)$, $X(i, s, f_1)$, and $X(i, c, f_1)$.

Due to the phase coherency over the block and since frequency corresponds to logic, we can employ predetection integration and form for B_j ($j = 0, 1$):

$$Z(B_j, s, f_0) = \sum_{i=1}^N (-1)^{b_{j,i}} X(i, s, f_0)$$

$$Z(B_j, c, f_0) = \sum_{i=1}^N (-1)^{b_{j,i}} X(i, c, f_0)$$

$$Z(B_j, s, f_1) = \sum_{i=1}^N (-1)^{[b_{j,i} + 1]} X(i, s, f_1)$$

$$Z(B_j, c, f_1) = \sum_{i=1}^N (-1)^{[b_{j,i} + 1]} X(i, c, f_1)$$

Now since the initial phase of any bit signal at either frequency is unknown, we form for block B_j ($j = 0, 1$) the block type envelopes at each frequency; i.e., we form $E(B_j, f_0) = \sqrt{Z^2(B_j, s, f_0) + Z^2(B_j, c, f_0)}$ and $E(B_j, f_1) = \sqrt{Z^2(B_j, s, f_1) + Z^2(B_j, c, f_1)}$. Then we form for B_j ($j = 0, 1$), $\mathcal{E}(B_j) = E(B_j, f_0) + E(B_j, f_1)$ and we make a block decision by deciding that B_0 was transmitted if $\mathcal{E}(B_0) > \mathcal{E}(B_1)$ and that B_1 was transmitted if $\mathcal{E}(B_1) > \mathcal{E}(B_0)$. If $\mathcal{E}(B_0) = \mathcal{E}(B_1)$, then we flip an unbiased coin to reach a decision. From References 1 and 2, we see that this technique as described above is optimum for high E_b/N_0 ratios. For low E_b/N_0 ratios, the optimum form of this technique is obtained by replacing the block type envelopes $E(B_j, f_0)$ and $E(B_j, f_1)$ by $E^2(B_j, f_0)$ and $E^2(B_j, f_1)$ ($j = 0, 1$).

Diagram 3 gives an implementation of the NCB2FSK-Add, Subtract Block Decision Technique receiver for low E_b/N_0 with $Y(B_j, s, f_k)$ and $Y(B_j, c, f_k)$ replaced by $Z(B_j, s, f_k)$ and $Z(B_j, c, f_k)$ for $j = 0, 1$ and $k = 0, 1$. Given N and E_b/N_0 (low E_b/N_0 ratio) and assuming an equi-distributed random orthogonal block encoding scheme, we have from Appendix 3, assuming the B_0 block was transmitted, that $\mathcal{E}(B_0)$ is determined to within a constant C by a non-central Chi-Squared Distribution with 4 degrees of freedom and non-central parameter $N E_b/N_0$ and that $\mathcal{E}(B_1)$ is determined to within the same constant C by a Chi-Squared Distribution with 4 degrees of freedom. Comparing these distributions for $\mathcal{E}(B_0)$ and $\mathcal{E}(B_1)$ with those for the equi-distributed complementary case of the NCB2FSK-Add Block Decision Technique given above we find that for this decision technique the P_{eB} curves for B_0 and B_1 blocks (of length N) belonging to an equi-distributed random orthogonal block encoding scheme are given by the P_{eB} curves for the equi-distributed complementary block encoding case of the NCB2FSK-Add Block Decision Technique at a redundancy $\hat{N} = N/2$.

The CB2FSK Block Decision Technique

For this decision technique we assume that binary FSK modulation is employed with modulation index $m = 1$, frequency corresponds to logic, and there is phase coherency over the block such that for either frequency the initial phase of all possible bit signals at that frequency is the same and this value is known.

If we assume that the B_0 and B_1 blocks (of length N) belong to a simple complementary block encoding scheme, then from Reference 6 we see that we can optimally matched filter process the received block signal with the resulting P_{eB} for a given N and E_b/N_0 being given by: $P_{eB} = \frac{1}{2}[1 - \text{erf}(\sqrt{N E_b}/2N_0)]$. These curves are given in Figure 7 and were computed on a 300 Series Wang calculator using Reference 5.

The CB2PSK Block Decision Technique

For this decision technique we assume that binary PSK modulation is employed and there is phase coherency over the block such that for either bit signal the initial phase is the same and this value is known for N repetitions of the bit signal.

If we assume that the B_0 and B_1 blocks of length N belong to a simple complementary block encoding scheme, then we can optimally process the received block signal with the resulting P_{eB} for a given N and E_b/N_0 being given by: $P_{eB} = \frac{1}{2}[1 - \text{erf}(\sqrt{N E_b}/N_0)]$. These curves are given in Figure 8 and were computed on a 300 Series Wang calculator using Reference 5.

A Comparison of Decision Techniques

Suppose binary FSK modulation is employed with modulation index $m = \frac{1}{2}$ or 1, frequency corresponds to logic and the initial phase of each of the N possible bit signals at either frequency is different and this value is unknown. Clearly one can employ only the NC2FSK signaling case of the Bit by Bit Decision Technique or the NC2FSK-Sum Block Decision Technique in making a block decision. If we compare these alternatives, then from Figures 3 and 4 we see that for any given N , the P_{eB} curve for the NC2FSK-Sum Block Decision Technique show a processing gain advantage of approximately 2 dB per bit with respect to the P_{eB} curves for the NC2FSK signaling case of the Bit by Bit Decision Technique. We note that this comparison holds for all types of block encoding schemes.

Now suppose that $m = 1$ and the initial phase of each of the N possible bit signals at either frequency is the same but this value is unknown. This allows us to employ the NCB2FSK-Add Block Decision Technique in making a block decision. If we recall the relation between the P_{eB} curves for the different types of block encoding schemes for this

decision technique and then examine Figures 5 and 6, then we see that the P_{eB} curves of Figures 5 and 6 bound the variation for the different types of block encoding schemes for the NCB2FSK-Add Block Decision Technique except we must remember that for the equi-distributed random orthogonal block encoding schemes we have an effective redundancy of $\hat{N} = N/2$, thus these P_{eB} curves at a redundancy of N are bounded by the P_{eB} curves of Figures 5 and 6 for a redundancy of $\hat{N} = N/2$.

If we compare, from a processing gain advantage per bit standpoint, the NCB2FSK-Add Block Decision Technique with the NC2FSK-Sum Block Decision Technique using Figures 4, 5, and 6, then we see that this advantage will be a function of N , the block encoding scheme employed and the value of P_{eB} chosen as a reference. For any block encoding scheme and any value of P_{eB} , we see that the NCB2FSK-Add Block Decision Technique has a processing gain advantage over the NC2FSK-Sum Block Decision Technique for any $N \geq 4$ and this advantage clearly increases as N increases. For example, if we employ equi-distributed complementary encoding and set $P_{eB} = 10^{-3}$, then for $N = 4$ the advantage is about 1 dB per bit whereas for $N = 2048$ the advantage is about 12 dB per bit. Using these comparisons of the NCB2FSK-Add technique with the NC2FSK-Sum technique we can, using the results previously obtained, easily extend these results to comparisons of the NC2FSK Bit by Bit technique with the NCB2FSK-Add technique.

Next let us suppose that we can employ coherent signaling per bit and there is phase coherency over the block with respect to each of the bit signals in the binary signaling set. If the block encoding scheme can be any of the various types mentioned, we must employ the Bit by Bit Decision Technique. Due to the fact that we can employ coherent signaling per bit, we can utilize either the C2PSK case or the C2FSK case of the Bit by Bit Decision Technique. If we compare these alternatives, then from Figures 1 and 2 we see that for any N and any type of block encoding scheme, the P_{eB} curves for the C2PSK case show a processing gain advantage of approximately 3 dB per bit with respect to the P_{eB} curves for the C2FSK case.

Now if we restrict the block encoding schemes to the simple complementary block encoding scheme, then we can employ the CB2FSK and CB2PSK Block Decision Techniques. If we compare these alternatives, then from Figures 7 and 8 we see that for any N the P_{eB} curves for the CB2PSK technique show a processing gain advantage of 3 dB per bit with respect to the P_{eB} curves for the CB2FSK technique. If we compare the CB2PSK technique and the C2PSK Bit by Bit technique or the CB2FSK technique and the C2FSK Bit by Bit technique, then we see from Figures 1 and 8 and 2 and 7 that the Bit by Bit technique shows approximately a 2 dB loss in processing gain per bit versus the corresponding technique for any N and when simple complementary block encoding is employed.

THE INTELLIGENT RECEIVER

Let $N_{j,k}$ denote the number of bits i for which $b_{0,i} = j$ and $b_{1,i} = k$ where $j = 0, 1$ and $k = 0, 1$ and $i = 1, \dots, N$. Suppose we employ a block encoding scheme which has the property that, for any pair of B_0 and B_1 blocks belonging to this scheme, $N_{11} \neq 0$ and $N_{00} \neq 0$. Clearly an equi-distributed random orthogonal block encoding scheme has this property since $N_{00} = N_{11} = N/4$, but a simple complementary, complementary, or equi-distributed complementary block encoding scheme does not have this property. Now suppose that, in addition to implementing a particular block decision technique, for each of the $N_{00} + N_{11}$ bits where the blocks agree, the receiver makes a hard decision on which of the bit signals was transmitted. Thus, the receiver makes a hard bit decision d_i on the transmitted bit $b_{j,i}$ for these $N_{00} + N_{11}$ bits i . Due to the fact that the B_0 and B_1 blocks are available at the receiver, the receiver knows precisely the value of $b_{j,i}$ for these $N_{00} + N_{11}$ bits i . Hence, the receiver can compute $r_0 = \sum d_i$, where the summation is over i s.t. $b_{0,i} = b_{1,i} = 0$ with $i = 1, \dots, N$; and $r_1 = \sum (d_i \oplus 1)$ where the summation is over i s.t. $b_{0,i} = b_{1,i} = 1$ with $i = 1, \dots, N$, which represent the number of obvious bit errors with respect to the N_{00} and N_{11} bits, respectively. Assuming a block encoding scheme is employed where $N_{00} \neq 0$ and $N_{11} \neq 0$, a receiver which, in addition to implementing a particular block decision technique, operates in a manner described above to compute the numbers r_0 , r_1 and N_{00} , N_{11} will be called an intelligent receiver. An implementation of the intelligent portion of the receiver for NC2FSK signaling is given in Diagram 4.

Now let us examine the utilizations of the intelligent receiver. Basically we can distinguish two types of utilizations of the intelligent receiver. These involve either direct or indirect use of the measured values r_0 , r_1 and N_{00} , N_{11} .

An example of a direct use of the measured values would be using these values to measure the actual probability of a bit error. $\hat{P}_{e,b}$ where $\hat{P}_{e,b}$ is simply the relative frequency of all obvious bit errors, i.e., for a particular data bit transmission $\hat{P}_{e,b} = \frac{r_0 + r_1}{N_{00} + N_{11}}$. From Reference 7, pages 191-209, we see that for $N_{00} + N_{11}$ sufficiently large it follows from the Laws of Large Numbers that $\hat{P}_{e,b}$ converges to $P_{e,b}$ assuming the conditions used to determine $P_{e,b}$ are valid. If $N_{00} + N_{11}$ is not sufficiently large so that $\hat{P}_{e,b}$ converges to $P_{e,b}$ we can form $\hat{P}_{e,b}$ with respect to a number of data bit transmissions; i.e., we can add the r_0 and r_1 values for these transmissions together and add the N_{00} and N_{11} for these transmissions together and then determine the relative frequency $\hat{P}_{e,b}$ with respect to these sums.

An example of an indirect use of the measured values would be using these values in testing a hypothesis concerning the nature of the noise in

the communication system. Suppose we let H_0 be the hypothesis that the noise is white gaussian noise. In the case when H_0 is true and given a binary signaling technique (C2PSK, C2FSK, or NC2FSK) we can determine $P_{e,b}$. In order to test the hypothesis H_0 we choose an error probability α such that we want our test to decide correctly that H_0 is true with probability $1 - \alpha$. We use the probability α to determine a threshold R such that if $r_{00} + r_{11} \leq R$, then by choosing H_0 to be true we can be correct with probability $1 - \alpha$. Thus, when we reject the hypothesis H_0 for $r_{00} + r_{11} > R$, we are incorrect only with probability α . Clearly R is a function of $P_{e,b}$, α , and $N_{00} + N_{11}$ and R is determined by the equation:

$$\sum_{K=0}^R \binom{N_{00} + N_{11}}{K} P_{e,b}^K (1 - P_{e,b})^{N_{00} + N_{11} - K} = 1 - \alpha$$

AREAS FOR FURTHER INVESTIGATION

In the area of redundant encoding techniques, concatenated or nested codes will be investigated since they show promise of high noise resistance. In the area of modulation and signaling techniques, multi-level or M-ary techniques such as MPSK, MFSK and combined modulation techniques will be investigated. A previous report (see Reference 9) will provide the background basic to this investigation. In the area of detection techniques, non-parametric detectors will be investigated due to their promise of a lower probability of error when the noise is not additive white gaussian noise.

It is also planned that physical implementation of these techniques will be pursued in the form of a real time digital receiver with ample consideration being given to software as well as hardware oriented digital receiver design.

We would like to thank J. W. Linnehan (NRL Code 5414) for his helpful attitude and constructive criticism in the preparation of this report, and Dorothy M. Creamer for her patient and expert typing help.

APPENDIX 1

For the low E_b/N_0 ratio case of the NC2FSK-Sum Block Decision Technique we investigate the distribution of $\mathcal{E}(B_j)$ assuming that the B_j block was transmitted and that the B_i block was not transmitted. In what follows, we will use the symbols given in Diagram 2 and let s be the signal power, σ^2 be the average noise power and ϕ_i be the phase distortion of the signal for the i^{th} bit.

First let us suppose that the B_i block was not transmitted. It is well known (see Reference 1, page 168) that, for all $i = 1, \dots, N$, $\sqrt{Z_{j,i}}$ is a Rayleigh distributed random variable with density function $P(\sqrt{Z_{j,i}}; X)$ given by:

$$P(\sqrt{Z_{j,i}}; X) = \begin{cases} \frac{X}{\sigma^2} \exp[-X^2/2\sigma^2], & X > 0 \\ 0 & , X \leq 0 \end{cases}$$

From Reference 8, page 79 it follows that the density function of $Z_{j,i}$ is:

$$P(Z_{j,i}; Y) = \begin{cases} \frac{1}{2\sigma^2} \exp[-Y/2\sigma^2], & Y > 0 \\ 0 & , Y \leq 0 \end{cases}$$

Thus from Reference 8, page 173 we see that for all $i = 1, \dots, N$, $Z_{j,i}$ is an exponential random variable with parameter $1/2\sigma^2$. Now

$\mathcal{E}(B_j) = \sum_{i=1}^N Z_{j,i}$ is the sum of N independently and identically distributed exponential random variables with parameter $1/2\sigma^2$. From Reference 8, pages 194-5 we have that the moment generating function of each $Z_{j,i}$ is given by:

$$M(Z_{j,i}; t) = \frac{\frac{1}{2\sigma^2}}{\frac{1}{2\sigma^2} - t} \quad \text{for } t < \frac{1}{2\sigma^2}$$

From Reference 8, page 203 we see that the moment generating function of $\mathcal{E}(B_j)$ is given by:

$$M(\mathcal{E}(B_j); t) = \left(\frac{\frac{1}{2\sigma^2}}{\frac{1}{2\sigma^2} - t} \right)^N \quad \text{for } t < \frac{1}{2\sigma^2}$$

Now $M(\mathbf{E}(B_j); t)$ is the moment generating function of the random variable $\mathbf{E}(B_j)$ where $\mathbf{E}(B_j)/\sigma^2$ has a Chi-Squared Distribution with $2N$ degrees of freedom. Thus $\mathbf{E}(B_j)$ is determined to within the constant $C = 1/\sigma^2$ by a Chi-Squared Distribution with $2N$ degrees of freedom.

Next let us suppose that the B_j block was transmitted. We consider first the distribution of $Z_{j,i}$. Clearly $Z_{j,i} = X^2(j, c, i) + X^2(j, s, i)$ where $X(j, c, i)$ and $X(j, s, i)$ are the quadrature components associated with B_j for the i^{th} bit. From Reference 1, page 168 we see that, since B_j was transmitted, $X(j, c, i)$ has a normal distribution with mean $= \sqrt{s} \cos \varphi_i$ and variance σ^2 and $X(j, s, i)$ has a normal distribution with mean $= \sqrt{s} \sin \varphi_i$ and variance $= \sigma^2$. From Reference 8, page 169 and Reference 4, pages 48-52 we see that $X^2(j, c, i)/\sigma^2$ and $X^2(j, s, i)/\sigma^2$ have a non-central Chi-Squared Distribution with one degree of freedom and non-central parameters $s \cos^2 \varphi_i/\sigma^2$ and $s \sin^2 \varphi_i/\sigma^2$, respectively; hence from the additive property $Z_{j,i}/\sigma^2 = X^2(j, c, i)/\sigma^2 + X^2(j, s, i)/\sigma^2$, has a non-central Chi-Squared Distribution with two degrees of freedom and non-central parameter $s/\sigma^2 = 2E_b/N_0$. Using the additive property and since the $Z_{j,i}$ are independently and identically distributed, we see that

$$\mathbf{E}(B_j)/\sigma^2 = \sum_{i=1}^N Z_{j,i}/\sigma^2 \text{ has a non-central Chi-Squared distribution with } 2N$$

degrees of freedom and non-central parameter $2N E_b/N_0$. Thus $\mathbf{E}(B_j)$ is determined to within the constant $C = 1/\sigma^2$ by a non-central Chi-Squared distribution with $2N$ degrees of freedom and non-central parameter $2N E_b/N_0$.

For the low E_b/N_0 ratio case of the NCB2FSK-Add Block Decision Technique, with equi-distributed complementary block encoding, we investigate the distribution of $\mathbf{E}(B_j)$ assuming that the B_j block was transmitted and that the B_i block was not transmitted. In what follows we will use the symbols given in Diagram 3 and let s be the signal power, σ^2 be the average noise power and φ_0 and φ_1 be the initial, unknown signal phases at f_0 and f_1 , respectively.

First let us suppose that the B_j block was not transmitted. From Reference 1, page 168 we see that the quadrature components appearing in $Y(B_j, s, f_0)$, $Y(B_j, c, f_0)$, $Y(B_j, s, f_1)$ and $Y(B_j, c, f_1)$ have normal distributions with mean = 0 and variance = σ^2 . From Reference 8, page 200 it follows that $Y(B_j, s, f_0)$, $Y(B_j, c, f_0)$, $Y(B_j, s, f_1)$, and $Y(B_j, c, f_1)$ have normal distributions with mean = 0 and variance $N\sigma^2/2$. Thus from Reference 8, pages 169, 180 it follows that $Y^2(B_j, s, f_0)/(N\sigma^2/2)$, $Y^2(B_j, c, f_0)/(N\sigma^2/2)$, $Y^2(B_j, s, f_1)/(N\sigma^2/2)$ and $Y^2(B_j, c, f_1)/(N\sigma^2/2)$ have a Chi-Squared Distribution with one degree of freedom. Hence $E^2(B_j, f_0)/(N\sigma^2/2) = Y^2(B_j, s, f_0)/(N\sigma^2/2) + Y^2(B_j, c, f_0)/(N\sigma^2/2)$ and $E^2(B_j, f_1)/(N\sigma^2/2) = Y^2(B_j, s, f_1)/(N\sigma^2/2) + Y^2(B_j, c, f_1)/(N\sigma^2/2)$ have, from Reference 8, page 201, a Chi-Squared Distribution with two degrees of freedom. Using this additivity property again we see that $\mathbf{E}(B_j)/(N\sigma^2/2) = E^2(B_j, f_0)/(N\sigma^2/2) + E^2(B_j, f_1)/(N\sigma^2/2)$ has a Chi-Squared Distribution with four degrees of freedom. Thus $\mathbf{E}(B_j)$ is determined to within the constant $C = 2/N\sigma^2$ by a Chi-Squared Distribution with four degrees of freedom.

Next let us suppose that the B_j block was transmitted. From Reference 1, page 168, we see that the quadrature components appearing in $Y(B_j, s, f_0)$, $Y(B_j, c, f_0)$, $Y(B_j, s, f_1)$ and $Y(B_j, c, f_1)$ have a normal distribution with means = $\sqrt{s} \sin \varphi_0$, $\sqrt{s} \cos \varphi_0$, $\sqrt{s} \sin \varphi_1$ and $\sqrt{s} \cos \varphi_1$, respectively and variance = σ^2 . From Reference 8, page 200 it follows that $Y(B_j, s, f_0)$, $Y(B_j, c, f_0)$, $Y(B_j, s, f_1)$ and $Y(B_j, c, f_1)$ have a normal distribution with means = $N\sqrt{s} \sin \varphi_0/2$, $N\sqrt{s} \cos \varphi_0/2$, $N\sqrt{s} \sin \varphi_1/2$ and $N\sqrt{s} \cos \varphi_1/2$, respectively and variance $N\sigma^2/2$. Thus from Reference 8, page 169 and Reference 4, pages 48-52 it follows that $Y^2(B_j, s, f_0)/(N\sigma^2/2)$, $Y^2(B_j, c, f_0)/(N\sigma^2/2)$, $Y^2(B_j, s, f_1)/(N\sigma^2/2)$ and $Y^2(B_j, c, f_1)/(N\sigma^2/2)$ have a non-central Chi-Squared Distribution with one degree of freedom and non-central parameters $Ns \sin^2 \varphi_0/2\sigma^2$, $Ns \cos^2 \varphi_0/2\sigma^2$, $Ns \sin^2 \varphi_1/2\sigma^2$ and $Ns \cos^2 \varphi_1/2\sigma^2$, respectively. Using the additive property we see that $E^2(B_j, f_0)/(N\sigma^2/2) = Y^2(B_j, s, f_0)/(N\sigma^2/2) + Y^2(B_j, c, f_0)/(N\sigma^2/2)$ and $E^2(B_j, f_1)/(N\sigma^2/2) = Y^2(B_j, s, f_1)/(N\sigma^2/2) + Y^2(B_j, c, f_1)/(N\sigma^2/2)$ have a non-central Chi-Squared Distribution with two degrees of freedom and non-central parameter $Ns/2\sigma^2 = N E_b/N_0$. Using the additivity property once again we see that $\mathbf{E}(B_j)/(N\sigma^2/2) = E^2(B_j, f_0)/(N\sigma^2/2) + E^2(B_j, f_1)/(N\sigma^2/2)$ has a non-central Chi-Squared Distribution with four degrees of freedom and non-central parameter $2N E_b/N_0$. Thus $\mathbf{E}(B_j)$ is determined to within the constant $C = 2/N\sigma^2$ by a non-central Chi-Squared Distribution with four degrees of freedom and non-central parameter $2N E_b/N_0$.

For the low E_b/N_0 ratio case of the NCB2FSK-Add, Subtract Block Decision Technique with equi-distributed random orthogonal block encoding we investigate the distribution of $\mathbf{E}(B_j)$ assuming that the B_j block was transmitted and that the B_k block was not transmitted. In what follows we will use the symbols given in Diagram 3 with $Y(B_j, s, f_k)$ and $Y(B_j, c, f_k)$ replaced by $Z(B_j, s, f_k)$ and $Z(B_j, c, f_k)$ for $j = 0, 1$ and $k = 0, 1$ and let s be the signal power, σ^2 be the average noise power and φ_0 and φ_1 be the initial, unknown signal phases at f_0 and f_1 , respectively.

First let us suppose that the B_j block was not transmitted. Due to the encoding employed and from Reference 1, page 168 we see that, for each of the sums $Z(B_j, s, f_0)$, $Z(B_j, c, f_0)$, $Z(B_j, s, f_1)$ and $Z(B_j, c, f_1)$, $N/4$ of the $N/2$ positive and $N/4$ of the $N/2$ negative quadrature components appearing in the sum have a normal distribution with means = $\sqrt{s} \sin \varphi_0$, $\sqrt{s} \cos \varphi_0$, $\sqrt{s} \sin \varphi_1$ and $\sqrt{s} \cos \varphi_1$ respectively and variance = σ^2 and the other $N/4$ positive and $N/4$ negative quadrature components appearing in the sum have a normal distribution with mean = 0 and variance = σ^2 . Hence the sum of the $N/2$ quadrature components with respect to either the negative or the positive portion of each sum has from Reference 8, page 200 a normal distribution with means = $N\sqrt{s} \sin \varphi_0/4$, $N\sqrt{s} \cos \varphi_0/4$, $N\sqrt{s} \sin \varphi_1/4$ and $N\sqrt{s} \cos \varphi_1/4$ respectively and variance $N\sigma^2/2$. Hence taking into account the signs associated with each portion we see from Reference 8, pages 199-200 that $Z(B_j, s, f_0)$, $Z(B_j, c, f_0)$, $Z(B_j, s, f_1)$ and $Z(B_j, c, f_1)$ each have a normal distribution with mean = 0 and variance = $N\sigma^2$. Thus from Reference 8, pages 169, 180 we see that $Z^2(B_j, s, f_0)/N\sigma^2$, $Z^2(B_j, c, f_0)/N\sigma^2$, $Z^2(B_j, s, f_1)/N\sigma^2$ and $Z^2(B_j, c, f_1)/N\sigma^2$ each have a Chi-Squared Distribution with one degree of freedom. From Reference 8, page 201 it follows that $E^2(B_j, f_0)/N\sigma^2$ and $E^2(B_j, f_1)/N\sigma^2$ each have a Chi-Squared Distribution with two degrees of freedom. Using this additivity property once again it follows that $\mathbf{E}(B_j)/N\sigma^2 = E^2(B_j, f_0)/N\sigma^2 + E^2(B_j, f_1)/N\sigma^2$ has a Chi-Squared Distribution with four degrees of freedom. Thus $\mathbf{E}(B_j)$ is determined to within a constant $C = 1/N\sigma^2$ by a Chi-Squared Distribution with four degrees of freedom.

Next let us suppose that the B_j block was transmitted. In this case each of the $N/2$ positive quadrature component terms appearing in the sums $Z(B_j, s, f_0)$, $Z(B_j, c, f_0)$, $Z(B_j, s, f_1)$ and $Z(B_j, c, f_1)$ has a normal distribution with means = $\sqrt{s} \sin \varphi_0$, $\sqrt{s} \cos \varphi_0$, $\sqrt{s} \sin \varphi_1$ and $\sqrt{s} \cos \varphi_1$ respectively and variance = σ^2 and each of the $N/2$ negative quadrature component terms appearing in these sums has a normal distribution with mean = 0 and variance = σ^2 . Thus from Reference 8, page 200 it follows that the sum of $N/2$ positive quadrature component terms in these sums have a normal distribution with means = $N\sqrt{s} \sin \varphi_0/2$, $N\sqrt{s} \cos \varphi_0/2$, $N\sqrt{s} \sin \varphi_1/2$ and $N\sqrt{s} \cos \varphi_1/2$ respectively and variance = $N\sigma^2/2$ and the sum of the $N/2$ negative quadrature component terms in these sums have a normal distribution with mean = 0 and variance = $N\sigma^2/2$. Hence taking into account the signs associated with each type of sum we see from Reference 8, pages 199 and 200 that $Z(B_j, s, f_0)$,

$Z(B_j, c, f_0)$, $Z(B_j, s, f_1)$ and $Z(B_j, c, f_1)$ have a normal distribution with means = $N\sqrt{s} \sin \varphi_0/2$, $N\sqrt{s} \cos \varphi_0/2$, $N\sqrt{s} \sin \varphi_1/2$ and $N\sqrt{s} \cos \varphi_1/2$ respectively and variance = $N\sigma^2$. Thus from Reference 8, page 169 and Reference 4, pages 48-52 it follows that $Z(B_j, s, f_0)/N\sigma^2$, $Z(B_j, c, f_0)/N\sigma^2$, $Z(B_j, s, f_1)/N\sigma^2$ and $Z(B_j, c, f_1)/N\sigma^2$ have a non-central Chi-Squared Distribution with one degree of freedom and non-central parameters $Ns \sin^2 \varphi_0/4$, $Ns \cos^2 \varphi_0/4$, $Ns \sin^2 \varphi_1/4$ and $Ns \cos^2 \varphi_1/4$ respectively. Using the additivity property we see that $E^2(B_j, f_0)/N\sigma^2 = Z^2(B_j, s, f_0)/N\sigma^2 + Z^2(B_j, c, f_0)/N\sigma^2$ and $E^2(B_j, f_1)/N\sigma^2 = Z^2(B_j, s, f_1)/N\sigma^2 + Z^2(B_j, c, f_1)/N\sigma^2$ have a non-central Chi-Squared Distribution with two degrees of freedom and non-central parameter $Ns/4 = N E_b/2N_0$. Using the additivity property once again we see that $\mathcal{E}(B_j)/N\sigma^2 = E^2(B_j, f_0)/N\sigma^2 + E^2(B_j, f_1)/N\sigma^2$ has a non-central Chi-Squared Distribution with four degrees of freedom and non-central parameter $N E_b/N_0$. Thus $\mathcal{E}(B_j)$ is determined to within the constant $C=1/N\sigma^2$ by a non-central Chi-Squared Distribution with four degrees of freedom and non-central parameter $N E_b/N_0$.

REFERENCES

1. "Extraction of Signals from Noise," by L. A. Wainstein and V. D. Zubakov, Prentice-Hall, Inc., Englewood Cliffs, New Jersey, 1962 (R. A. Silverman, trans.)
2. "Statistical Theory of Signal Detection," by C. W. Helstrom, Pergamon Press, Oxford, 1960
3. "Handbook of Mathematical Functions," Edited by M. Abramowitz and I. A. Stegun, National Bureau of Standards, Applied Mathematics Series #55, 1964
4. "Applications of Characteristic Functions," by E. Lukacs and R. G. Laha, Griffins Statistical Monographs & Courses #14, Hafner Pub. Co., N. Y., 1964
5. "Tables of Normal Probability Functions," National Bureau of Standards, Applied Mathematics Series #23, 1953
6. "Radar Detection" by J. V. DiFranco and W. L. Rubin, Prentice-Hall, Inc., Englewood Cliffs, New Jersey, 1968
7. "An Introduction to Probability Theory and Its Applications, by W. Feller, Volume 1, John Wiley and Sons, Inc., New York, 1950
8. "Introductory Probability and Statistical Applications," by P. L. Meyer, Addison-Wesley Pub. Co., Inc., Reading, Massachusetts, 1965
9. "Certain M-ary Digital Satellite Communication Systems," by Noel C. Balthasar and Hugo M. Beck, Naval Research Laboratory Report 1929, October 9, 1968

BIT BY BIT DECISION TECHNIQUE C2PSK SIGNALING

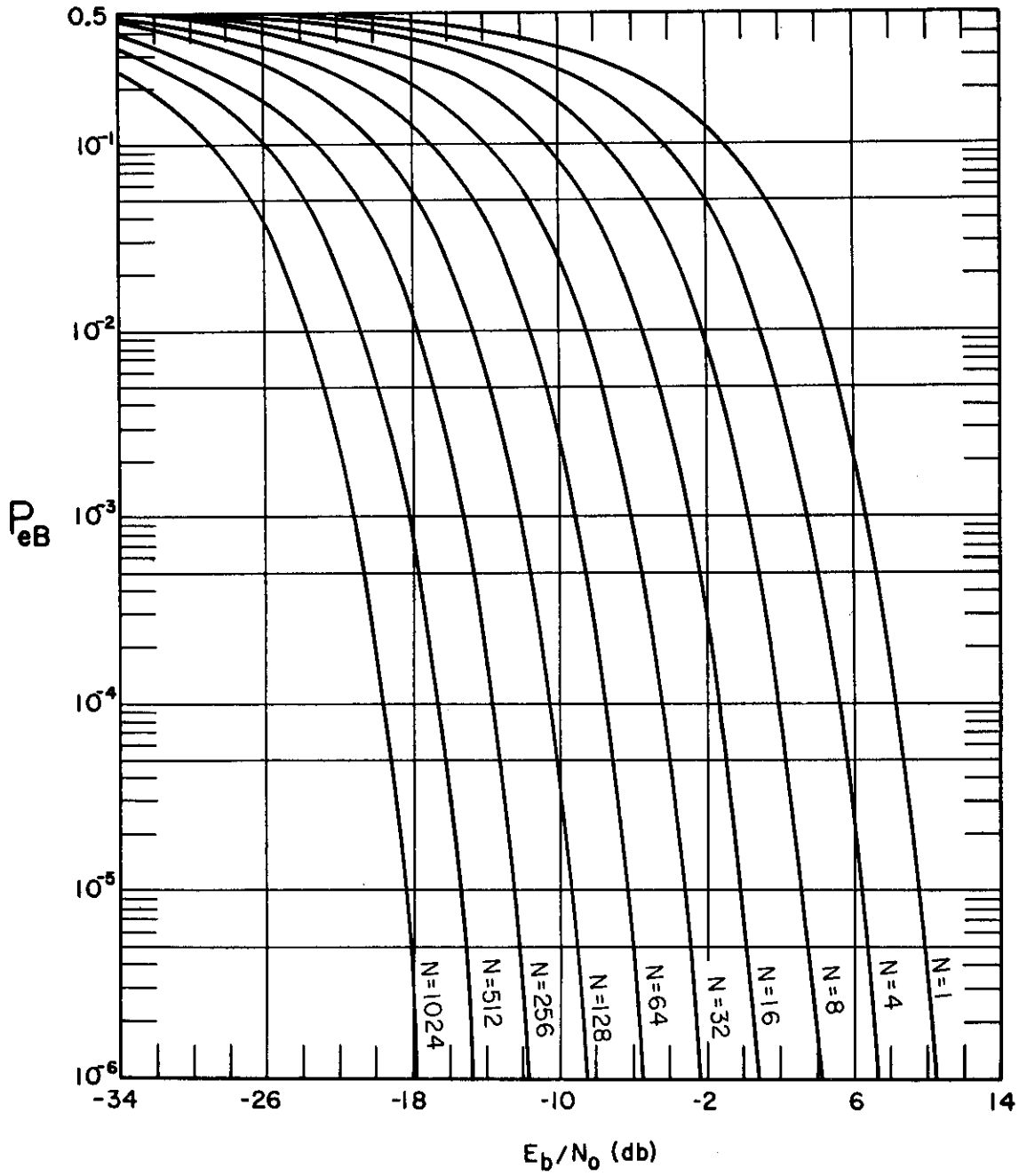


Figure 1

BIT BY BIT DECISION TECHNIQUE C2FSK SIGNALING

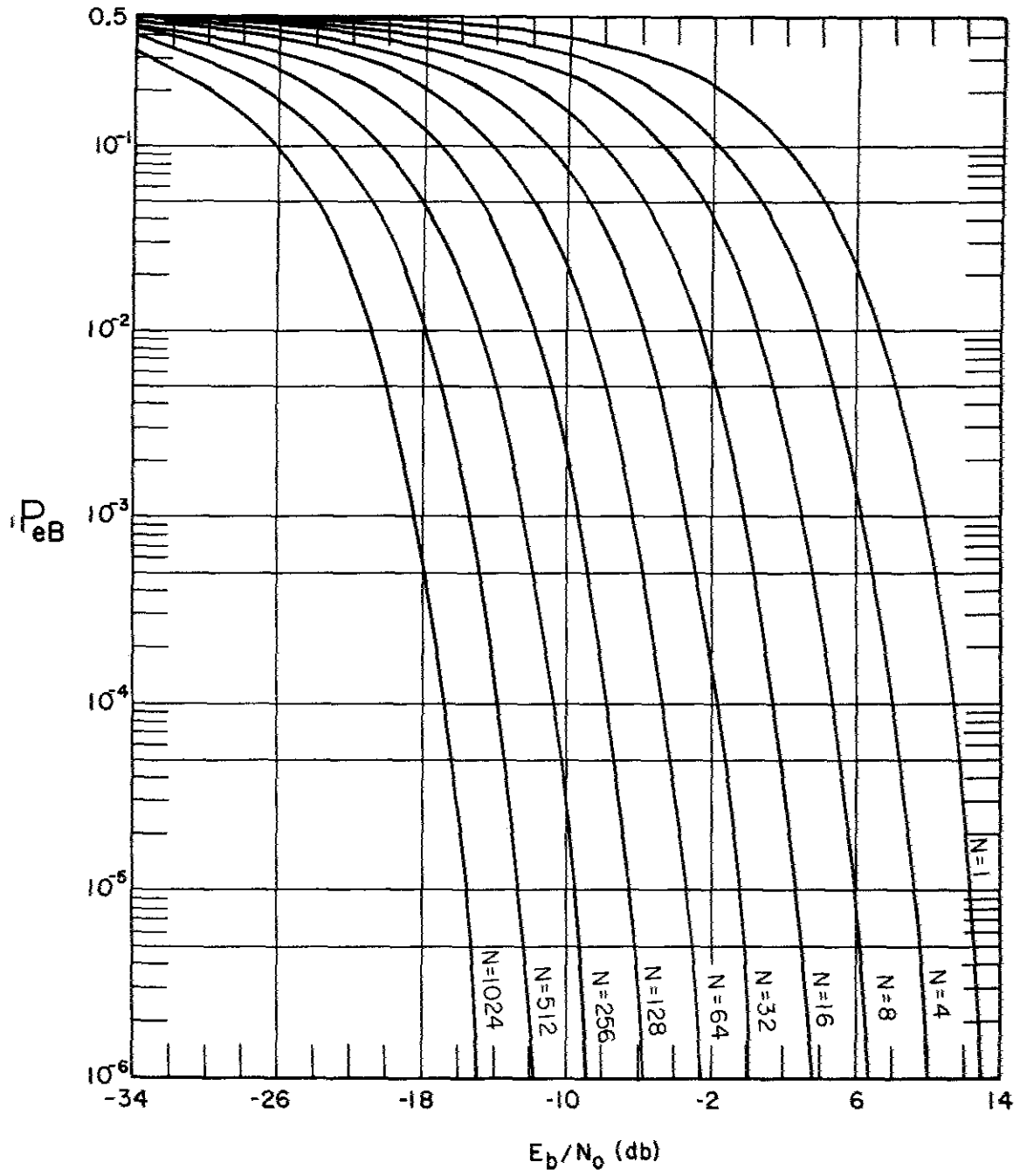


Figure 2

BIT BY BIT DECISION TECHNIQUE NC2FSK SIGNALING

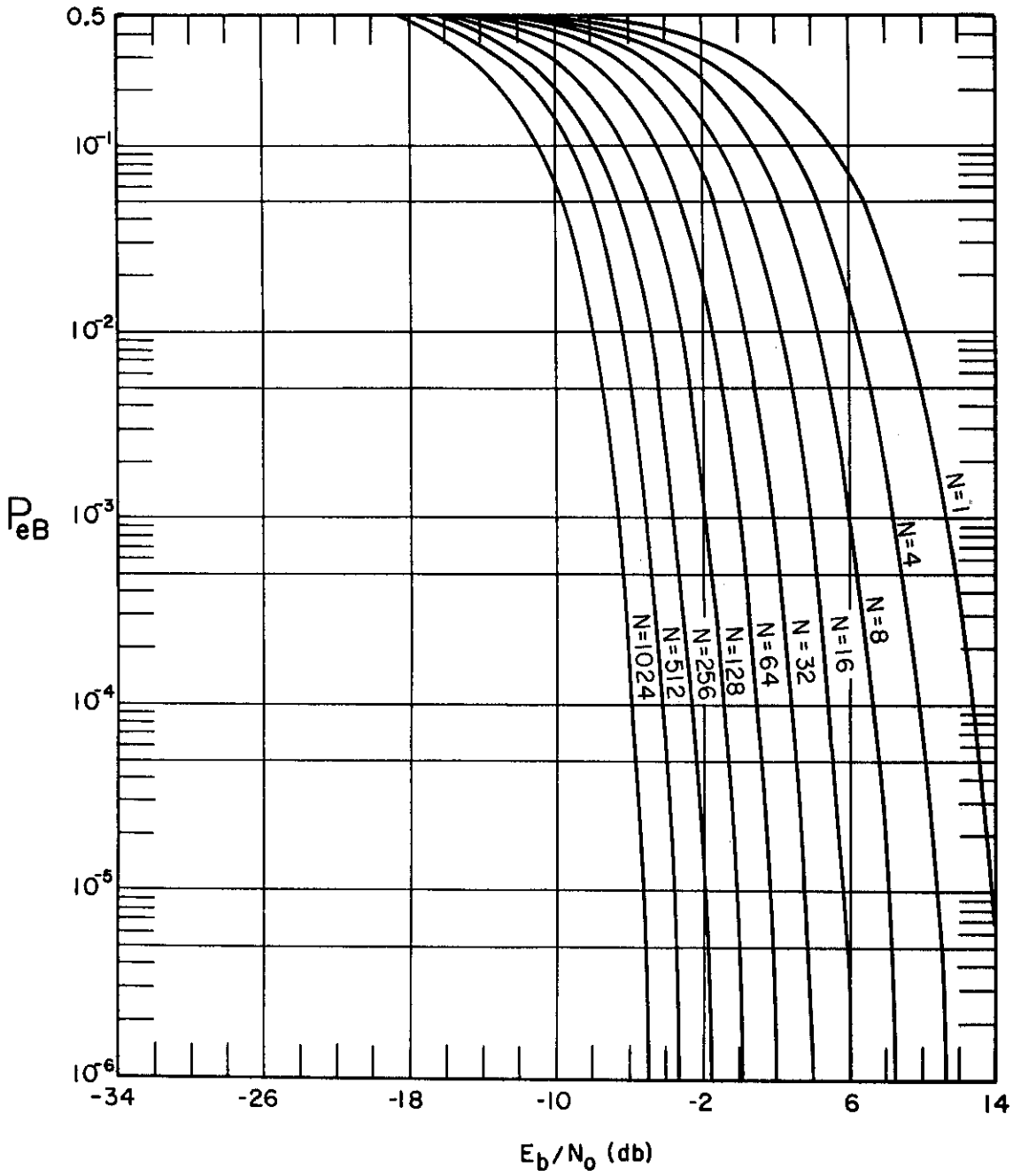


Figure 3

NC2FSK-SUM BLOCK DECISION TECHNIQUE

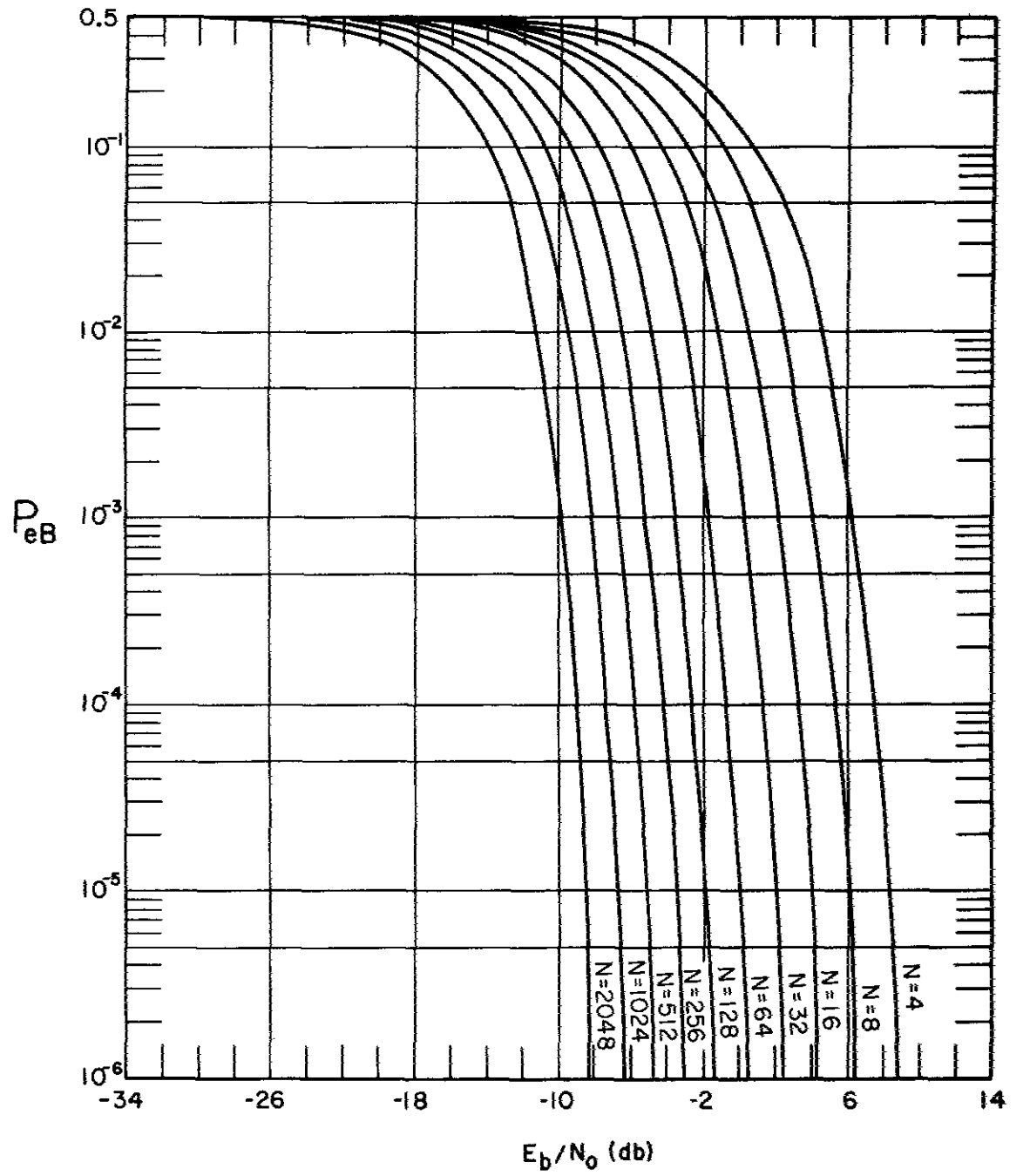


Figure 4

NCB2FSK-ADD BLOCK DECISION TECHNIQUE
SIMPLE COMPLEMENTARY ENCODING

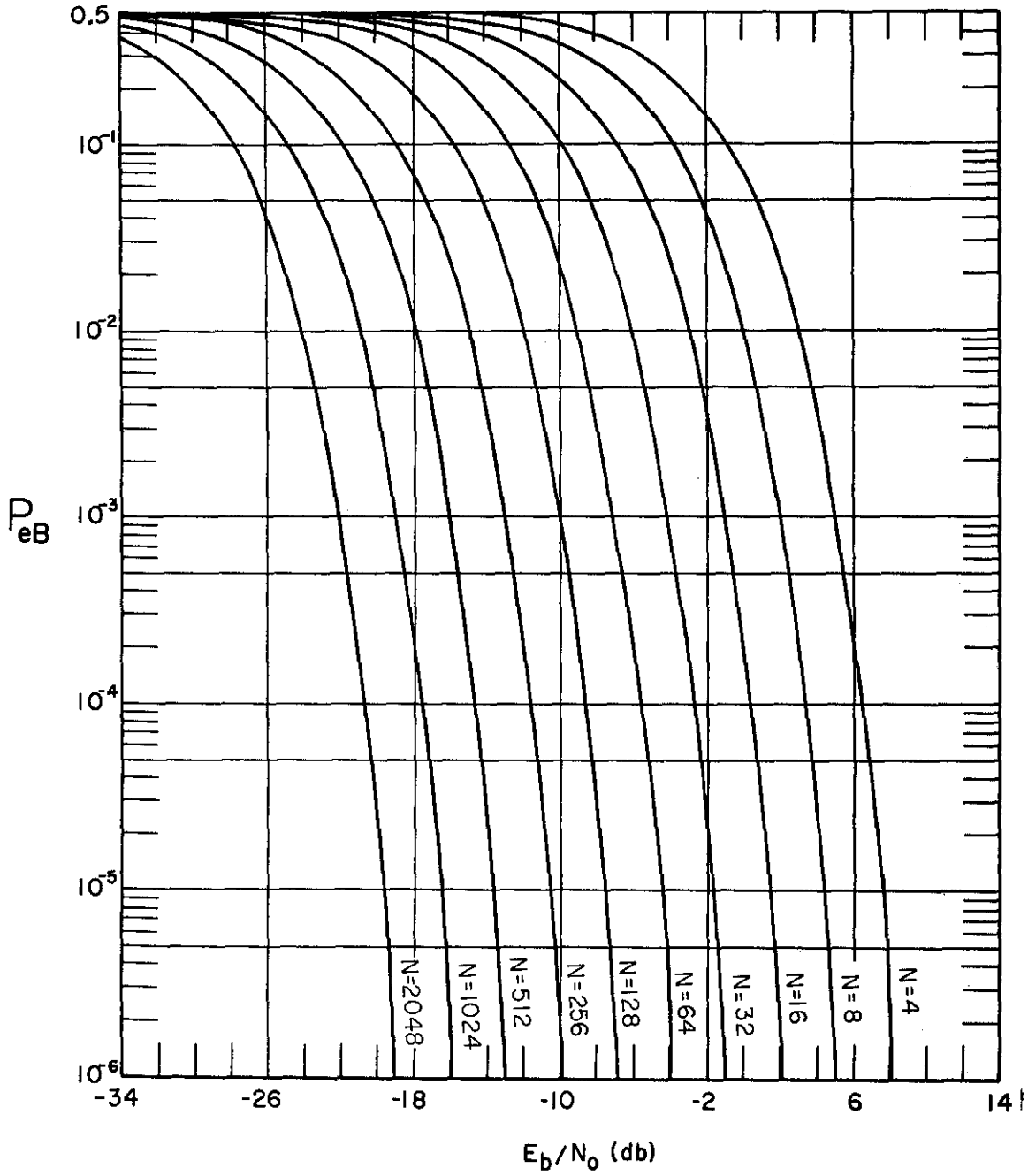


Figure 5

NCB2FSK-ADD BLOCK DECISION TECHNIQUE
EQUI-DISTRIBUTED COMPLEMENTARY ENCODING

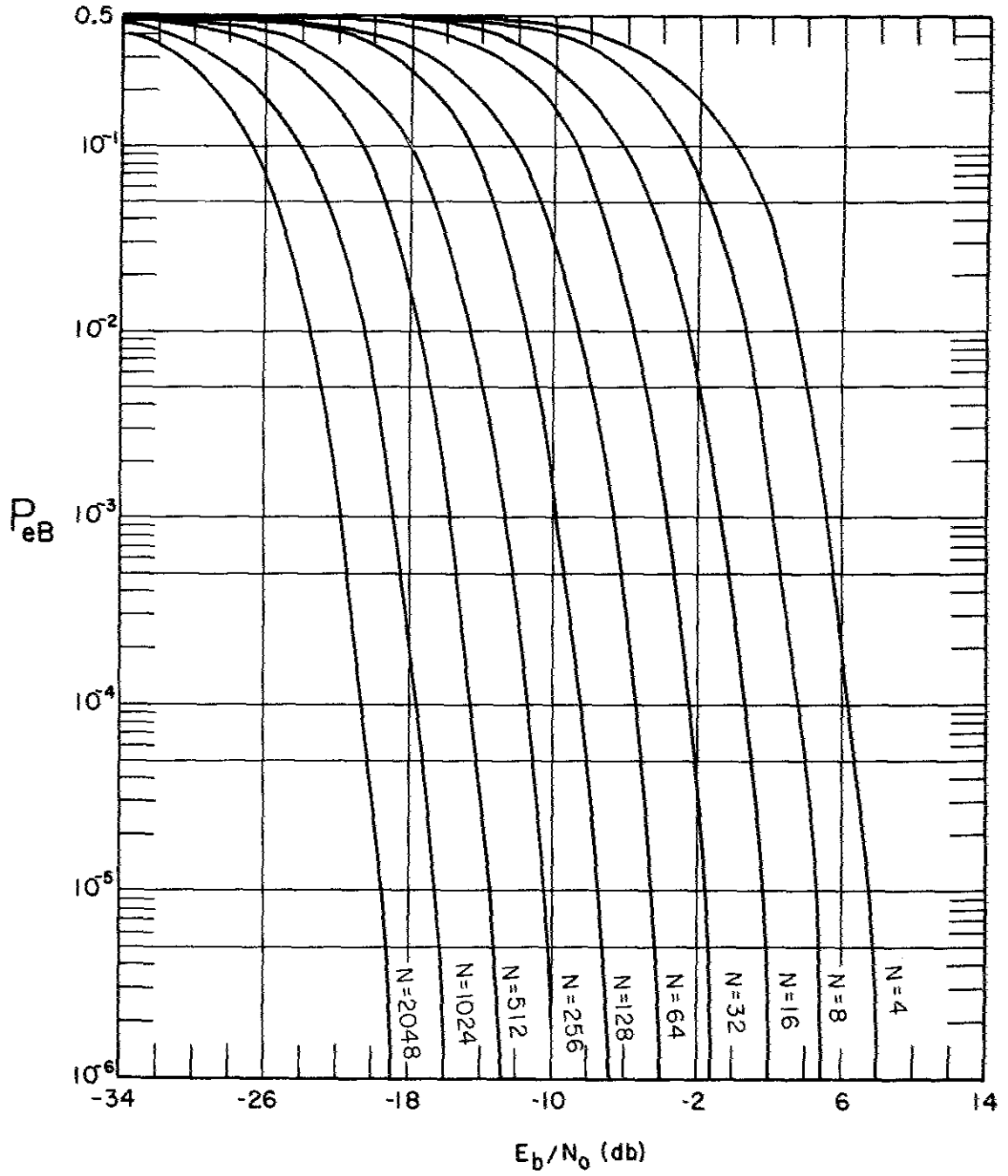


Figure 6

CB2FSK BLOCK DECISION TECHNIQUE

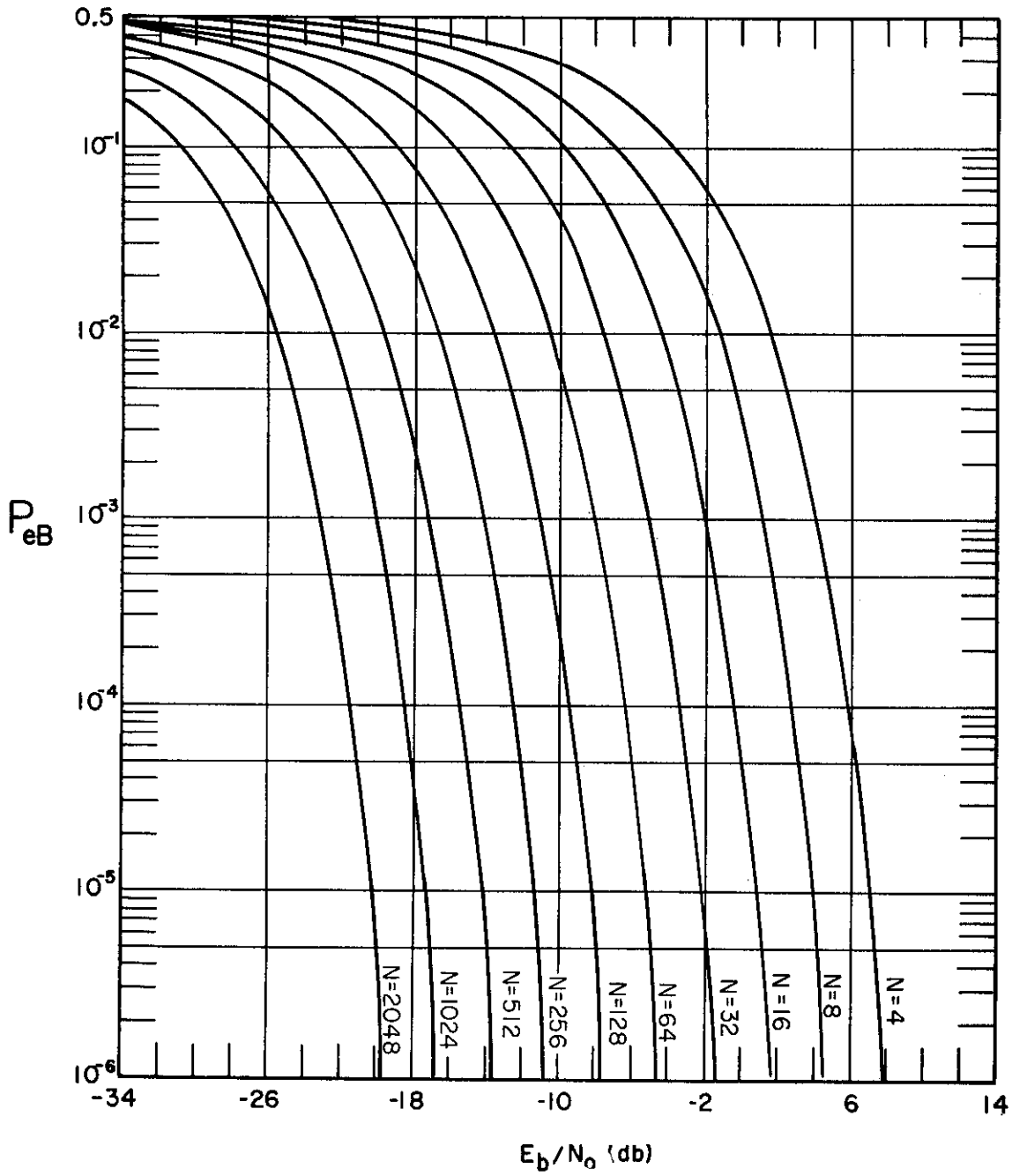


Figure 7

CB2PSK BLOCK DECISION TECHNIQUE

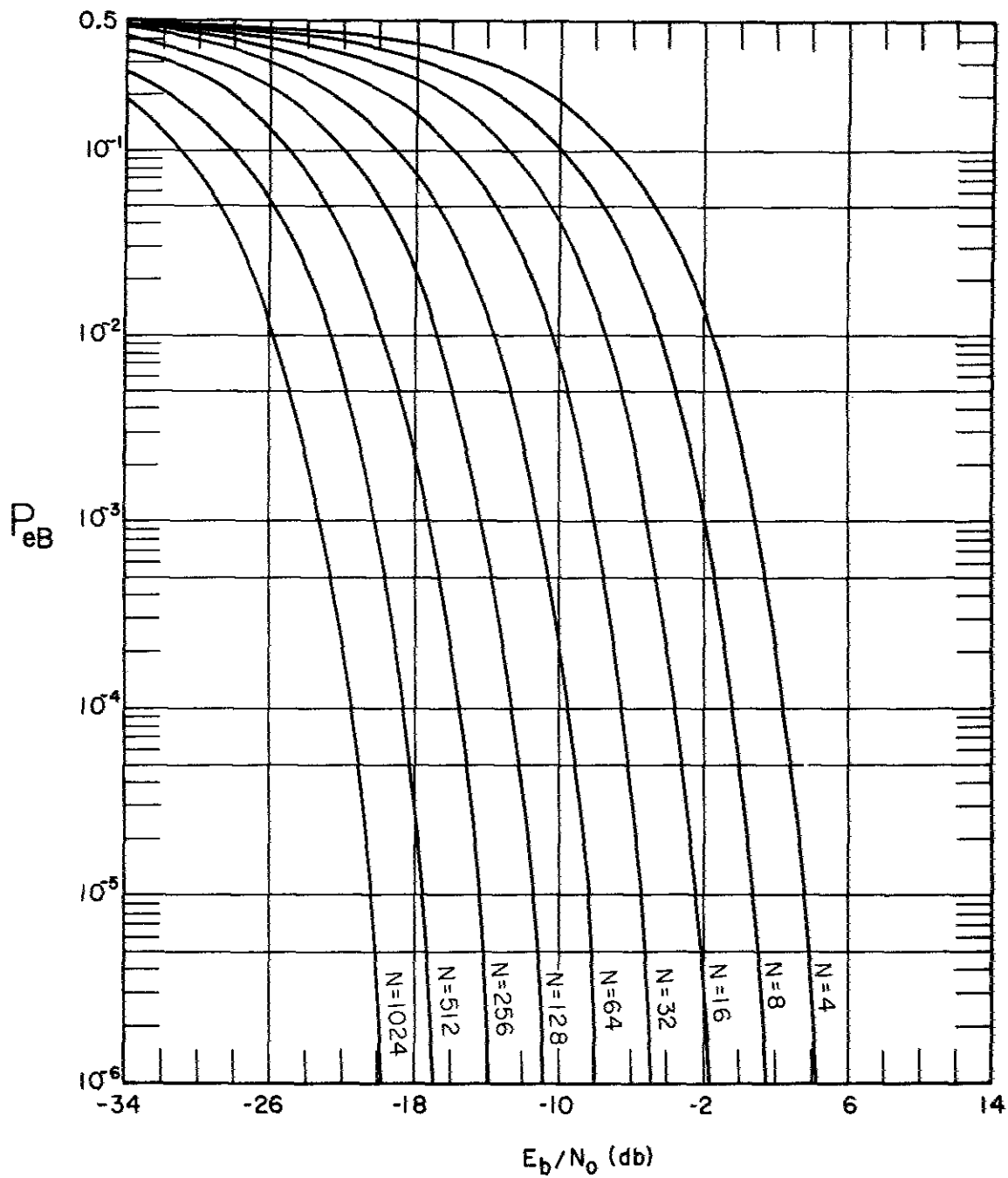


Figure 8

BIT BY BIT DECISION TECHNIQUE RECEIVER (NC2FSK SIGNALING)

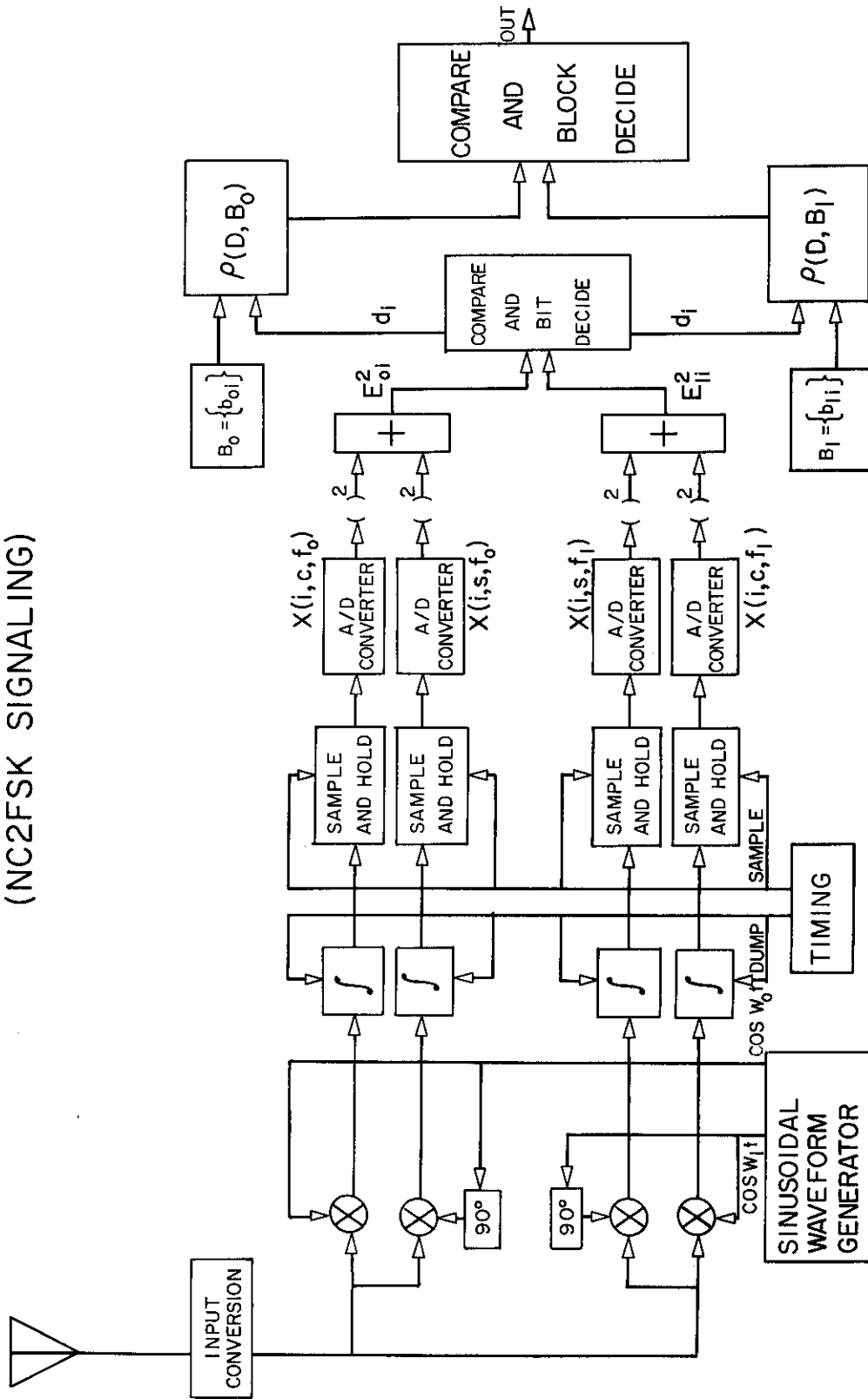


Diagram 1

NCB2FSK-ADD BLOCK DECISION TECHNIQUE RECEIVER

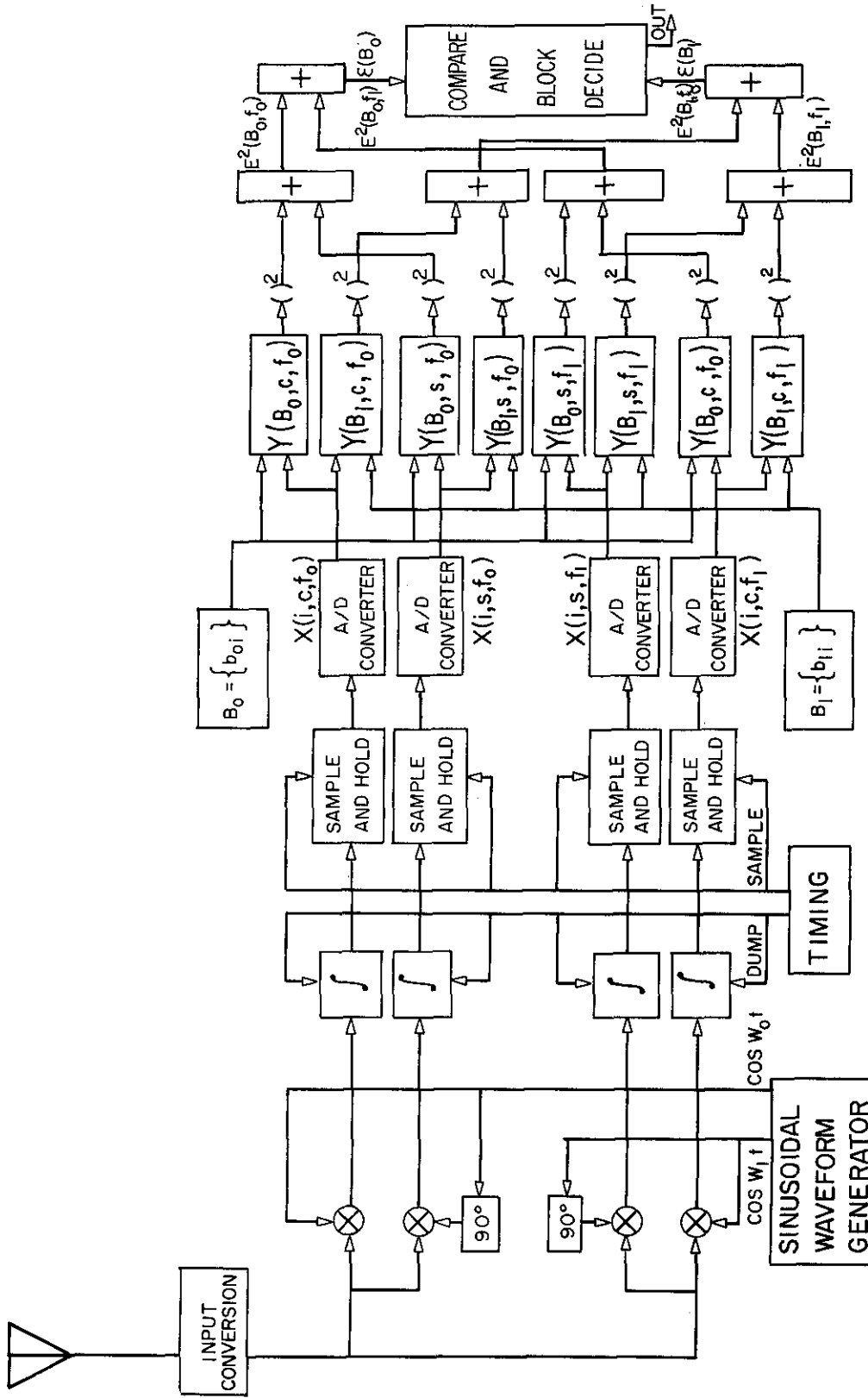
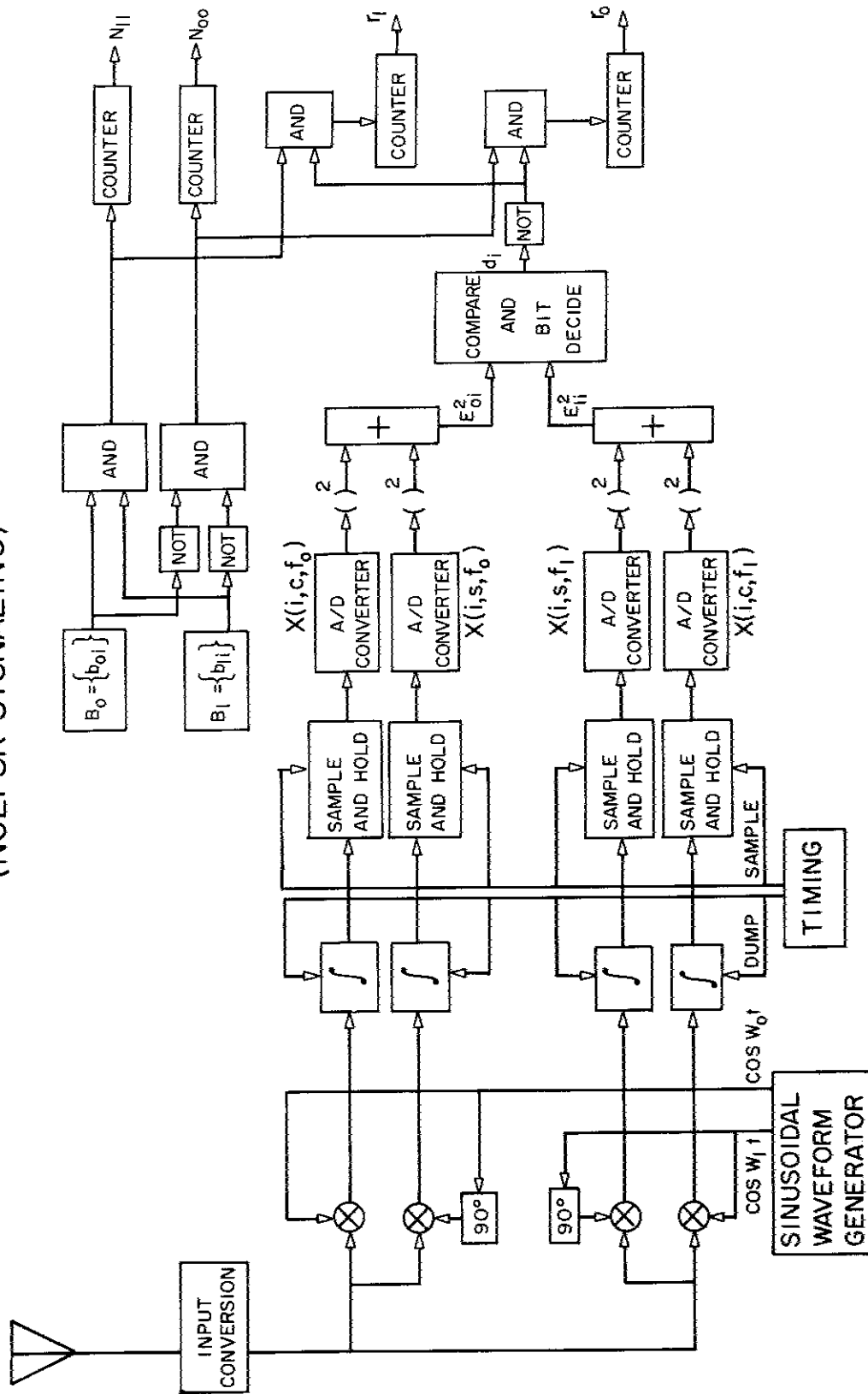


Diagram 3

INTELLIGENT PORTION OF A RECEIVER (NC2FSK SIGNALING)





SHIPBOARD SHOCK AND NAVY DEVICES FOR ITS SIMULATION

INTRODUCTION

Purpose

Information is presented on the characteristics and operation of the devices specified by MIL-S-901 for shock testing shipboard equipment — the Navy HI Class Shock Machines and the Floating Shock Platform. Other shock machines, such as the Shock Machine for Electronic Devices, the JAN-S-44 machine, air guns, and drop-tables, are also used by the Navy and other services but will not be considered here. The facts presented here have been accumulated from many sources, most of which are no longer readily accessible, and is intended to provide background information for potential users of MIL-S-901 shock machines. Equipments are accepted for shipboard use if they comply satisfactorily with the shock test and design procedures prescribed by MIL-S-901.

Background

Prior to World War II, damage to shipboard equipment resulted principally from direct hits by enemy shells and torpedoes or from firing the ship's own guns. The only acceptable protective measures available were mounting equipments as far away from the hull plating as possible and carrying as much armor as practicable. During this period a program to improve the resistance to gun-blast damage of equipments which required mounting in the vicinity of gun turrets resulted in the 3-ft-lb and 250-ft-lb shock machines. An extension of this work to improve the reliability of shipboard equipments in general resulted in the development of a combination rock-and-roll, shock-and-vibration test machine.

During World War II the problems of equipment reliability were increased by the emergence of large noncontact bombs and influence mines. Exploding at some distance from the ship, these applied an underwater pressure pulse to a large area of the hull; while the ship often sustained little structural damage, damage to equipments onboard was widespread. Heavy equipments in engine-room compartments, previously safe, became misaligned or inoperative from mount or casing fractures, or in extreme cases were broken free entirely and propelled through the compartment. Lighter equipments escaped this fate due to flexibility in their mounts and structures but were often rendered inoperative by permanent deformation and interference of internal parts due to excessive motion. Although equipments in superstructure and above-deck locations suffered least from underwater explosions, they remained most susceptible to blast and shell damage. The problem was complicated further by the growing necessity for complex and delicate electronic devices, such as radar and sonar. While protecting equipments from combat environments was more difficult, newer equipments were less resistant to combat environments.

In 1939 the British developed (on a somewhat ad hoc basis) a shock machine which produced damage to items under test similar to that sustained in service. This machine was capable of testing items weighing a few hundred pounds. In 1940 the U.S. Navy had

a modified version of this machine built by General Electric Corporation as the Navy High-Impact Shock Machine for Lightweight Equipments. This machine provides a satisfactory test for items weighing up to 250 lb, although tests on items of up to 400 lb are considered acceptable. Due to the need to test heavier items, the first Navy High-Impact Shock Machine for Mediumweight Equipments was built by Westinghouse Electric Corporation in 1942 and was rated for testing items weighing from 250 to 4500 lb. The maximum rating of this machine has since been extended to 6000 lb. Various devices for testing still heavier items were proposed and evaluated, and in 1959 the Floating Shock Platform, built by the Underwater Explosion Research Division, now a part of the Naval Ship Research and Design Center (NSRDC), was placed in service. The original version of this device was rated from 6,000 to 30,000 lb and a later, slightly longer version from 40,000 to 60,000 lb. A still larger version of this device is presently being constructed. A somewhat similar device is the Submarine Shock Test Vehicle, which was recently placed in service.

MEASUREMENT OF SHOCK MOTIONS

Shock Motion Waveforms

Shipboard shock motions are complex and varied, but in many situations useful information may be derived by considering simplified waveforms which possess a few selected characteristics of the actual complex waveform.

Motion Parameters

A motion may be described in terms of the time-dependent history of the displacement, velocity, acceleration, or jerk associated with it. Which description is preferred will depend on the nature of the system under study, the type of information desired, the manner in which the motion is excited, and possibly the instrumental limitations. As a rule, large displacements will be associated with low frequencies, and the displacements at high frequencies will be small, while the accelerations will be large at high frequencies and small at low. If a considerable range of frequencies is involved in the motion under study, both displacement and acceleration will likely be parameters having wide dynamic range. (Jerk, the derivative of acceleration, is of even greater dynamic range but is of little interest in the study of shock per se.) Velocity is a much more uniform parameter over the frequency range and shows a much lower dynamic range. Dynamic range can be reduced by such expedients as filtration of one sort or another, but this implies that it is permissible to restrict the study to motions with some range of frequencies. If this is not the case, velocity remains as the motion parameter of choice.

Generally the properties of a shock motion which will be of concern will include the amplitudes of the chosen motion parameter, the frequencies involved, the durations of various aspects of the motion, and derived quantities such as shock spectra and Fourier spectra.

Simple Pulse Shock

In many cases the shock motion may be described adequately by a simple pulse of acceleration (Fig. 1) — a body striking an elastic member may undergo a half-sine pulse

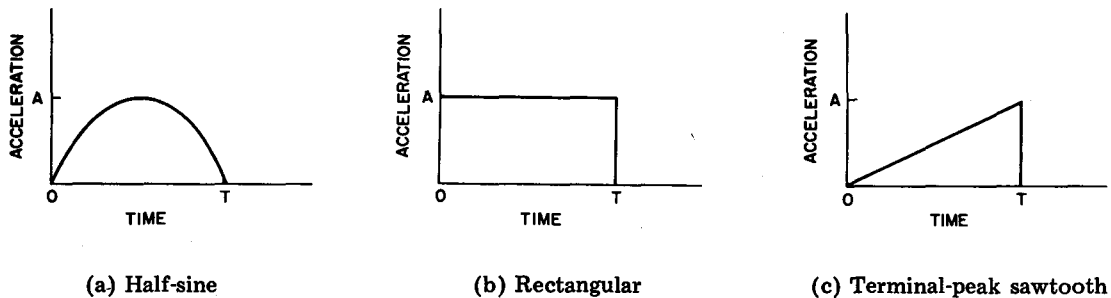


Fig. 1 — Some of the more common simple acceleration pulse waveforms

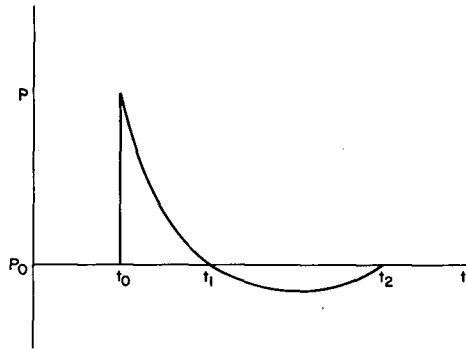
of acceleration, for example. If the pulse is sufficiently short in terms of the response time of the affected system, the exact shape of the pulse becomes of little concern, and it may be regarded as an impulse. The excitation then is in essence a velocity step, a great mathematical convenience. In other cases the excitation may be represented as a simple pulse of displacement. The most useful simplistic characterization of the shock motion is determined not only by its waveform but also by the system in which it occurs and the nature of the problem being studied.

Shipboard Shock

Shipboard shock is of such a type that broadly applicable simplifications usually cannot be made. Each primary exciting mechanism produces ship structure motions more or less peculiar to it. Air blast, such as from firing the ship's guns, produces very high, short-duration loadings at exposed areas of the deck and superstructure and leads to a basic motion resembling a velocity step with exponential decay (1) (plus oscillations of the excited system). The motion may consist of a train of such pulses due to the difference in arrival time of the blasts from different sources and echoes. Shell burst provides a similar excitation, complicated by thermal effects, and perhaps direct mechanical action if close enough to the point of detonation. Like underwater shock, air-blast shock has become a much more serious problem with the introduction of larger weapons: surface or air burst of nuclear weapons also provide pressure excitations with extensive, near-planar wavefronts. The study of this extended form of air-blast shock is incomplete.

Underwater shock (1,2) produces perhaps the most complex excitation pattern. The primary shock wave arrives first and is a steep pressure step with exponential decay. Next — significant for large weapon attack — might be a negative pressure pulse of similar shape due to surface reflection and possibly another positive pulse from bottom reflection. Other dominant features of the excitation are the arrival of the surge of water displaced by the expansion of the gas bubble (which is responsible for practically all of the rigid body motion of the ship), of the "bubble pulse" (the pressure pulse emitted by the gas bubble when it has contracted to minimum radius), and of the bubble-pulse reflections. The relative placement of these features in the overall excitation train depends on the depth of the detonation, the depth of the water, and the distance of the ship from the detonation. The bubble may oscillate for several cycles, emitting pressure pulses at each radius minimum. Sometimes the first bubble pulse will be of sufficient magnitude to warrant consideration, especially for low-frequency systems. The bubble has a natural tendency to rise to the surface and may vent to the atmosphere. If this occurs during the first expansion, no bubble pulse will be emitted. The velocity of the

rise is by far the greatest when the bubble radius is at a minimum, and for relatively shallow shots the bubble oscillations will be terminated by venting rather than by dissipation of the driving energy. The venting itself causes surface waves which arrive at the ship late in the proceedings. Their effect is usually negligible compared to what has gone before but can occasionally be significant to the response of low-frequency, lightly damped systems. The salient features of air blast and underwater shock pressure waves are outlined in Fig. 2.



(a) Air blast starts suddenly from ambient P_0 at time t_0 , reaching peak pressure P (overpressure $P - P_0$). At time t_1 the overpressure phase is succeeded by the underpressure phase lasting until time t_2 . Pressure fluctuations following this phase are essentially negligible.

(b) The pressure wave from an underwater explosion starts suddenly from ambient at t_0 , reading a peak value P (far greater, of course, than the value attained in air blast). At time t_1 "surface cutoff" occurs when the wavefront reflected with opposite sign from the water surface interferes destructively with that traveling the direct path. Surface cutoff may in fact result in some underpressure, as indicated. At time t_2 the wave front reflected from the bottom arrives, and at time t_3 the first bubble pulse arrives.

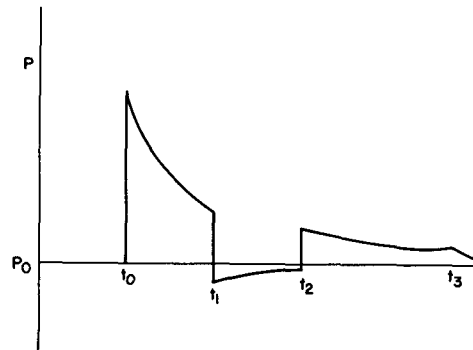


Fig. 2 — Simplified free-field pressure-time histories for (a) airblast and (b) underwater explosions

For some items it is permissible to regard the input shock motion as a velocity step, or as a velocity change with exponential decay. For an average item, however, the shock motion will have been transmitted through a structural path which accentuates some frequency components and suppresses others, leading to a complex and highly individualistic waveform. Since the item of equipment itself may have many components, hence many modes, its response motions may be even more complicated. Shipboard shock is accordingly characterized by a complex and relatively unpredictable waveform having components over a considerable range of frequency (Fig. 3). The ranges of typical parameters which might be encountered are: frequency, from near 0 to 5 kHz; displacement, zero up to a few feet, velocity, 0 to about ± 30 ft/s (although velocities of up to 140 ft/s have been reported); and acceleration, 0 to $\pm 10,000$ g.

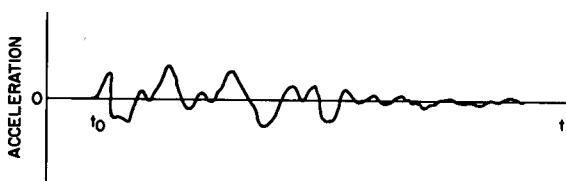


Fig. 3 — A typical acceleration waveform found in shipboard shock. Starting at time t_0 , the acceleration amplitudes may reach several hundred (or even several thousand) g and remain significant for about a second.

For conventional explosive attack the severity of an underwater shock input to a ship is often indicated by the "shock factor," determined by the TNT equivalent weight of the charge, the depth of the detonation, and its distance from the ship. This factor was originally assigned as an index of the ship's hull motion and was derived for a particular ship with a particular orientation to the detonation and for a particular charge size. Scaling laws have been empirically defined which should be applied to extend this concept so that a stated value of shock factor means the same shock severity on all ships for all variables, such as orientations and charge weights. These laws continue to be the topic of some discussion. Even so, the shock factor is a valuable parameter since workers in the field agree on its general definition, if not always on its detailed application.

Instrumentation Systems

To study shock motions some characteristic or waveform description of them must be captured in a comparatively permanent form (1). Some shock pickups are self-recording, such as the scratch gage, lead gage, putty gage, reed or dynamic load factor gage, ball-crusher accelerometer, and a variety of other peak-reading devices. Some optical measurement methods lead naturally to filmed readouts (high-speed movies, for example). However, the vast majority of shock pickups in use today transduce the shock parameter to which they are sensitive into an electrical signal, permitting great convenience in signal transmission, computation, and recording. Figure 4 shows a block diagram of a typical modern measurement instrumentation system.

Practically all motion pickups may be regarded as single-degree-of-freedom (s.d.o.f.) systems (Fig. 5). If a s.d.o.f. system is regarded as a "test mass," a "spring," a "base," and a "sensor," the character of the sensor and the relationship of the frequencies involved in the motion of the base to the natural frequency of the mass on the spring (base fixed) determine the parameter of motion to which the pickup responds. If the base-motion frequencies are well below the natural frequency of the pickup, the relative displacement of the mass with respect to the base is proportional to the acceleration of the base. If the base-motion frequencies are well above the natural frequency, the relative displacement is identical to the base displacement since the test mass remains still — it is seismically suspended. Now, the most commonly used sensors fall into two categories: those which produce an indication proportional to the displacement of the mass relative to the base and those which produce an indication proportional to the velocity of the mass relative to the base. The application of these sensors in the first instance above (relative displacement proportional to base acceleration) produce an accelerometer or

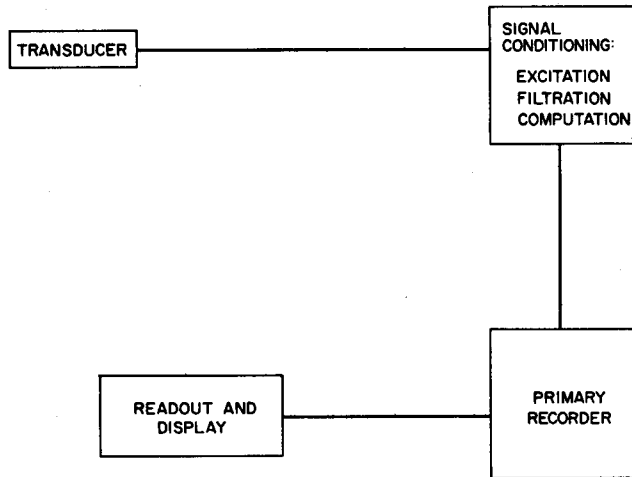


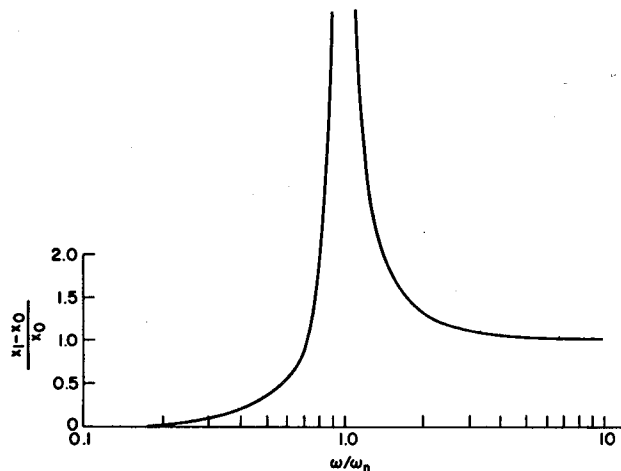
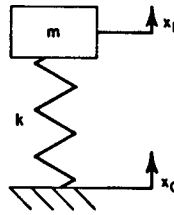
Fig. 4 — Block diagram of a basic measurement instrumentation system

jerkmeter, respectively. (Jerk is a motion parameter of concern in the study of physiological effects of shock motions, but will not be considered further here.) In the second instance (relative displacement proportional to base displacement), the pickup produced is a displacement meter or a velocity meter, respectively. Note that a high-speed camera hung on its "soft" bungee cord is a prime example of a displacement meter. Another pickup variation is the highly overdamped s.d.o.f. system, whose relative displacement is proportional to base velocity for a substantial range of frequencies centered about its natural frequency.

Pickups of the seismic type have one common disadvantage: they are large and heavy. The size is necessary because the relative displacement is ideally the input motion; the weight is a product partly of sheer bulk, partly of the necessity for low natural frequency in spite of large component sizes, and partly of the requirement for robust construction to keep the natural frequencies of the component parts high enough to avoid contaminating the response of the instrument. The requirement for large displacement capability along the sensitive axis renders seismic pickups somewhat fragile with regard to cross-axis excitations, detracting from their utility as practical shock pickups.

Another pickup of great historical importance in shock studies is the reed gage, or dynamic load factor gage, which consists of an array of cantilever springs with end masses. The spring length and thickness and the magnitude of the end mass are adjusted so that the natural frequencies of the array members span a frequency range of about 40 to 450 Hz. The masses are fitted with scribes permitting the maximum deflections of the array to be recorded by scratching a suitable surface with varying degrees of legibility. The recorded deflections allow the "shock spectrum" of the shock motion to be determined (with some error). Now that large fast computers are available these primitive devices are dying out; nevertheless, they retain the virtue of requiring no external power or readout and recording circuitry.

(a) Undamped s.d.o.f. system



(b) Steady-state response of a s.d.o.f. system. The forcing (radian) frequency is ω and the system natural (radian) frequency $\omega_n = \sqrt{K/m}$. The seismic region is where $\omega/\omega_n > 2$, where the relative displacement is essentially the same as the absolute displacement of the base. Accelerometers operate in the region $\omega/\omega_n < 0.6$, where the relative displacement is small and proportional to the acceleration of the base.

Fig. 5 — Single-degree-of-freedom (s.d.o.f.) system and its response

Transducers

Transducers may be sensitive to any of the major motion parameters: displacement, velocity, and acceleration.

Displacement

Displacement is often the most important parameter of motion and also the most difficult to measure satisfactorily. Its importance arises from the greatest interest in a study often being the distortion or deformation of some structure, which can generally be evaluated only if the displacements of structural members relative to one another are

known.* These desired relative displacements are often small differences between large absolute displacements, requiring that the measurements be made with extreme accuracy over a great dynamic range.

Displacement is difficult to measure satisfactorily because the available measuring devices are not sufficiently accurate over large dynamic ranges. Devices capable of measuring large displacements, such as linear potentiometers and linear variable differential transformers, are inherently limited to low frequencies for one reason or another and usually lack the requisite accuracy and fine resolution as well. The high-frequency devices, such as the capacitive pickup and the various interferometers, are restricted to small displacements. All of these devices actually measure displacement of the measured object relative to themselves. Absolute displacements can be measured if an inertial reference is available, such as a fixed frame which does not partake of the shock motion or a seismic test mass.

Because of these difficulties, it is not common to measure displacement directly but to calculate it from measurements of another motion parameter.

Velocity

Velocity transducers generally consist of a coil moving about a seismically suspended magnet or a magnet moving along a seismically suspended coil. The seismic nature of the pickup imposes the restrictions on size, weight, and frequency range remarked previously. Either the coil or magnet is fixed to the base and exposed to the entire shock environment. Even though ruggedly built, they tend to break up and/or lose magnetization with use.

Acceleration

Acceleration transducers, or accelerometers, have many desirable features as shock pickups since they operate below their natural frequencies. This means not only that their relative displacements are small but also that the higher the natural frequency the better. Both factors lead to small, light pickups and wide frequency range. The instrumentation problems unique to accelerometers are due largely to their sensor mechanisms. Those mechanisms using strain gage bridges and linear variable differential transformers are relatively susceptible to damage by cross-axis shock (although not to the extent of seismic pickups) and are relatively limited in maximum acceleration capability. The more common piezoelectric types present very high impedances and have low sensitivities, requiring elaborate specialized signal-handling circuitry, and may exhibit "zero shift" under shock excitation. Zero shift appears as a sudden, spurious dc component in the accelerometer's output; while it may not be sufficiently pronounced to prevent reasonably good acceleration values to be read, it is disastrous to efforts to compute other shock parameters from the record. Fortunately, zero shift can be avoided by careful selection of accelerometers. In addition to these problems, the piezoelectric pickup is essentially undamped. If the shock motion possesses perceptible energy in the region of the accelerometer's natural

*Often a great deal of such information can be extracted from measurements of dynamic strains at judiciously selected regions of a structure. However, these measured values are used as inputs or constraints to some semiempirical model of the structure from whose action the displacements of the actual structure are inferred. This is greatly different from measuring the actual displacements directly.

frequency, the accelerometer will ring to some extent. If the natural frequency is high enough, this false signal may be filtered out electrically.

These problems may be regarded as the effects of the shock motion as a mechanical environment for the pickup rather than as the subject of a measurement. Since these aspects of the shock motion will rarely be the same, the shock motion can be mitigated as "environment to the pickup" without affecting the shock motion as "phenomenon to be measured" by suitable mounting and padding arrangements. By these means accelerometers can be exposed to shock environments far in excess of their capability and yet obtain very good measurements of the shock motions.

Strain

The study of equipment response to shock environments is greatly facilitated by the strain gage, which may now be obtained in a wide variety of shapes and forms. In its original form, the strain gage used the fact that when a conductor is deformed, its resistance varies in such a way that the relative change in resistance is proportional to the relative elongation of the conductor. The relative elongation is the strain, hence the name of the gage, and the coefficient of proportionality, or gage factor, is close to 2 for most metals. The basic resistance of the gage is from about 100 to 500 ohms, so the resistance changes are quite small, but noise is generally not a problem. Strain gage instrumentation is well developed commercially, and a great variety of bridge and amplifier packages are readily available. The most common form for the strain gage was at one time the fine-wire grid with a paper backing. While still widely used, this form has been largely supplanted by the foil grid with plastic backing, which is more convenient for use with modern adhesives. The choice of backings and adhesives is largely determined by the temperature range which must be tolerated.

Thermal effects are usually compensated by matching the gage characteristics to the expansion coefficient of the material to which it is to be attached. Elaborate compound gages can be obtained which contain a resistance thermometer element matched to the strain gage element which allows the temperature effect to be canceled. Thermal effects on the wiring connecting the strain gage installation to the bridge circuitry are also a source of error but can be compensated by such techniques as the "six-wire" connection.

More recent strain gages use the piezoresistive effect and may have gage factors of one or two thousand for fairly small strains. The gage factor of these gages is usually strongly affected by temperature and varies somewhat with strain. Readout circuitry with appropriate compensation is available for this type of strain gage also. They are used as the sensor devices in the piezoresistive accelerometers, where their high strain sensitivity allows the natural frequency of the accelerometer to be kept much higher than is possible when other types of strain gage are used.

Signal Conditioning

The signal output from the transducer is generally not suitable for display and recording. It may appear at an inconvenient voltage level or at a high impedance, or it may contain ac carriers or ringing frequency components. The circuitry which accepts the transducer output signal and adapts it to the requirements of recording and display devices is referred to as signal conditioning equipment. In many cases the signal conditioning also provides electrical excitation to the transducer.

Excitation and Impedance Transformation

Pickups using sensors, such as strain gages, piezoresistive elements, and capacitors, require that dc power or ac carriers be supplied to them, and linear differential transformer types require an ac carrier. The self-generating types are the coil-and-magnet velocity meter and the piezoelectric accelerometer. The velocity meter is the least demanding of all transducers as far as circuitry is concerned. It is a current generator with an impedance typically of a few ohms; signal lead characteristics and dress are thus of comparatively little concern, input impedances of readout circuitry are largely a matter of academic interest, and practically any necessary signal voltage can be supplied by appropriate resistor networks. In spite of these advantages, the velocity meter is a poor pickup in other respects.

The piezoelectric accelerometer, on the other hand, is a very high (capacitive) impedance charge generator. It requires high input impedance readout circuitry to obtain satisfactory low-frequency performance, which, in the past, was provided by cathode-followers, emitter-followers, electrometer circuits, and the like. These have largely been supplanted by the so-called charge-amplifiers and more recent operational amplifier circuits, such as "zero-drive." Because the piezoelectric accelerometer is a charge generator, it is desirable to keep the signal cabling to the readout circuitry as short as possible. The capacity of the cable shunts the signal voltage (although it does help the time constant), and, even with low noise cable, the signal generated by the moving cable becomes a serious problem when the total capacity at the input of the electronics is represented mostly by the cable. The requirement for short cabling frequently leads to the placement of at least some circuit elements close to the pickup, exposed to some shock motion, or even built into the accelerometer housing. This approach is often unsuccessful due to inadequate shock resistance in the exposed circuitry. The charge amplifier (current integrator) is not much affected by input capacity variations and is attractive for moderately long cable runs. Its problems are that the noise level is largely determined by input capacity and that the accelerometer is operated in an effectively short-circuited condition, lowering its natural frequency.

Filtration

After, in some such manner, having achieved a signal at convenient impedance and voltage levels, it may need to be filtered for various reasons, such as removing carrier frequency or (if the transducer is a piezoelectric accelerometer) removing the ringing contribution at its natural frequency. In the case of simple pulse shock, it should not be necessary, nor desirable, to filter the output if the piezoelectric accelerometer has been selected properly. In the case of shipboard shock, it will probably be necessary to filter in order to tell anything about the shock motion, and it is generally advantageous to limit the signal bandwidth to no more than that of the primary recording system. The filter characteristic is a matter of serious concern. It will almost invariably be of the low-pass type, preferably direct-coupled. It is much more important that the phase shift be linear with frequency than that the cutoff be sharp, because nonlinear phase shift introduces envelope distortion. This requirement applies to all elements of the measurement and analysis instrumentation chain, from the transducer to the final chart.

Computation

It is most desirable to make the primary recordings at the most primitive level of signal handling possible; i.e., when the transducer signal has been modified to the point where the recording system can stomach the signal, it should be recorded. Each additional component in the electronic chain is an additional source of noise, distortion, and unreliability. Nevertheless, there may be occasions when it is necessary to perform some computation prior to recording. For example, it may be essential to record an accelerometer output of very high dynamic range, beyond the capacity of the recording system, and yet retain the dynamic range of the signal. In this case it would be advisable to integrate the acceleration signal and record the resulting velocity signal.

Recording and Display

Primary Records

The use of magnetic tape as the medium for primary records is now almost universal. The frequency range of interest in shock studies is usually below a few kHz but extends almost to dc, making the use of FM recording mandatory. The low upper-frequency requirement permits low-density recording (54-kHz center frequency at 60 ips) to be used, improving dynamic range and noise level. It is also possible to frequency-multiplex several shock signals onto one direct record channel, but the dynamic range limitation and relatively high noise level often make this technique inadvisable.

Readout Devices

For many purposes the storage oscilloscope is adequate for displaying shock waveforms. Shipboard shock motions last too long and have too high a frequency content for this to be satisfactory. Streak photography is still used to some extent, but has largely been supplanted by the string oscillograph family. Galvanometers for these instruments are now available with a frequency capability of 10 kHz or more, and amplifiers suitable to drive them are common. Direct print photographic papers require no processing to produce a legible, though evanescent, recording. If it is feasible to play the magnetic tape back at greatly reduced speed, the time-honored pen recorder can be used for display. Time considerations usually place this procedure in the category of desperation measures, unless only a few records are involved.

ANALYSIS OF SHOCK MOTIONS

Shock Motion Waveforms

The waveforms of shock motions are multitudinous as are the waveform parameters required to describe them. If a shock motion consists of a velocity step, there is nothing to describe except its height; if it is not quite a step, its rise time in addition to its height may adequately describe it. If the velocity waveform's shape during the rise time is sufficiently complicated to require more description, it is better described by an acceleration pulse, which (if ideal) is described by its height, duration, and shape. Since it will rarely be ideal, additional parameters will be required to indicate the closeness with which it approaches an ideal shape.

Shipboard shock is another matter entirely. Descriptive parameters would include peak value, dominant frequencies, time-to-peak value, and decay time. The variety of waveforms is great, and the appropriate waveform parameters depend on both the nature of the individual waveform and the intended use of its description. The intended application will at least partially determine which group of the waveform parameters are pertinent.

Shock Spectra

Because of the complexity of the waveforms of shock motions, it is desirable to have a way to describe a shock motion which informs of its character but which is not sensitive to small waveform variations. This cannot be done simply with waveform parameters; even a slight shift in the phasing of high-frequency components can alter a waveform to an immense degree. One such description is provided by the shock spectrum, which in essence describes a shock motion in terms of the results it produces, thus giving a convenient basis for the comparison of shock motions (1,3,4).

Definitions

The shock spectrum of a motion may be defined as follows: Let the shock motion be applied as the input excitation to an assembly of s.d.o.f. systems, each having a different natural frequency (Fig. 6). Plotting the absolute value of the maximum relative displacement of each s.d.o.f. system against its natural frequency yields the shock spectrum of the motion. As a convenience in plotting, the maximum relative displacements may be scaled by natural frequency or its square, the most commonly used scaling factors being ω , the natural circular frequency, and ω^2/g (Fig. 7). Not only is this scaling a graphical convenience but also the undamped shock spectra (the plot derived when the s.d.o.f. systems are undamped) may be regarded as indicating the displacement step, velocity step, or static acceleration (depending on whether the plot is scaled by 1 , ω , or ω^2/g), which is equivalent to the shock motion. The basis of equivalence is that a s.d.o.f. system of a given natural frequency will undergo the same maximum relative displacement when subjected to the shock motion which it would experience when subjected to a displacement step, velocity step, or static acceleration of magnitude equal to the value of the shock spectrum of the shock motion at the natural frequency of the s.d.o.f. system. This is not the case if the shock spectrum is damped. Since the shock spectrum is strongly affected by the degree of damping of the elemental s.d.o.f. assembly, the amount of damping for which a shock spectrum has been obtained should always be specified.

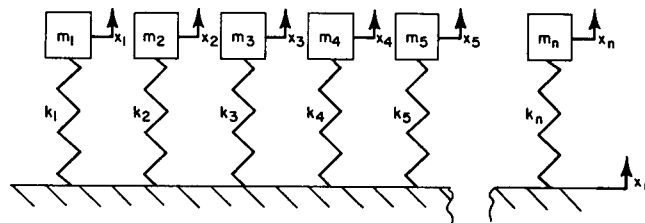


Fig. 6 — An array of undamped s.d.o.f. systems on a common foundation. The shock motion is the motion of the foundation x_0 .

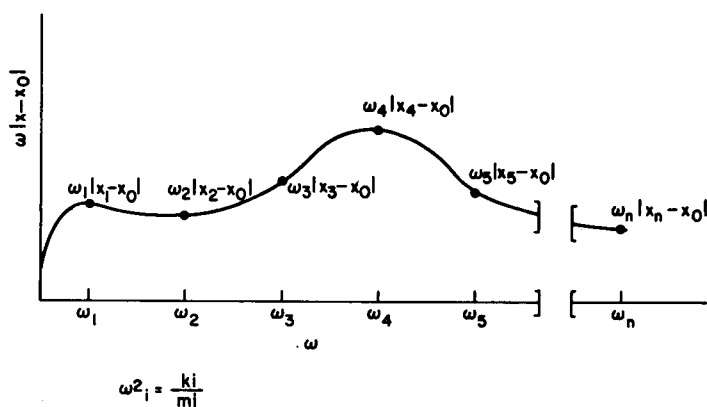


Fig. 7 — The shock spectrum of the foundation motion x_0 of Fig. 6. The absolute value of the largest relative displacement, regardless of sign or time of occurrence, of each array element is multiplied by its natural (radian) frequency and plotted against the natural (radian) frequency.

There are subspecies of shock spectra. The term shock spectrum is usually reserved for the quantity defined above, based on the maximum relative displacement, which is sometimes called the "overall" shock spectrum. Two more shock spectra are the positive and negative shock spectra, based on plots of the maximum positive relative displacement and the maximum negative relative displacement, respectively, as functions of system natural frequency. Obviously, at each frequency point the value of the shock spectrum will coincide with one or the other of the positive and negative shock spectra; the shapes of the three curves may be considerably different. Yet another variety of shock spectrum may be defined from the epoch of observation. If the relative displacements plotted are those which occur while the shock motion is still in progress, the resulting shock spectra are spoken of as "primary" or "during" shock spectra. If only the relative displacements occurring after the shock motion has come to an end are considered, the shock spectrum is the "residual" shock spectrum. Again, the term shock spectrum is usually accepted as referring to maximum relative displacement, regardless of when it may occur and regardless of its sign. To recapitulate, the varieties of shock spectra are

1. shock spectrum
2. primary shock spectrum
3. residual shock spectrum
4. positive shock spectrum
5. negative shock spectrum
6. positive primary shock spectrum
7. negative primary shock spectrum
8. positive residual shock spectrum
9. negative residual shock spectrum.

Figure 8 shows the response of a typical s.d.o.f. system and the extreme which would be plotted for the various subspecies of shock spectra. The latter two are distinct only if the shock spectra are damped. Damped shock spectra are of relatively limited use, and they are more often of concern with a specific piece of equipment than with a general type of analysis. The shock spectra normally encountered are traditionally undamped.

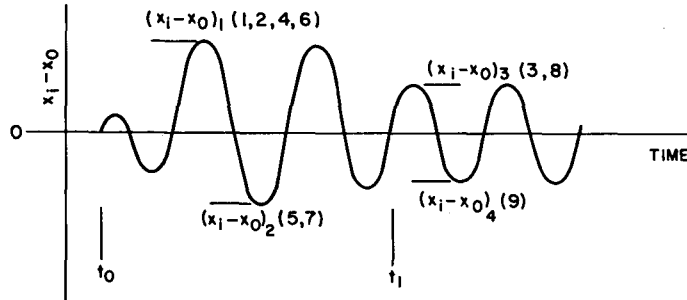


Fig. 8 — The relative displacement response, as a function of time, of the i th member of the array shown in Fig. 6. The shock motion x_0 starts at time t_0 and ends at t_1 ; it is zero outside the range $t_0 \leq t \leq t_1$. The response extrema indicated are those which would be plotted for the various subspecies of shock spectra listed in parentheses. The numbers refer to the list on page 13. The first extremum $(x_i - x_0)_1$ is the largest value regardless of sign or time of occurrence; the largest value, regardless of sign, which occurs while the shock motion x_0 is still in progress; the largest positive value regardless of time of occurrence, and the largest positive value which occurs while the shock motion is in progress. The value $(x_i - x_0)_1$ is thus the value plotted for shock spectra varieties 1, 2, 4, and 6. The second extremum $(x_i - x_0)_2$ is the largest negative value regardless of time of occurrence and also the largest negative value occurring while the shock motion is in progress, and accordingly is the value plotted for shock spectra varieties 5 and 7. The third extremum $(x_i - x_0)_3$ is the largest positive value and the largest value, regardless of sign, which occurs after the shock motion has ceased. So this value is used for shock spectra varieties 3 and 8. The final extremum $(x_i - x_0)_4$ is the largest negative value occurring after the shock motion has ceased and gives the value for the final shock spectrum variety 9.

Descriptions of Shock Spectra

The simple pulse waveforms have some generic features of interest. Any symmetrical pulse will have zeros in the residual spectrum at frequencies related to the reciprocal of the pulse duration. Pulses which are mirror images will have identical residual spectra. At frequencies which are low with respect to pulse duration, the shock spectra of simple pulses are relatively little affected by pulse shape. A particularly interesting simple pulse is the terminal peak sawtooth, all of whose shock spectra coincide for frequencies above the reciprocal of twice the duration (Figs. 9 through 11).

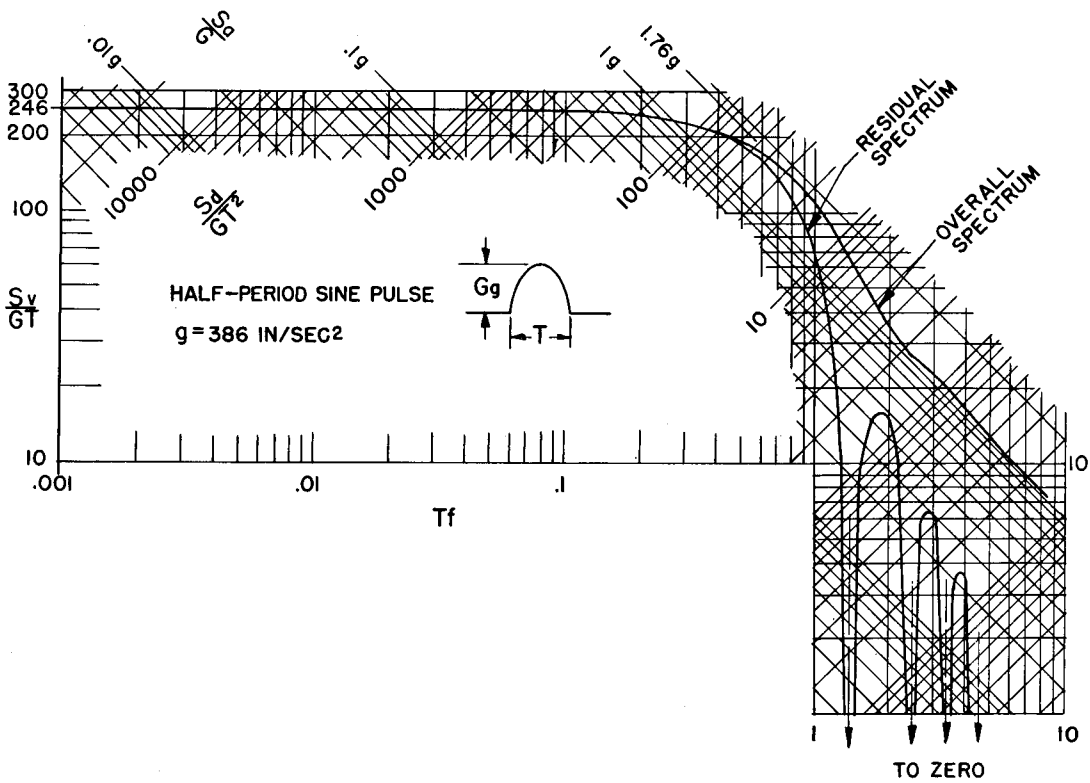


Fig. 9 — Residual and overall shock spectra of the half-sine acceleration pulse shown in the inset. The overall spectrum is the usual shock spectrum, i.e., the maximum response regardless of when it occurs. S_a , S_v , and S_d are respectively acceleration, velocity, and displacement shock spectra expressed in units of in./sec², in./sec, and in. G is the acceleration expressed in units of gravity g . T is the pulse duration; f is frequency. If the pulse length is 0.006 sec and the amplitude is 200 g , for a frequency of 100 Hz ($Tf = 0.6$) the overall shock spectral values of S_a , S_v , and S_d are 340 g , 200 in./sec, and 0.32 in. respectively.

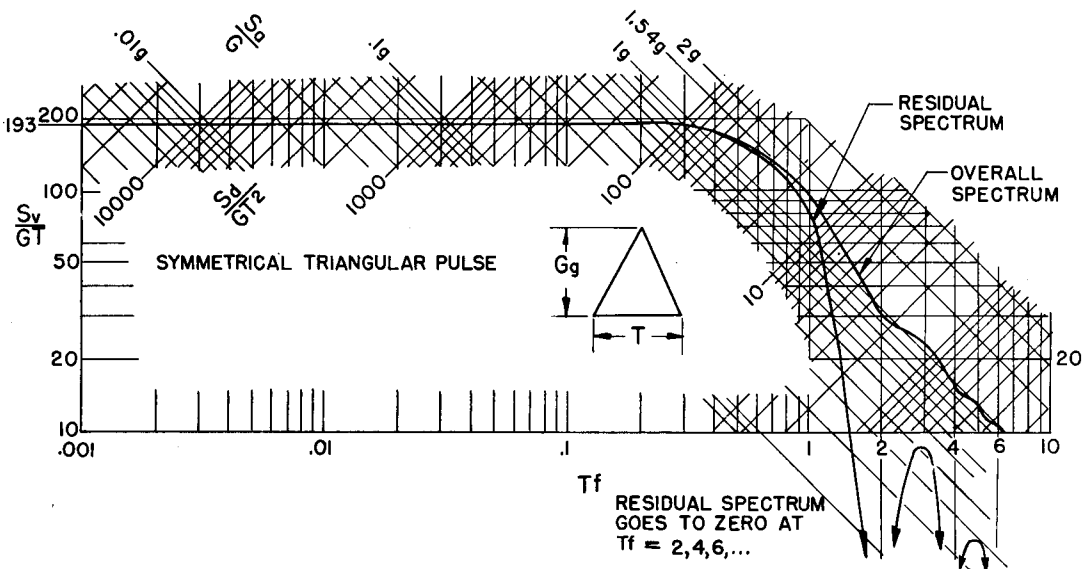


Fig. 10 — Shock spectra of a symmetrical triangular acceleration pulse

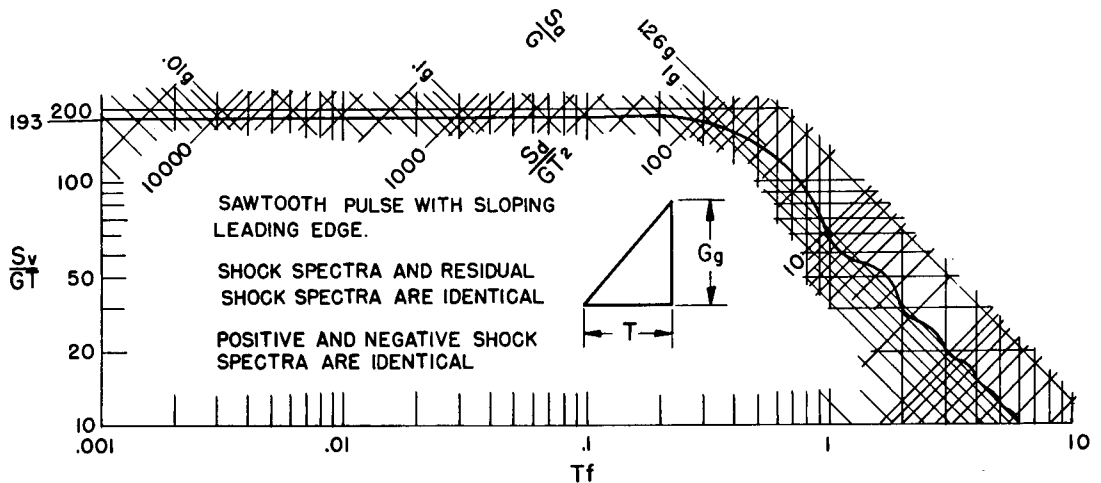


Fig. 11 — Shock spectra of a sawtooth acceleration pulse

The more complex waveforms such as shipboard shock, have more complex spectra (idealized in Fig. 12) which can generally be regarded as consisting of four frequency domains:

1. At very high frequencies, the spectrum value becomes equal to the maximum value of acceleration of the shock motion.
2. At lower frequencies, the spectrum will have peaks and valleys indicating response to dominant frequencies associated with the shock motions and may have values much greater than those of the actual motions.
3. At still lower frequencies, the shock motion will be in effect a simple change in velocity, and the spectral value will be that of the velocity change.
4. Finally, at very low frequencies, the value of the shock spectrum becomes equal to the maximum displacement involved in the shock motion.

Analysis Instrumentation Systems

Data reduction with self-recording pickups, such as the reed gage or putty gage, requires the reading of often barely detectable markings by means of a traveling microscope or a dial gage. This procedure is time consuming and laborious, and the errors can be large. The information derived from such pickups is primarily related to the shock spectrum, the reed gage in fact being the embodiment of the definition. Unfortunately, the reed gage has less than ideal characteristics. Its cantilevers ("reeds") are really not s.d.o.f. systems, their deflections often are not recorded properly due to collisions and other mishaps, and most importantly, the frequency range is not covered adequately. The self-recording pickups are generally making an unlamented departure except for special applications. The modern procedure is to do some preliminary analysis at the test site (sometimes a very complete analysis) and to perform any additional analysis, particularly that involving large volumes of data, at a large digital data processing facility.

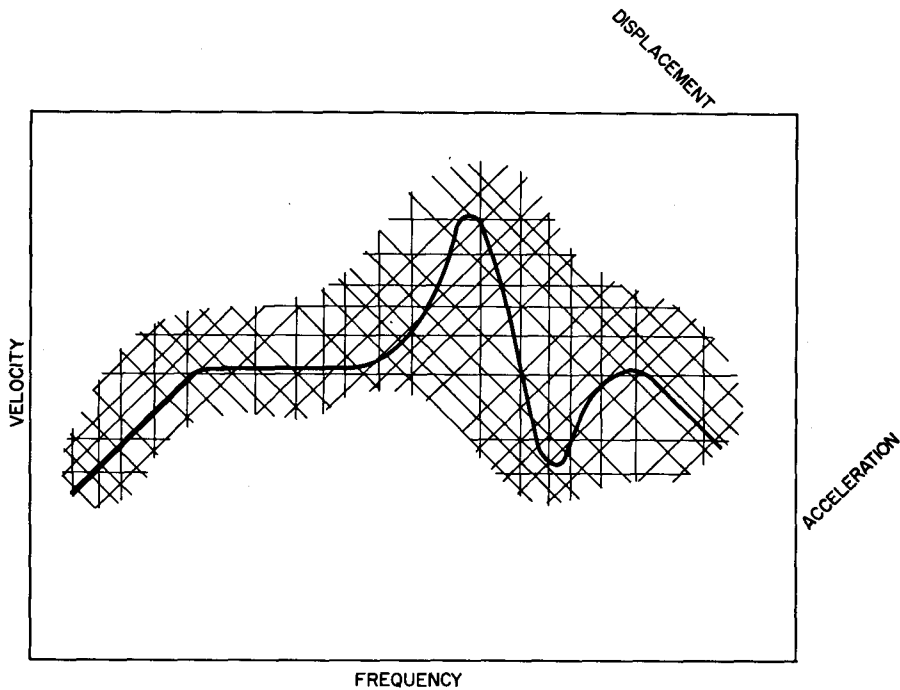


Fig. 12 — An idealized shock spectrum plotted on four-coordinate graph paper. System natural frequency (Frequency) is plotted along the abscissa, and maximum relative deflection multiplied by radian frequency (Velocity) is plotted along the ordinate. Lines of constant maximum relative deflection (Displacement) rise from left to right, and lines of constant product of maximum relative deflection and radian frequency squared (Acceleration) fall from left to right. Scale factors are usually chosen so that the units of these are hertz, in./sec, in., and g respectively. The hypothetical shock spectrum shown illustrates the four basic frequency domains. At high frequency, the shock spectrum value is equal to the highest acceleration contained in the input motion. At somewhat lower frequencies the shock spectrum value reflects resonant reactions to the input motion. At still lower frequencies the shock spectrum value is the value of the velocity change associated with the input motion, and at the lowest frequencies the shock spectrum value is equal to the maximum displacement involved in the input motion.

The on-site analysis equipment may often be analog since extreme accuracy is probably less important than pictorial output. It may include amplifiers, filters, integrators, differentiators, summing amplifiers, harmonic analyzers, shock spectrum analyzers, and graphic recorders. The most recent trend is to replace this ensemble of dedicated analog devices by an analog-digital converter, a small digital computer, and a graphic recorder, a combination which can perform any analysis function. The saving in hardware can be substantial, and the elimination of the need to input the signal to many individual analyzing instruments can yield even greater saving in time and effort.

SHOCK RESPONSE OF STRUCTURES

Dynamical Properties of Structures

The problem of describing the dynamic behavior of a real structure is extremely complicated. Even structures with as few as three degrees of freedom must be analyzed as somewhat special cases, in the sense that some of the structural coefficients must be assigned specific values or ranges of values. As the number of degrees of freedom increases, numerical procedures become mandatory, and shipboard equipments can be exceedingly complex structures. In practical cases, it is almost universal policy to make the assumption that the structure is linear, that it can be described by a lumped-constant model (i.e., an assemblage of properly chosen ideal springs and pure masses), and that it is essentially undamped. Variations on this theme may be undertaken at times, but not to any great degree; a few elastic elements may be assumed nonlinear, for example, or structural components in a restricted area be subject to damping. The computational requirements soon become prohibitive.

Normal Modes

A linear, lumped-constant structure has a number of natural frequencies equal to its number of degrees of freedom. Each natural frequency is a property of the entire structure, but the individual components of the structure will participate in motions at some frequencies more than at others. Each mode of vibration of the structure thus is characterized by a natural frequency and a mode shape, a configuration showing the degree to which each structural component participates in the motion of the whole. The natural frequencies and mode shapes are the eigenfrequencies and eigenfunctions of the characteristic equation of the structure (1,5,6).

There are several numerical methods for the solution of characteristic equations; one of the more useful is the Schmidt orthogonalization procedure. This method requires that the influence coefficients of the structure be calculated. This calculation may be made by applying a force at a measurement point of the structure and noting the motion at all of the measurement points; this provides one row of the influence coefficient matrix. Applying the forces at all of the measurement points completes the matrix. Since reciprocity applies to structures of the type hypothesized, the influence coefficient matrix must be symmetric, simplifying the calculation. The influence coefficient matrix is post-multiplied by the mass matrix to provide the dynamical matrix of the structure. A set of displacements representing the first mode shape is assumed, and the structure's equation of motion $(D - (1/\omega^2) I) \{q\} = 0$ solved. The resulting column is then used as the second trial column, and the iteration proceeds until the modal column produced coincides with the trial column to the desired degree of closeness. The second mode may be found similarly by adding the constraint that the modal column must be orthogonal to the first. This in effect postmultiplies the dynamical matrix by a "sweeping matrix" which sweeps out the first mode contributions (7). The third mode is constrained to be orthogonal to the first two, and so forth. The process is continued until it is considered that the higher-mode contributions are negligible. This method typically loses one significant figure per mode, so that numbers become impressively long if many modes must be retained.

Application of normal mode analysis permits the response of a structure to a known input motion to be calculated. The procedure allows the structure to be decomposed into an assembly of uncoupled s.d.o.f. systems whose responses may be calculated and

reassembled by a formula allowing for modal masses and participation factors to provide the net motions of each inertial element of the model. For many applications it may be sufficient to calculate just the modal responses.

Mechanical Impedance

Calculation of the dynamic properties of a structure by the normal mode or similar methods often involves idealizing the structure into a lumped-constant model. The most critical step of any dynamic analysis method (or, to a lesser degree, static analysis) lies in the selection of the model. This process has no sure procedure — general guidelines exist, but the greatest reliance is on the experience and intuition of the individual deriving the model. In practical cases, where structures may be extremely complex, it is often necessary to perform experimental measurements even to tell what the structure is. Complete reliance on blueprints can lead to some nasty surprises.

One promising method for the experimental study of structures relies on the concept of mechanical impedance. By analogy to the theory of electrical multiport networks, the mechanical impedance matrix of a structure may be defined as the matrix of coefficients relating driving forces to resulting velocities, evidently a close relative of the influence coefficient matrix. Most commonly, the velocity is measured at the same point to which the force is applied, and the complex ratio of force to velocity is called the driving point impedance. For a simple structure, the plot of driving point impedance vs frequency may be divided into three regions. At high frequencies, the structure is predominantly spring-like, and the impedance declines with increasing frequency; at low frequencies, the structure is masslike, and the impedance increases with frequency; at intermediate frequencies the impedance has peaks and valleys due to the resonant responses of the structure (Fig. 13). Suppose that the structure consists of a set of masses and springs and that the driving point impedance is measured at one of the masses. Its response will null at the fixed-base natural frequencies of the substructures connecting to it, and so the driving point impedance will peak at these frequencies. By measuring impedances at each mass of the structure, the natural frequencies of all of the substructures may be determined (in principle) and the fixed-base natural frequencies of the structure as a whole may be calculated. In practice this may be exceedingly difficult to do since practical structures rarely resemble clear-cut mass-spring assemblies, and accessibility to many of the masses is usually poor.

Commonly the measured quantities are force and acceleration, impedance being obtained via multiplication of the force/acceleration ratio by circular frequency. Transducers for both measured quantities are incorporated in an "impedance head," which is connected between the driving point on the structure and the electromagnetic shaker which provides the driving force. These transducers are usually piezoelectric, and subject to the same foibles mentioned previously. In addition, the technique for measuring impedance has its own pitfalls.

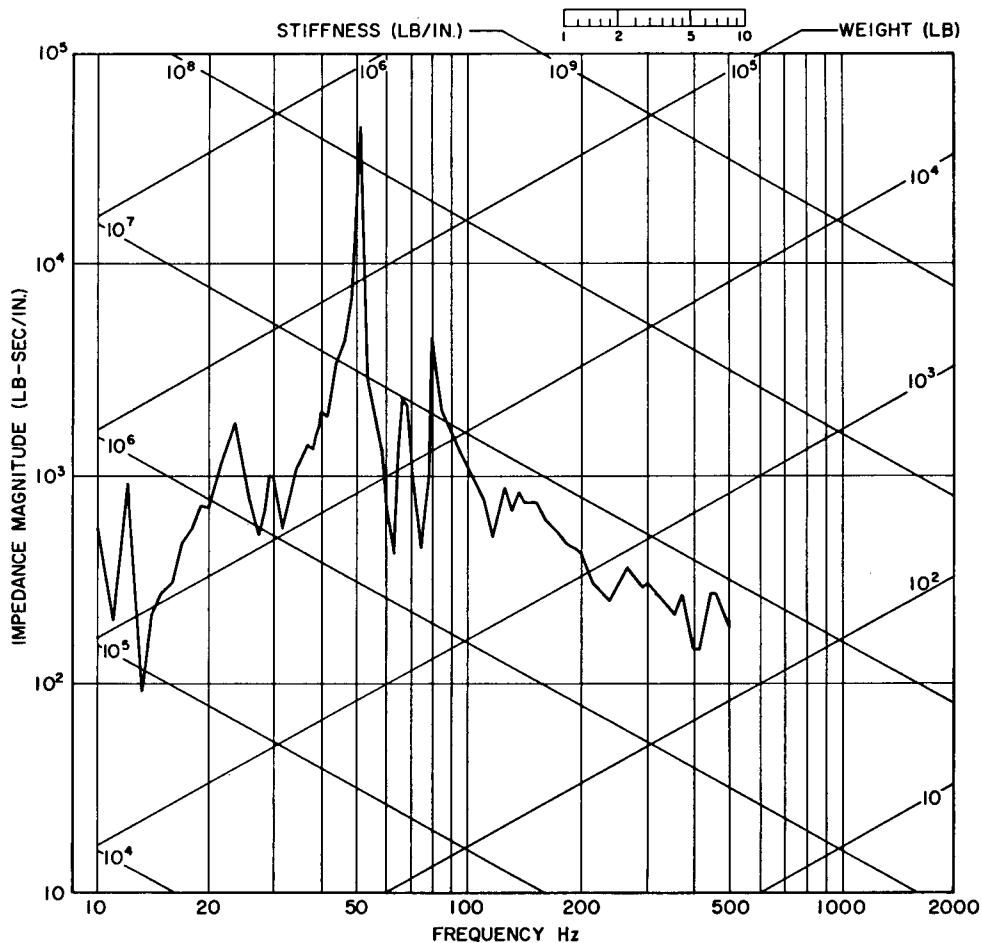


Fig. 13 — Driving-point impedance of a test structure. Lines of constant weight slope upward from left to right; lines of constant stiffness slope downward. The test structure is strongly springlike above 100 Hz, more or less masslike below 40 Hz, and mixed in-between.

It is possible that the measurement procedure itself can impose an abnormal constraint, so that the structure during measurement differs from the natural structure.* The mechanical linkage of the driving and measuring apparatus to the structure must be carefully considered. Alignment is very critical. Since it is impractical to apply great driving forces, it is necessary to measure some very small accelerations, and noise (electrical and

*Apart from experimental mishaps, the nature of the measured parameter may be such that the measurement procedure requires abnormal constraints to be imposed. For example, to measure the impedance matrix Z (where $F = ZV$) directly requires that a velocity be applied to one of the measurement points, the velocities at all other measurement points be held to zero, and the forces present at each measurement point determined. This gives one row of coefficients in the impedance matrix; the procedure is repeated for each measurement point. Due largely to the experimental difficulty and messy bookkeeping requirements the direct measurement approach is rarely used. It is much simpler, both in theory and in application, to measure the mobility matrix M (where $V = MF$) and invert. To measure mobility, a force is applied to a measurement point and the resulting velocities measured at all of the measurement points. No additional constraints are imposed on the structure.

mechanical) is a problem. To cap it off, the impedance plot may be so complicated as to baffle even an experienced interpreter. It is not surprising, therefore, that different investigators will frequently reach different conclusions about the dynamic properties of the same structure. Nonetheless, these difficulties are gradually being overcome. Instrumentation is being improved, and guidelines for experimental procedures are being established.

Fixed-Base Response of Structures

The natural frequencies usually calculated by the normal mode theory are the structure's "fixed-base" natural frequencies, which imply that the body to which the structure is attached and which furnishes its input motions is of such a nature that its motions are entirely unaffected by whatever the structure may do. When the motion input to the structure is a shock motion, the relative displacements of the structural elements will correspond to the shock spectrum, each normal mode behaving like a s.d.o.f. system having the same natural frequency as the mode. The maximum relative deflection associated with the excited mode shape as compared to the rest configuration will be as indicated by the shock spectrum. The motions of the individual structural elements will be determined by the participation factors and the relevant influence coefficients, and there need be no individual structural elements which actually attain the values given by the shock spectrum.

The structure's modal response will be characterized by a high-frequency region where the peak response acceleration is the maximum acceleration in the input motion, a low-frequency region where the peak response displacement is the maximum displacement of the input motion, a lower-intermediate region where the peak response velocity is the velocity change of the input motion, and a higher-intermediate range in which the modal response is of a resonant character. It is clear that amplification of motion can occur only when a resonant type of response takes place, and so the structural response will be dominated by the energy content of the input motion at the structure's fixed-base natural frequencies.

All modes are excited by the shock motion, but each has a characteristic propagation time. At different times, therefore, different modes may dominate the structural response. There may also be considerable flow of energy between modes. If two modes, for example, have natural frequencies fairly close together, and one is excited (in some improbable manner) but not the other, its motion will decrease while that of the other builds up. The magnitude of this effect and the rapidity with which it takes place are again functions of the participation factors and influence coefficients involved.

Resilient Mountings

Shipboard equipments, particularly those of a fragile nature, are sometimes mounted on resilient elements to mitigate the deleterious effects of motion of the ship's structure. These elements may be called "vibration isolators" or "shock mounts" depending on which aspect of the shipboard environment they are intended to ease. As its name indicates, the aim of the vibration isolator is to afford the equipment a relatively seismic suspension, and isolators are chosen to yield a natural frequency for the equipment — isolator combination, which is low compared to shipboard vibration. A wide variety of isolators are available, and an extensive repertoire of techniques exists for selecting and

using them under any imaginable circumstance. This leads to a pitfall in shock resistance. A seismic system subjected to shock must be capable of large relative displacements, displacements which approximate the absolute displacements of the ship. If the isolator cannot accommodate such displacements, it will bottom, and the resulting shock input to the equipment may well be more severe than that it would receive if attached directly to the ship. If the isolator can provide the displacement, appropriate clearances must be provided for the equipment to prevent collisions with neighboring equipments and structures. In extreme cases, it may be necessary to furnish the equipment with a saddle to enable the operator to maintain contact with it.

The shock mount is not intended to minimize the equipment's motion but to limit the magnitude of impulsive forces transmitted to it. It is consequently required to have some capacity for energy storage but need not provide very low suspension frequencies. As is the case with vibration isolators, there are many varieties of shock mounts available, but the selection procedure is less well systematized due to the less well-defined nature of the term shock. Usually, the selection procedure produces a suspension frequency of about 20 Hz or so, which is well situated to give problems from the normal shipboard vibration environment (5 to 33 Hz).

If the mass of the resilient mount and its hardware is negligible, the effect of its addition to the equipment from the point of view of structural analysis is to add a relatively soft spring between the equipment and its mounting structure. If this mass is not negligible, and it frequently is not, it may have the effect of converting the equipment into a vibration absorber for the mount (8).

All in all, resilient mounts are a mixed blessing at best and should be resorted to in extremis. With proper design and careful attention to design guidelines, it is possible to keep the natural frequencies of most equipment above about 35 Hz, and they can probably ride things out without assistance.

Shipboard equipments are frequently classified as "rigid-mounted" or "flexibly mounted" when their mounting frequencies lie above 15 to 20 Hz or below 5 to 10 Hz, respectively. The intermediate range is sparsely populated.

Effects of Interactions

Foundation Impedance

In actuality the motions of the foundation to which the structure is attached will be affected by the motions of the structure. This may be due to the effective masses of structure and foundation being comparable for some modes or to flexibility in the foundation. In either event a portion of the foundation in effect joins with the structure to form an extended structure with different response characteristics (Fig. 14). Nevertheless, the structure's response will still be strongly affected by the components of the motion at its mounting points which have frequencies in the vicinity of its fixed-base natural frequencies. The effects of foundation flexibility may include geometrical ones, such as changes in mounting dimensions, but the principal effect will be one analogous to the addition of shock mounts, viz, to limit high-frequency components of the motion and enhance low-frequency components. As a rule, the effect of foundation impedance will be as if the structure were mounted to a finite reaction mass. Particularly for large,

Fig. 14a — A simple equipment item on a fixed-base foundation

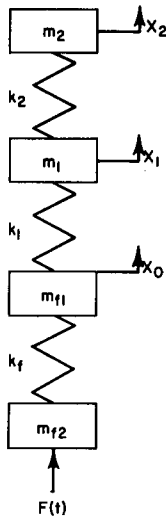
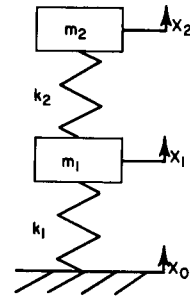


Fig. 14b — The same item on a reactive foundation, such as its actual shipboard installation

massive structures, the effective reaction mass may become small enough for the structure to act as a vibration absorber. Obviously any physically realizable object must have a finite impedance. The decision of what is structure and what is foundation may become an arbitrary one based on how much calculation is justified or reasonable.

Shock Spectrum Dip

If the response motions of the structure affect the motion of the foundation, they must affect the shock spectrum measured at the foundation (9,10). Since the components of the foundation motion at the structure's natural frequencies are the ones which determine its response, they are soaked up by the structure due to the vibration absorber effect. Therefore, little motion will be present at these frequencies in the foundation motion or its shock spectrum. Evidently the most important frequencies with regard to structural response are those associated with the dips in the shock spectrum (more precisely, the minima of the residual shock spectrum). For this reason shock tests based on spectral envelopes may be unduly severe.

Energy Transfer

Just as energy may flow between modes of a structure, it may also flow between structures on a common foundation of finite impedance. The response motions of each structure will be coupled into the other by reaction to the foundation. The details of the phenomenon will depend on the participation factors and influence coefficients of the extended structure (structure 1-foundation-structure 2) and the relation of the natural frequencies of the two structures (11,12). The study of structural response to shipboard shock motions can be complicated to any degree desired.

LABORATORY SIMULATION OF SHOCK ENVIRONMENTS

In view of the problems of shock theory, it is highly desirable to maintain an experimental program in which structures can be exposed to shock motions of known characteristics. If the shock motions are simple, the response characteristics may permit critical structural parameters to be evaluated. If the shock motions duplicate those to which the structure will be exposed in service, the response of the structure will indicate suitability for its intended service.

The study of shipboard shock is a field which exists for one purpose: to assure that essential Navy shipboard equipments will operate safely and reliably in combat. An obvious way to generate shock motions for experiments and acceptance tests for this purpose is to blow up a ship. Although done occasionally, this method is far too expensive and inconvenient to become a regular procedure. It is necessary to be able to generate shock motions of a controllable, or at least known, nature in the laboratory.

Equivalence Criteria

Two basic types of shock machines are widely used. One type (exemplified by the drop tester in Fig. 15) presents a high foundation impedance to its test packages and generates simple acceleration pulses, such as half-sine, sawtooth, and rectangular. The waveform parameters of these pulses can easily be measured with a high degree of precision and they constitute well-known excitation inputs of shapes which simplify the computations involved in extracting structural parameters of the test package from its measured response motions. Shock pulses of this type are also useful for providing arbitrary test environments. If the service environment is unknown or widely variable, this type of shock motion can be a useful acceptance test environment (13,14).

The other major type of shock machine endeavors to approximate the actual service shock environment. The Navy HI Class Shock Machines are of this type and generate complex shock motion waveforms similar to those of shipboard shock. With complex waveforms it is more difficult to decide when shock motions are similar, and the problem is complicated further by the fact that the response of equipments to the shock motions is of more concern than the motions themselves. For acceptance testing, shock motions are regarded as equivalent if they cause the same damage in equipments subjected to them. For purposes of design and prediction, it is necessary to know what parameters of the shock motions are critical to equipment response, what their values are, and how they are related.

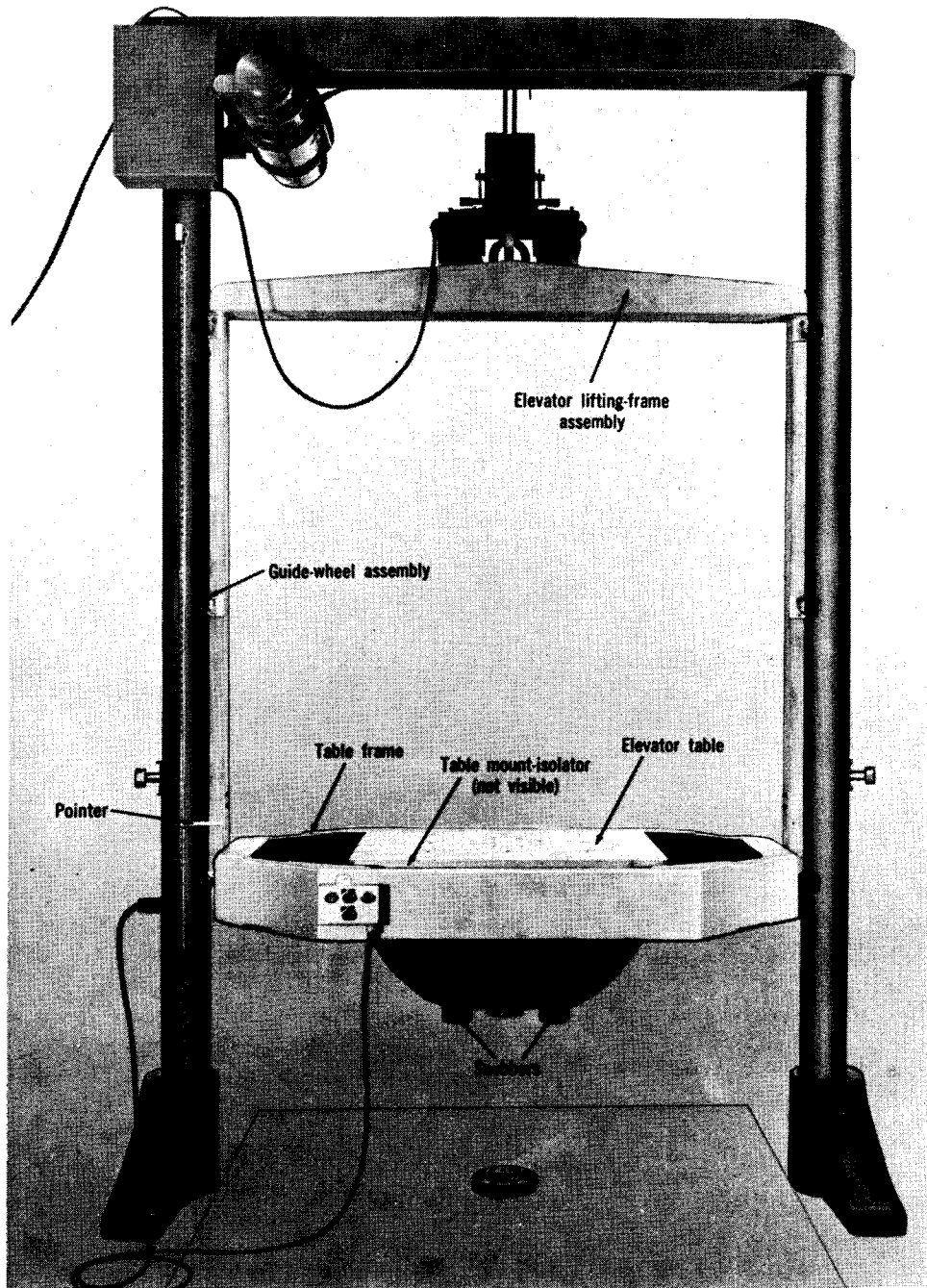


Fig. 15 -- A large drop tester of 400-lb load capacity. Shock machines of this type present a high impedance to the test package and generate simple acceleration pulse waveforms by dropping the test table with the test package fastened to it on appropriate impact moderating devices.

Waveform Parameters

Establishing the equivalence of shock motions having simple pulse waveforms is simply a matter of determining the pulse form and the allowable deviations from it. Any shock motions whose motion-time curves lie within the band of values so specified would be considered equivalent. The same sort of thing can be done for the more complex waveforms: a shock motion can be defined as a standard and permissible deviation limits defined. Obviously, this process is unreasonable from several aspects. First, the instrumentation systems which provide the motion-time curves may be different. A slight difference in frequency response or slight nonlinear phase shift at high frequencies is sufficient to render two recordings of the same waveform completely unrecognizable. Second, the high-frequency components of a motion may well represent local oscillations of small amplitude which do not propagate to any extent and are beyond the range of frequencies to which any practical structure can respond. Third, the response of a structure, which is really the primary concern, is determined largely by the components of the shock motion at its fixed-base natural frequencies, and other features of the waveform may be mostly irrelevant from this regard.

Despite these objections, it is sometimes possible to establish equivalence of the basis of waveform comparison. The first complaint can be alleviated by standardizing instrumentation systems, which has been done in a sense for the simple pulse shock machines. There the characteristics of the instrumentation system used to establish the pulse waveform parameters are specified in some detail. This approach would be of limited value in the study of shipboard shock because so much of the data available have been gathered by many groups over several years with instruments representing the phylogeny of the genus. Since it is rational to restrict the frequency content to some sensible range, the second problem can be solved by doing so. Restriction should not apply to the simple pulse shock motions, though, since the placing of frequencies involved in these waveforms is such that the high-frequency components are an important factor in the pulse makeup. The third problem is minimized concurrently with the second.

The conclusion remains that a waveform specification is an unsatisfactory method for comparing shipboard-type shock waveforms in general. There are special cases when general comparisons can be made, and they may be as simple as requiring only that peak velocities and dominant frequencies shall be comparable.

Shock Spectrum Envelope

A more reasonable way to compare shock motions is by means of the shock spectra. If a shock motion has a certain shock spectrum and permissible deviations can be specified, it is possible to compare others to it in the same way as proposed for waveforms. The advantages are that now the emphasis is placed on response to the shock motion rather than on fine details of its waveform — two waveforms may look very different yet lead to the same peak relative deflections at frequencies of significance. Also, it is possible to compare a shock motion with a group of shock motions; a group of shock motions may each have a shock spectrum very different from that of the one to which they are compared, but if the envelope of all their shock spectra are comparable to it, then the group of shock motions may be considered equivalent to the one. Unfortunately, this procedure tacitly assumes that all shock spectra are obtained from infinite foundation impedances (remember shock spectrum dip). If in fact some or all of the shock spectra were obtained from foundations which were affected by structure reaction, envelope comparisons can be very misleading.

Shock Spectrum Minima

Where structure-foundation interactions are significant, the critical points of the shock spectrum tend to lie away from the peaks (15), as shown in Fig. 16. If the shock spectral values are read off at the structure's fixed-base natural frequencies, it is possible in principle to calculate the effective mass ratios for the various modes and compensate for differences in foundation impedance. The effects of other structures on the same foundation may also be compensated for to an extent.

Foundation Impedance

In many shipboard installations the structure-foundation combination forms a relatively low-frequency system and the initial energy input to the system is accomplished in such a short time that it is the impulse of the primary excitation which matters, rather than its waveform. In this case, instead of examining the motion of the foundation-structure interface, an equivalent shock motion can be developed by attaching the structure to a foundation having the same impedance as its service foundation, suddenly feeding in an appropriate amount of energy to the system and allowing the structure and foundation to sort things out to suit themselves. As may be imagined, the practical difficulties of duplicating a foundation impedance may be formidable. This is, nonetheless, the principle on which the Navy HI Class Shock Machines operate.

Shock Test Specification

A shock test may be specified in several ways. It may be required that the shock motion input have a certain arbitrary waveform selected for mathematical tractability, as with the simple pulse shock machines. It may be required that the input shock motion possess a certain shock spectrum, which may also be arbitrary, or possibly derived from measured service environments. It may be required that the shock motion's shock spectrum have certain values at critical frequencies, also derived from measured service environments. Finally, it may be required that an appropriate foundation impedance be provided and that a certain energy be input to the structure-foundation system. The shipboard shock test procedure of MIL-S-901 follows the last tack implicitly, by specifying a shock test machine, a mounting arrangement, and an operating procedure. The primary criterion used for setting these specified items is production of the same damage to the test equipment by the shock test as by the service environment. The secondary criterion is generality of the shock test, by that an equipment which passes the shock test may be placed at any location on any ship with confidence that it will survive the service environment. There are some classes of equipment to which this specification is not applied and for which specifications of a different type are authorized. In such cases it is sometimes possible to use the same machine but to vary the mounting arrangement and operating procedure to provide the specified shock test.

Shock Test Machine

The shock test machine specified by MIL-S-901 may be one of three depending on the weight of the equipment to be tested. If the weight is less than 250 lb, the Navy High-Impact Shock Machine for Lightweight Equipment (LWSM) is applicable; if between 250 and 6000 lb, the Navy High-Impact Shock Machine for Mediumweight Equipment (MWSM)

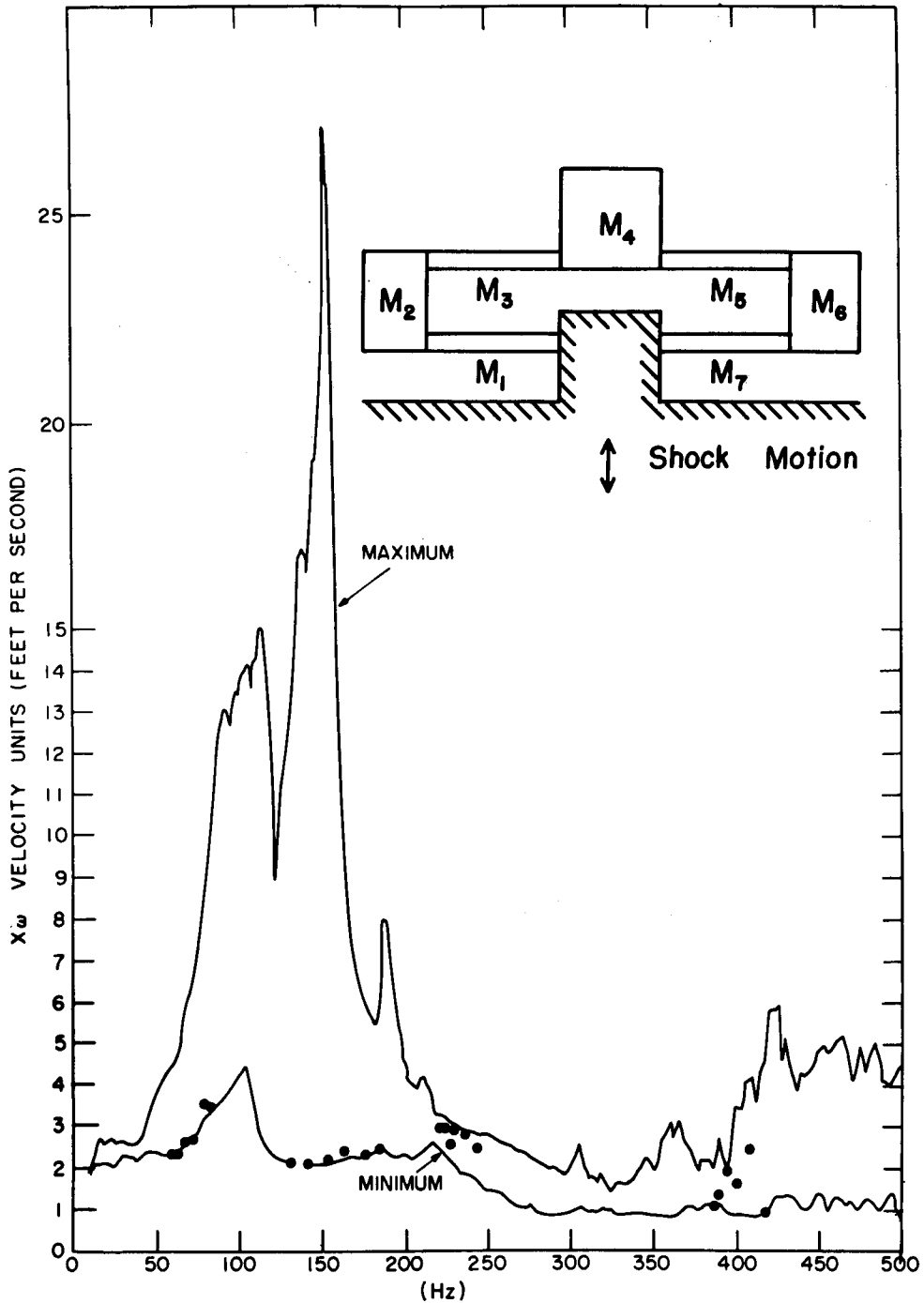


Fig. 16 — Maximum and minimum envelope of shock spectra of shock machine for medium-weight equipment with load as shown in inset. The beam lengths were varied, but the total mass on the table remained constant. The points represent the values of shock spectra which would be required to compute the values of stress measured in the beam.

is to be used; and if between 6,000 and 30,000 or 40,000 lb, the Navy Floating Shock Platform (FSP) is required. Items weighing between 250 and 400 lb may be tested on either the LWSM or MWSM, but the test report must indicate which. The initial FSP is somewhat shorter than the later models and has a maximum load rating of 30,000 lb compared to 40,000 lb for the longer ones. Items of up to 60,000 may be tested on the FSP if the center of gravity is not too high. Plans are in progress for the construction of the Large FSP, with a nominal load capacity of 320,000 lb. Until this device is completed, items too heavy or too large for the Navy's family of shock machines must rely on calculations by some method of dynamic analysis, such as the Dynamic Design Analysis Method (DDAM) (7).

These machines are completely different in geometry and construction; their mounting arrangements and operating procedures are also different. In general, the preferred procedure is to test entire assemblies as a unit on the appropriate machine. Where this is not feasible, as in a sonar system which may consist of 50 cabinets of electronics and numerous hydrophone domes, the subsidiary equipments may be tested individually on whichever machine is appropriate.

Since specified shock tests are mandatory, designing equipments to pass the test will inevitably come to be an end in itself. However many of the characteristics of shipboard shock the test machine may reproduce, there will still be some which it does not, simply because a test machine is not a ship. Designing around the shock test is not objectionable, since this indeed is what is supposed to be done, but taking advantage of characteristics peculiar to the shock machine to mitigate shock levels in ways which can be tolerated on the test machine but which cannot be tolerated on shipboard. For example, suppose an equipment is designed with a bottom structure of very soft foam rubber, permitting relative motion between the equipment proper and its mounting feet of, for example, 4 in. This item then would pass a test on the MWSM easily, even on the anvil table, since the maximum displacement of the MWSM is 3 in. If this same equipment were placed on board ship, where shock may mean gross ship motions of feet, it would likely be reduced to scrap metal when the first shot was fired.

Things like this have been known to happen, although in less blatant form. Inexperienced designers frequently show an exaggerated enthusiasm for shock mounts and vibration isolators, and even experienced ones may become so intent on the details of the test that they forget its purpose. To overcome this potential problem, practices are discouraged or forbidden that are clearly incompatible with shipboard conditions, even though they may enable an equipment to pass the shock test. Sometimes a special shock test has to be designed to simulate different aspects of shipboard shock than those simulated by the normal specification test.

Test Equipment Mounting Arrangement

In shock testing to specified waveforms or spectra, the foundation impedance presented to the test package by the shock machine and fixtures is kept as high as possible. When operated as specified, the HI Class Shock Machines are used with a mounting arrangement for the test package which provides it with a foundation impedance approximating that of its service installation. This is done by introducing compliant members into the mounting structure, as in the LWSM and MWSM, or by duplicating the service installation, as in the FSP. In all cases, it is required that the test package be attached

to the shock machine in the same way that it is attached to the ship, or as nearly as possible.

Shock Machine Operating Procedure

If the shock test is of the specified waveform or specified spectrum type, the shock motion input may be generated by dropping the mounting table and test item onto a suitable impacting surface, by feeding a suitable electrical signal into the drive amplifier of an electrodynamic shaker, or by rapidly applying high pressure to a hydraulic drive cylinder. The operating procedure for the HI shock machines is merely to introduce a specified quantity of energy into the test equipment-shock machine system in a time short with respect to the system's natural frequency. In the LWSM and the MWSM this is done by raising an impacting hammer to a specified height and in the FSP by detonating a charge of specified size at a specified depth and at a specified distance from and orientation to the FSP. The specification does not require that any particular waveform or spectrum be produced, nor that the one which is produced be known. (These may, of course, be required in those special cases for which shock test procedures other than that of MIL-S-901 are applied.) A specification shock test requires several such blows. The earlier ones are less severe than the later and serve an exploratory function. The condition of the test package and shock machine should be identical for each of the individual blows. After each blow, therefore, any mounting bolts and nuts which may have loosened should be retightened.

Test Equipment Performance

The performance required of the equipment being tested is a function of the importance of the equipment to the effective operation of the ship. The requirement may be no more than that the equipment or parts thereof shall not take flight or otherwise prove a hazard to personnel, or it may be that the equipment shall perform its function without any interruption, or anywhere between. Specification MIL-S-901 separates shipboard equipments into two grades:

Grade A — Grade A items are machinery, equipment, and systems essential for the safety and continued combat capability of the ship. The design shall be suitable to withstand shock loadings without significant effect on performance and without any portion of the equipment coming adrift or otherwise creating a hazard to personnel or vital systems.

Grade B — Grade B items are machinery, equipment, and systems not required for the safety or continued combat capability of the ship. The design shall be suitable to withstand shock loadings without the equipment or any external portion of the equipment coming adrift or otherwise creating a hazard to personnel or vital systems.

Standardization of Shock Machines

A desirable result of specifying test machines, mounting arrangements, and operating procedures is that a fair amount of test standardization comes about naturally. This is of great importance for two major reasons. First, standardization assures adequacy of a shock test regardless of at which shock testing facility the test is performed. Second, consistency in the severity of the shock environment generated by identical conditions on

different machines, and by identical conditions on the same machine at different times, allows the severity of the shock test to be reduced without loss of adequacy. The shock resistance of equipments, like all else, is not an absolutely fixed quantity but varies from equipment to equipment according to some distribution law. The shock test severity must be set high enough to reduce the number of equipments which pass the shock test but fail in service to some acceptable fraction. Shock test severity also has some distribution due to variation between test machines and procedures and variation between performance of any individual machine at different times. The percentage of equipments which pass the shock test but fail in service is then given by the overlap of the two distributions. If this area of overlap is held constant, the mean value of the shock test severity distribution is much less when the distribution is narrow, representing consistency, than when it is broad (Fig. 17). Consistency is thus a highly desirable attribute in a shock machine.

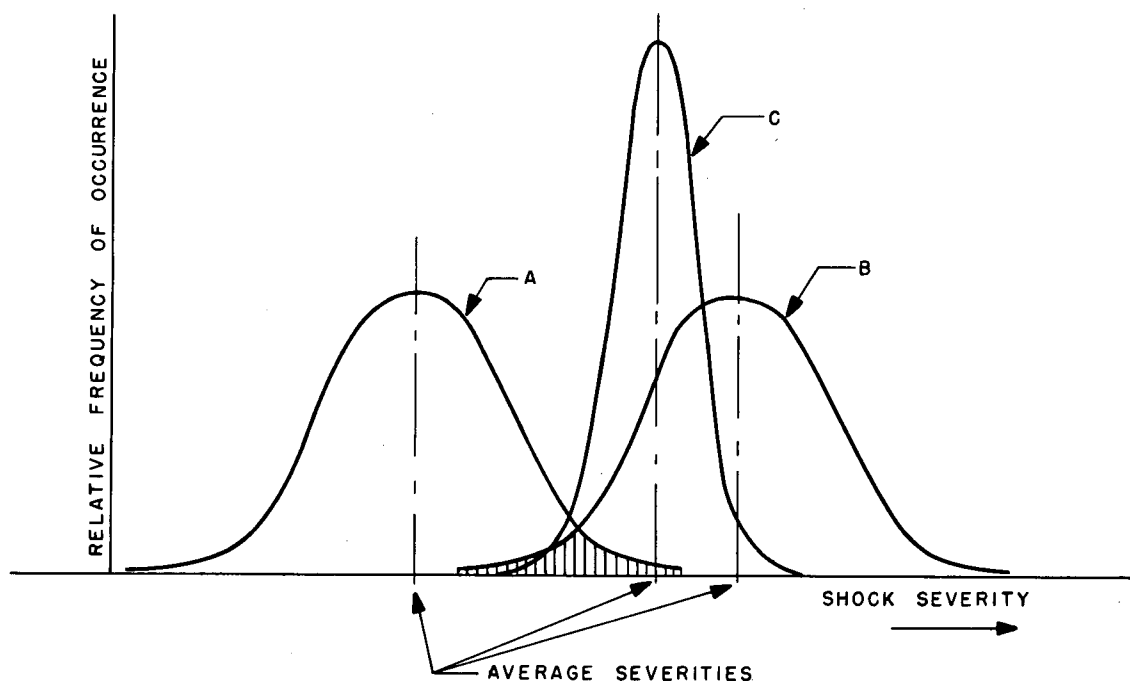


Fig. 17 — Distribution A represents the shock environment found aboard ship; distributions B and C represents the shock environments developed by two shock testing machines. Ideally, the shock severity used for design and acceptance testing should be above any level found in the field: the service failure rate of tested equipments would then be zero. In fact, it is not practical to do this but to accept a certain failure rate related to the probability that the test level will be exceeded by the service level. This possibility is represented in the figure by the cross-hatched region of overlap between distributions A and B. Note that when distribution C, representing a more consistent machine than that for B, is arranged to yield the same area of overlap, hence the same service failure rate, the average test severity is substantially lower than that for distribution B. Consistency is a highly desirable attribute in a shock machine.

In general, the shock motions generated by shock machines under some standard conditions should not vary more than 5% for frequencies under 200 Hz unless they undergo some plastic deformation of parts. Some plastic deformation does occur in the structures of the LWSM and FSP when operated at maximum severity. It does not occur in the MWSM (except for some slight bending of the mounting channels), which uses

hardened impacting surfaces. Considerable variation may be expected in shock spectra peak values since these are largely determined by damping losses. Damping arises from the relative motion of structural parts and strongly depends on bolt tightness and friction between mating surfaces.

THE NAVY HIGH-IMPACT SHOCK MACHINE FOR LIGHTWEIGHT EQUIPMENT

History

The ancestral LWSM was assembled in Britain in 1939, purportedly out of parts selected from the local junk yard (16). Its success in predicting shock performance of shipboard equipments soon attracted the interest of the U.S. Navy, which had a modified version built by General Electric Corporation in 1940. Further modifications have been made as the need for them has been revealed by use and as the increasing number of machines made standardization necessary (17). The major structural modifications to date have been installation of hammers with spherical impacting surfaces, to increase the lateral arm stiffness of the swinging hammer, standardization of the anvil travel at 1.5 inches to position stops, and replacement of the original leaf springs by coil springs and most recently by coil springs with closed and ground ends. The major operational changes have been to reduce the normal maximum load rating from 400 lb to 250 lb (when the MWSM was introduced) and to specify swinging hammer drop heights in feet of vertical rise rather than degrees of inclination. Other substantial modifications have been made to some machines for special applications. Since these machines no longer conform with the specified structure of the LWSM, they should probably be renamed.

Description (18).

The LWSM in Fig. 18 consists of a welded framework of standard steel structural sections; two hammers, one swinging in a vertical arc and the other dropping vertically; an electric hoist by which either may be raised; and an anvil plate which can be turned to present either its back or its side edge to the swinging hammer. This combination of two hammers and two anvil-plate orientations permits a test item to be subjected to shock along three orthogonal axes without remounting. Remounting would usually be simpler than rotating the anvil plate. Each hammer weighs 400 lb and can be raised to a vertical height of 5 ft above its impact position for a maximum energy input capability of 2000 ft-lb.

The anvil plate is a steel plate measuring $34 \times 48 \times 5/8$ inches, reinforced by steel I-beams welded to its back surface. Steel impact pads are welded to its top and side edges and over the stiffeners at the center of its back surface. For back and top blows the anvil plate is positioned across the main frame and rests on two enclosed coil springs. It is attached to the main frame by a set of four through bolts, each with a pair of springs, one of which is active (in compression) during the initial forward motion of a back blow and the other during the motion backward past the rest position later in the blow. These are called the "forward" and "rebound" springs respectively. The four through bolts pass through slots in the anvil plate with washers and spacers to permit free motion for top blows, where only the enclosed springs on which the anvil plate rests are active. For edge blows the anvil plate is rotated 90° about a vertical axis and is supported by rollers bearing on tracks above and below it. It is positioned along these tracks by two bolts, each with

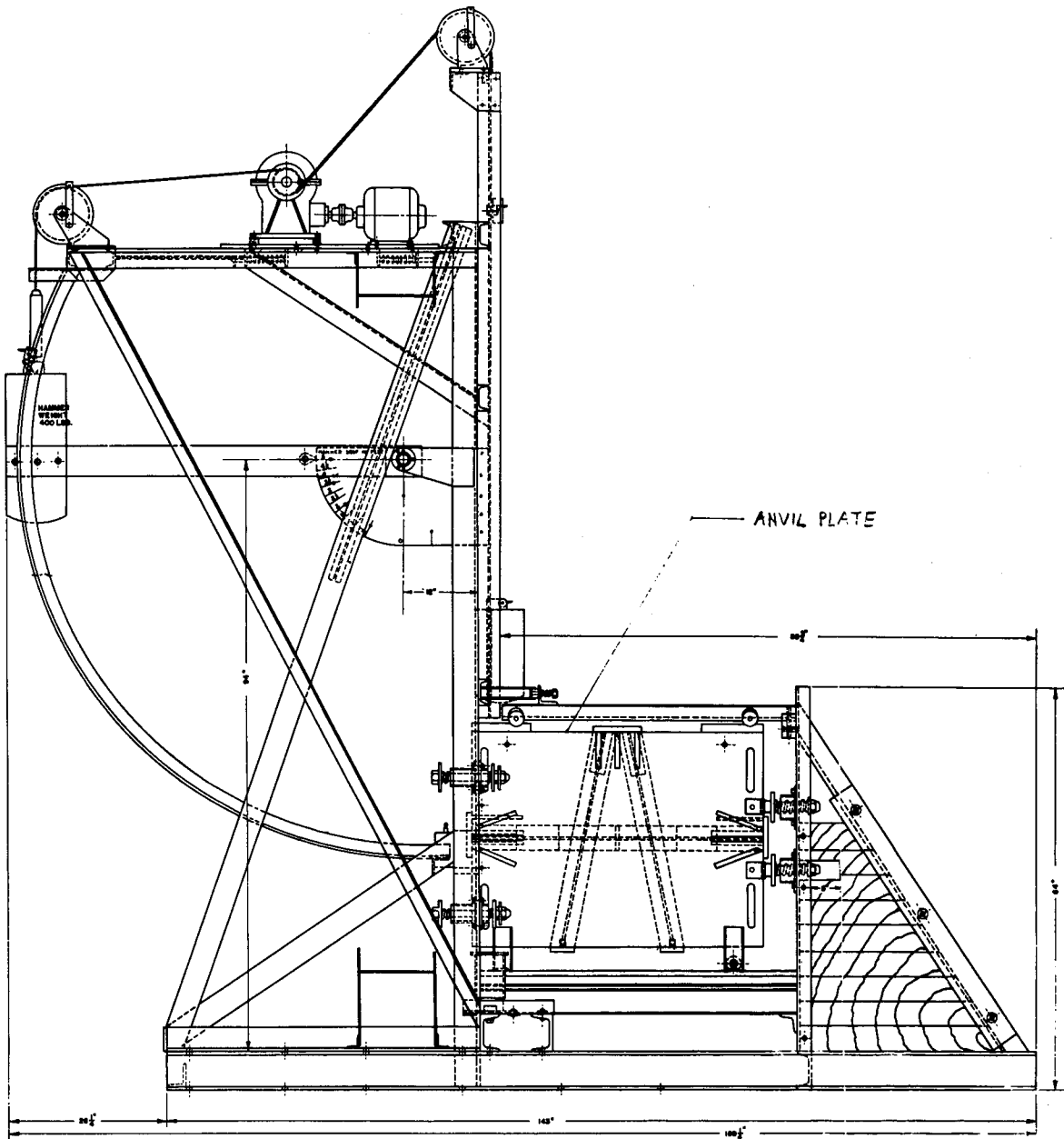


Fig. 18 — The Navy High-Impact Shock Machine for Lightweight Equipment. The LWSM is shown with the anvil plate oriented for edge blows. For back and top blows the anvil plate is rotated 90° and attached to the LWSM frame so as to present its back to the swinging hammer.

a pair of springs, attached to its forward edge, and is struck on the impact pad at its rear edge by the swinging hammer. In all directions, forward springs are furnished with limit stops which bottom after 1.5 inches of forward motion. The rebound springs for back and edge blows, which are much stiffer than the forward springs, are also fitted with limit stops, but these springs reach their solid height after about 0.4 inch of displacement, before the stops are reached. There are no rebound springs for top blows, the travel being limited by a captive bolt.

The forward motion for back and edge blows is set to 1.5 inches by adjustment of the through bolts, precompressing both the forward and rebound springs. When the anvil table starts forward, both springs act for about the first 0.1 inch of travel, at which time the rebound spring reaches its free height. The effective force-deflection curve for the anvil plate is thus bi linear (Fig. 19).

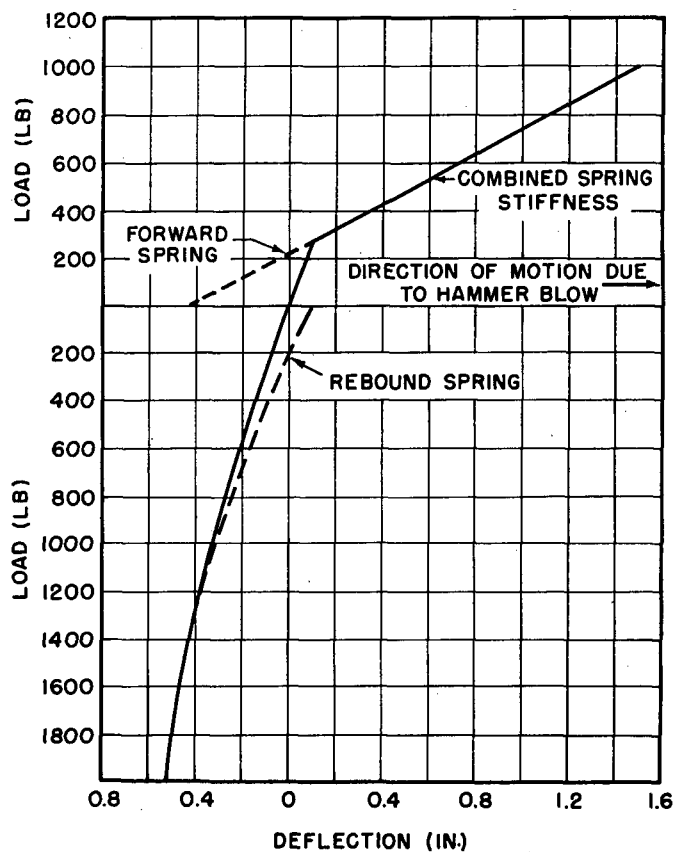


Fig. 19 — Force-deflection curves for the springs acting for back blows

Mounting Arrangements

The flexibility necessary to produce the desired foundation impedance is introduced by the 4A plate and the shelf plate specified by MIL-S-901. The 4A plate (Fig. 20) is a steel plate $27 \times 34 \times 1/2$ inches used for bulkhead-mounted equipments; its name is derived from the number of its illustration in an early shock test specification. The shelf plate (Fig. 21) is used for platform-mounted equipment and resembles the 4A plate with a reinforced shelf added to the bottom. Both plates are attached to the anvil table with reinforced 4-inch car-building channels as separators along their vertical edges. Test items are bolted to the mounting plates by drilling holes in appropriate places — when the holes become too numerous, the plates are replaced. For some types of equipment, such as circuit breakers, other mounting plates are specified in addition to the 4A or shelf plates. These are described in the shock test specification.

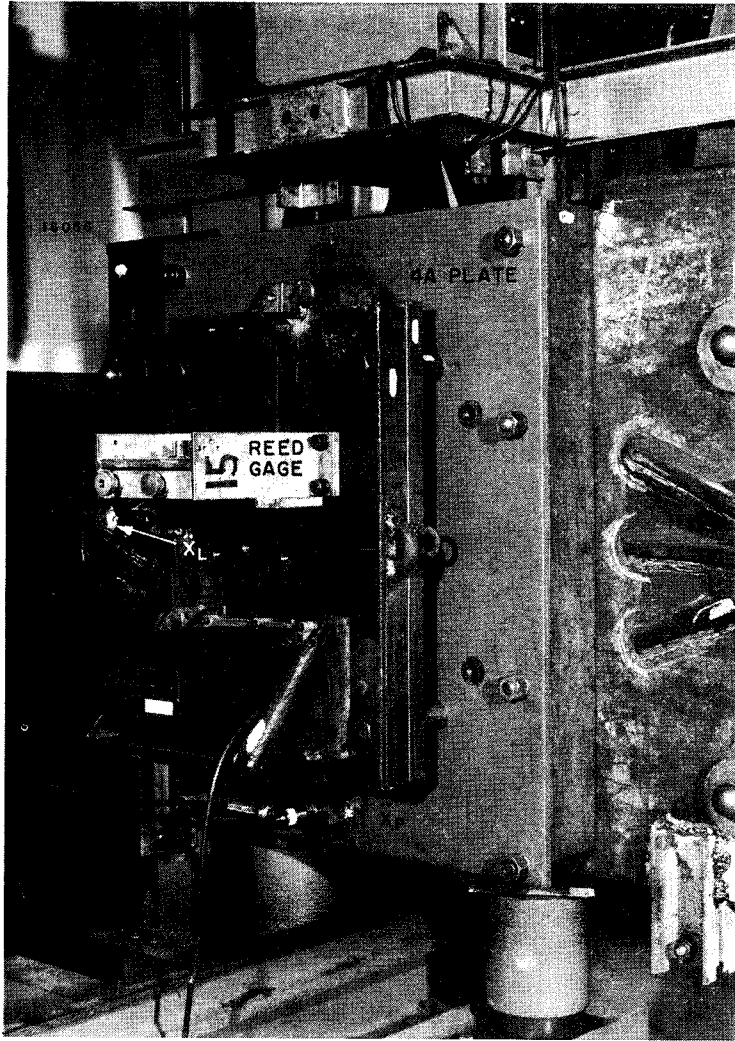


Fig. 20 — Calibration load of 389 lb mounted on the 4A plate in the vertical orientation. For the horizontal mounting orientation the load structure was rotated 90° about its thickness axis. Two of the four mounting holes used for the horizontal orientation are visible to the right of the load structure. The arrangement shown is for back blows.

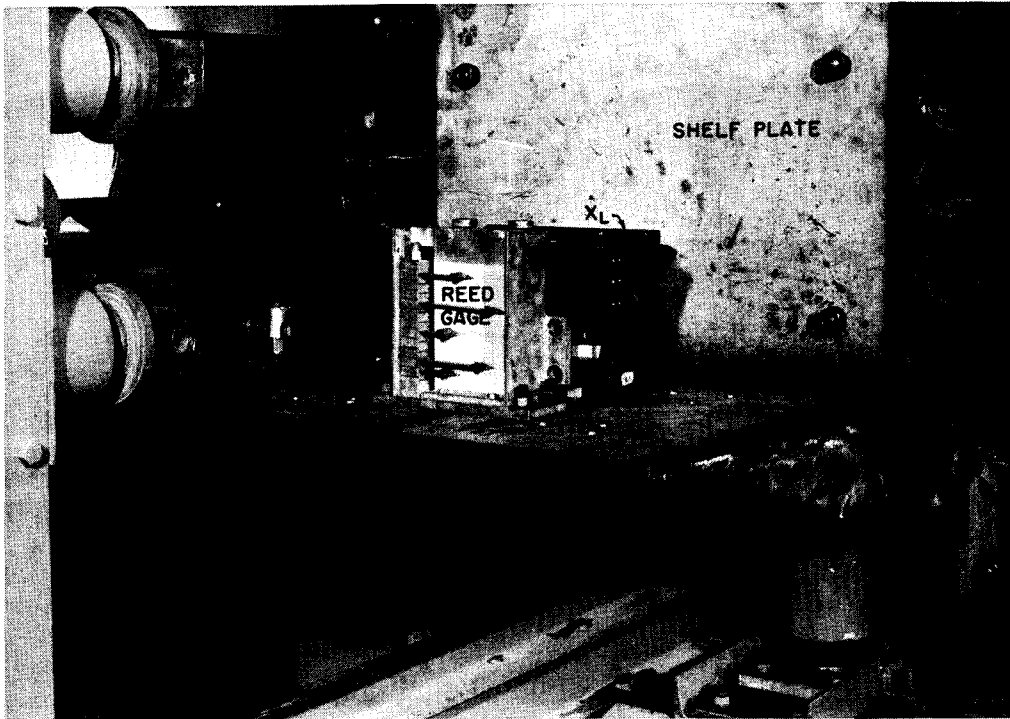


Fig. 21 — Calibration load of 57 lb mounted on the shelf plate; the arrangement is for top blows

Operating Procedure

The shock test specification requires that when the test item has been attached to the LWSM appropriately it shall be subjected to blows of 1-, 3-, and 5-foot hammer drops (in that order) in each of the three operating orientations — back, top, and edge. The order in which these orientations are to be tested is not specified nor is it required that tests be performed with the shock motion aligned in each direction along each axis. Mounting bolts and nuts are checked after each blow and retightened as necessary. The test item is also checked after each blow for conformance to whatever performance requirement has been set for it. The test proceeds until the test item is judged to fail, either for inadequate performance or structural collapse, or until the full series of nine blows has been completed.

An essential part of the operating procedure is maintaining the LWSM in the specified condition. This machine does deform plastically in use with associated changes in shock characteristics. It is required that the LWSM be inspected regularly to detect and repair cracked welds (which are generally found in the anvil-plate structure) and to replace the impact pads when their deformation becomes pronounced. Deformation is considered excessive when it results in a separation greater than 1 inch of the center of the impact pad from a chord extended from its ends.

Calibration of Shock Outputs (19-21)

As experience with the LWSM grew, the need for information about its output motion became apparent. The design information that can be derived from a go/no-go type of test consists largely of failure statistics for items of various constructions: This can be of great value in weeding out poor designs from equipments on hand and providing general guidelines for what methods and materials of construction to prefer or avoid: this was, after all, the LWSM's *raison d'être*. When this knowledge had been assimilated and was being practiced, failure rates dropped and the opposite problem of overdesign arose. While this is a far better problem to have, excessive strength of material or construction is uneconomical due to unnecessary costs, weight, and size. The cut-and-try method for optimizing construction of equipments is effective but can be highly expensive and time consuming if it is approached blindly. It was thus considered advisable to ascertain the salient characteristics of the shock motions developed by the LWSM and to distribute this information to provide a starting point for equipment design.

If machines are to be compared, the methods and procedures by which these calibrations are performed must be standardized or at least be of such a nature that results from a machine with one calibration arrangement can allow computation of what the results will be with another arrangement. If the information is to be of any use to equipment design, the calibration arrangement should not be specialized. Ideally, the arrangement should be of such a nature that the calculations required to interpret the calibration information in terms of the performance of some particular equipment design will be as simple as possible.

The shock outputs of the LWSM are affected by test equipment weight, frame stiffness, and mounting dimensions; by the tightness of the mounting-plate bolts; and by the condition of the anvil plate. These factors influence the modes of vibration of the mounting plates, shift natural frequencies, and change their phase relationships. The shock waveforms measured with two nearly identical equipments can consequently vary considerably in shape, although their magnitudes remain comparable. Consequently, it is desirable that the calibration arrangement should be representative of the average equipment actually tested or should use an equipment variable as a controlled parameter. The operating procedures should be those used for equipment tests.

Test Arrangement

The calibration test structure's interaction with the shock machine affects the shock motions measured at the machine/structure interface and on the test structure. For design, it is necessary to calculate (given these measurements and knowledge of the test structure) what the shock motions will be with a different test structure. This is most easily done if the original test structure is a dead weight, i.e., a load whose compliance is so low that its natural frequencies are well above the range of concern. Therefore, the one used for the calibration of the LWSM was of this type (22). Since the most widely varying parameter of equipments which are tested is weight, the calibration load structure was arranged accordingly to permit the weight to be varied over the rated range of the machine. Another variable of tested equipments is mounting dimension. Since this varies less widely, the mounting dimensions of the test load structure were taken as an average of those of equipment most often tested and were arranged as the corners of a rectangle. This permitted the effects of change in mounting dimension to be found by orienting the test load so that its long mounting axis was either vertical (Fig. 20) or across

the LWSM mounting plate. When the long axis lies across the mounting plate, the mounting points are closer to the spacer channels between the mounting plate and the anvil plate, and the configuration is much stiffer than when the long axis is vertical.

The calibration structure consisted of dead-weight loads of 57, 121, 145, 192, 261, and 389 lb. These weights were bolted to the mounting plate at the corners of an 18-by-13-inch rectangle and separated from the mounting plate by spacers to reduce binding. The 57-lb load (Fig. 21) consisted of the measuring instruments and their mounting adaptors welded along the vertical axis of the mounting plate. The 121-, 145-, and 192-lb loads were supplied by bolting steel plates to a welded steel frame; the 261- and 389-lb loads were provided by heavier steel plates without the frame but using the same mounting holes. The calibration load was attached to the 4A plate in both (load) orientations and to the shelf of the shelf plate. Blows of 1-, 2-, 3-, 4-, and 5-foot drop were delivered for back, edge, and top anvil-plate orientation.

Measurement Instrumentation

Measurement instrumentation (Figs. 20 and 21) consisted of a quartz accelerometer, a seismic-coil velocity meter (natural frequency 2.5 Hz, maximum travel 3 inches), and a reed gage, all mounted on the calibration load, and a quartz accelerometer attached to the mounting plate. The latter accelerometer was located at the center of the lower edge of the 4A plate and at the center of an outboard stiffener of the shelf plate. Each accelerometer output was fed into a high-impedance cathode follower and recorded on two channels, one filtered at 1000 Hz (low pass) and the other at 300 Hz for one blow and 5000 Hz for the next. Signals were recorded by 35-mm streak photography of a five-channel cro display. The records were then analyzed for peak accelerations and velocities, dominant load frequencies, and shock spectra.

Output Shock Motion Waveforms (20)

Description

The shock waveforms (Fig. 22) produced for a given load arrangement have the same general characteristics for different heights of hammer drop but are greatly different for different loads, load orientations, mounting plates, and blow directions. Back blows are more severe than edge or top blows. Back and edge blows with the load oriented across the 4A plate are much more impulsive in nature than those with the load oriented vertically, while top blows are not much affected by load orientation. Motions of the shelf plate have a much more pronounced rotary component for back blows than those of the 4A plate due to the low center of mass.

Peak accelerations occur shortly after impact on approximate half-sine pulses with superposed hash. These are followed by irregular perturbations from the interplay of the numerous vibratory modes excited by the impact. The durations of the half-sine pulses are about 2 ms on the mounting plates and about 4 ms on the load. After the pulse, slight variations in the uncontrolled parameters of the machine lead to large changes in the acceleration waveforms, particularly at high frequencies. The 300-Hz filter removes most of the high frequencies, so that the frequencies which dominate these records are those which dominate the velocity meter records, but this filter seriously deforms the

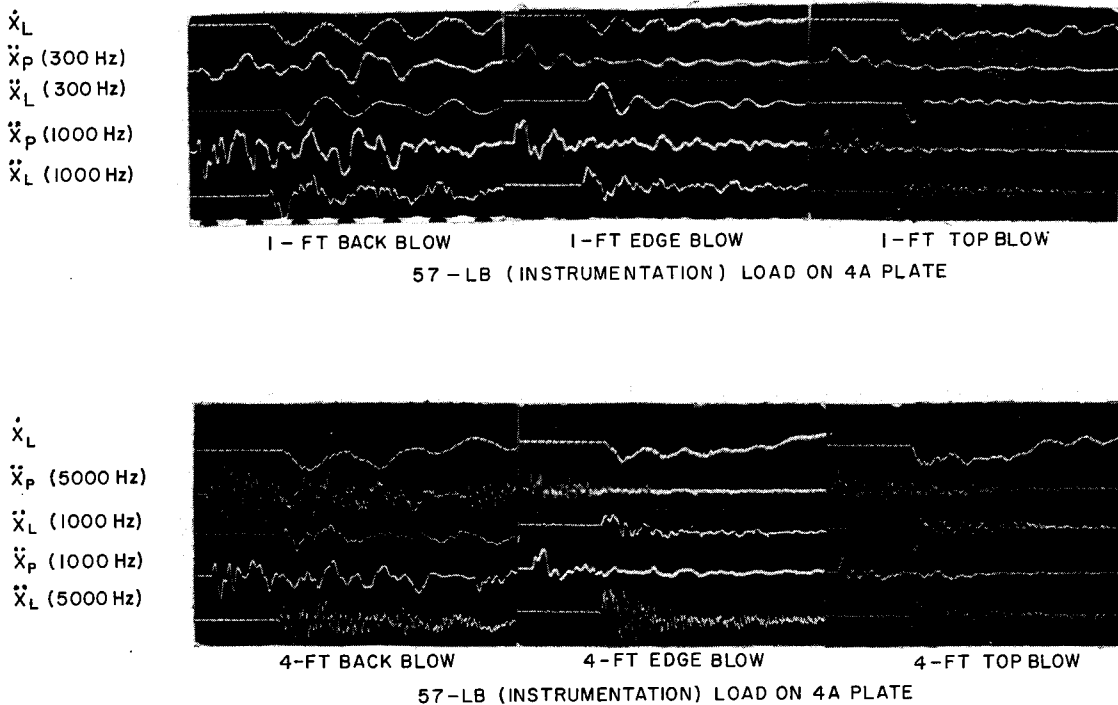


Fig. 22 — Typical waveforms measured on the LWSM. In these records, \dot{X}_L , \ddot{X}_L , and \ddot{X}_P represent load velocity, load acceleration, and mounting-plate acceleration respectively. The latter two are low-pass-filtered at the cutoff frequency indicated in parentheses. Time scale is indicated by blanking each trace at a rate of 1000 Hz. The offset between traces 2 and 4 and the rest is due to the geometry of the recording device. The deflections of all traces begin essentially simultaneously.

initial pulse. The 5000-Hz filter provides records which are almost unintelligible in terms of load response. The best compromise seems to be the 1000-Hz cutoff.

Mounting Plate Acceleration

Mounting plate acceleration depend very strongly on the location of the measurement — accelerations measured at other regions of the mounting plate may confidently be expected to differ from those reported here. It is likely that the differences would be mainly in acceleration level and frequency and that the pattern of changes caused by load arrangement, blow direction, and drop height would not be affected greatly. It should be pointed out that the mounting plate accelerometer was positioned to provide comparable relationships between mounting plate and load motions on the 4A plate and shelf plate. Thus, while the location is similar with respect to the load on both mounting plates, it is of very different character with respect to the structure of the mounting plates.

The peak mounting-plate acceleration (bottom section of Figs. 23 through 31) rises with hammer impact velocity, both slope and intercept being strongly affected by the load arrangement and direction of blow. There is a tendency for peak acceleration to decrease with increasing load, but it is by no means pronounced. Edge and top blows are comparable regardless of load orientation on the 4A plate. When the load is mounted

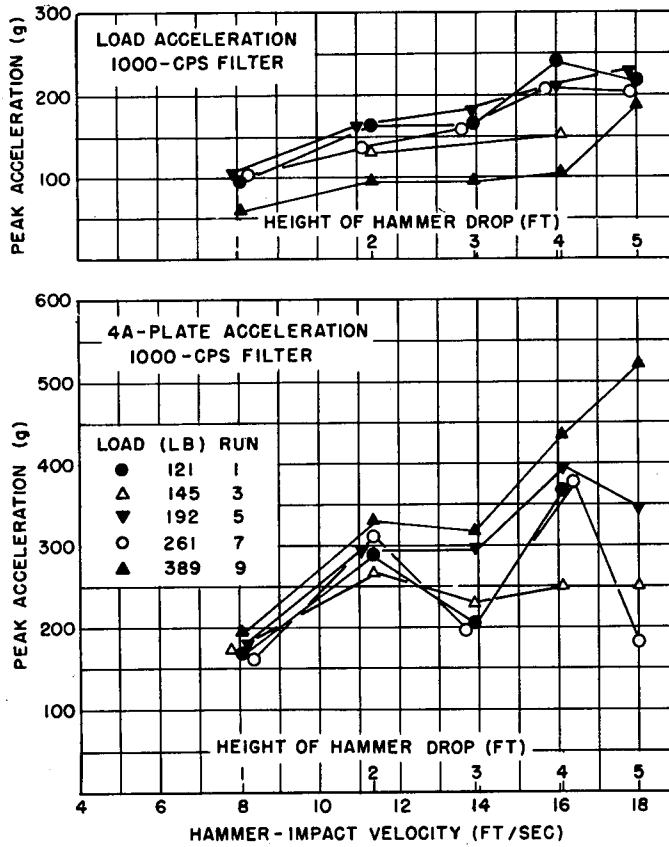


Fig. 23 — Peak load and 4A plate accelerations for back blows, load axis vertical

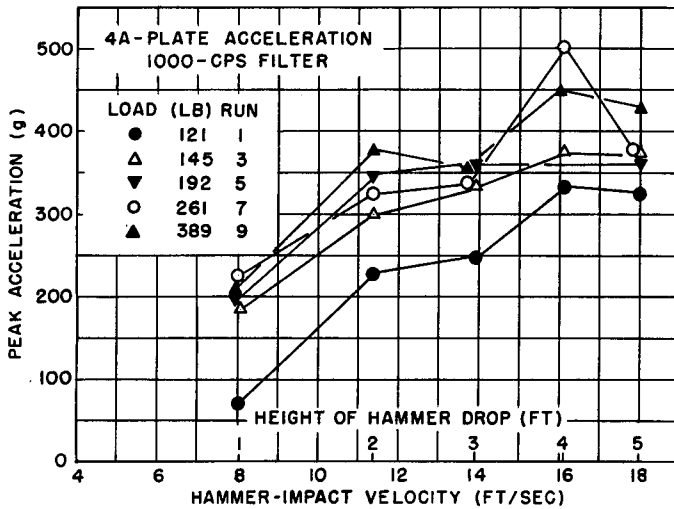
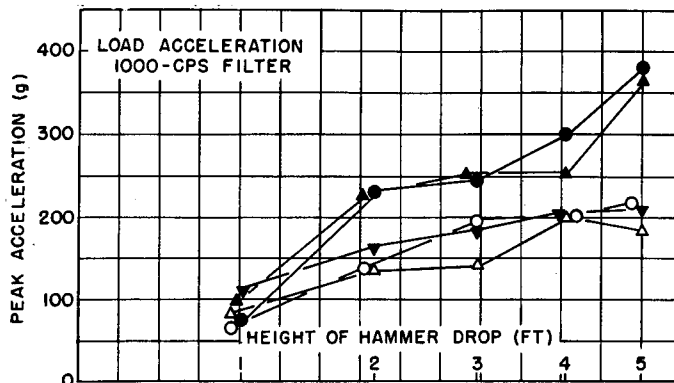


Fig. 24 — Peak load and 4A plate accelerations for edge blows, load axis vertical

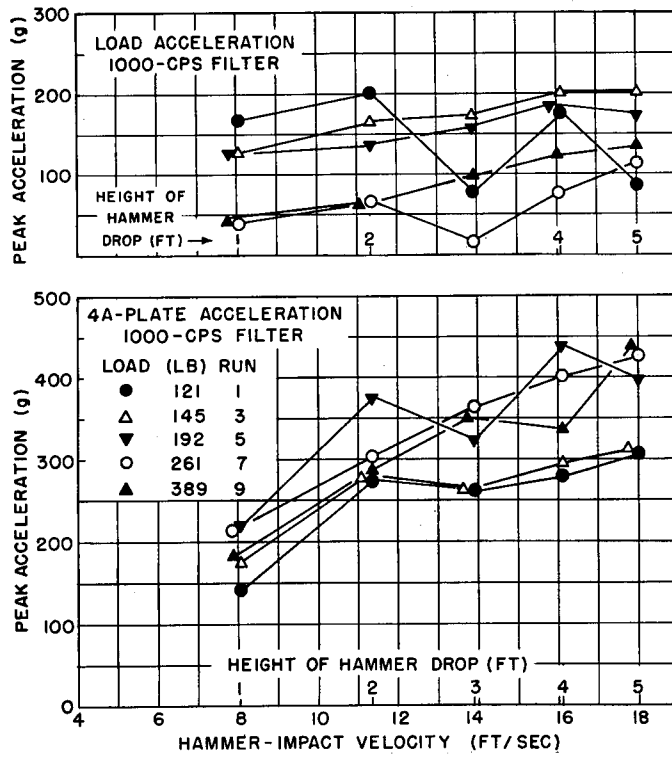


Fig. 25 — Peak load and 4A plate accelerations for top blows, load axis vertical

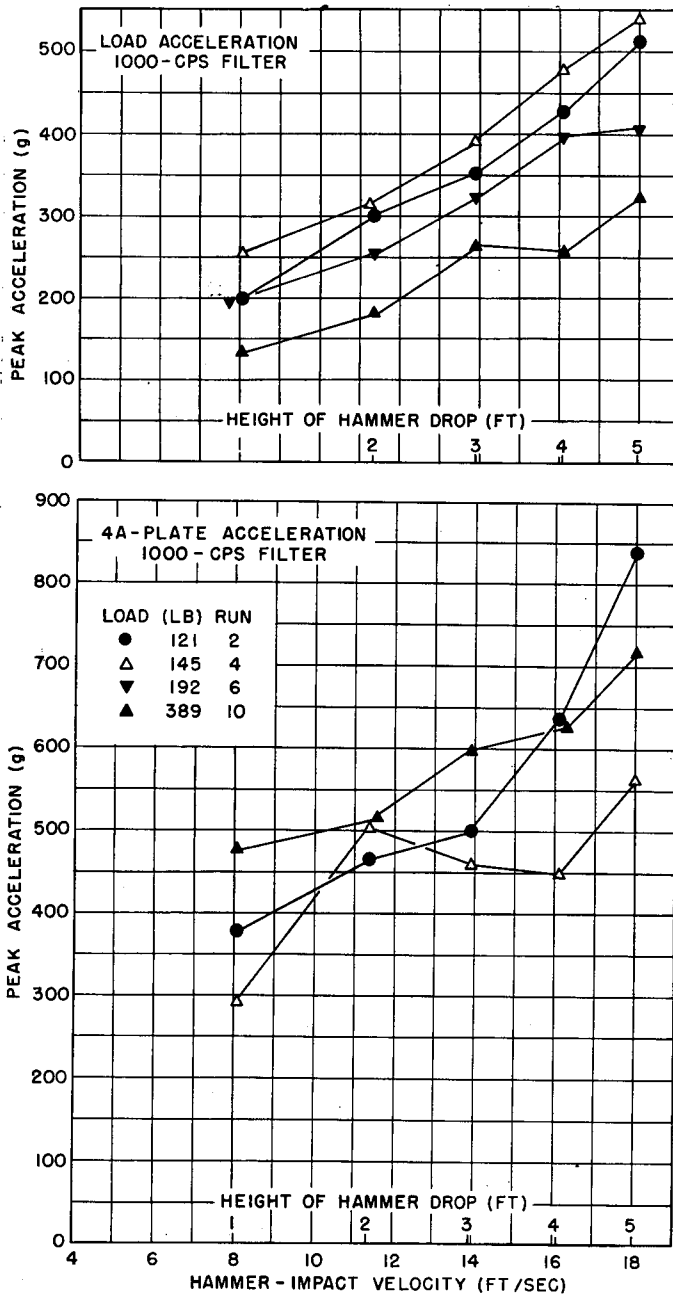


Fig. 26 — Peak load and 4A plate accelerations for back blows, load axis horizontal

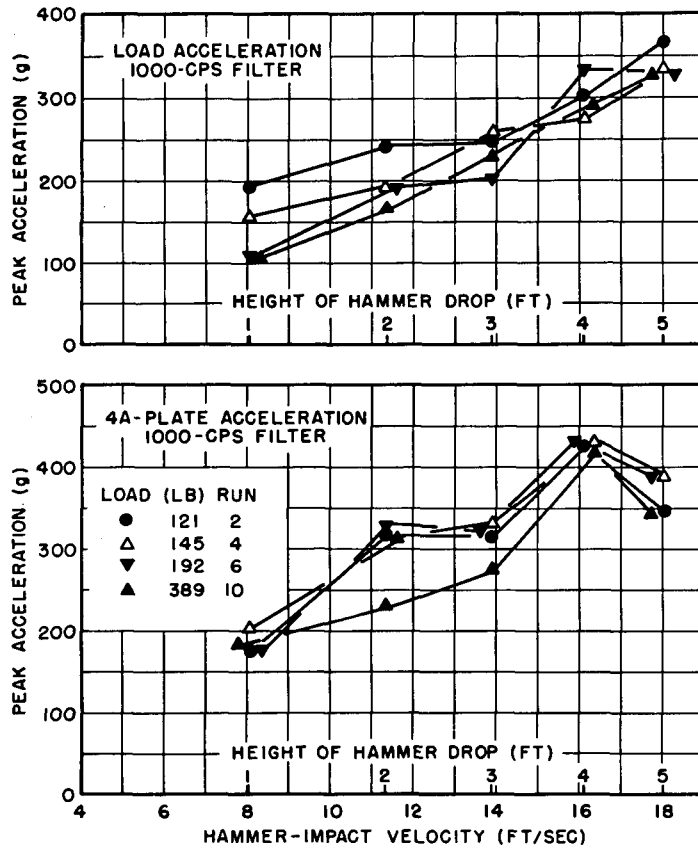


Fig. 27 — Peak load and 4A plate accelerations for edge blows, load axis horizontal

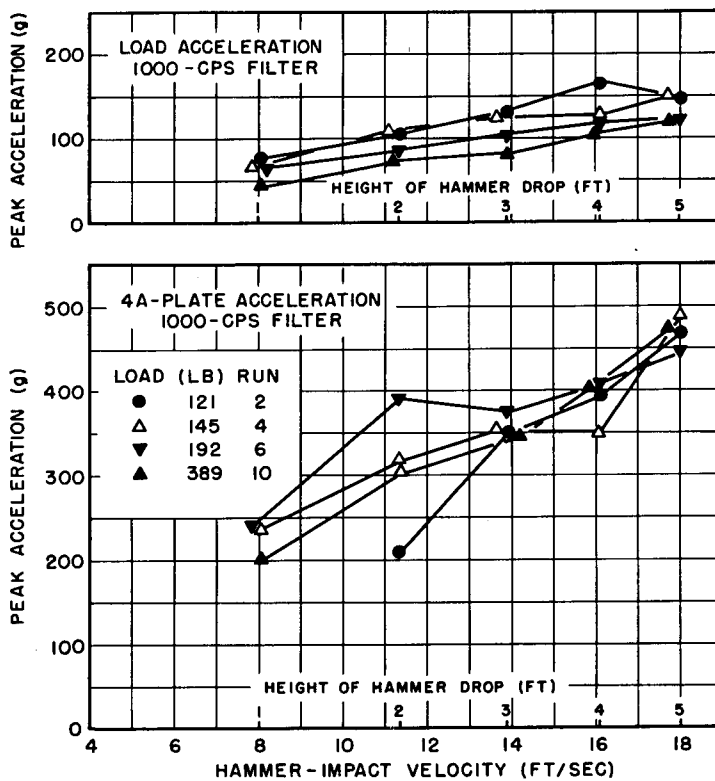


Fig. 28 — Peak load and 4A plate accelerations for top blows, load axis horizontal

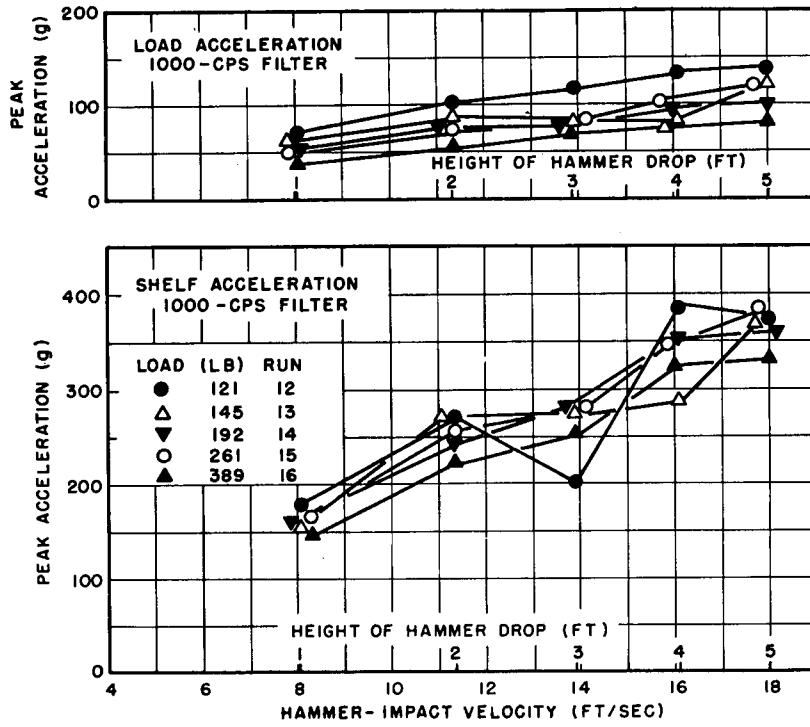


Fig. 29 — Peak load and shelf plate accelerations for back blows

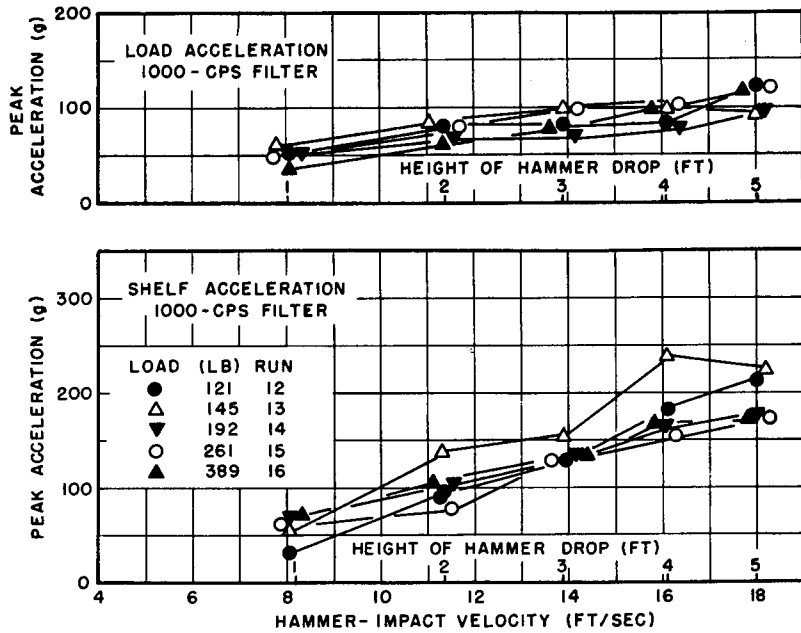


Fig. 30 — Peak load and shelf plate accelerations for edge blows

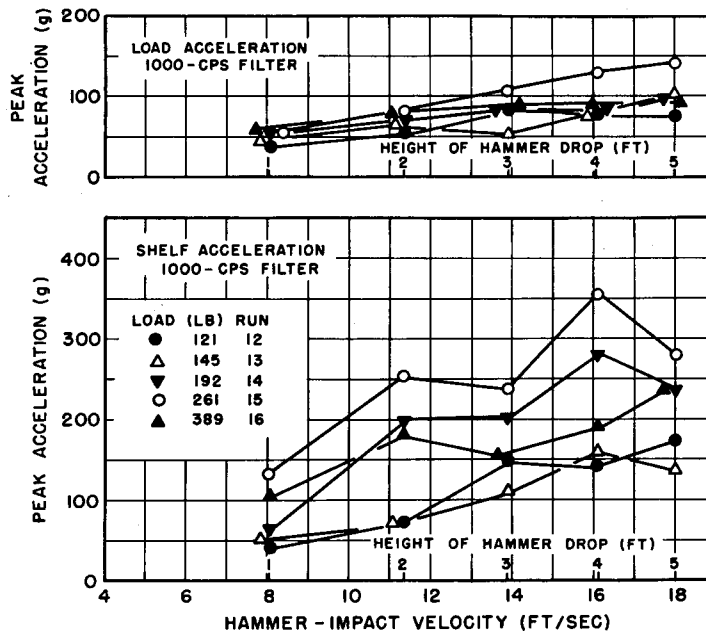


Fig. 31 — Peak load and shelf plate accelerations for top blows

on the shelf plate or vertically on the 4A plate, the severity of blows in all three directions are comparable. When the load is mounted horizontally on the 4A plate, back blows are considerably more severe than edge, and edge somewhat more severe than top blows. This is due primarily to the decreased span from support channel to mounting point, and it may be that some binding between the load and 4A plate is present also. In all cases, the peak accelerations measured on the 4A plate are much larger than those on the shelf plate under equivalent conditions. The maximum value recorded was 840 g, the minimum was 32 g, and the average of all values for all test blows was 241 g.

Load Acceleration

Load accelerations (top section of Figs. 23 through 31) show much the same trends as the mounting-plate accelerations, except that there is a slightly more consistent decrease as load is increased. Decreases are small, especially with the shelf plate. The maximum peak load acceleration recorded was 537 g, the minimum was 17 g, and the average value for all blows was 161 g.

Load Velocity

The load velocity waveform varies over the continuum between two extreme types, one a comparatively smooth, damped (1 - cos) type and the other a step type which reaches its maximum velocity quickly and is garnished with high-frequency, low-amplitude hash. The former type is found in the more flexible test conditions, back and edge blows with loads mounted vertically on the 4A plate. The latter is connected with the stiffer conditions, top blows with either load orientation on the 4A plate and blows in any direction with loads mounted horizontally. For loads mounted on the shelf plate, the velocities and frequencies are lower, and the distinction between waveform types is less pronounced.

Shelf plate waveforms are also more difficult to analyze due to a substantial rotational component of unknown magnitude.

Velocity as a motion parameter is less sensitive than acceleration to the high-frequency components, hence, shows rigid-body motions to better advantage. Peak load velocity (Figs. 32 through 40) for a given test arrangement is essentially linear with hammer impact velocity except at the high velocities, where flattening of the curve indicates some plastic deformation in the struck members. Loads mounted on the 4A plate attain the greatest peak velocities for edge blows and the least for top blows; the orientation of the load on the 4A plate has little effect. Loads mounted on the shelf plate have substantially lower peak velocities. The peak velocities measured ranged from 15.4 ft/sec to 2.3 ft/sec. The average peak velocity for all blows was 8.2 ft/sec.

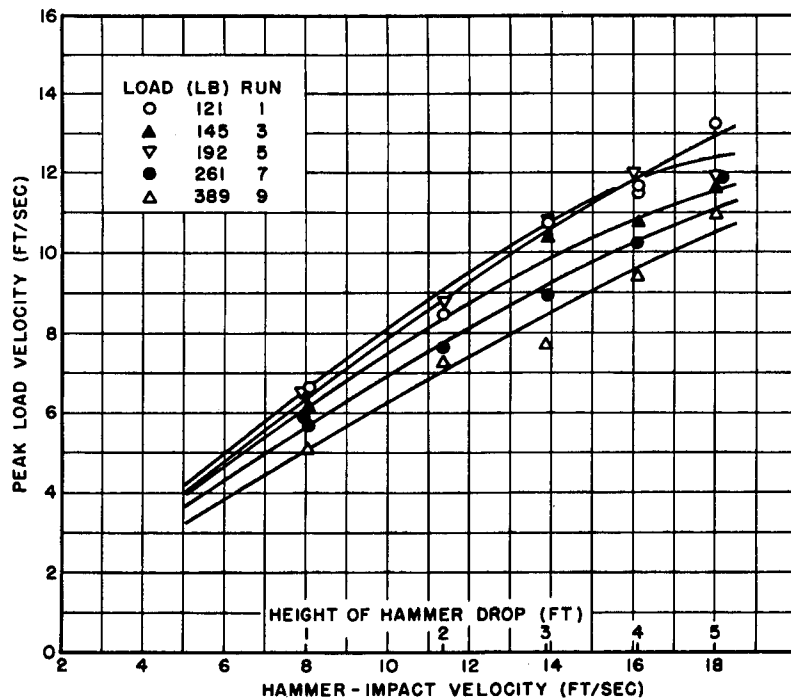


Fig. 32 — Peak load velocity for back blows on 4A plate, load axis vertical

As implied by the behavior of load velocities and accelerations, dominant load frequencies decrease with load increase when mounted on the 4A plate but are not greatly affected on the shelf plate (Fig. 41). Loads mounted horizontally on the 4A plate have higher frequencies than vertically mounted loads for back and edge blows, while the opposite is true for top blows. Loads mounted on the shelf plate have lower frequencies than those on the 4A plate. The highest dominant frequency found was 220 Hz, the lowest was 41 Hz, and the average of all load arrangements was 122 Hz.

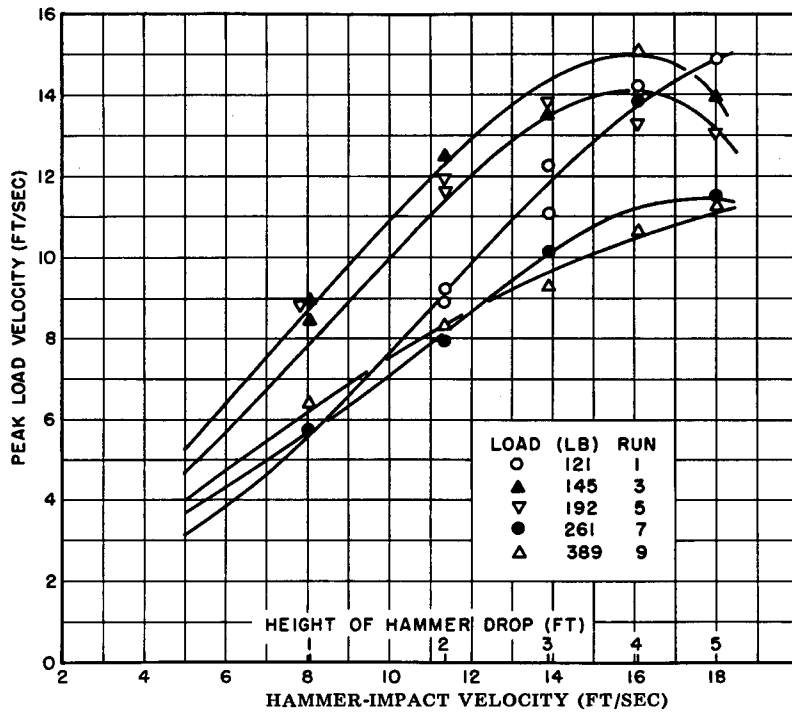


Fig. 33 — Peak load velocity for edge blows on 4A plate, load axis vertical

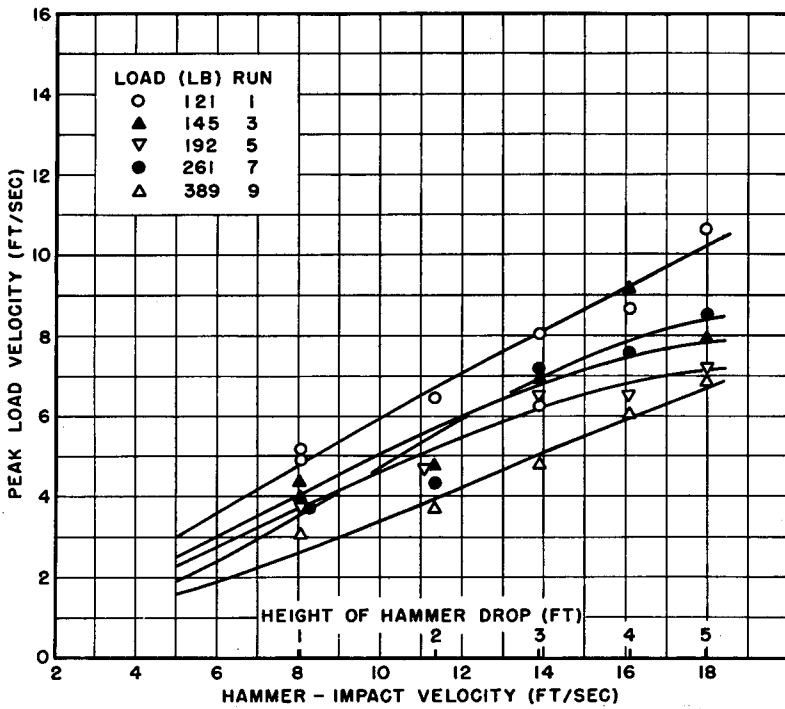


Fig. 34 — Peak load velocity for top blows on 4A plate, load axis vertical

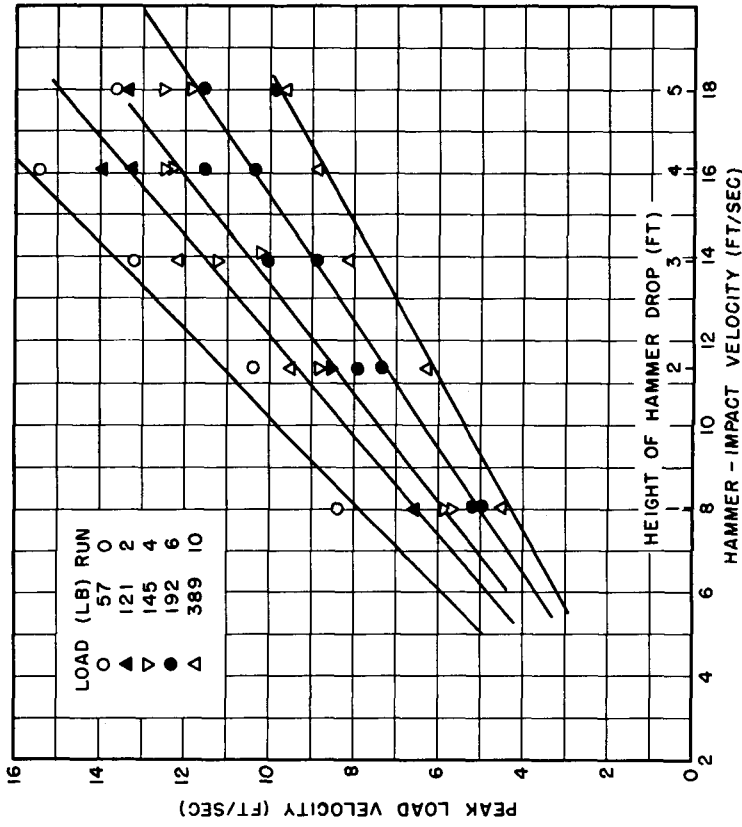


Fig. 36 -- Peak load velocity for edge blows on 4A plate, load axis horizontal

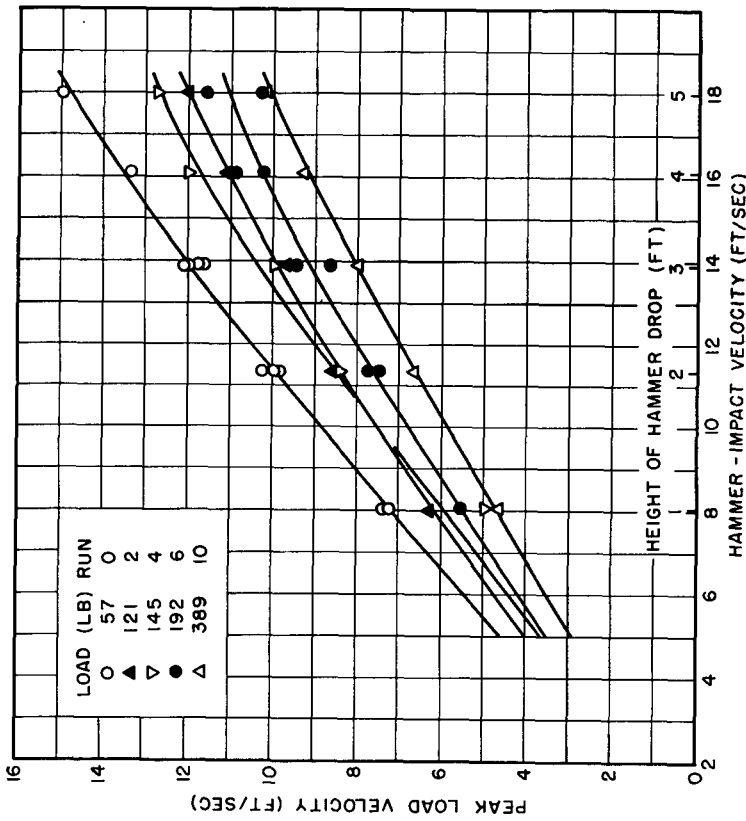


Fig. 35 -- Peak load velocity for back blows on 4A plate, load axis horizontal

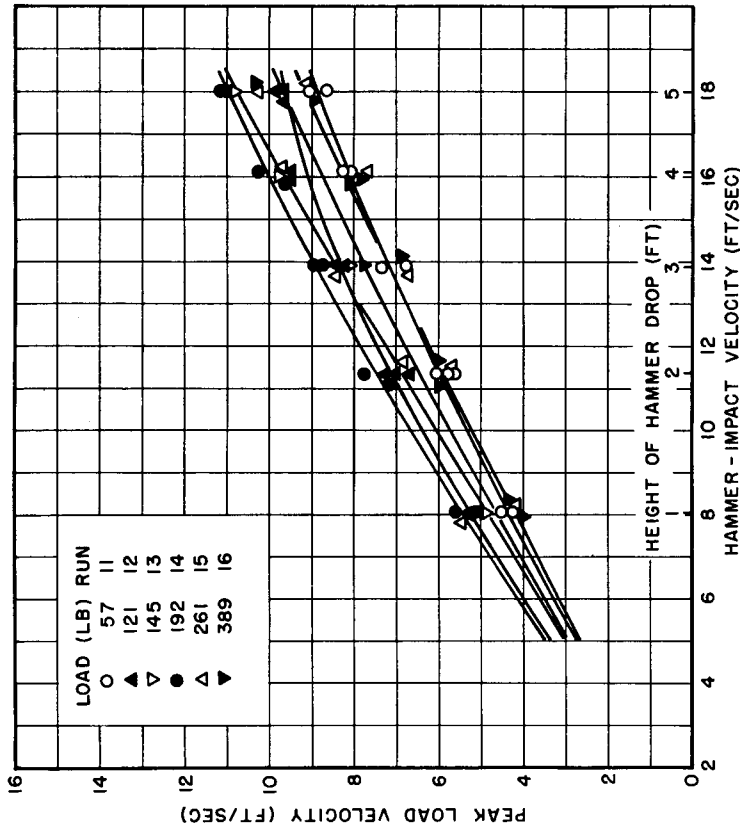


Fig. 38 — Peak load velocity for back blows on shelf plate

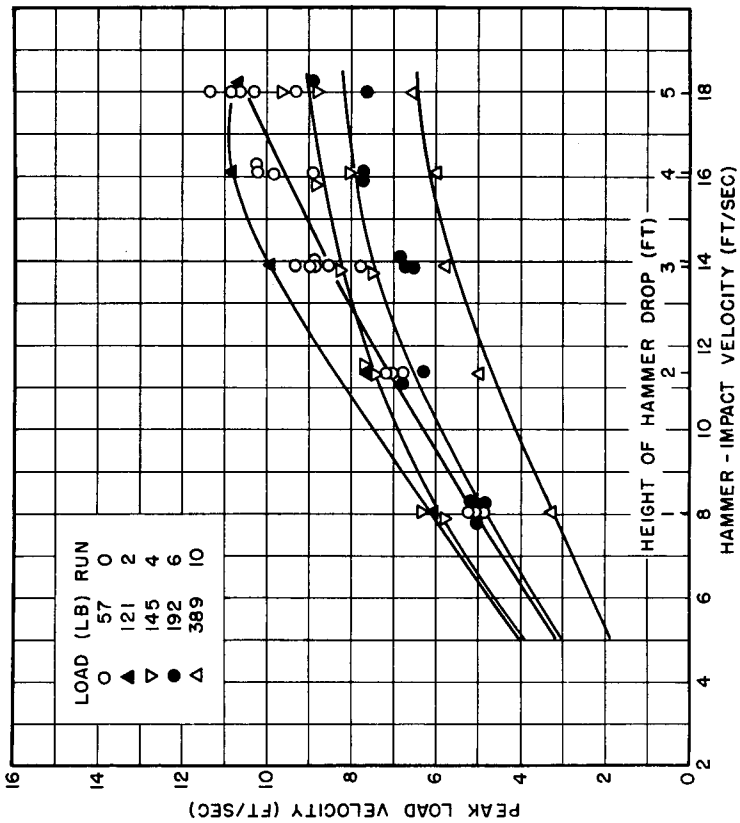


Fig. 37 — Peak load velocity for top blows on 4A plate, load axis horizontal

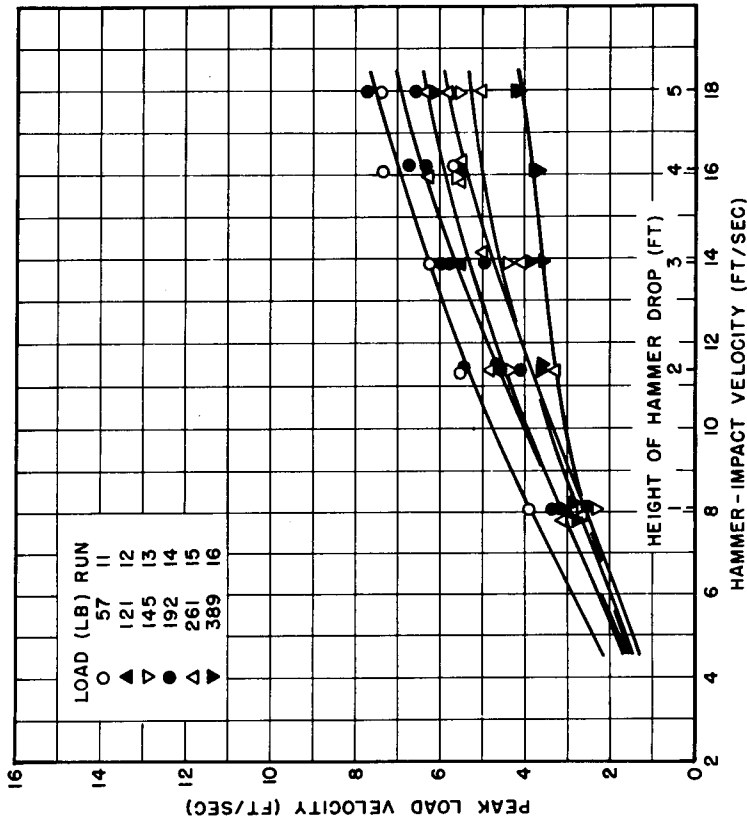


Fig. 40 — Peak load velocity for top blows on shelf plate

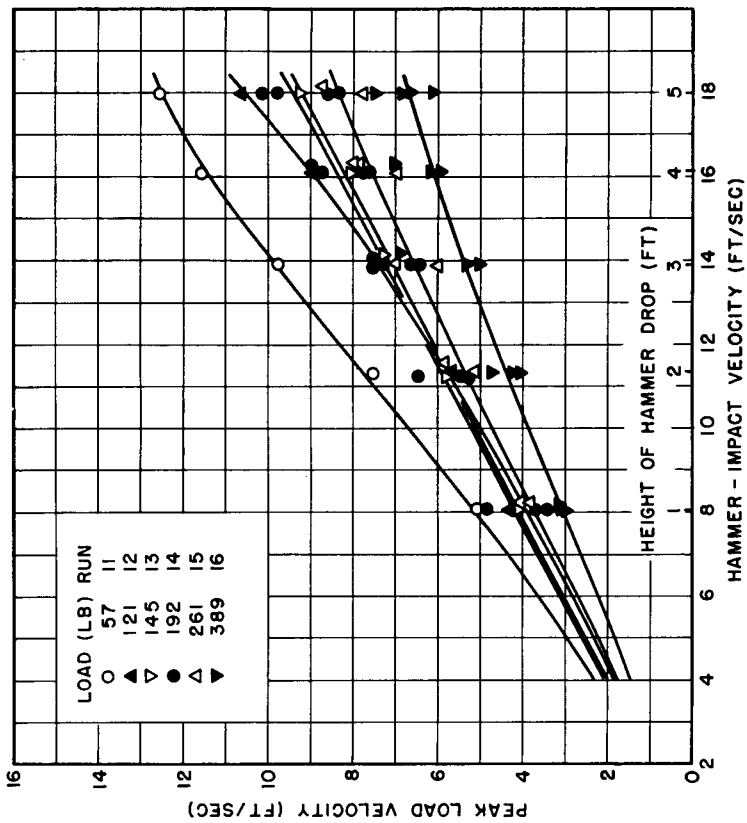


Fig. 39 — Peak load velocity for edge blows on shelf plate

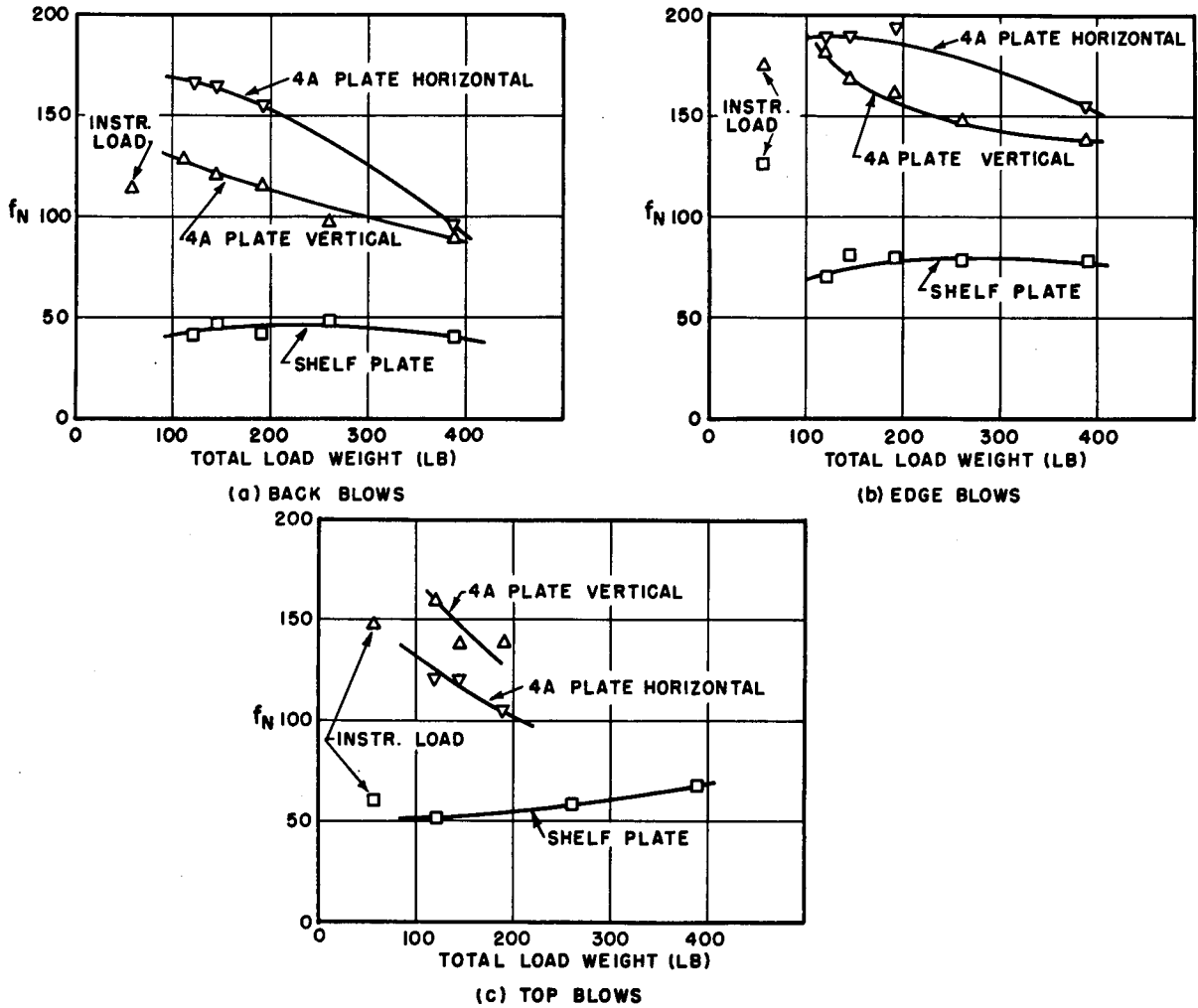


Fig. 41 — Predominant load frequencies

Load Displacement

Selected load velocity records were integrated graphically to provide curves of absolute load displacement vs time. For 5-ft blows, the time to peak displacement varies from about 20 ms (instrument load on 4A plate) to about 40 ms (389-lb load). Since the natural frequency of the velocity meter is 2.5 Hz, the error introduced in the graphical integration should be only a few percent.

When the 4A plate is lightly loaded, the displacements produced by blows in the three directions are very similar (Fig. 42a). The extra flexibility of the 4A plate with regard to back blows introduces an oscillatory component, but the center-of-mass displacement closely follows the curves obtained for top and edge blows. Adding a 389-lb load not only increases the time to peak displacement but also introduces considerable differences in the displacements for the different blow directions (Fig. 42b). Back blows

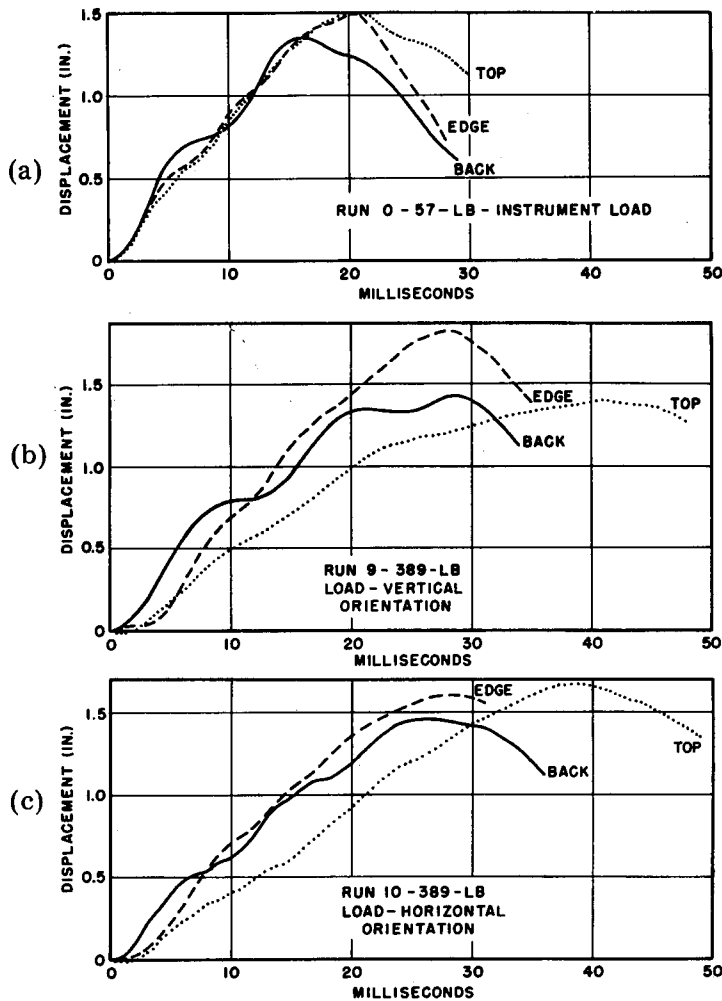


Fig. 42 — Displacement-time curves for 5-ft drops on the 4A plate

get underway faster but do not reach so great a displacement due to the phasing of the oscillatory component. Edge blows start more slowly but reach high peak displacements in comparable times, indicating lower but more consistent velocities. Load orientation seems relatively unimportant with regard to peak displacement or time to peak (Fig. 42c). Displacement curves for shelf-mounted loads are quite different. Large variations for the different blow directions are apparent even for light loads (Fig. 43a), and insignificant changes in time to peak displacement are occasioned by large increases in load (Fig. 43b). Peak displacements are found to exceed the 1.5-inch limit of the anvil table. This can be accounted for by flexibility of the machine framework responsible for stopping the anvil plate at the end of its travel and the phasing of the local vibrations of the load.

Reproducibility

The nature of the LWSM is such that its structure deforms plastically in use. Obviously there must be some attendant variation of output characteristics. To estimate the

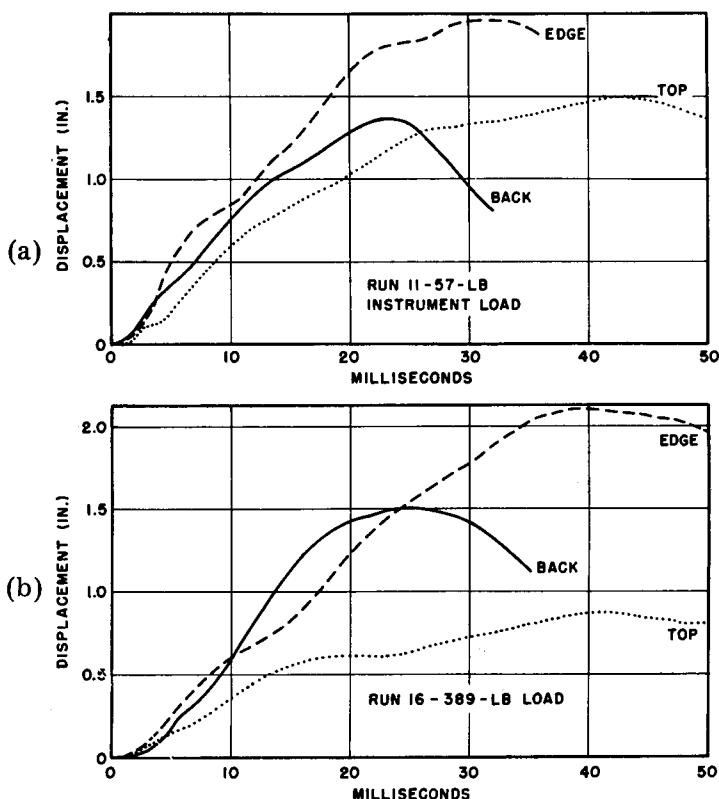


Fig. 43 — Displacement-time curves for 5-ft drops on the shelf plate

significance of these changes, a series of blows with instrumentation load on the 4A plate was made at the beginning of the calibration sequence, and a similar sequence at the end, after some 400 blows of all descriptions (Fig. 44). With only the instrumentation load, mounting plate and load accelerations are approximately the same, and during the initial sequence peak accelerations showed a small amount of scatter and an approximately linear relation to hammer impact velocity. This was also true of the later sequence, but the general level ran about 60% higher than for the initial. Peak velocities showed the same trend, although with less scatter (as would be expected for a lower-order function), and the later sequence ran about 25% higher than the initial level. This tends to indicate that the differences probably arise from changes in the stiffness of the anvil assembly arising from work hardening and impact pad deformation. The variation in damage potential is more likely to follow the trend of the peak velocity measurements than that of the accelerations because damage more generally results from the lower-frequency components of the shock motions.

Consistency (23,24)

To estimate the degree of similarity between the shock motions generated by different machines, four machines were calibrated using the same 4A plate, loads, and measuring instruments. The loads were 57 lb and 261 lb oriented vertically on the 4A plate with blows of 1-, 3-, and 5-ft hammer heights delivered in all three directions: the

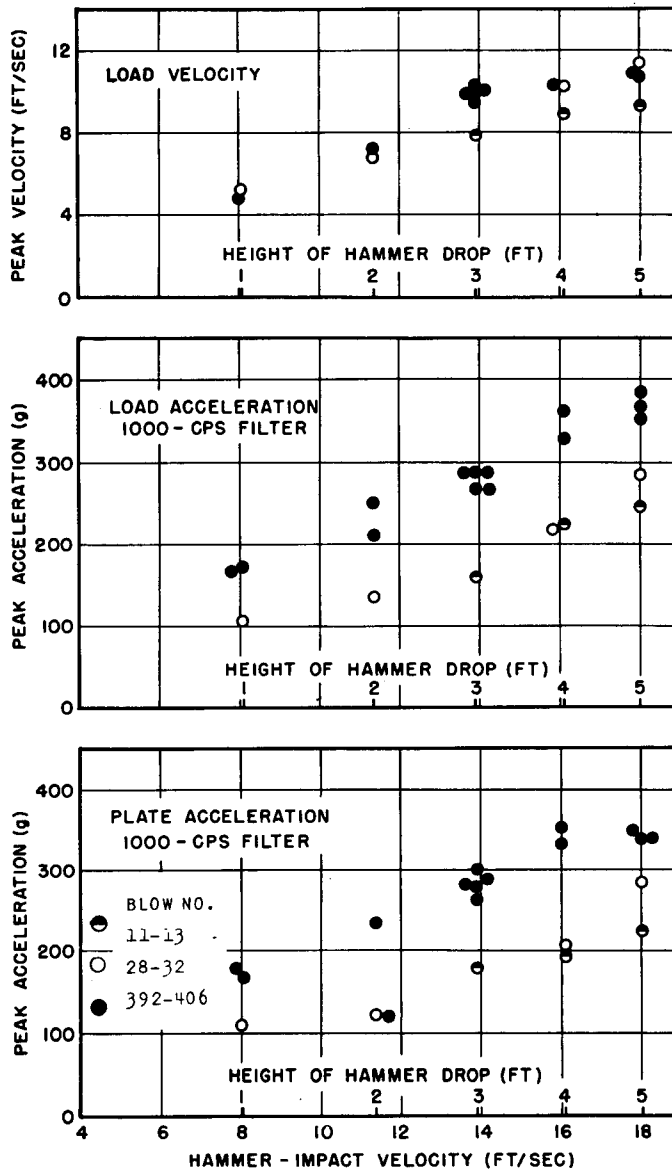


Fig. 44 — Peak load velocity, peak load acceleration, and 4A plate acceleration resulting from repeated top blows with a 57-lb load

measuring instruments were a velocity meter and a reed gage attached to the load. The motion parameters measured were peak load velocity (Fig. 45), time to peak load velocity (Table 1), and dominant load frequency (Table 1). The maximum spread of lowest peak velocities was 2.8 to 3.7 ft/sec for 1-ft top blows with a 261-lb load. For the highest velocities, the maximum spread was 14.1 to 17.9 ft/sec for 5-ft edge blows with a 57-lb load. The greatest variation of time to peak velocity for the slowest rise was 5.5 to 6.0 ms for 5-ft drops with a 57-lb load. The highest load frequency showed a spread of 142 to 167 Hz (3-ft blows with a 260-lb load) and the lowest 90 to 97 Hz

(1-ft blows with a 261-lb load), while the most extreme spread was 120 to 174 Hz for 3-ft blows with a 57-lb load. In all, the variations between machines are entirely comparable to those which might be expected between blows on any one of them.

Output Shock Spectra (18,21)

Before the calibration series was undertaken, it was known that the LWSM tends to have dominant frequencies at about 100 Hz (from 4A plate flexibility) and at about 350 Hz (from the anvil-plate structure). These frequencies would be expected to be important in the shock spectra; therefore, the reed gage used was provided with reeds having natural frequencies in these regions. Among the less fortunate characteristics of the reed gage are: (a) reeds below about 40 Hz cannot be used effectively because of the clearance requirements, (b) reeds above about 450 Hz are of little value because of errors in reading the very small deflections, and (c) the number of reeds which can be used is limited. The resulting shock spectrum is a sampling of a few points and may well miss the most important features of the actual continuous shock spectrum. For this reason the shock spectrum derived from reed gage recording is generally drawn as a polygon of straight-line segments joining the measured points rather than a smooth curve. This tradition helps to remind the beholder that the actual values of the shock spectrum between points may be vastly different from the lines which join them.

Preliminary trial showed that for the calibration study only five reeds could be used effectively. They were selected to have natural frequencies of 40, 100, 198, 345, and 430 Hz.

Description

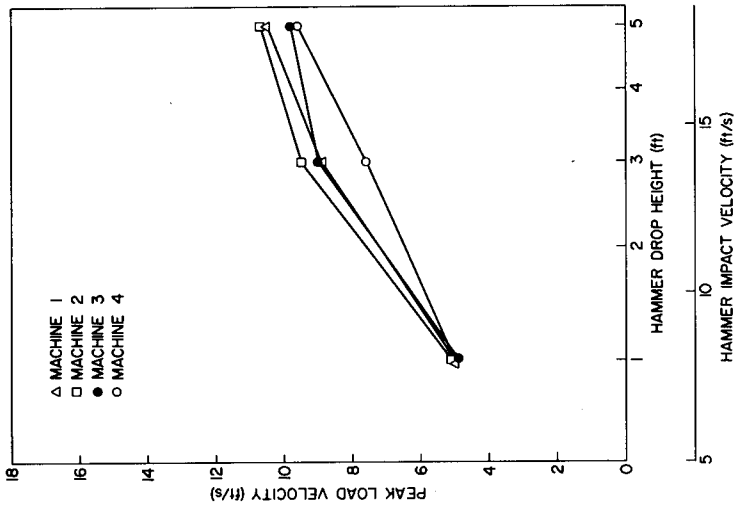
The shock spectrum's shape is determined by structural parameters of the test package-shock machine system. Accordingly, the effect of increasing the energy input to the system should be to raise the overall level of the shock spectrum unless the energy input becomes so great that nonlinear interactions become considerable. For this reason the following discussion will be primarily concerned with the effects on the shock spectra for 5-ft drop heights of variations in the loading arrangement.

Effects of Hammer Drop Height

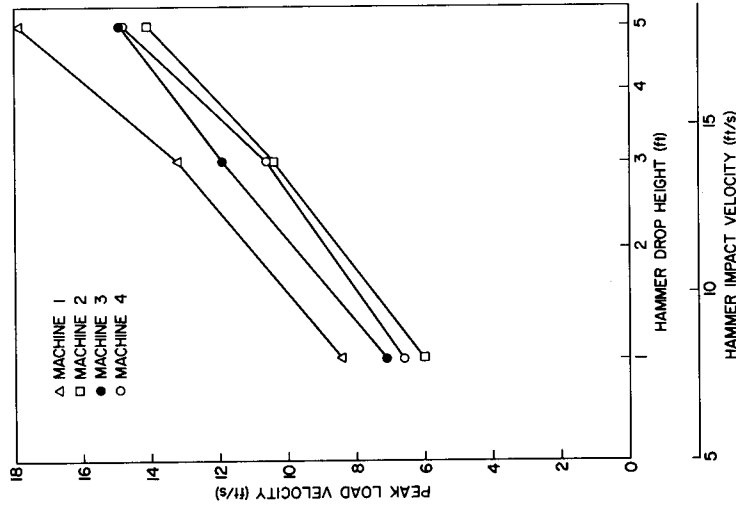
The overall level of the shock spectrum rises with drop height, as expected, but does not remain proportional to hammer impact velocity. This was also remarked with regard to load velocity. For drop heights beyond 3 ft, the increase in spectral level is considerably less than that for heights below. The shock spectra for 3-ft blows are in fact comparable with those for 5-ft blows (Fig. 46).

Effects of Blow Direction and Mounting Plate

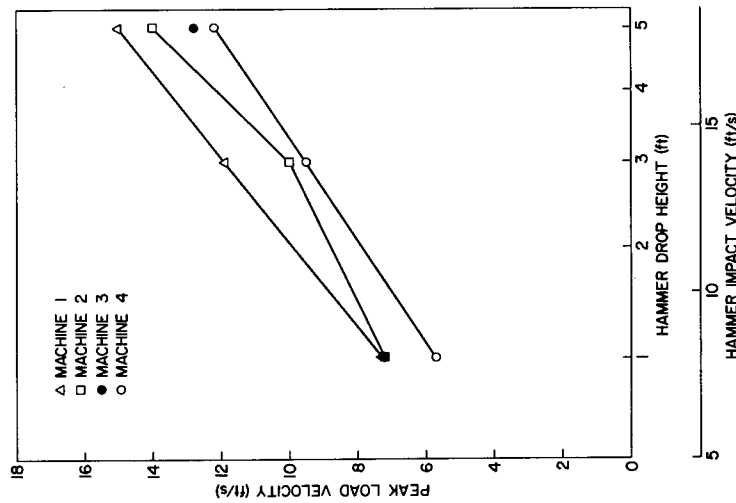
For the 57-lb instrument load on the 4A plate, back blows provide a shock spectrum with peaks at 100 and 345 Hz from the 4A plate and anvil plate vibrations. These peaks are absent from the spectra for top and edge blows, which are reasonably well described in straight lines. This is in keeping with the steplike waveform of the load velocities (Fig. 47). For the 57-lb load on the shelf plate, the back blow retains the 345-Hz peak, but the 100-Hz peak characteristic of the 4A plate vanishes, naturally



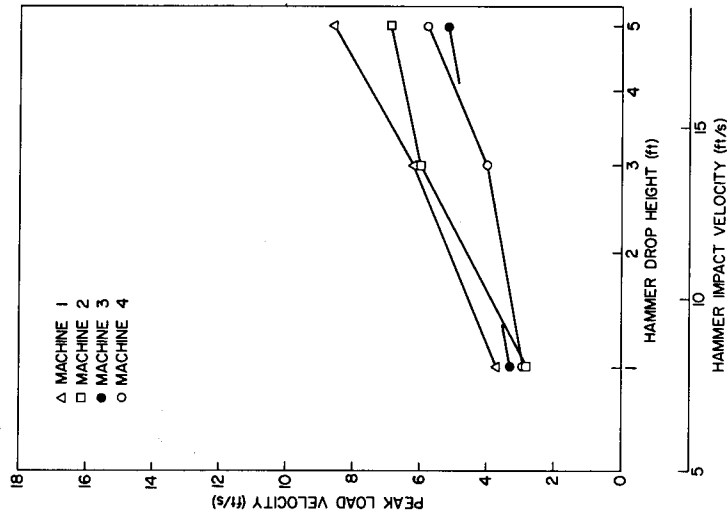
(a) Back blows for a 57-lb load



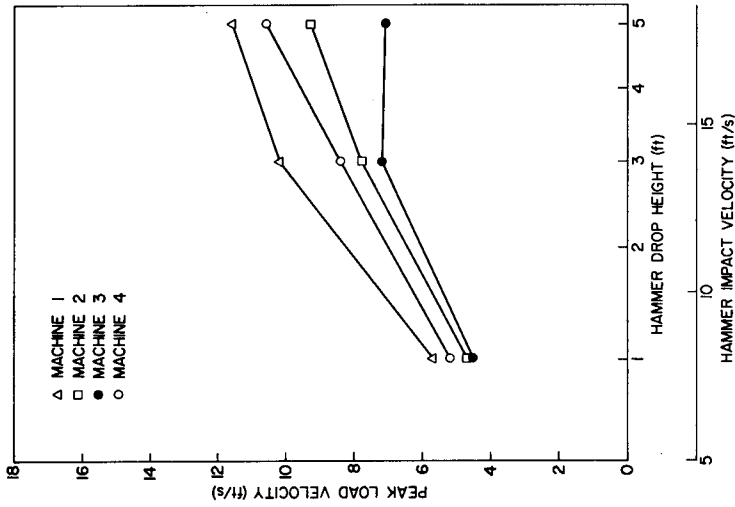
(b) Edge blows for a 57-lb load



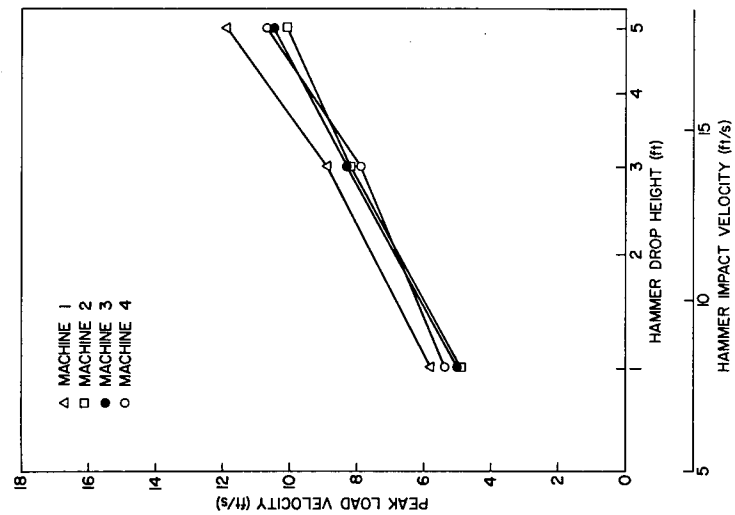
(c) Top blows for a 57-lb load



(d) Back blows for a 261-lb load



(e) Edge blows for a 261-lb load



(f) Top blows for a 261-lb load

Fig. 45 — Peak load velocities for 57-lb and 261-lb loads on the 4A plate, load axis vertical, on four different LWSM's

Table 1
4A Plate Frequencies and Time to Peak
Load Velocities for Four LWSM's

Blow Direction	Frequency (Hz) for Average 4A Plate				Time to Peak Velocity (ms)			
	Machine 1	Machine 2	Machine 3	Machine 4	Machine 1	Machine 2	Machine 3	Machine 4
<u>57-lb load</u>								
Back	112	99	100	114	4.1	4.5	3.6	—
Edge	125	136	120	174	4.2	4.0	4.2	—
Top	118	124	110	148	3.9	4.7	3.5	—
<u>261-lb load</u>								
Back	92	95	90	97	3.8	3.9	3.9	—
Edge	—	—	—	—	3.9	3.7	4.1	—
Top	167	142	150	147	6.0	6.0	5.5	—

enough. Edge and top blows produce shock spectra similar to those found on the 4A plate but much lower (Fig. 49a). The level for the edge blow is only half that found on the 4A plate and that for the top blow is even lower. With the other test loads, the back and edge blows produce consistently higher spectra than does the top blow, and the 4A plate spectra are consistently higher than those from the shelf plate (Figs. 48 through 50).

Effects of Load Weight

As would be expected, the major effect of increasing load weight is to lower the level of the shock spectrum in general and to shift the peaks to lower frequencies (Figs. 47 through 50). The change in level is substantial, the level with the 389-lb load being only about half that with the 121-lb load, and is greater on the 4A plate than on the shelf plate. The effect becomes less important as the load approaches the capacity of the machine, inasmuch as the shock spectra for the 389-lb load are not much lower than those for the 261-lb load (Fig. 51).

Effects of Mounting Dimension

The 4A plate is bolted to the anvil plate with reinforced 4-inch channels as separators; the bolts fastening this assembly are 24 inches apart. The edges of the channels are flush with the edges of the 4A plate, giving a free span between channels of 22 inches. It is evident that if an equipment has a mounting dimension of 22 inches or more the flexibility of the 4A plate will be bypassed, and the equipment will be in effect mounted directly on the anvil plate. The mounting points of the calibration load arrangement lay 2 inches or 4-1/2 inches from the edges of the spacer channels, depending on the load orientation. For back blows, the effect of orientation is drastic, greatly exceeding that of load weight (Figs. 48 through 50). The shock spectrum for a 389-lb load mounted horizontally is mostly higher in level than of a 121-lb load mounted vertically. Top and edge blows show little or no such effect, although it would presumably appear if the test load was of such a geometry that rocking modes allowed 4A plate flexibility to come into play for these directions of blow.

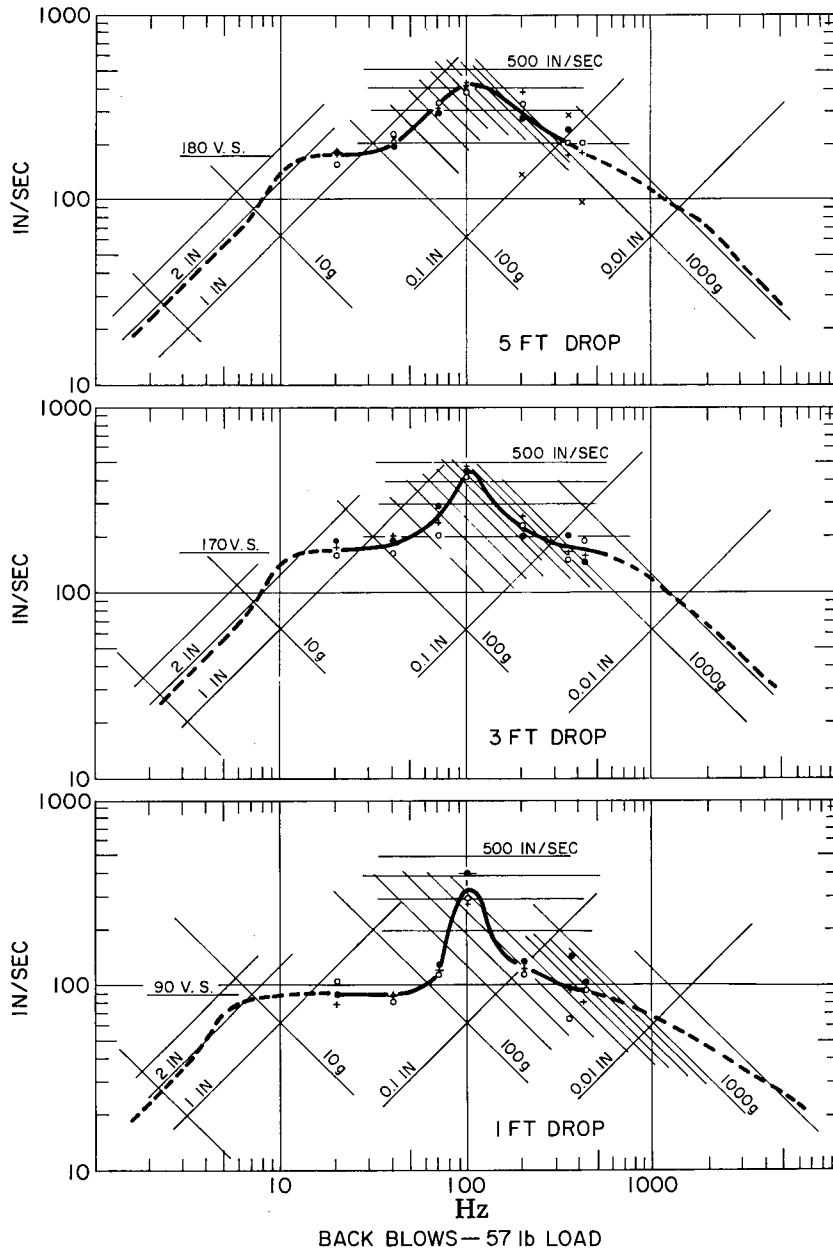


Fig. 46 — Shock spectra for 1-ft, 3-ft, and 5-ft back blows with a 57-lb load on the 4A plate for four different LWSM's

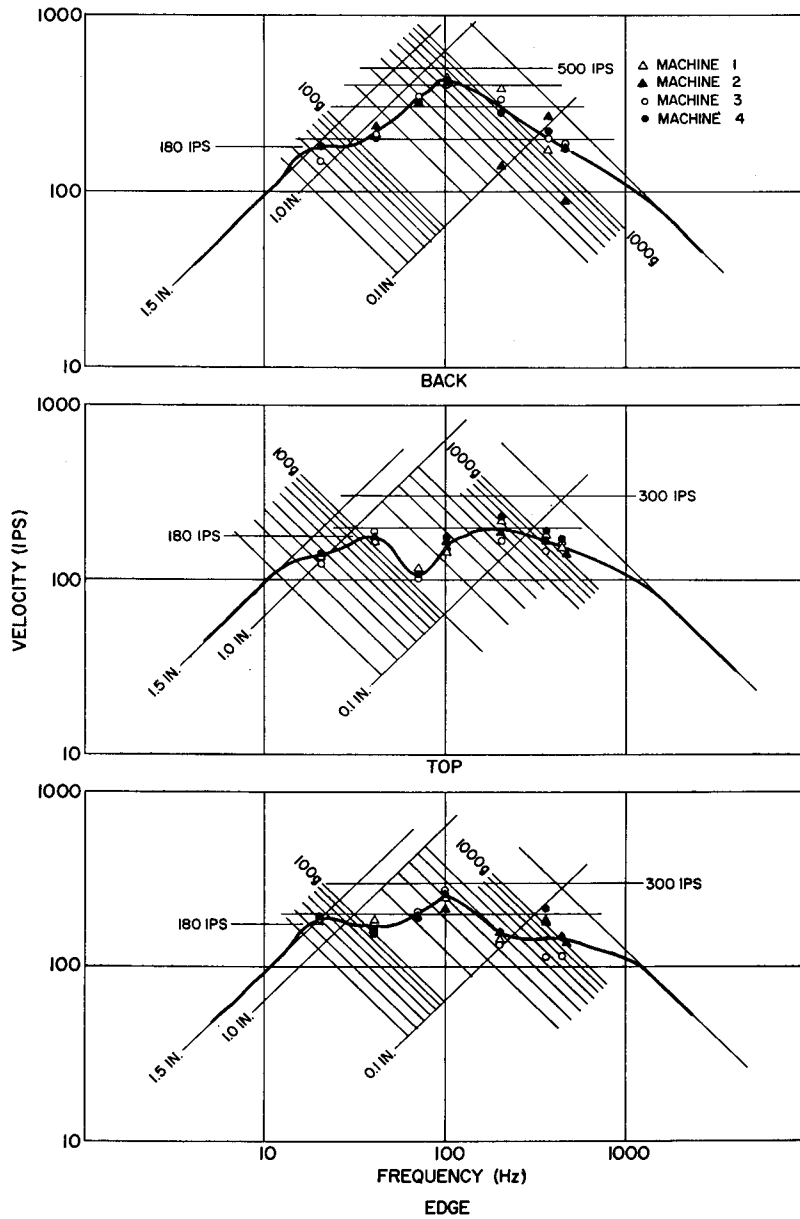


Fig. 47 — Shock spectra for 5-ft blows with a 57-lb load on the 4A plate for four different LWSM's

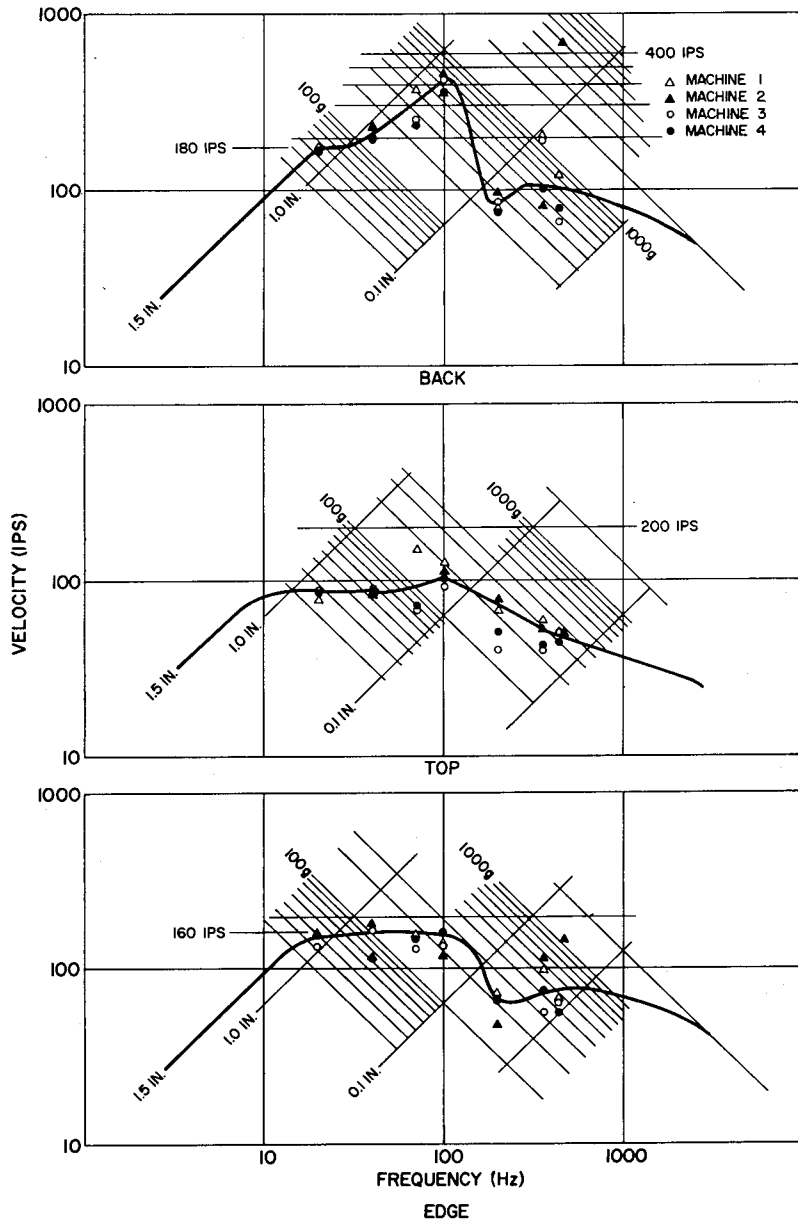


Fig. 48 — Shock spectra for 5-ft blows with a 261-lb load on the 4A plate, load axis vertical, for four different LWSM's

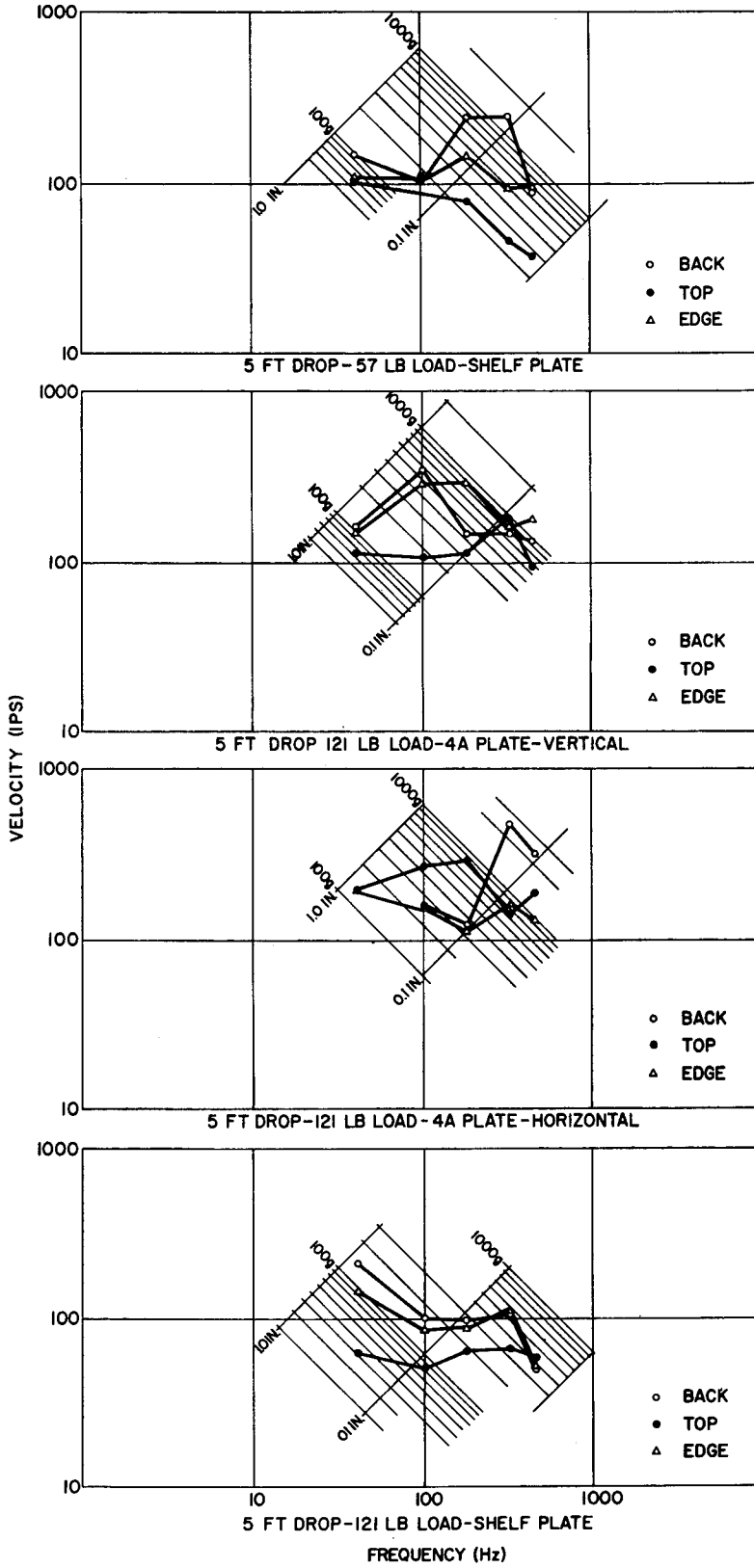


Fig. 49 — Shock spectra for 5-ft blows with 57-lb and 121-lb loads

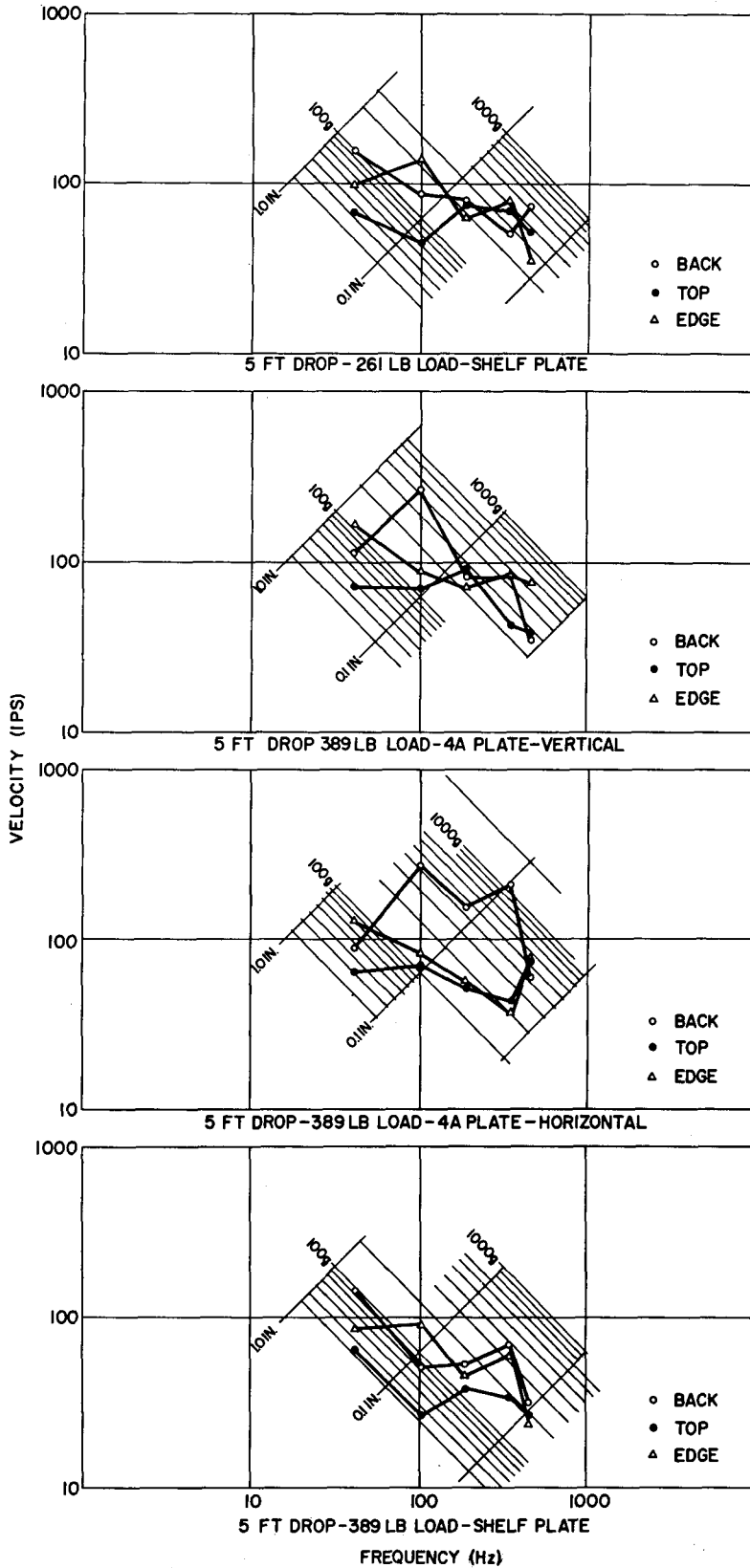


Fig. 50 — Shock spectra for 5-ft blows with 261-lb and 389-lb loads

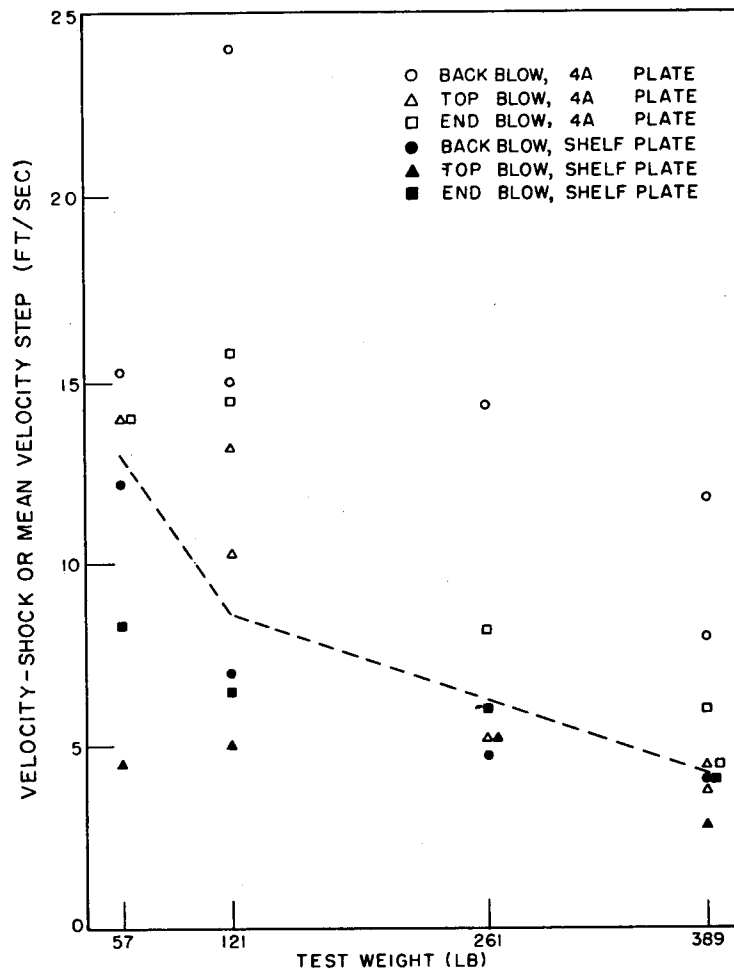


Fig. 51 — Values of velocity-shock for 5-ft blows as a function of load weight

Reproducibility

The reproducibility of shock spectra for repeat blows is generally good, particularly if the blows are given in succession. If other blows intervene, and particularly if the machine test arrangement is changed between blows, the agreement is less dependable, although still good. Deviations are mostly at the high-frequency end, which is most strongly affected by changes in the uncontrolled variables of the test arrangement (Fig. 52).

Consistency (23,24)

The variation in shock spectra between machines has much the same pattern as that between blows on one machine — deviations are mostly at high frequencies and are greatest with “stiff” test arrangements (light load and top or edge blows). The amount of variation is also comparable with that found for repeat blows on the same machine. All in all, the consistency of shock motions produced by the LWSM is much better than expected (Figs. 46 through 48).

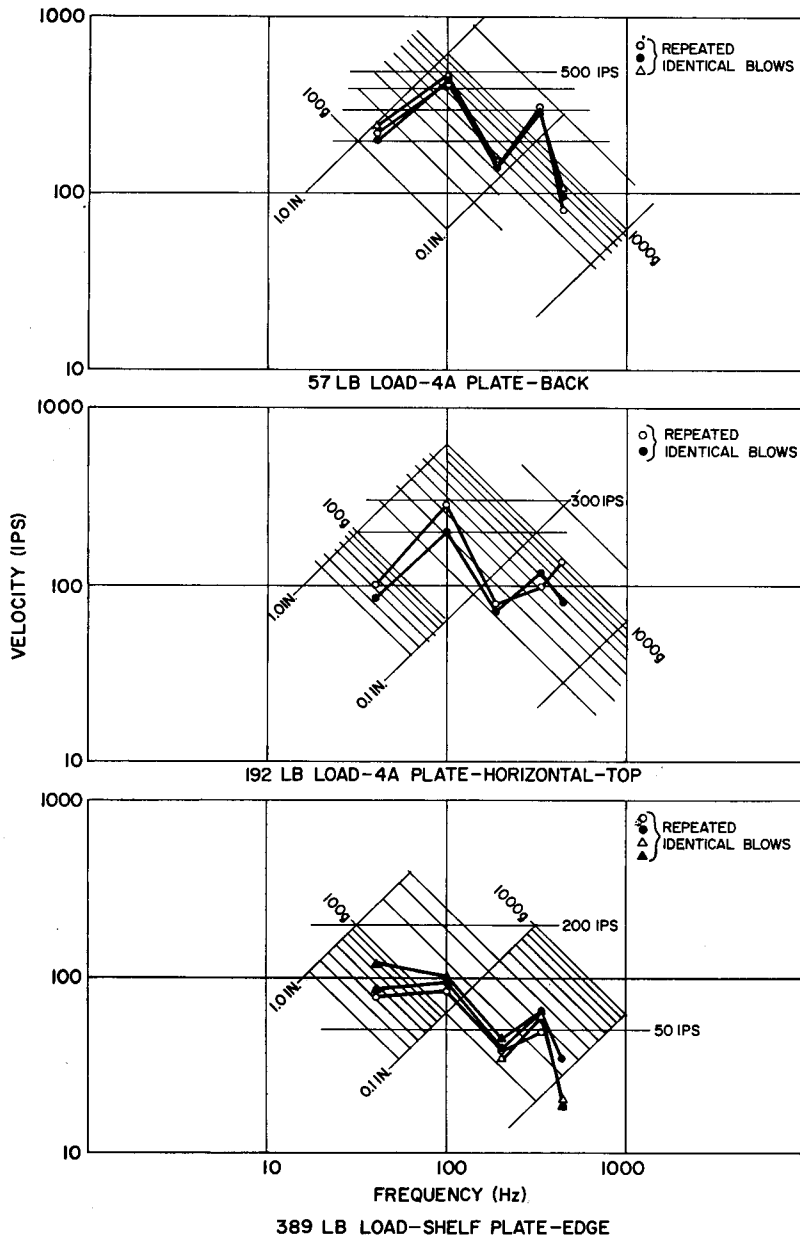


Fig. 52 — Shock spectra for repeated 5-ft blows

Nonstandard Operation (25)

The shock motion produced at the deck by an underwater explosion is much different from that at the hull or at bulkheads. It is characterized by large deflections, low frequency, and low acceleration. Extensive modifications were made (by NSRDC) to an LWSM in an attempt to generate such motions. The modifications consisted of resting the anvil-plate/load assembly on a guiding track and introducing a liquid spring between hammer and impact pad. The spring provides a 60-g, 12-ms half-sine pulse, and the anvil-plate/test-equipment assembly is braked at a rate of -4 g by shock absorbers; an overall travel of 12 inches is provided. A folding linkage permits 1 inch of free travel before the shock absorbers act, in order to prevent interference with the 12-ms input pulse. This makes operation of the machine critically dependent on the velocity change imparted by the pulse, so this is held at about 15 ft/sec by maintaining the total test load on the machine at 400 lb by adding dead weights as required.

This arrangement has not been used much. It was reasonably successful in simulating deck motion and has the feature of demonstrating the consequences of improper use of resilient mounts in dramatic fashion. The suggestion has been made, unfortunately, that this arrangement should replace the specified shock test for some equipments, which would represent a retreat from the Navy policy of universality. The end result would be to require a different test, and presumably a different shock machine, for each item of equipment on each class of ship and for each possible shipboard location. The more different the shock motions are, the more important it is not to provide a special machine or test to simulate them.

THE NAVY HIGH-IMPACT SHOCK MACHINE FOR MEDIUMWEIGHT EQUIPMENT

History

The LWSM brought about rapid and substantial improvements in the shock resistance of equipments in its weight range. While design guidelines and rules of thumb could be and were derived from this experience and applied to heavier equipments, it was appreciated that there is no substitute for an actual shock test. It was the feeling at that time that 400 lb was really too great a load for the LWSM, and that 250 lb would be a more reasonable limit.* Most shipboard equipments, particularly the relatively fragile electronic systems, weigh less than 4500 lb, or can be disassembled into free-standing subsystems in this range. It was decided that a shock machine should be built to be capable of testing equipments in the weight range of 250 to 4500 lb and that this machine should be an extension of the LWSM in the sense that a test item should experience equivalent shock environments on the two machines. Under a BuShips contract, Westinghouse Electric Corporation designed and constructed (in 1942) the first Navy High-Impact Shock Machine for Mediumweight Equipment (MWSM), which was installed at the Naval Engineering Experiment Station (now NSRDL) Annapolis, Maryland, in 1943.

*In actuality the shock environment produced by the LWSM with a 400-lb load is not much less severe than that with a 250-lb load. However, when the load is an actual equipment rather than a dead weight, the modal masses will probably be higher for the heavier items and item-machine interactions more noticeable. This could cause concern, particularly since the "shock spectrum dip" phenomenon was not appreciated at that time. In addition, heavy shipboard equipments tend to be bulky, leading to inconvenient or unsatisfactory test installations on the LWSM.

The basic design of the MWSM consists of an anvil table struck from below by a swinging hammer. The requirement for shock intensity equivalent to that of the LWSM was to be met for a 250-lb load, and the criterion was taken to be anvil-plate starting velocity. Studies on the LWSM at that time indicated that the starting velocity of the anvil plate with a load of 250 lb was about 7 ft/s for 5-ft back or edge blows. It was considered that shock intensity on shipboard would decrease as equipment weight increased, so 6 ft/s was arbitrarily selected as the proper velocity for a 4500-lb load. These two points were connected by a straight line, and this graph of anvil-table starting velocity vs equipment weight served not only to set MWSM design parameters but also, after it had been built, to determine the schedule of hammer drop heights comprising the shock test for various weights of equipment.*

The medium-weight shock test specification is thus based entirely on anvil-table velocity, although no equipment is mounted directly to the anvil table for a normal specification test. The mounting flexibility provided in the LWSM by the 4A or shelf plate is provided in the MWSM by an arrangement of channels and support rails. The evolution and intent of this mounting system have been since lost and remain today a subject of speculation.

Changes in the MWSM itself have not been great. Most changes have been made for convenience, such as the quick-release mechanism and solenoid operation for dropping the hammer, automatic brake application on the backswing to prevent a second impact, and the installation of pneumatic jacks for positioning the anvil table. Structural changes have been almost entirely to add reinforcing to the anvil-table structure. The operating changes have been much more important and permit (for some items) the use of non-standard mountings to provide a specified fixed-base fundamental frequency, the use of the 30° corner bulkhead for specification testing, and extending the rated load of the machine to items weighing 6000 lb. Both of the latter changes are questionable.

Description (18,26)

The MWSM consists of a 3000-lb hammer which swings through an arc of up to 270°. At the end of the swing it strikes a 4500-lb anvil table from below, imparting an upward velocity to it. The anvil table is restrained by 12 2-inch-diameter bolts passing through both it and the shock machine's foundation which permit a free motion of 3 inches. When this limit is reached, the bolts sharply stop the motion of the anvil table ("anvil-table reversal") and it drops back onto the foundation. Since the reversal impact is somewhat elastic, the anvil table drops considerably faster than it would under the action of gravity alone. The machine is embedded in a massive concrete block resting on coil springs which bear on a heavy concrete shell isolated from the rest of the building by a layer of some absorbent material (Fig. 53).

The anvil table has a mounting surface of 60 × 60 inches provided with threaded holes for attaching the various mounting arrangements. Beneath the mounting surface 12 heavy reinforcing webs run from the edge of the table to the impact column. Four of these webs rest on pneumatic jacks which can raise the anvil table 1.5 inches above

*The hammer drop heights specified for the standard shock test were evidently derived on the assumption that the test load would be attached directly to the anvil table, which is rarely done.

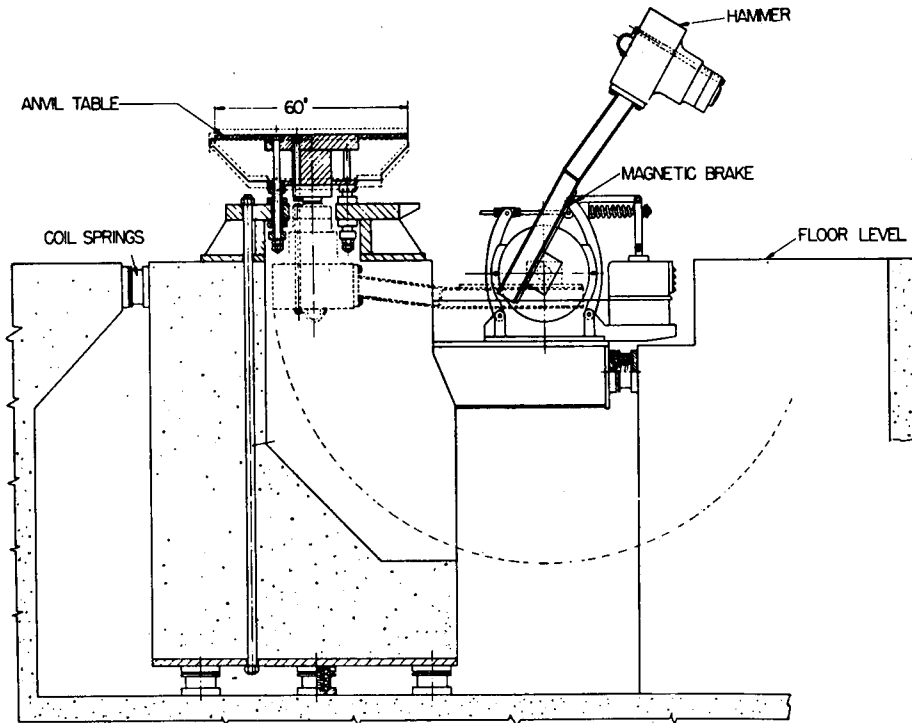


Fig. 53 — The Navy High-Impact Shock Machine for Mediumweight Equipment (MWSM). The position of the hammer at the instant of impact is shown by the dotted lines.

its normal rest position. When adjusted for 1.5-inch travel, the anvil-table has a slightly higher velocity when the top stops are reached than in the 3-inch travel configuration; since it drops back onto the jacks rather than the foundation, its final collision is softer.

The impacting surfaces of both hammer and anvil table are fitted with spherical, hardened-steel impact plates. Unlike the LWSM, this impact is highly elastic and most energy loss takes place in the structure of the anvil table itself by gradual cracking of welds. This makes the MWSM inherently a simpler, more predictable, and more consistent machine than the LWSM. It has been the mainstay of the Navy's shock testing program for many years.

The MWSM is not an ideal machine, however. When the travel is changed, the point of impact also is changed. This imparts a rotary component to the motion of the anvil table. Relatively tall equipments have a tendency to tilt in one direction or another anyway, causing the anvil table to bind on its through bolts and also causing uneven contact at the limit stops, which imparts a rotary motion component at the anvil table reversal. This predilection is accentuated by the off-center impact of the hammer. The machine is normally adjusted so that the impact area is central for 1.5-inch travel; it is accordingly on the side of the impacting surfaces toward the hammer axis for 3-inch travel blows.

Mounting Arrangements

The desired flexibility is introduced by mounting the test equipment on support channels. These are pairs of 4-inch standard or carbuilding channels bolted back to back with a space between; T-shaped blocks with threaded holes fit into this space and the bolts securing the test equipment attach to them. The support channels are separated from the anvil table by spacer rails at each end, to which the channels are clamped (Fig. 54). The spacer rails may be fabricated from sections of 7-inch shipbuilding channel or, since these may deform with the heavy loads now permitted, the rails may be built up from sheet stock. The spacer rails are bolted directly to the mounting surface of the anvil table.

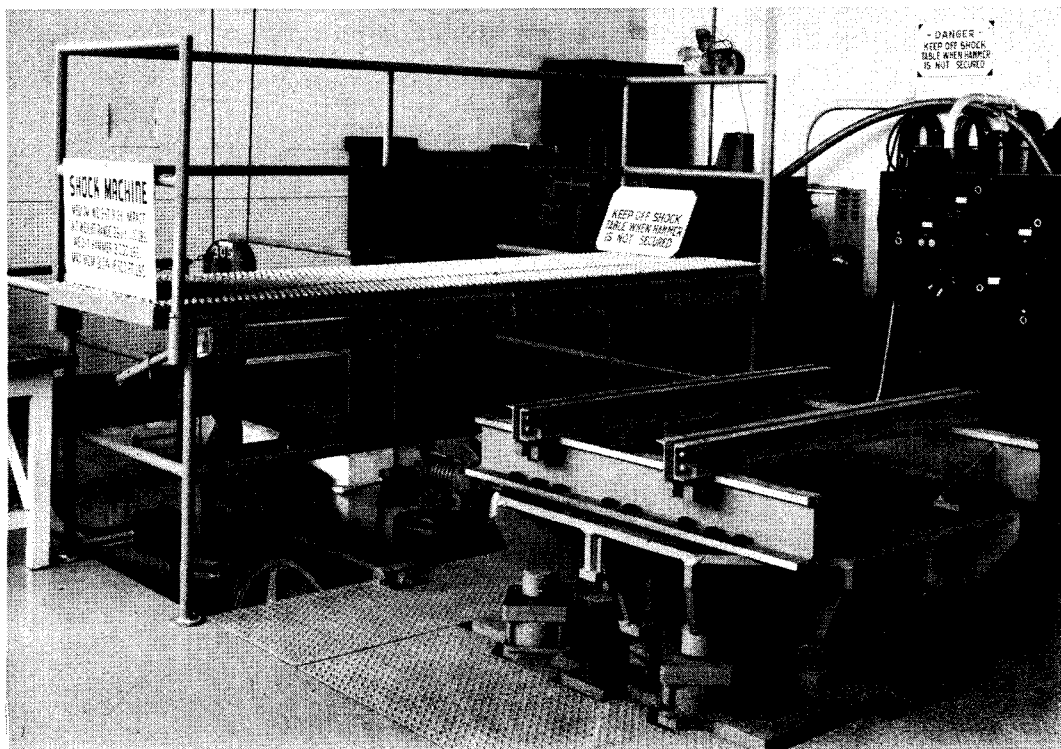


Fig. 54 — View of the MWSM anvil table showing the mounting channels and support rails

The number and type of support channels to be used for a particular test item are specified by a table contained in MIL-S-901. Entries are made in this list by test equipment weight and distance between mounting holes. Fewer channels are called for as the mounting hole separation increases, or the free span of the supporting channels decreases. This tends to keep the natural frequency of the test-equipment/channel/anvil table system more or less constant; it has been found to vary from about 55 Hz to about 72 Hz, with most cases being around 65 Hz. However, this does not seem to be the criterion on which the table was originally set up. The reason remains yet another mystery in the provenance of the MWSM, but apparently the aim was to keep the calculated maximum stress in the channels below 35,000 psi in a static acceleration field of 50 g.

Additional permissible mounting arrangements were introduced in MIL-S-901C (27). There is no provision in the MWSM to change the direction of the blow, and it is usually impracticable to change the orientation of the test equipment. It is now permissible to use a pair of slanted spacer rails which tilt the support channels and test equipment at an angle of 30° , allowing the shock input to be directed along two equipment axes. Although no acknowledgment of the fact is made in the specifications, this tilt places a sidewise loading on the support channels which they are unprepared to handle, and in some circumstances it may well be advisable to use additional sets. Yet another mounting arrangement which may be used is a 30° corner bulkhead (Fig. 55), which directs motion along all three axes and which is convenient for equipments which require bulkhead support. This consists of a fairly stiff framework arranged on a stiffer floor, all being constructed of 4-inch heavy I-beam and channels and clamped to a set of spacer rails roughly similar to those used with the support channels. Its motion waveform is much like that of the anvil table embellished with liberal quantities of high and middle frequencies.

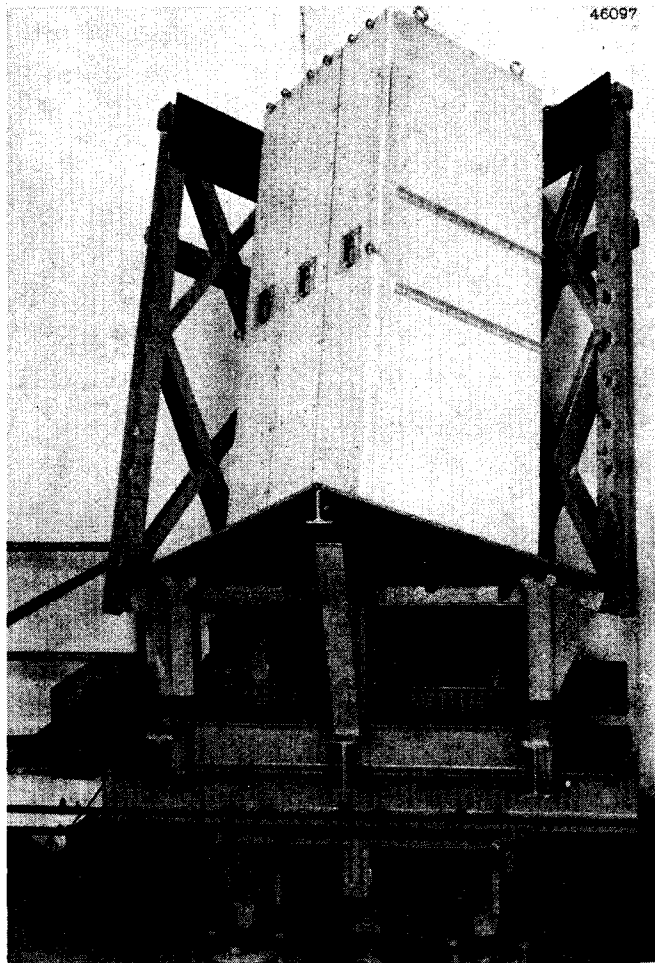


Fig. 55 — An item of shipboard equipment mounted on the MWSM with the 30° corner bulkhead

Operating Procedure

The operating variables of the MWSM are the energy input to the equipment/channel/anvil system and the free travel of the anvil table. The energy input is specified in terms of vertical height of hammer drop and is usually read off an indicator of the rotation of the hammer axis from the position 180° away from its impact position. No allowance is to be made for the 1.5-inch difference resulting from the anvil table travel setting. The specification lists required hammer heights against the total weight on the anvil table, including all mounting arrangement and fixtures as well as the test equipment itself. The shock test consists of six blows encompassing two drop heights and two anvil table travels. As specified, two blows of the lower height are delivered with 3-inch travel (Group I blows), then two blows of the greater height (Group II blows), also with 3-inch travel, and finally two blows of the greater height with 1.5-inch travel (Group III blows). Each group of blows is required to include one in an inclined mounting. As with the LWSM, mounting nuts and bolts are to be tightened after each blow.

Mathematical Models

In contrast to the LWSM, the simple nature of the MWSM has made it highly desirable to theoreticians. The characteristic variables are reasonably well defined; it is an essentially elastic machine, and its largely uniaxial motions combine with controllable amounts of complexity to render it attractive to mathematicians. They have been quite pleased with the MWSM since its inception.

The MWSM with a dead-weight load may be regarded as a mass-spring-mass system. Next the limit on anvil table travel can be included, and also some damping, perhaps (Fig. 56). The details of the spring characteristic can stand considerable elaboration. The support channels rest on top of the spacer rails with their ends projecting slightly beyond, and the hold-down clamps are attached to this projecting part. This means that the effective free span of the channels is some 4 inches or more greater for motions of the load away from the anvil table than for motions toward it.* If the load, although a dead weight, has some compliance and permits some curvature in the part of the channels between the load mounting points, a new genus of intricacies is evolved and the load is still only a dead weight. When the test load is considered a structure, so that its reactions on the machine must be considered with more elaboration, it is evident that models of the MWSM may be complicated to any desired degree and sometimes are.

Although there is a limit to the amount of detail which can be justified in such a model, it is possible to derive considerable insight into the action of the MWSM from even a simple one. For most engineering purposes an adequate model is one which describes the MWSM as a mass (anvil table) and a spring (supporting channels) attached to the test

*Theoretically, this effect could be considerable and cause differences of 60% or more in the apparent load frequencies for upward and downward motions. In practice, some such difference can be seen, but it is small. One possible reason is that the spacer rails have some lateral compliance, which will be exercised by downward motions of the load, where the channel end forces are great, but not much by upward motions, where the end forces are accommodated by rotation of the end clamps about the spacer rail flange on which they bear. This additional compliance for motions in the stiff channel direction will help even things out. Another possible contribution is compliance in the test item, which would tend to make the channel end conditions less effective.

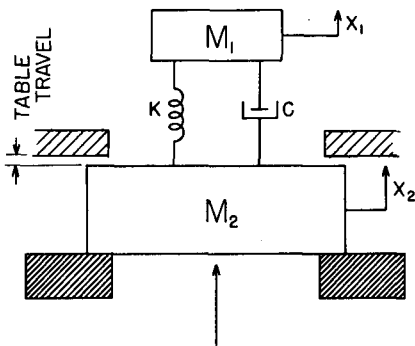


Fig. 56 — A simple model of a test load mounted on the MWSM. For many purposes an even simpler model ignoring damping and travel limitation can yield useful results.

equipment (with appropriate distribution of the channel mass), the input energy being supplied as an initial velocity of some value to the mass representing the anvil table.

Calibration of Shock Outputs (28)

Calibration of the MWSM is a more straightforward procedure than with the LWSM since there are fewer machine variables. The controlled variables are load weight and orientation, hammer drop height, and anvil-table travel. Since the MWSM is essentially elastic and the load mounting arrangement is not changed throughout the test, the uncontrolled variables are less effective. The test loads are of larger dimensions, but the MWSM is unencumbered by surrounding structure (unlike the LWSM) and it is not inconvenient to operate with large test packages.

Test Arrangement

The test load was of the dead-weight type and consisted of a number of weights which could be bolted to either of two base pieces. A welded steel frame with mounting point dimensions of 16 × 24 inches was used for loads below 2000 lb (Fig. 57) and an 1870-lb steel casting with mounting point dimensions of 24 × 32 inches for loads above 2000 lb (Fig. 58). Both base pieces were separated from the supporting channels by cylindrical spacers at each corner, through which the mounting bolts passed. Load weights of 1115, 2051, 3386, and 4423 lb were tested, each with its long axis directed both across and along the support channels. Channel arrangements for each load weight and orientation were those required by the shock test specification. The all-up weight on the anvil table ranged from 1783 to 5616 lb.

Hammer drop heights were also taken from the tables of the test specification, which at that time prescribed different heights for Class A and Class B equipments of the same weight and mounting dimension.* In addition to these blows, blows from drop heights of 50% of those specified for Class B and 150% of those specified for Class A were delivered (when feasible). Anvil-table travels were as specified by MIL-S-901.

*The earlier Navy shock test specifications grouped shipboard equipments in Class A and Class B, much like the present Grade A and Grade B. Rather than specifying different functional responses to the same test, as at present, the practice then was to require the same functional response to different tests.

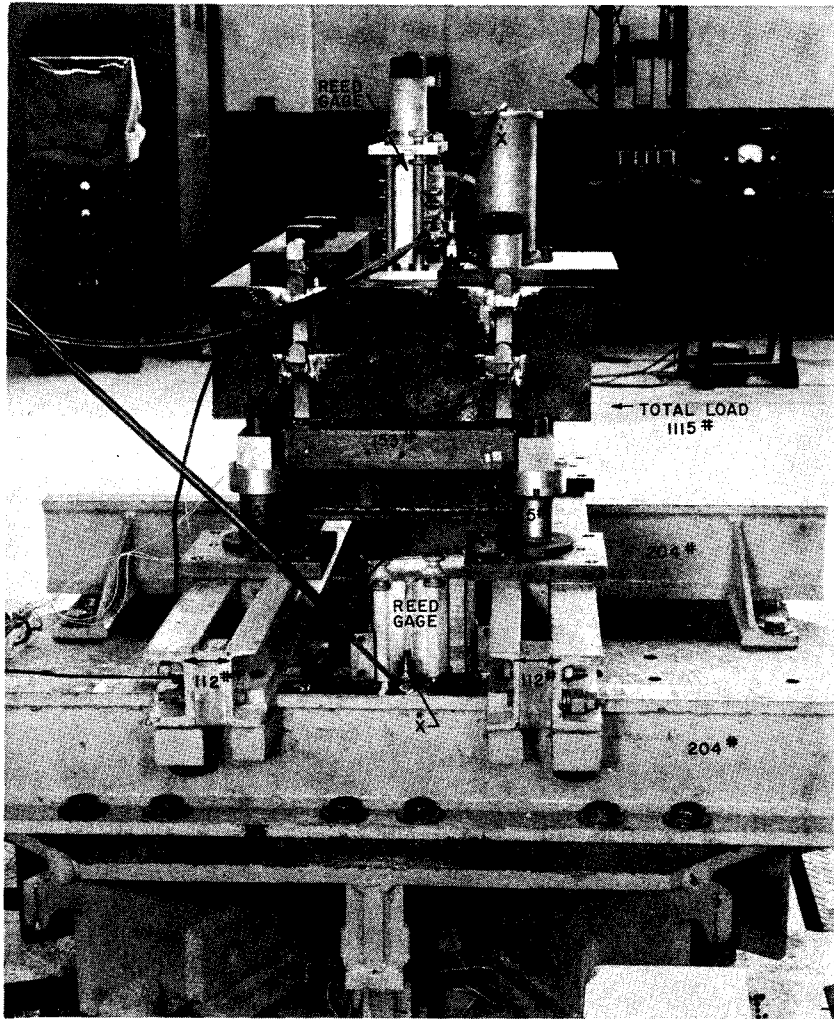


Fig. 57 — The 1115-lb calibration test load mounted on the MWSM

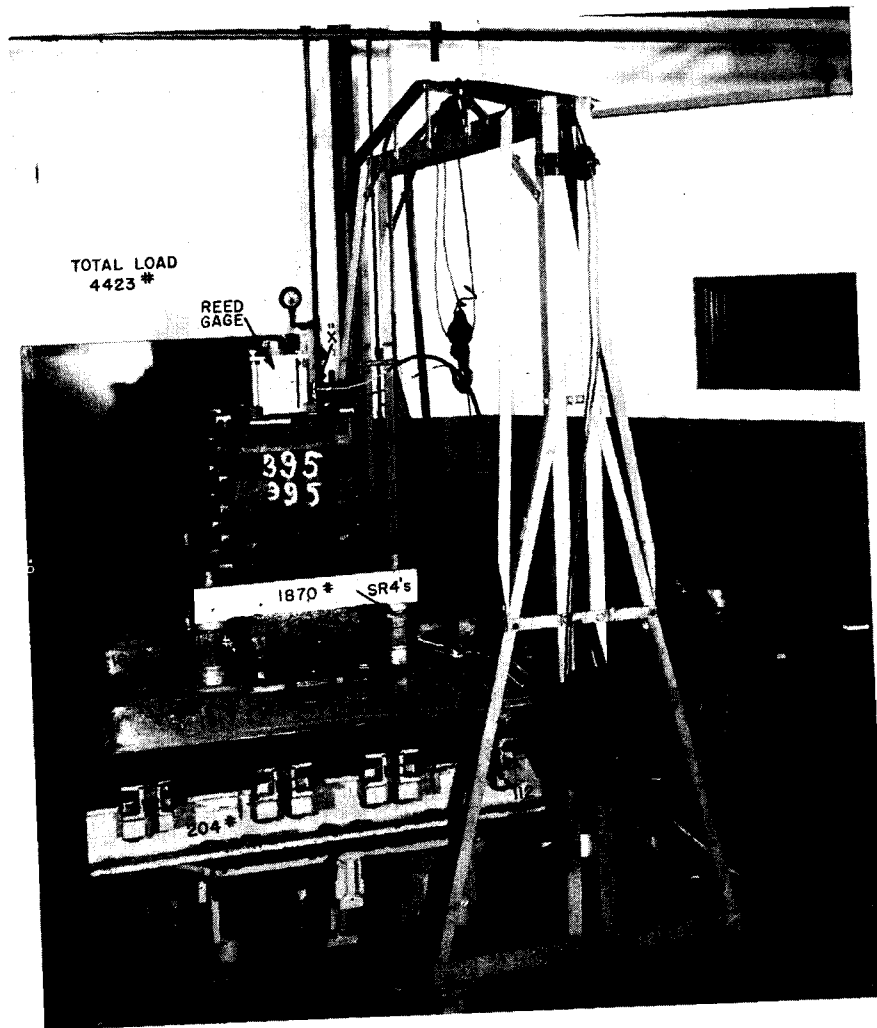


Fig. 58 — The 4423-lb calibration test load mounted on the MWSM

Measurement Instrumentation

The instrument package attached to the anvil table consisted of a reed gage, a quartz accelerometer, and a seismic-coil velocity meter having a natural frequency of 2.5 Hz and a displacement capacity of 3 inches. The calibration load carried a reed gage, a quartz accelerometer, and a seismic-magnet velocity meter having a natural frequency of 5 Hz and a displacement capacity of 5 inches. In addition, a strain gage was attached to the hammer to provide an indication of the dynamic forces involved in the impact, and a set of strain gages was attached to one of the load-mounting spacer cylinders and wired to measure the force exerted by the load on the supporting channels.

The reed gages are self recording; the electrical outputs of the velocity meters, accelerometers, and the spacer strain gages were recorded by 35-mm streak photography of a five-channel cro display. The velocity meter and strain gage signals were recorded without filtration, while the accelerometer outputs were low-pass-filtered at 300 or 1000 Hz before display. The strain gage on the hammer was not monitored regularly since the impact is elastic and consequently the dynamic forces are constant for a given drop height.

Output Shock Motion Waveforms (18,28)

Description

The MWSM in the calibration arrangement constitutes a mass-spring-mass system which is excited by imparting a sudden velocity to the mass representing the anvil table. This applies until the limit stops of the anvil-table travel are reached. The new set of transients introduced by this event may nullify or augment the motion already proceeding, depending on the stage of the motion at which it occurs. If the load mass has its maximum velocity away from the anvil table at the time, the load velocity change may be greater than that caused by the original hammer impact, theoretically as much as 2.5 times greater. In practice ratios so large are never encountered.

Anvil-Table Velocity

The hammer impact produces a half-sine pulse of acceleration having a duration of 1 ms; this not only imparts a velocity change to the anvil table but also excites elastic vibrations in it as well (Fig. 59). The frequency of these vibrations is about 750 Hz (longitudinal mode), and since the duration of the impact is larger than half the natural period, they build up so that the second peak is always larger than the first. The first peak, or "initial velocity," closely approximates the center line of the subsequent oscillations and is very nearly a linear function of the hammer impact velocity with a slope averaging from 0.45 to 0.58 (Fig. 60). The initial velocity is essentially independent of load when the load is channel mounted, although this would not be the case if the load were attached directly to the anvil table. The most probable value for the hammer-to-anvil table transfer coefficient may be taken as 0.54 for channel-mounted loads. The initial velocity varies from 3.4 ft/s for a drop height of 0.75 ft to 10.3 ft/s for the maximum drop of 5.5 ft (Figs. 61a through 61h).

In addition to the body vibration, the anvil table has gross body motions. These are the velocity step imparted by the hammer's impact, the linear rundown from gravity's deceleration, and the oscillation at the natural frequency of the test load-channel/anvil-table

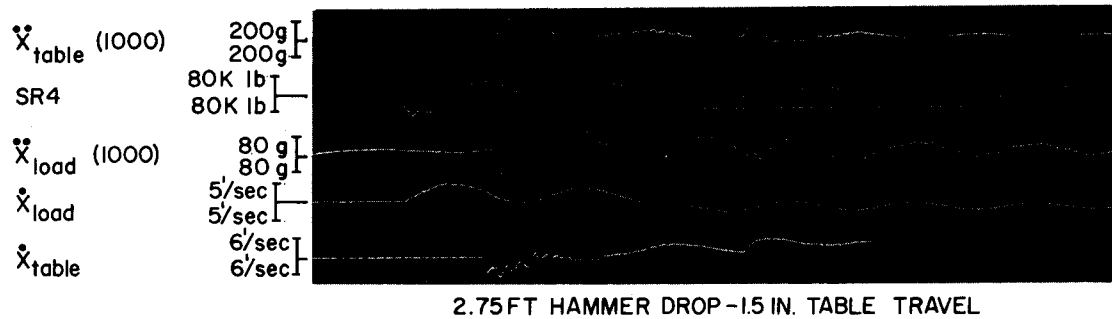


Fig. 59 — Typical waveforms from a blow with a 4423-lb load. The accelerometer records are low-pass-filtered with a 1000-Hz cutoff frequency. The record marked SR4 shows the force transmitted by one of the load's four support legs. Timing is indicated by blanking each record at a rate of 1000 Hz. The offset between the second and fourth traces and the other three is due to geometrical offset in the recording apparatus. The onset of shock is actually almost simultaneous in all channels.

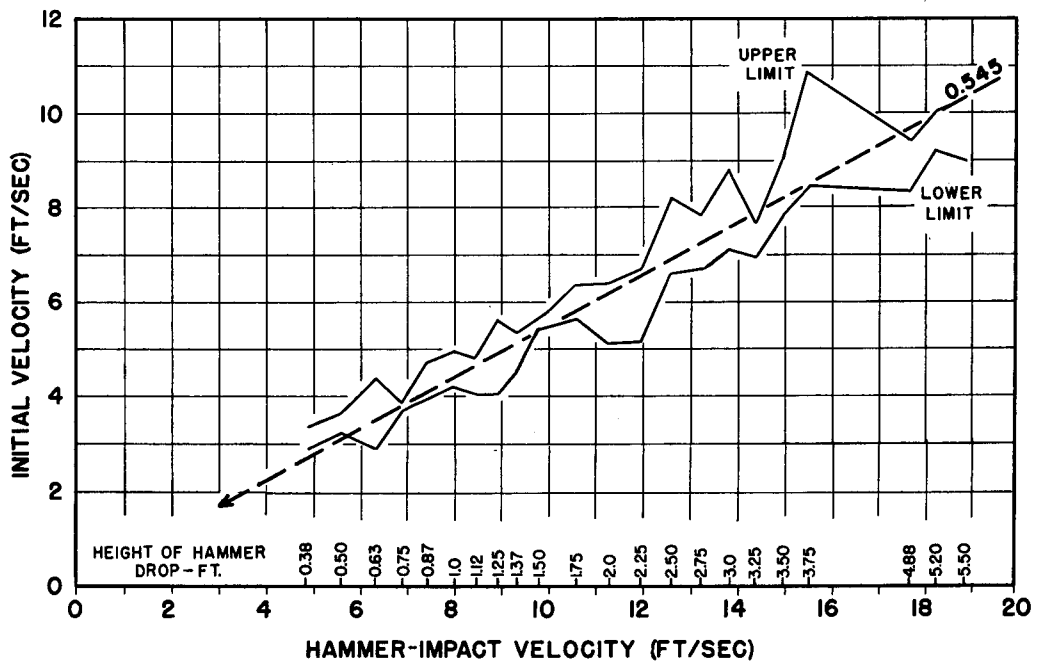
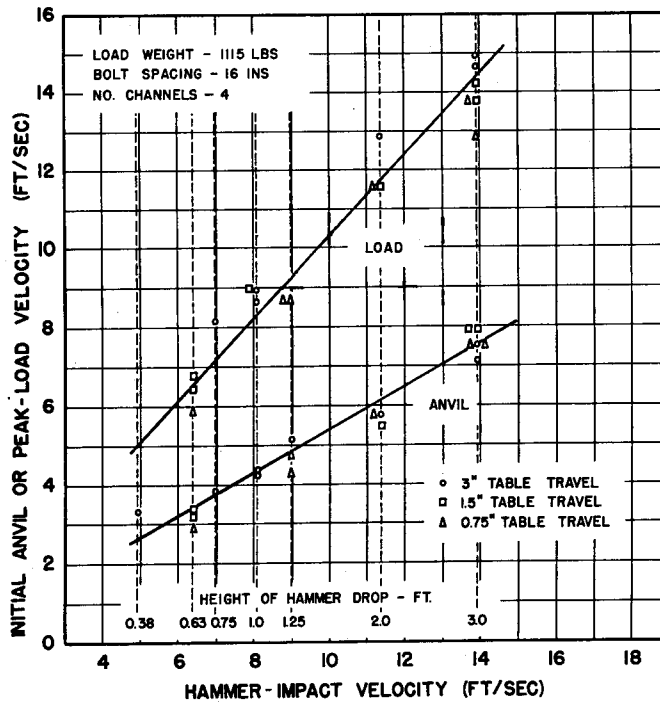


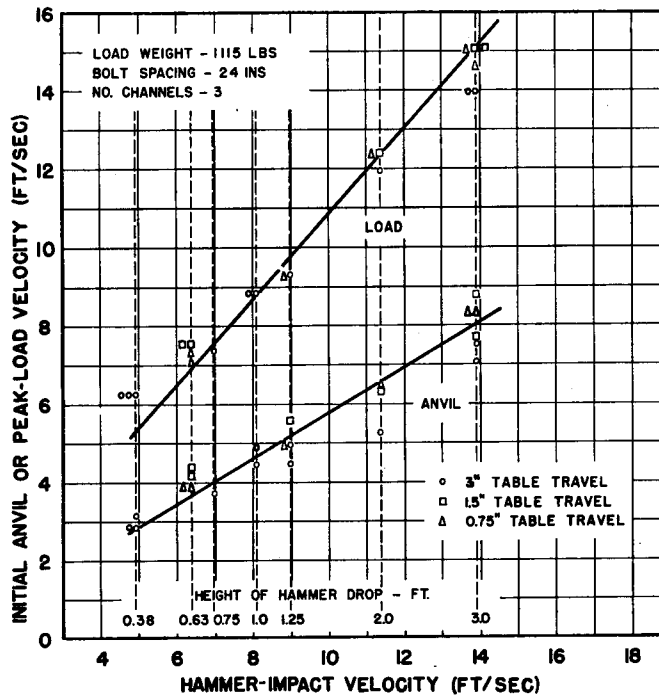
Fig. 60 — Initial anvil-table velocity for all blows

(mass-spring-mass) system. The magnitude of the last motion depends on the mass ratio of test load to anvil table and is of great importance in regard to the secondary shock arising from the anvil table striking its limit stops. It shall be referred to here as the "fundamental" oscillation of the mass-spring-mass system.

The average velocity is difficult to determine because the anvil table may attain a tilt of about 3.5° and velocity meters are imperfect instruments. The first means that the center of the anvil table may be as much as 0.75 inch below the level at which the hold-down bolts first strike their limit stops, which invalidates the simple procedure of dividing the nominal travel by the time interval between the impacts of the hammer and of the

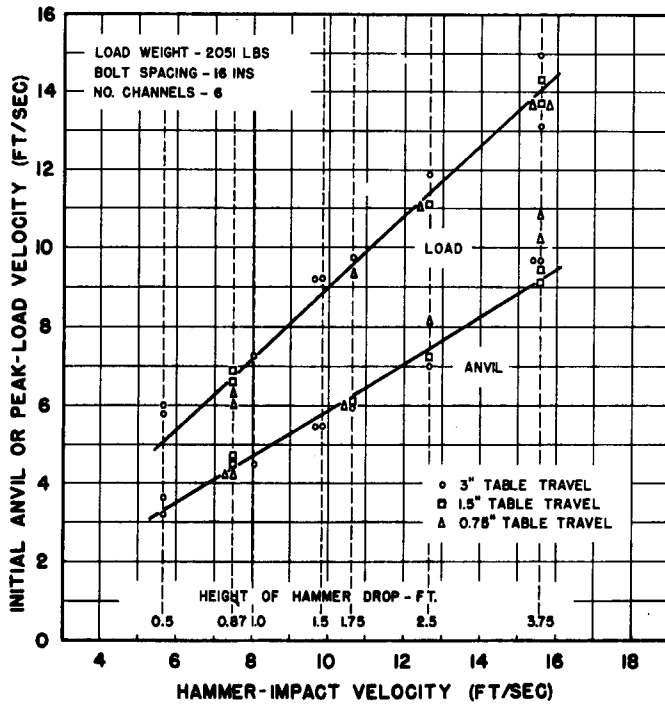


(a) Load weight = 1115 lb, bolt spacing = 16 in.,
and no. of channels = 4

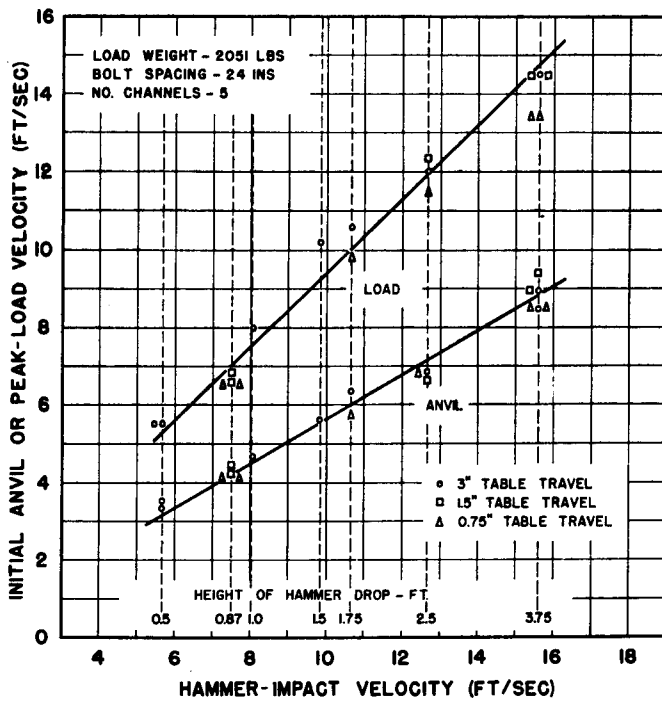


(b) Load weight = 1115 lb, bolt spacing = 24 in.,
and no. of channels = 3

Fig. 61 — Initial anvil-table and peak load velocities

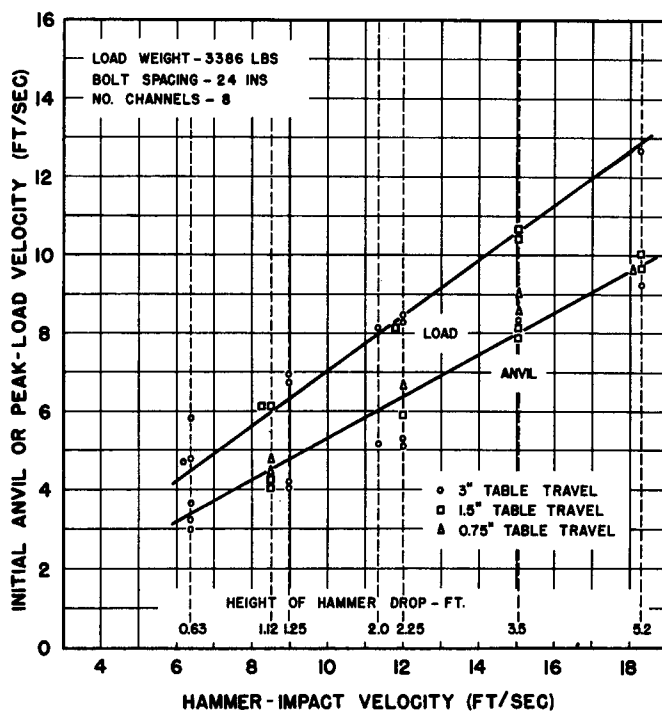


(c) Load weight = 2051 lb, bolt spacing = 16 in., and no. of channels = 6

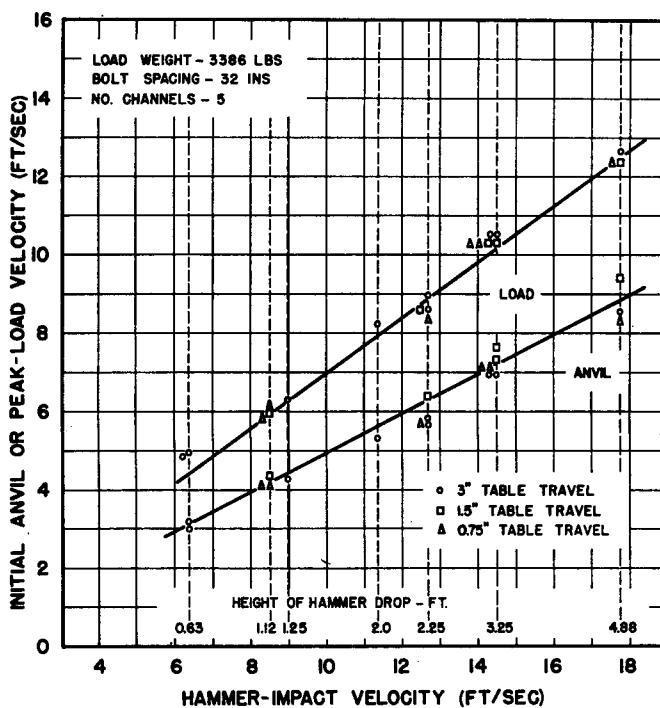


(d) Load weight = 2051 lb, bolt spacing = 24 in., and no. of channels = 5

Fig. 61 (Continued) — Initial anvil-table and peak load velocities

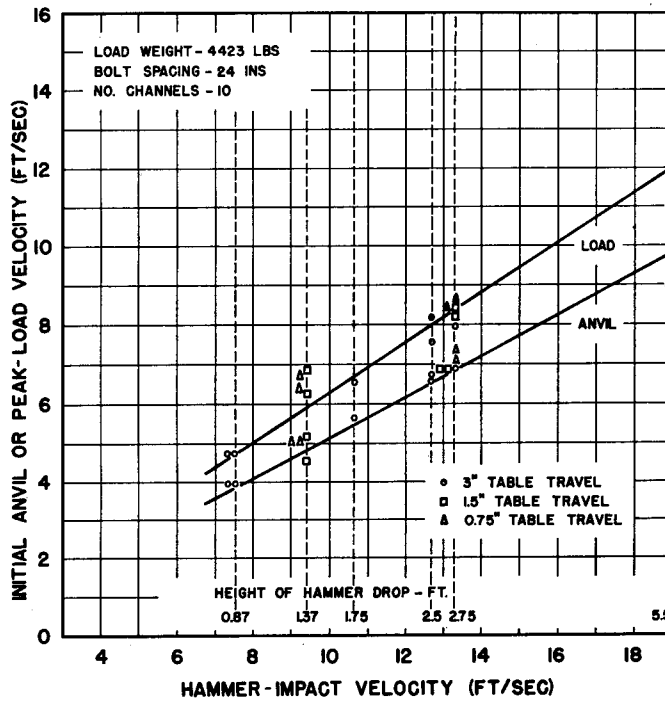


(e) Load weight = 3386 lb, bolt spacing = 24 in., and no. of channels = 8

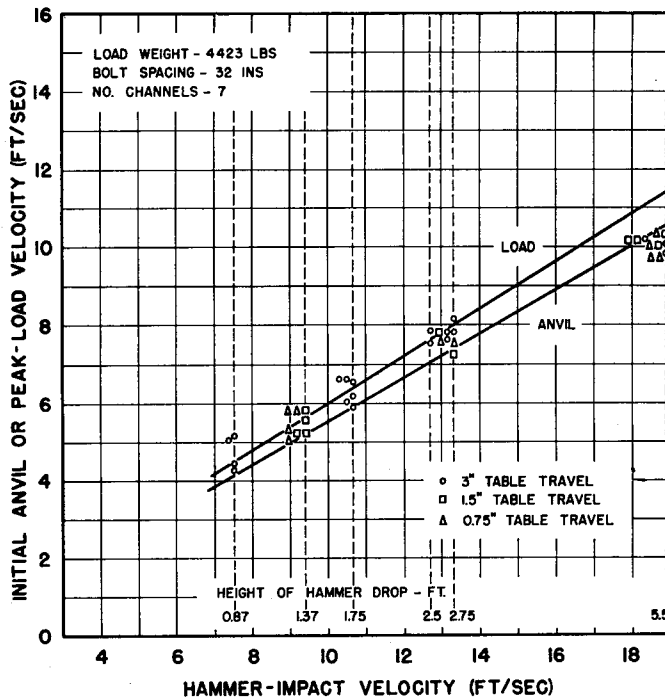


(f) Load weight = 3386 lb, bolt spacing = 32 in., and no. of channels = 5

Fig. 61 (Continued) — Initial anvil-table and peak load velocities



(g) Load weight = 4423 lb, bolt spacing = 24 in., and no. of channels = 10



(h) Load weight = 4423 lb, bolt spacing = 32 in., and no. of channels = 7

Fig. 61 (Continued) — Initial anvil-table and peak load velocities

limit stops. The second introduces discontinuities from bottoming of the velocity meter's seismic element and also a sinusoidal baseline due to its own natural frequency, which complicates the procedure of graphically averaging the velocity-time record over some integral number of oscillation cycles and allowing for the deceleration of gravity. The most reliable procedure is the most laborious and consists of integrating the velocity-time record up to the time at which its sign changes due to the anvil table reaching the limit stops and dividing this displacement by the time interval.

When the anvil table strikes the limit stops, it rebounds downward with a velocity depending on the coefficient of restitution and the striking velocity. Although bottoming discontinuities and motion of the velocity meter's seismic element prevent the measurement of absolute velocity in this epoch, differences may be measured reliably and so the velocity change due to the reversal is accurately displayed. Although there is considerable scatter in the values of this quantity, it is greatest when the striking velocity of the anvil table is greatest as would be expected. A plot of the magnitude of the reversal velocity step against the phase of the anvil-table fundamental oscillation shows maxima at integral cycles of the motion (Fig. 62). When the reversal occurs at the first peak, the reversal velocity change is about 1.3 times the initial velocity, and when at the second, about 1.15 times. It is lower than the initial velocity for the subsequent peaks. On the basis of velocity change, the reversal shock may consequently be more severe than hammer impact. The slope of the velocity change is less steep, however, so the accelerations involved are less than those due to hammer impact. The presence of this attribute led to the specification of two anvil-table travels as standard test procedure. If the secondary shock is relatively severe for one travel, it will most likely be proportionately less severe for the other. Frequency variations between identical types of equipment of slightly different weight are compensated in this way, so that neither is discriminated against because its weight, mounting arrangement, and rise time combine to produce a severe secondary shock blow.

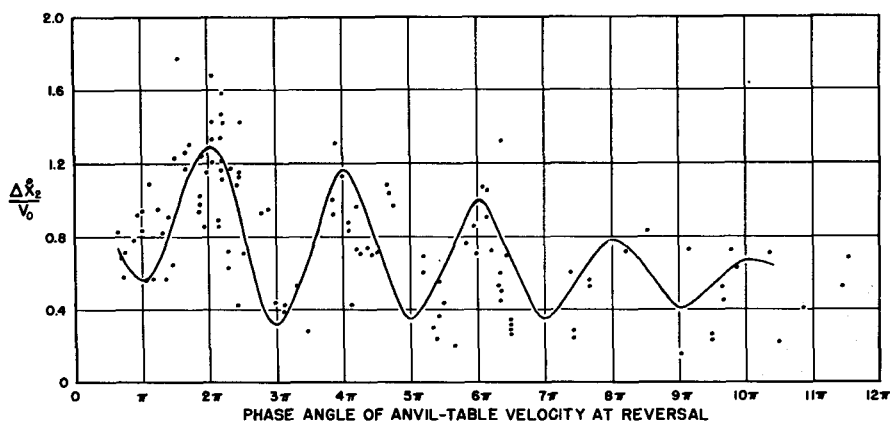


Fig. 62 — Variation of anvil-table reversal velocity with phase angle of fundamental oscillation

A third shock input is derived from the impact which occurs when the anvil table falls back onto its foundation. It is much less severe than the other two and is usually ignored, although not always. It is even less severe when the impact is on the air jacks (the 1.5-inch travel condition) rather than the machine foundation.

Anvil-Table Acceleration

Anvil-table acceleration shows active regions corresponding to the times of shock input to the motion (Fig. 59). At the hammer impact, the half-sine input pulse excites the 750-Hz longitudinal mode of the anvil-table structure. This appears at the accelerometer location as a damped vibration persisting for about 5 cycles. Peak accelerations associated with the hammer impact vary from 220 g (0.75-ft drop) to 580 g (5.5-ft drop) and, like the anvil-table initial velocity, are essentially linear with hammer impact velocity, again indicating that the MWSM is elastic (Figs. 63 and 64). The contribution of the fundamental oscillation to the acceleration is small since it is a low-frequency action, and gravity merely provides a constant level of 1 g.

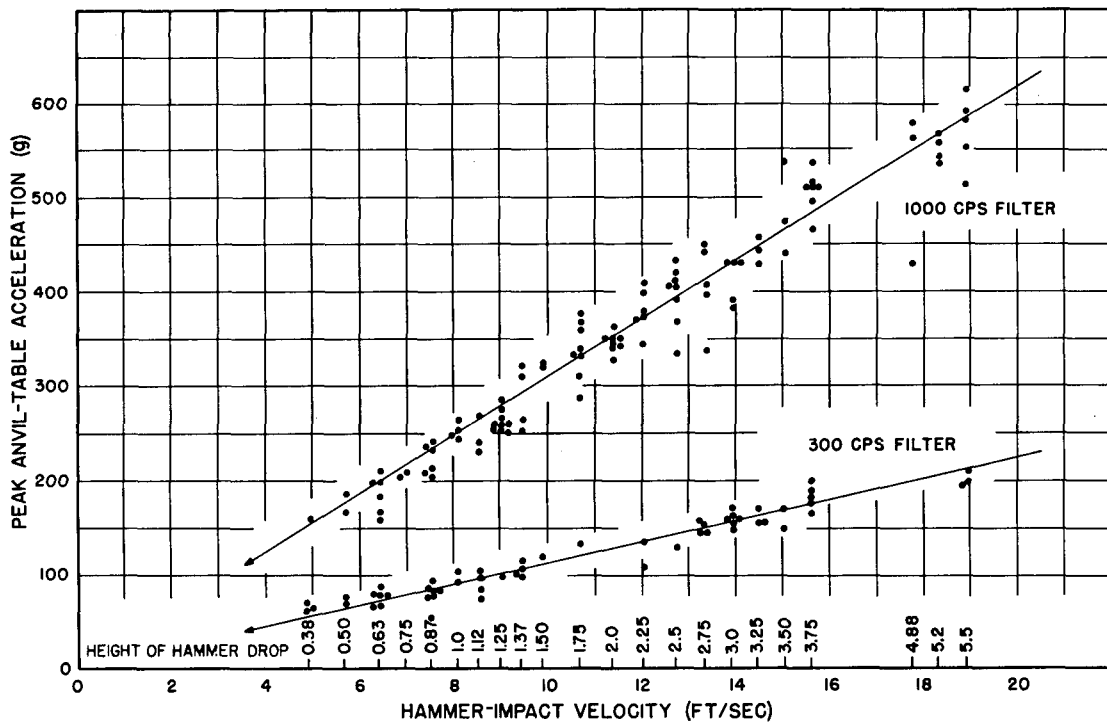
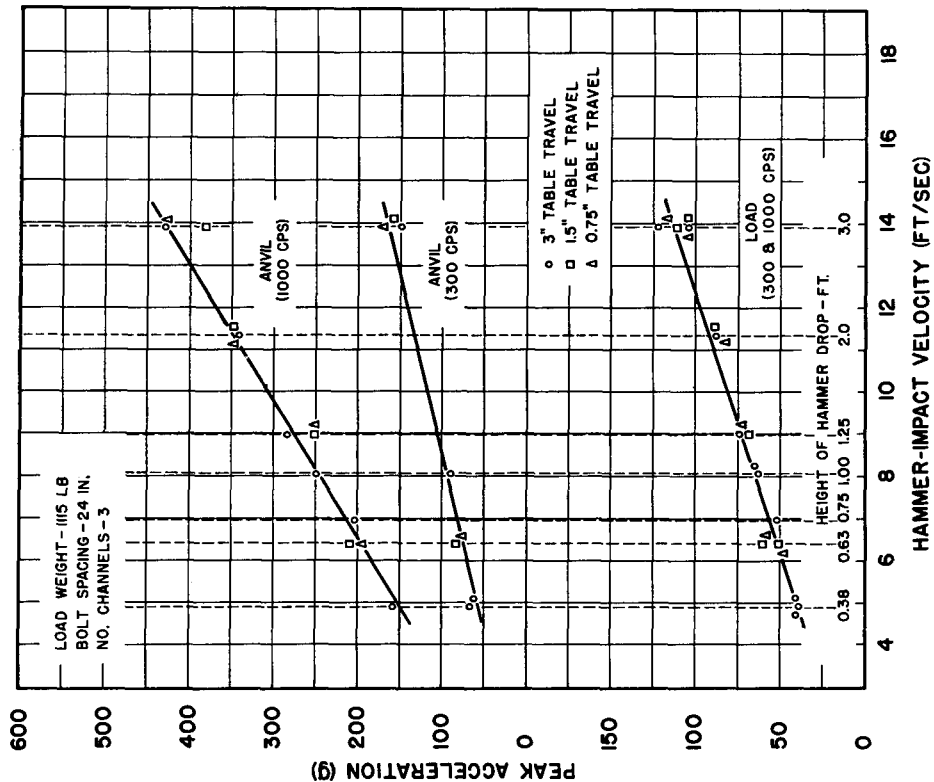
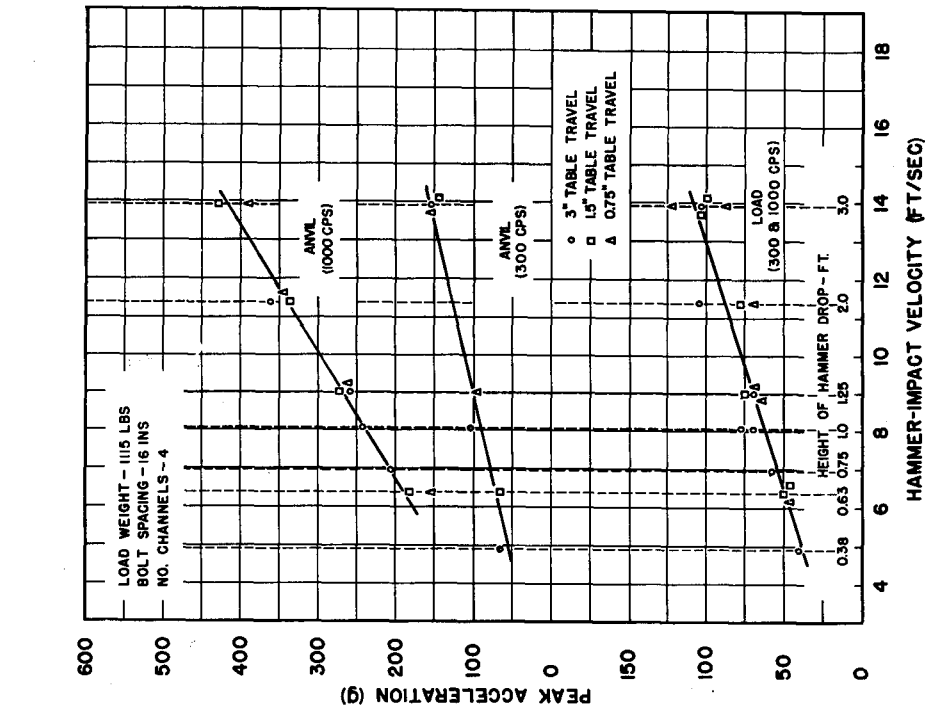


Fig. 63 — Peak anvil-table acceleration — all blows

The relative unimportance of the fundamental oscillation to the acceleration implies that the reversal acceleration will be somewhat insensitive to the phase of the fundamental at reversal. This is indeed the case. The reversal acceleration depends on the magnitude of the reversal velocity change and the time required for its occurrence (2 to 4 ms). Since the reversal velocity change depends on the phase of the fundamental at reversal, there is a remanent second-order dependence of the reversal acceleration also. Because the time required for reversal is so much larger than the hammer impact time, reversal accelerations are lower than the initial peaks, and anvil-table body vibrations are not excited. The reversal acceleration thus has the form of a fairly simple negative pulse. There is an additional positive pulse when the anvil table comes to rest, which is much longer and lower than the others.

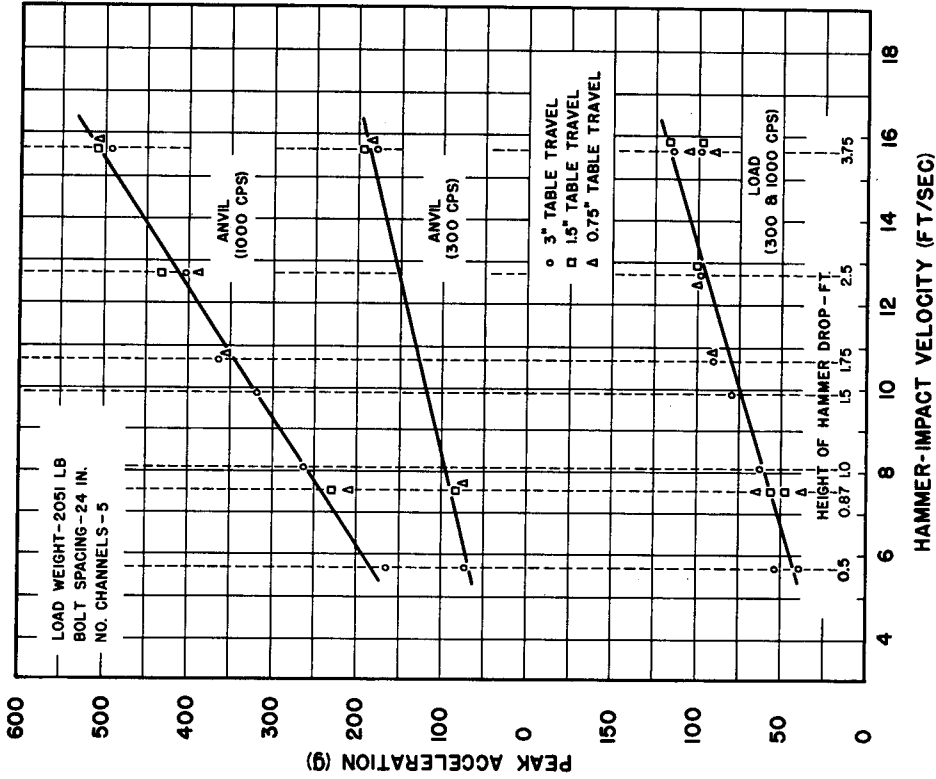


(a) Load weight = 1115 lb, bolt spacing = 16 in., and no. of channels = 4

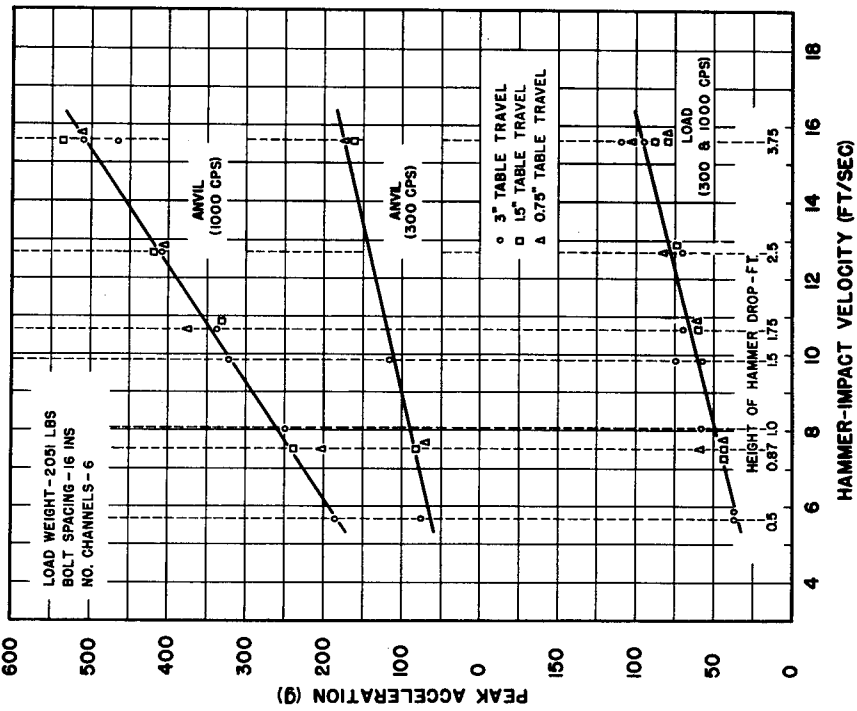


(b) Load weight = 1115 lb, bolt spacing = 24 in., and no. of channels = 3

Fig. 64 — Peak anvil-table and load accelerations

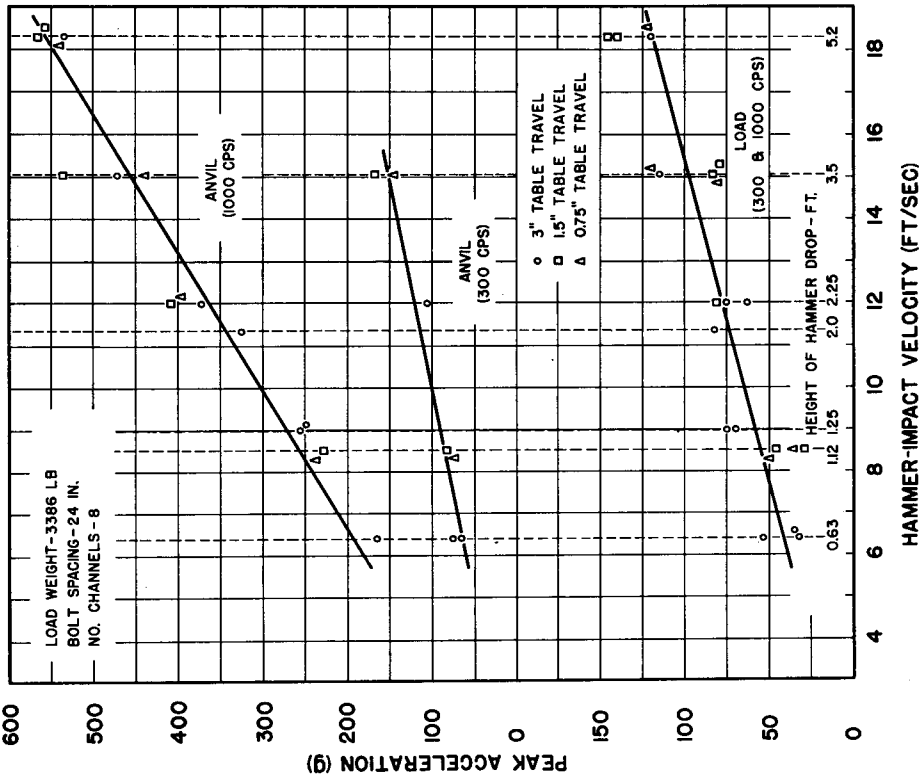


(c) Load weight = 2051 lb, bolt spacing = 16 in., and no. of channels = 6

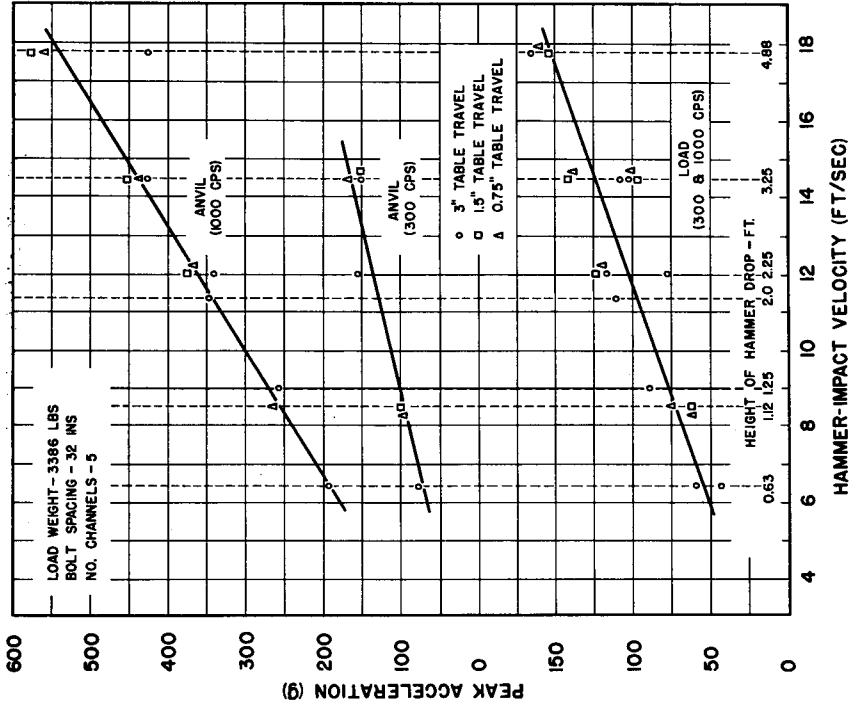


(d) Load weight = 2051 lb, bolt spacing = 24 in., and no. of channels = 5

Fig. 64 (Continued) — Peak anvil-table and load accelerations

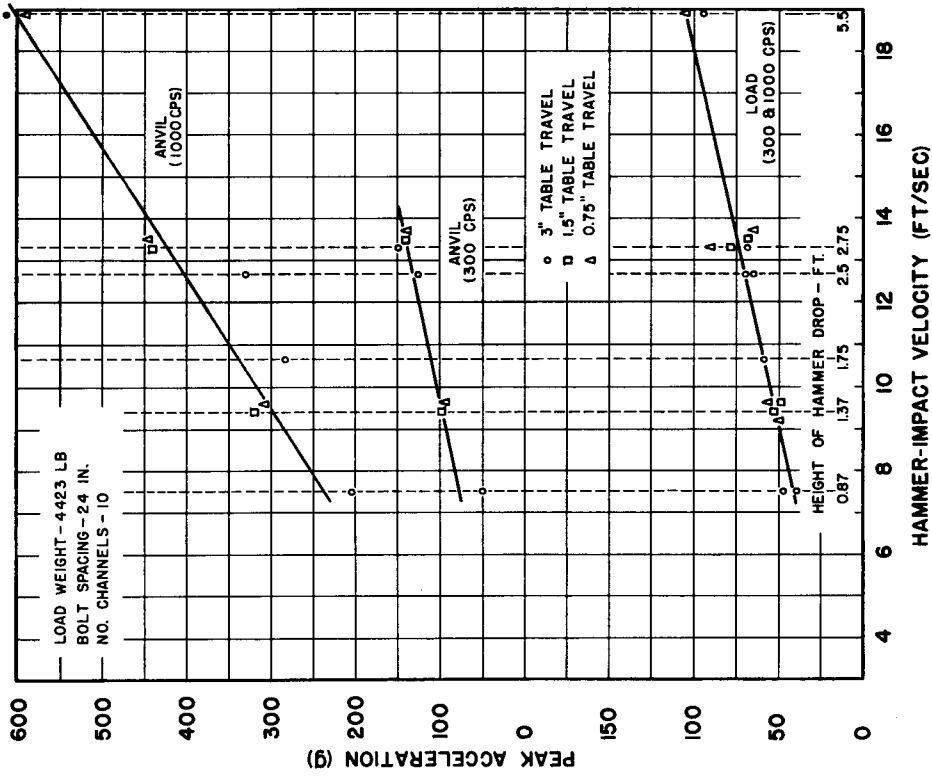


(e) Load weight = 3386 lb, bolt spacing = 24 in., and no. of channels = 8

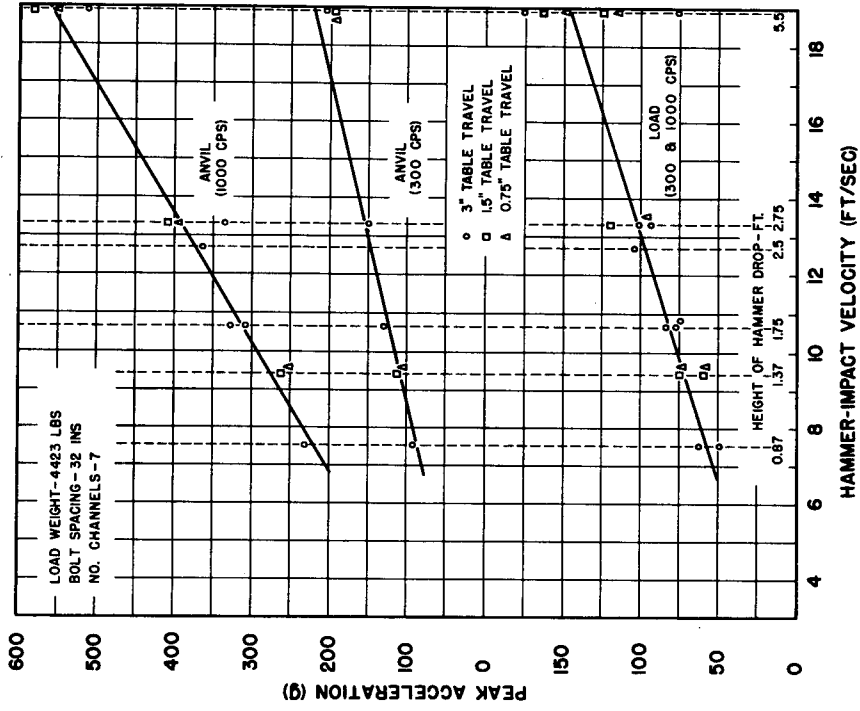


(f) Load weight = 3386 lb, bolt spacing = 32 in., and no. of channels = 5

Fig. 64 — Peak anvil-table and load accelerations



(g) Load weight = 4423 lb, bolt spacing = 24 in., and no. of channels = 10



(h) Load weight = 4423 lb, bolt spacing = 32 in., and no. of channels = 7

Fig. 64 — Peak anvil-table and load accelerations

The presence of high-frequency phenomena in the anvil-table acceleration waveforms requires the use of high-cutoff-frequency filters. A cutoff of 1000 Hz was found to be adequate. A cutoff of 300 Hz was also used, but while some useful information can be obtained, the frequencies involved in the motion at the time of hammer impact are so high that the waveform was seriously distorted.

Load Velocity

The low-pass filter formed by the support channels protects the load from the sudden changes in velocity seen at the anvil table. The most striking feature of the load velocity is the fundamental oscillation, with, of course, an underlying velocity step as a dc bias. The load velocity is basically of the $(1 - \cos)$ form (Fig. 59). If the anvil table does not strike the top stops, the fundamental oscillation will die down in about 10 to 12 cycles. With this degree of damping the maximum load velocity always occurs in the first half-cycle. If the anvil table does strike the limit stops, a new set of transients is generated which may act to increase or decrease the motions of the load, according to their phase.

The peak load velocity is always greater than the initial anvil-table velocity by a percentage depending on the mass ratio, and like initial velocity it is a near linear function of hammer impact velocity (Fig. 61). The slope of the relation depends on the mass ratio, varying from 0.6 for the heaviest load to 1.08 for the lightest, but it is not affected by the mounting dimension. As with the LWSM, the peak load velocity for a given hammer drop height decreases as the load increases, rapidly at first and then more slowly (Fig. 65).

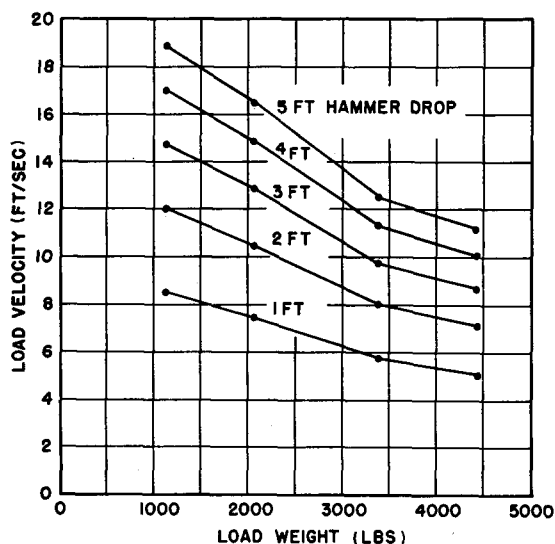


Fig. 65 — Peak load velocity for several hammer drop heights

As with the anvil-table velocity, the effect of reversal on the load velocity depends on the phase at which it occurs. The anvil-table reversal velocity step reaches maximum values when the phase of the fundamental oscillation is at whole cycles. Since the motion of the load is opposite to that of the anvil table, the load reversal velocity step has maxima when the fundamental is at odd half-cycles (Fig. 66). If the reversal occurs at the first

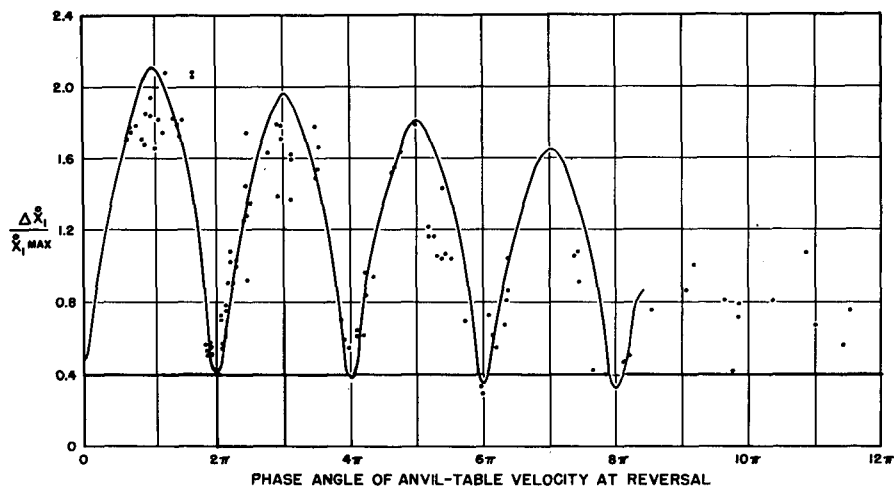


Fig. 66 — Variation of load reversal velocity with phase angle of fundamental oscillation

load velocity peak, the velocity change may be more than twice as great as that due to the hammer impact, although it never reaches the ratio of 2.5 which is theoretically possible.

Load Acceleration

The low-pass filter action mentioned with regard to the load velocity is even more apparent in the load acceleration. High-frequency components are small, and either 300- or 1000-Hz filtration is satisfactory (Fig. 59). As load and hammer drop height increase, the basically nonlinear nature of the supporting channels becomes noticeable. While the load acceleration waveform is nearly sinusoidal for low loads and drops, for high ones the positive half-cycles become shorter and higher than the negative.

Like the load velocity, load acceleration reaches its peak value due to the hammer impact during the first half-cycle of the fundamental oscillation. Also like the load velocity, this peak value is a linear function of the hammer impact velocity with a slope dependent on the mass ratio. It also depends to an extent on the mounting point dimension, a dependence which is not noticeable in the load velocity (Fig. 64). Peak accelerations range from 60 g (lightest load) and 96 g (heaviest load) for the lower drop heights of the test specification to 78 g (lightest load) and 144 g (heaviest load) for the higher. For a given mounting point dimension, the specified number of channels and drop heights will produce the same peak load accelerations regardless of load weight. The peak load acceleration increases as the mounting point dimension is increased, however (Fig. 67).

In contrast to the anvil-table acceleration, the load acceleration is dominated by the fundamental oscillation.* As would be anticipated, the reversal load acceleration is strongly

*This dominance is not due to the fundamental oscillation motions being vastly greater at the load than at the anvil table but to the absence of the very high accelerations excited in the anvil table by its impacts with the hammer and the limit stops. The relative magnitudes of the fundamental motions of load and anvil table are very nearly what would be expected for a mass-spring-mass system of appropriate mass ratio.

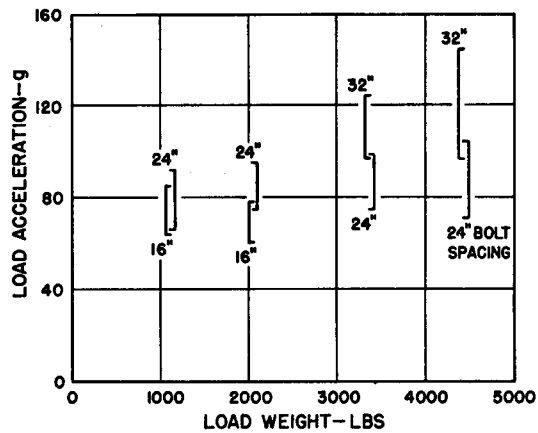


Fig. 67 — Load acceleration range for class A tests

affected by the phase of the fundamental oscillation at the time of reversal and may reach 1.2 times the peak acceleration due to hammer impact if the reversal occurs at the first half-cycle of the fundamental. Additional peaks occur at odd half-cycles, but after the first the reversal, acceleration is no greater than the initial peak, if as large.

Load Frequency

The waveform of the load motion is nearly sinusoidal for light loads and low drops, becoming more distorted as load and drop height increase. The distortion takes the form of negative half-cycles becoming longer and of lower amplitude as the hinge-pivot end constraint of the supporting channels for upward flexure is exploited more thoroughly and has the effect of lowering the net frequency. A more substantial variation of load frequency is caused by the mounting point dimension, especially for light loads. By far the greatest variation is found between loads of common dimension but of weights which fall on opposite sides of a demarcation line in the mounting specification table. The addition or subtraction of one or two supporting channels can result in substantial frequency changes. The lowest load frequency measured during the calibration procedure was 55.4 Hz, and the highest was 71.4 Hz. The average, and the value about which most of the measured values clustered, was 65 Hz (Table 2).

Reproducibility

As would be expected for an elastic machine, the MWSM does not show the systematic change in shock characteristics with use that the LWSM does. Its variations are all in the form of scatter. The predictability of waveform parameters is good and is better for those of the load motions than for those of the anvil table, and even better for velocities than for accelerations. The greatest variability is related to higher-frequency components and is probably due in part to the inevitable changes in mechanical details due to removal and reinstallation of loads and channels.

Table 2
Average Frequency of Fundamental
Oscillation (MWSM)

Load Wt (lb)	Dimension a (in.)	Number of Channels	Average Frequency (Hz)
1115	16	4	65.6
1115	24	3	71.4
2051	16	6	55.4
2051	24	5	57.5
3386	24	8	65.5
3386	32	5	68.1
4423	24	10	70.6
4423	32	7	67.7
Average			65.2

The least consistent parameters are the multipliers comparing the reversal parameters to those produced by the hammer impact. Even these adequately demonstrate the cyclic nature of the influence of fundamental oscillation phase.

Correlation with Model Predictions

The major features of the measured waveforms can be interpreted rather well in terms of a mass-spring-mass system with an impulsive input followed at some later time by a second oppositely directed impulsive input. Prediction of the effect of the latter input is improved by considering some damping and the effects of gravity to better estimate the appropriate initial conditions. The agreement is better for the load than for the anvil table, which when struck by the hammer reveals that it is not in fact a perfectly rigid mass. The most serious deviations in the measured load motions, at least with the compact dead-weight loads used here, are due to the nature of the velocity meter. This will not be the case for a more complex load structure, which would presumably have a higher center of gravity, making the rotational motion of the anvil table more substantial, and also have a multimodal response, making the rotation of more consequence.

In keeping with the order of the function, the velocity agreements are better than those of acceleration. Discrepancies of peak load velocities are less than 20%, and for the heavier loads 10% or less. The discrepancies for peak accelerations, on the other hand, are over 25% and as much as 57%. Interestingly, they are largest with the heavier loads, indicating the influence of the nonlinear spring characteristic of the supporting channels and the sensitivity of acceleration to the high-frequency structure of the waveform (Table 3).

On the measured frequencies and masses, the effective stiffness of the supporting channels may be calculated at 1 or 2×10^6 lb/ft/channel. The value of the damping coefficient may be estimated from the relative amplitudes of successive motional maxima and appears to be equivalent to about 4 or 5% of critical for normal load mounting methods. In general, it becomes larger as the amplitude decreases, indicating that it is largely of the frictional, or Coulomb, type.

Table 3
Comparison of Measured and Predicted
Peak Load Velocities and Accelerations

Mass Ratio	Ratio of Peak Load Velocity to Initial Velocity			Ratio of Peak Load Acceleration to Initial Velocity		
	Exper.	Theor.	% Error	Exper.	Theor.	% Error
0.25	1.91	1.60	16.2	14.4	10.2	29.2
0.24	2.00	1.61	19.5	15.0	11.2	25.3
0.46	1.67	1.37	17.6	11.5	7.4	35.7
0.45	1.74	1.38	20.3	13.9	7.7	44.6
0.70	1.30	1.17	10.0	12.0	7.5	37.4
0.70	1.30	1.17	10.0	15.7	7.8	50.3
0.90	1.17	1.05	10.3	10.4	7.2	30.8
0.90	1.11	1.05	5.4	14.3	7.0	57.0

Output Shock Spectra (18,29)

The reed gage attached to the calibration loads had reeds with natural frequencies of 40, 73, 91, 103, 122, 157, 203, 221, 353, and 418 Hz. The reed gage on the anvil table had reeds with natural frequencies of 20, 40, 103, 203, 353, 418, 554, and 920 Hz, unfortunately lacking any in the vicinity of the fundamental oscillation frequency.

Anvil-Table Shock Spectra

Since the reed gage attached to the anvil table lacked a reed near the fundamental oscillation frequency, its impression of the anvil-table motion was primarily the velocity step component. Therefore, the measured spectra are of simple velocity shock (Fig. 68). Since it also lacked a reed at 750 Hz, the ringing frequency of the anvil table is not indicated either. This is an excellent illustration of the failings of reed gages.

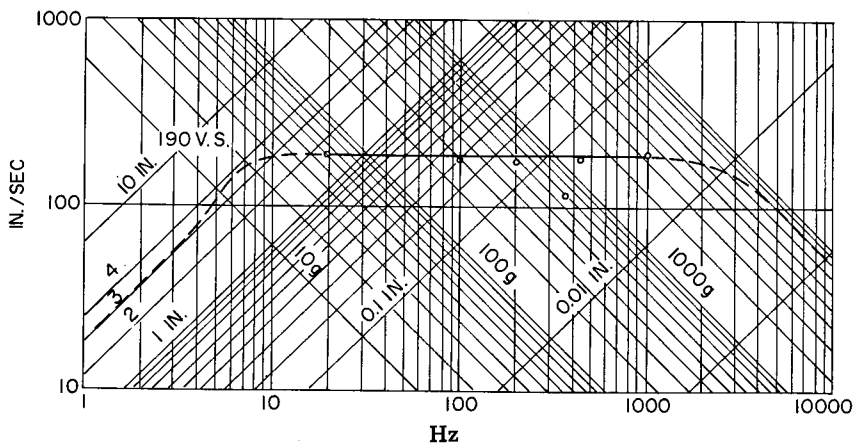


Fig. 68 — Shock spectrum of anvil table for 3-ft drop, 3-in. travel blow with a 1115-lb load

Load Shock Spectra

The load shock spectra are in more comforting circumstance. The 73-Hz reed, although removed from the fundamental frequencies to a greater or lesser degree, is close enough to indicate that this is the dominating feature of the load motions. The shock spectra demonstrate the limit to constant acceleration above this frequency and try to show the velocity shock region to the best of the reed gage's ability. As the shock machine control parameters are varied, the peak at 73 Hz rises and falls but largely continues to be the salient feature of the shock spectrum. This variation could be due to the fundamental oscillation frequency being shifted around in the selectivity band of the 73-Hz reed as much as to actual variation in its strength.

Effects of Hammer Drop Height

Increase in the height of hammer drop has the effect of raising the level of the shock spectrum without changing its shape. The level of the spectra for blows representing the higher drops of the standard shock test specification is about 150% that of the lower drops, roughly in the same ratio as peak load velocities and accelerations (Fig. 69).

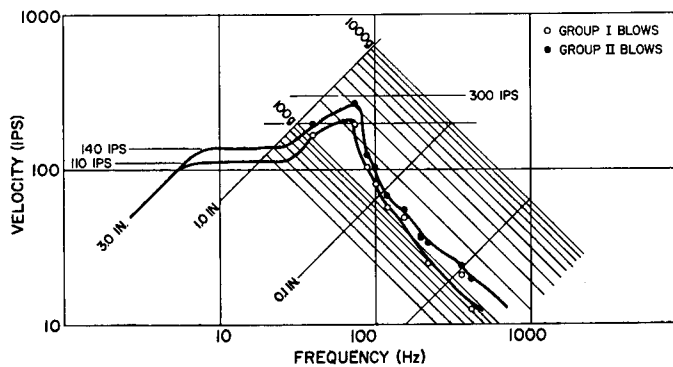


Fig. 69 — Effect of hammer drop height. Shock spectra of Group I (1.5 ft) and Group II (2.5 ft) blows for a 2051-lb load, mounting dimension 16 in.

Effects of Load Weight

Interestingly enough, increasing the load weight seems to increase the shock spectrum level, almost entirely at the high-frequency end, which is presumably due to the waveform distortion noted previously for high drop and heavy loads (Fig. 70). This might be somewhat alarming in view of the intention of the MWSM to provide less severe shock to heavier equipments. However, the frequencies which are most affected are from 353 Hz and beyond, while those below 200 Hz may decrease, and the 73-Hz level definitely decreases, as it should. The region between 200 and 353 Hz remains a mystery since no reed was located there. In any event, the frequency range below 200 Hz is certainly the only area of consequence for shipboard equipments, and it is reasonably safe to say that for practical purposes the shock severity does decrease with increasing load.

Effects of Mounting Dimension

Increasing the distance between mounting points also has the effect of selectively raising the shock spectrum levels at high frequencies (Fig. 70). This is in accord with the increased stiffness of the mounting arrangement indicated by the increase in fundamental oscillation frequency. The effect is probably not significant for practical test equipments.

Effects of Anvil-Table Travel

The anvil-table travel has no consistent effect. With the heavier loads, there is some tendency for the high-frequency (>200 Hz) end of the spectrum to be a trifle greater for 1.5-inch travel blows than for 3.0 inch. This tendency is reversed in the more important region of the fundamental oscillation frequency (Fig. 70). Such variations are much smaller than those due to the other machine variables. It is interesting that a parameter which can affect the load motion's waveform so strongly has so little influence on its shock spectrum. It is also noticeable that when the change in load velocity due to reversal is large, the time in which it takes place is relatively short, which would tend to stimulate the higher-frequency reeds more than the lower.

Reproducibility

The specification shock test calls for three groups of two identical blows. Comparison of the load shock spectra for these pairs of blows, plus two additional groups of three identical blows, shows the reproducibility to be generally good (Fig. 71). The variations above 200 Hz are commensurable with the uncertainties in reading the reed gage records. Variations below 200 Hz may be attributed to random variations in machine performance probably deriving from such sources as slight differences in bolt tightness.

Correlation with Model Predictions

The model used to calculate load shock spectra was the undamped mass-spring-mass system with rigid stops, and allowing for gravity. Spectra were computed for mass ratios of 0.45 and 0.9, corresponding approximately to the loads of 2051 lb and 4423 lb, and were computed for the epochs before and after the reversal event. The agreement between these curves and the measured spectral points is reasonably good for frequencies below about 2.5 times the fundamental oscillation frequency. Above this value, it remains fairly good for the lighter load, but the measured points are much higher than the theoretical curve for the heavier load (Fig. 72). This indicates the inadequacy of the simple model to express the actual mass distribution when the load mass is close to that of the anvil table, as was also exemplified by the departure of the load-velocity waveform from the simple shape predicted by the model.

Nonstandard Operation

Like the LWSM, the MWSM has also been used to generate special waveforms. These waveforms and the methods used to produce them do not form part of the standard shock test or its specification.

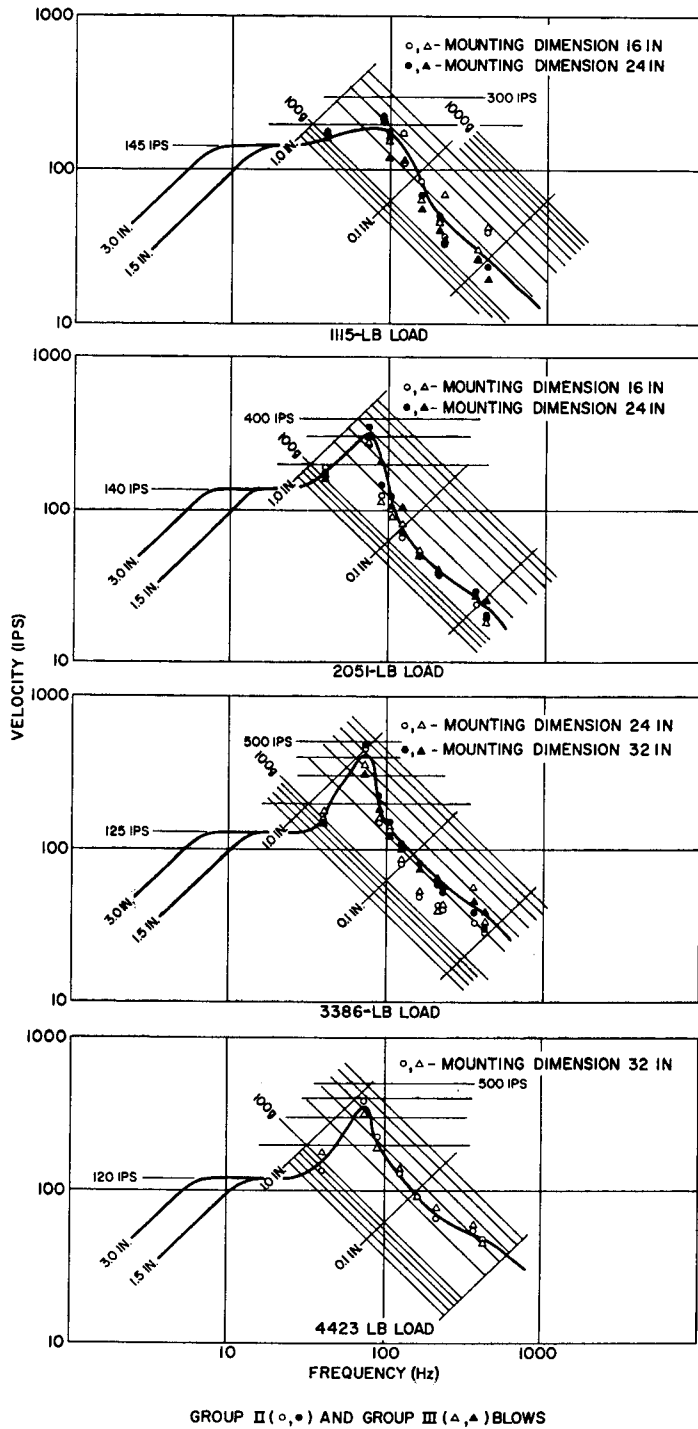


Fig. 70 — Shock spectra for Group II and Group III blows

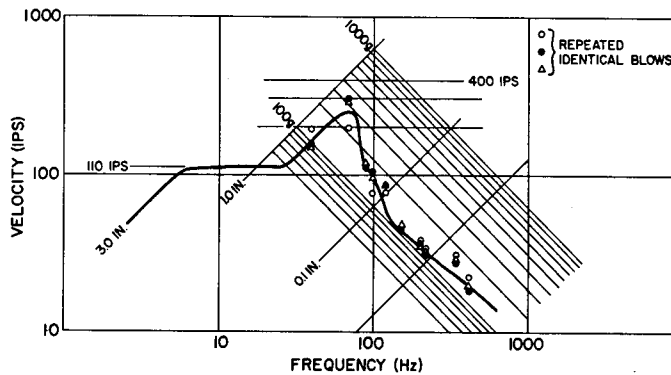


Fig. 71 — Shock spectra for repeated Group I (1.5 ft) blows with a 2051-lb load, mounting dimension 24 in.

Simple Pulse Shock (30)

The MWSM may easily be used to provide the commonly required initial ramp sawtooth and half-sine pulse shock waveforms. The test equipment is attached directly to the anvil table, with no flexible fixtures intervening unless they are considered part of the test equipment. All impacting surfaces of the MWSM (anvil-table impact pad, anvil-table travel top limit stops and bottom stops) are padded with appropriate shock moderating material. For sawtooth pulses the material, shown in Fig. 73, is plastic (lead or solder), and for the half-sine pulses it is elastic (polyurethane).

The plastic element attached to the anvil-table impact pad is a cone whose weight is appropriate to the desired pulse duration. When the hammer impacts, the anvil table accelerates for 6 to 8 ms, until the velocities of the anvil table and hammer are matched. The acceleration then drops to -1 g in 1 or 2 ms. This represents an elastic contribution mostly from the machine, setting a lower limit to the possible buildup time and imparting a slight velocity difference between hammer and anvil table. The anvil table rises until it strikes the elements at the top limit stops, which are also padded plastically, and decelerates over a period of some 25 to 30 ms. During this epoch, the hammer may catch up with the anvil table and impact again. It then swings back and the anvil table drops onto the bottom stops. The material for the bottom stop elements may be plastic or elastic since these elements do not play a significant role in the shock production. Elastic elements are more convenient since they need not be replaced. Peak accelerations from the primary hammer impact of up to 60 g (Figs. 74 and 75) may be produced. The peak accelerations from the secondary hammer impact (if any) may run from 10 to 20 g (Fig. 74).

The elastic elements, shown in Fig. 76, used for half-sine pulses are formed from polyurethane with a Shore A durometer reading of 65. The loading on the anvil-table impact pad element is so great that it is quite nonlinear, and the resulting anvil-table acceleration waveform departs seriously from half-sine if drops above a few inches are used. However, drops of up to 3 inches can produce reasonable half-sine pulses of up to about 7 g, with durations of 20 to 30 ms (Fig. 77).

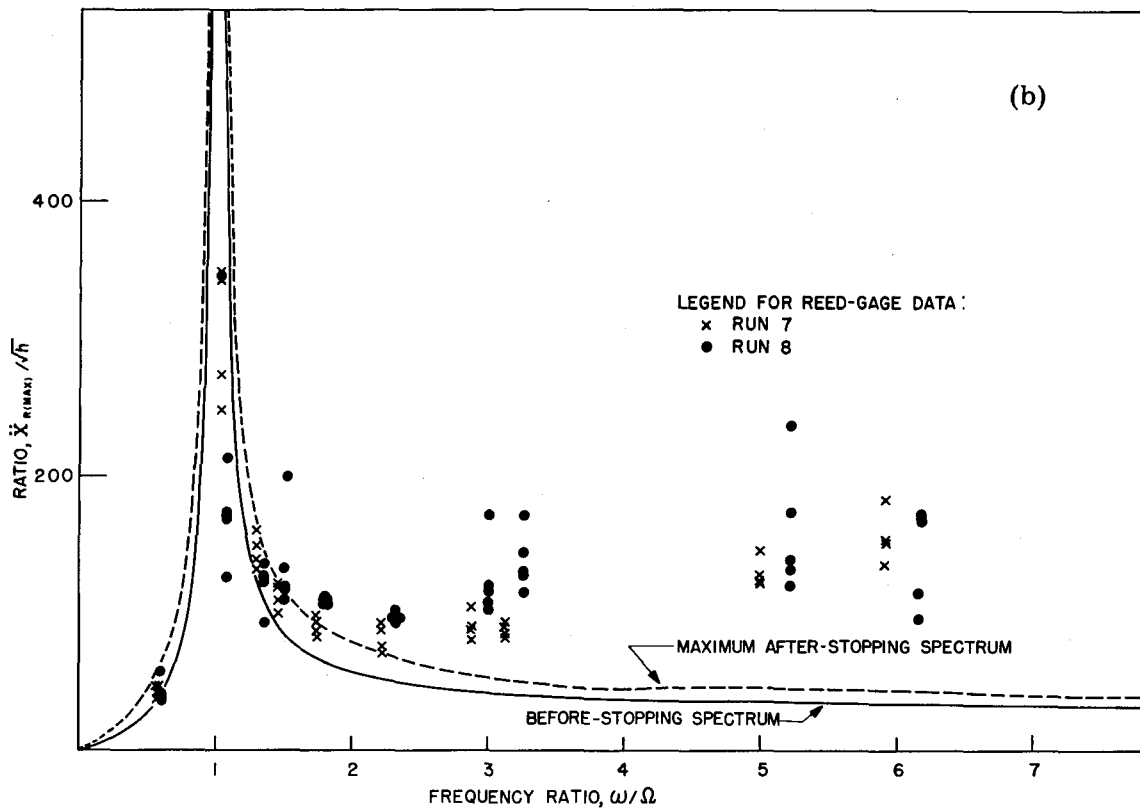
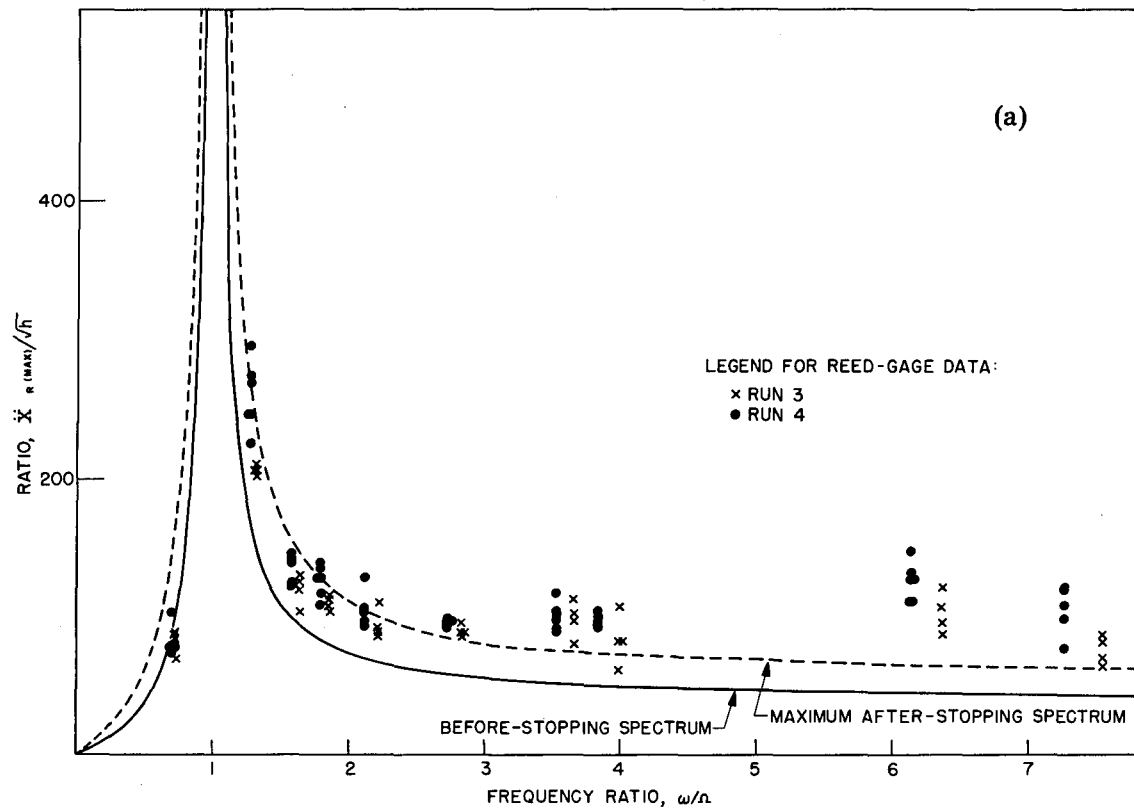


Fig. 72 — Theoretical and experimental shock spectra for mass-ratios of 0.45 and 0.9. These are plotted as equivalent static acceleration. Ω is the frequency of the fundamental oscillation.

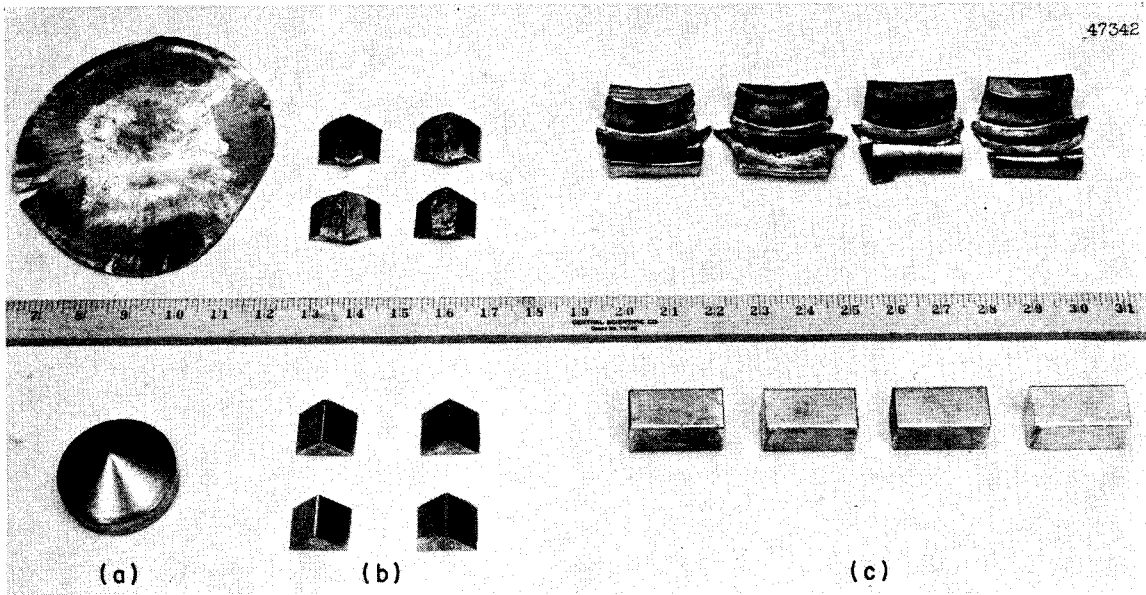


Fig. 73 — Plastic (solder) elements for generating sawtooth pulses with the MWSM. Shown (lower) before deformation and (upper) after, these elements are attached to (a) the anvil, (b) the bottom stops, and (c) the top stops.

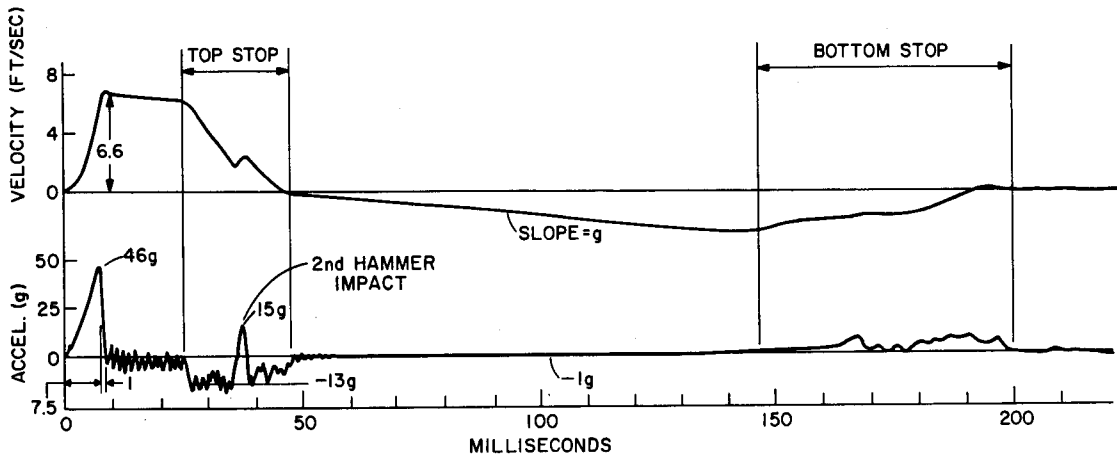


Fig. 74 — Anvil-table motion for a 4-ft hammer drop with a 21-oz plastic (solder) element

Plate Mounting

Some types of equipment, such as reactor components, are required or permitted to be shock-tested by procedures different from those of MIL-S-901. Typically, these shock tests are required to provide a mounting system such that a specified fixed-base natural frequency shall result and that hammer drop heights and table travels shall be as given by the schedule of MIL-S-901 for the all-up weight on the anvil table. Another type of specification might require that a mounting system and machine operation procedure shall be such that a specified fundamental oscillation frequency and peak load velocity shall be

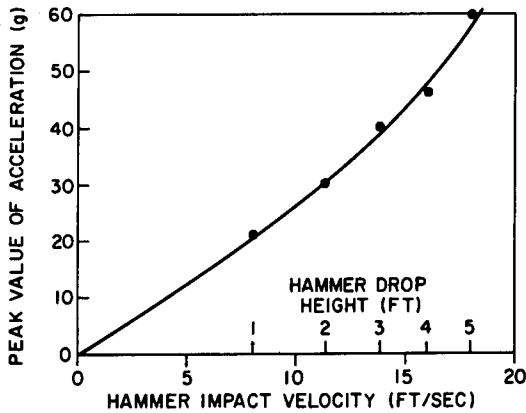


Fig. 75 — Sawtooth pulse amplitude as a function of hammer impact velocity

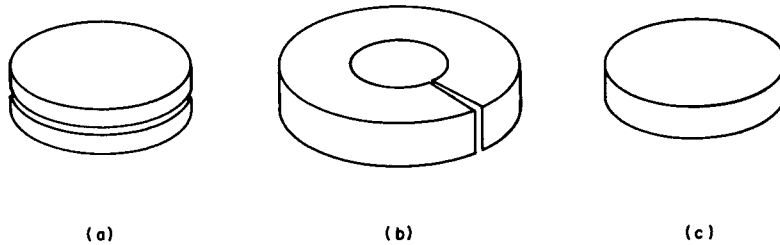


Fig. 76 — Elastic elements (polyurethane) used between the impact surfaces: (a) anvil, (b) top stops, and (c) bottom stops. All are 1 in. thick, (a) and (c) have 4-in. diameters, and (b) has a 5.2-in. O.D. and a 2.3-in. I.D.

produced. Still another may require that a specified shock spectrum envelope shall be produced at the load mounting points. This last procedure was once fairly common, then fell into abeyance as the complexities of interpreting shock spectra properly became appreciated. It is now reappearing. Since its renaissance is largely localized in fields with little previous acquaintance with shock and shock design, there seems little reason to hope that the present practitioners are any more knowledgeable than the last.

The frequencies specified for tests of the two former types are generally too low to be provided by the usual support channels. The dynamic stresses are entirely too high, and bending may be so rapid that the fundamental oscillation persists for only a cycle or less. A convenient way around this problem is to interpose a steel plate between the support channels and the test equipment, which is arranged so that its long axis lies parallel to the support channels. This system may be tuned by moving the support channels in and out to vary the effective free span of the plate and by such traditional tricks as judicious use of spacers. The plate will still yield somewhat, but the depth of plastic penetration is vastly less than would occur in the support channels alone and has no noticeable influence on the load motions. In time, the deformation may accumulate to an unsightly extent, whereupon the plate can be turned over for the next test.

Deck Motion Simulation

NSRDC is investigating ways to modify the operation of the MWSM to provide the large displacements and low frequencies characteristic of deck motions. The projected technique would not entail the extensive modifications of the machine structure that

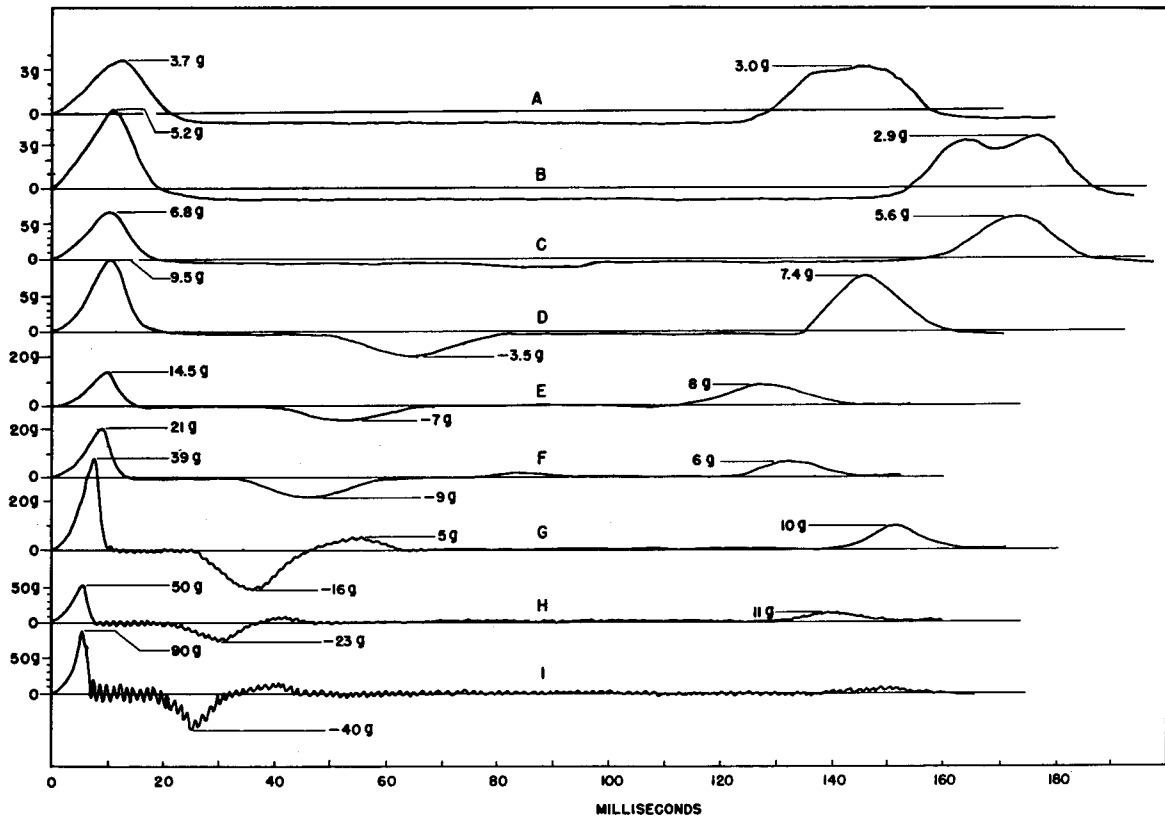


Fig. 77 — Acceleration curves using polyurethane elements of the dimensions shown in Fig. 76 and with a 65 Shore A durometer hardness. Hammer drop heights were (a) 1 in., (b) 2 in., (c) 3 in., (d) 5 in., (e) 8 in., (f) 1 ft., (g) 2 ft., (h) 3 ft., and (i) 4 ft.

were used with the LWSM but would constitute an elastic mounting system to be placed between the anvil table and the test equipment. The displacements involved would accordingly be limited to much less than the 12 inches permitted by the modified LWSM.

30° Corner Bulkhead

The 30° corner bulkhead (Fig. 55) is an auxiliary mounting adapter which permits shock motion to be induced along all three axes of a test equipment simultaneously. It is intended as an adjunct to the standard mounting arrangement, not as a replacement for it.

The bulkhead is a stiff and massive structure which is attached to spacer rails mounted on the anvil table. It has so many response modes of its own that the response of an equipment mounted in it is difficult to forecast, but by and large the normal modes of the overall structure will be those of the bulkhead, little influenced by those of the test equipment. The velocity measured at the corner of the bulkhead (the most compliant part of its structure) has the same character as that of the anvil table with strong, well-sustained sinusoidal components at 250 Hz and integral multiples, and a minor 150-Hz component. The displacements associated with these components are small. A severe input to the test equipment may be the racking occasioned by the motion of the bulkhead's

sides, which flap considerably. However, there are equipments which have inadequacies that are best revealed when shock is directed along two or three axes simultaneously, and for this reason it is desirable that some blows of the shock test should be delivered with the equipment on a 30° mounting.

Excessive Load Weights

The original schedule of specification blows provided peak load velocities of 11.5 ft/sec. Equipments weighing up to 4800 lb still receive tests of this severity. Dead-weight loads in excess of 4800 lb cannot be given this velocity; since the hammer is 5.5 ft long, it cannot be dropped from a height greater than 5.5 ft. With the current standard load limit of 6000 lb the peak attainable load velocity is 9.5 ft/sec at best, and usually lower. In view of this decrease in test severity at the high end of the load range, it may be desirable to modify the test procedure for items in the 5000- to 6000-lb range. For example, tests of such items could simply be transferred to the Floating Shock Platform, or light-weight mounting components could be fabricated from high-strength alloys. In any event, it would be well to hold the total load on the anvil table to around 6000 lb.

THE NAVY FLOATING SHOCK PLATFORM

History (31)

In the absence of suitable shock machines for testing equipments weighing in excess of about 4500 lb, actual shock testing of heavy shipboard items was limited to what could be installed on board a ship undergoing a series of shock tests. The situation largely involved calculating shock response plus occasional spot checks by actual test. Although capable of providing the best proof test imaginable, a ship undergoing shock tests is not a convenient device for equipment development. The expense is great and the shock severity is usually limited to a level which assures survival of the ship.

In 1959 the first Floating Shock Platform (FSP) was designed and built by the Underwater Explosion Research Division (UERD) of NSRDC at the Norfolk Naval Shipyard. It consists of an open steel barge capable of handling all-up loads to 30,000 lb (40,000 lb with restrictions on the location of the center of gravity) which is exposed to a series of underwater explosions. Test equipments are installed as they are on shipboard, and the test hopefully approaches the actual service conditions while providing the conveniences of accessibility, controlled shock environment, and economy obtained with a laboratory test machine. Since 1959, additional FSP's have been built, most of them somewhat larger than the original. The larger version has a total load capacity of 40,000 lb (or 60,000 lb if the center of gravity is not too high), and plans are in progress for the construction of a similar device for loads up to 320,000 lb.

A somewhat similar shock test device is the Submarine Test Vehicle (SSTV), which has recently been placed in service. This is essentially a submersible FSP, consisting of a segment of submarine hull in which equipments are attached with their normal foundations. The SSTV is then submerged and exposed to a series of underwater explosions.

Description

The original FSP is a rectangular double-bottomed barge 22 ft long by 16 ft wide; the double-bottom structure is heavily reinforced and 3 feet deep. Sides 3 feet high and 1 foot through enclose the usable workspace of 20 × 14 ft. Freeboard is further increased by the addition of 3-ft-high bulwarks atop the sides for a total height of 9 ft. The structure is topped with a canopy which provides protection from weather and plume spray and can be removed to permit free access to the workspace for installation and removal of test equipments. The larger version is similar except for its 6 ft greater length. The deck and bottom reinforcing members are 20.4-lb HY-80 plate, the bottom and sides are 40-lb STS plate, and the bulwark structure is 5.1-lb mild steel plate. The waterproof cover of the original FSP is steel-framed canvas, but this item is irrelevant to the shock characteristics and wide design variations are permitted.

The unloaded FSP weighs about 85,000 lb, draws about 4 ft of water, and provides an internal volume of 20 (or 26) ft long by 14 ft wide by roughly 15 ft high to the center of the canopy (Fig. 78).

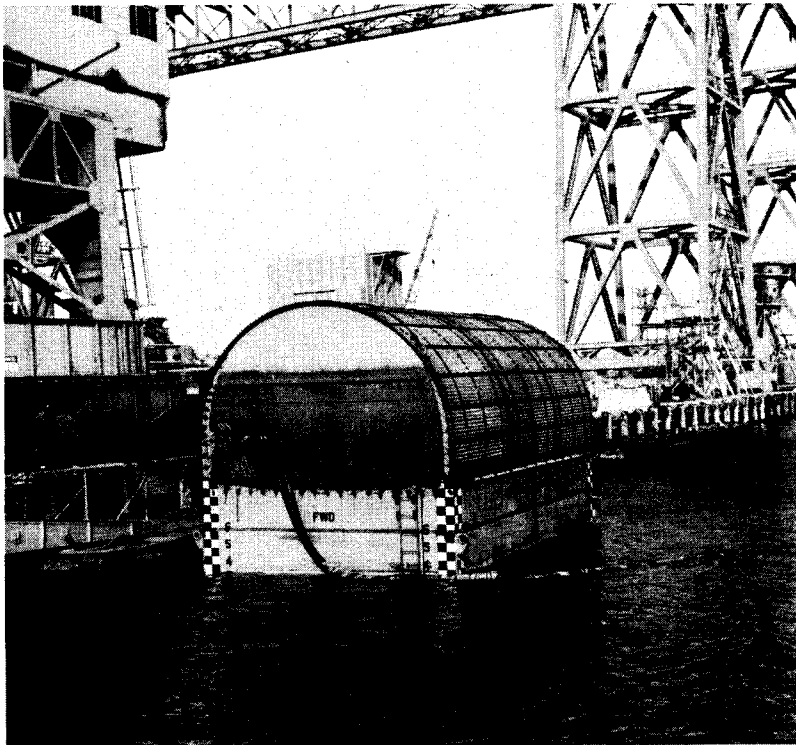


Fig. 78 — The Navy Floating Shock Platform (FSP). This FSP is one of the larger version (28 ft × 16 ft) and is located at the West Coast Shock Facility (WCSF), Hunters Point Naval Shipyard, San Francisco, California.

Mounting Arrangements

The test equipment should be mounted on a foundation structure which duplicates that of its shipboard mounting or approaches this ideal as closely as possible. For most equipments this may be done simply by bolting or welding their standard shipboard mounting foundations to the FSP deck. For some it is necessary to first erect a structure which simulates a particular region of the ship and to attach the shipboard mounting foundation to this structure.

Operating Procedure

The normal test procedure is to tow the loaded FSP to the test area and subject it to a series of underwater explosions at increasing proximity, the last being close enough to cause shock motions on the FSP which approximate those found on ships during severe shock attack (Fig. 79). The charge weight is standardized at 60 lb, the depth of detonation at 24 ft below the surface of the water, and the orientation such that a straight line from the charge to the center of geometry of the FSP bisects its long axis at right angles. The shock test control variable is "standoff," the horizontal distance from the near side of the FSP to the charge. The shots of the test series are detonated at standoffs of 60, 40, 30, 25, and 20 ft, in that order. A recent modification of this procedure requires the second (40-ft standoff) shot of the test series to be performed with the charge located forward of the FSP and on its projected center line. It is anticipated that this requirement for a fore-and-aft input will be retained in future editions of MIL-S-901.

After each shot the test equipment and installation are inspected, and mounting fasteners are retightened as necessary. As with the LWSM and MWSM equipment, performance is evaluated on the basis of its assigned category of importance. Water depth is not specified but should be around 35 to 40 ft at least. The maximum radius of the gas bubble on the first expansion is slightly less than 15 ft so that the bubble does not vent and the first bubble pulse is radiated. During the contraction phase the bubble's velocity toward the surface is greatly increased, and the bubble vents on the second expansion.

Calibration of Shock Outputs (32)

The shock motions of the FSP are considerably different from those of the LWSM and MWSM in several important respects. First, the shock input is not unidirectional but has strong vertical and athwartship, or vertical and fore-and-aft, components, which depend on the test orientation. Second, the rigid-body displacements are not limited by travel stops but by the characteristics of the detonation and the FSP response. These displacements are sizable in vertical and athwartship or vertical and fore-and-aft translations and in the rotations which couple them. Third, the relative strengths of vertical and athwartship input components are not the same for all shots since they are given at constant depth but varying standoff. Fourth, the test-item/shock-machine interactions are much more significant. Test loads in this weight range are so large, and the FSP structure required to support them must be so rigid, that its test load cannot be considered as simply a rigid dead-weight load. These differences add great complications to the calibration procedure, and the last prevents output descriptions as simple as those for the LWSM and MWSM. To reduce the data from the FSP to the same basis, it is necessary to compensate for the reactance of the test structure, which is unfortunately ill defined.

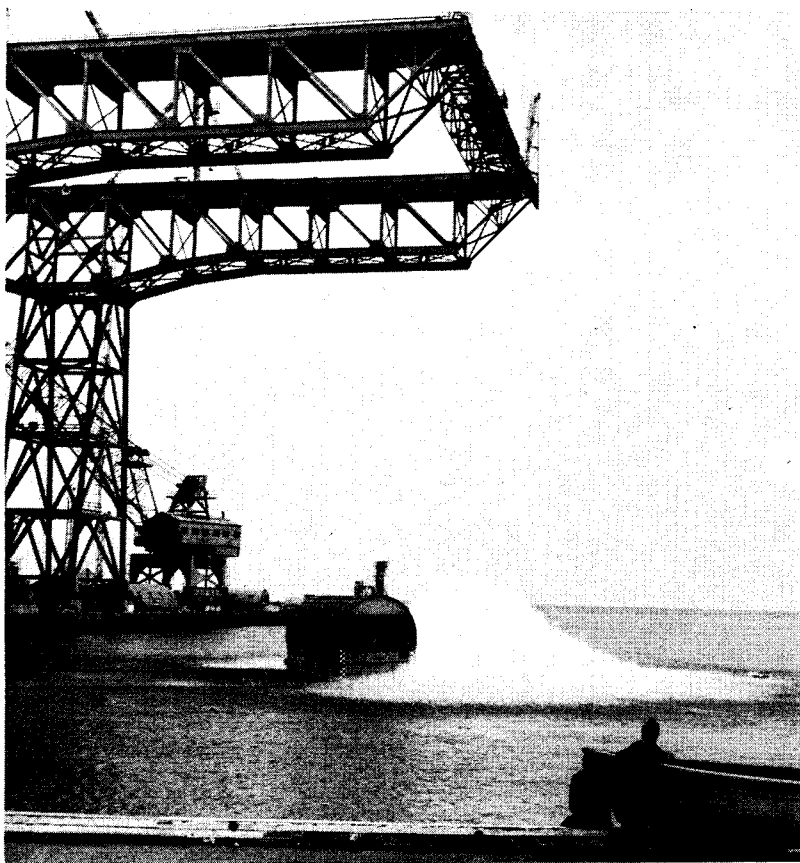


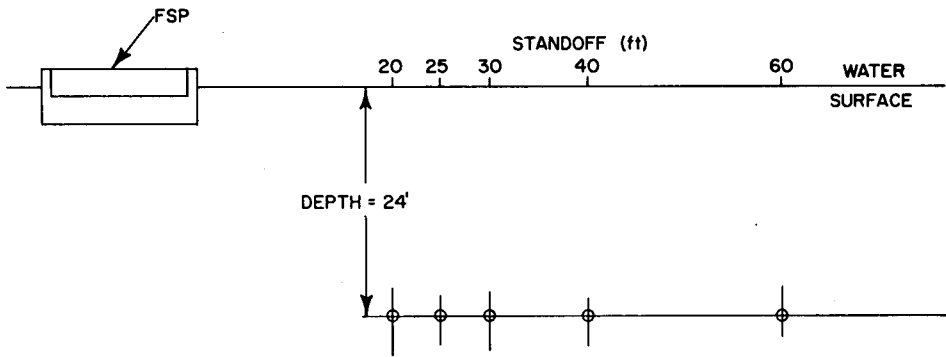
Fig. 79 — The FSP at an early stage of a close-in shot

Test Arrangement

The factors which influence the shock behavior of the FSP are the test-load weight, the charge weight, and the geometry of the test setup. Three test-load weights were selected: 35,800 lb, 18,400 lb, and 9,000 lb. Charge weights were mostly the standard 60 lb, but some were 90-lb charges. Some of these were placed at locations chosen to produce the same shock severity as the standard 60-lb charges (to check the shock factor scaling law) and others were placed close in to provide higher shock severities than those of the standard test specification. The test geometry was varied by changing the standoff (20, 30, 40, 60, and 80 ft) and depth (10, 15, 20, 25, and 30 ft) of the charge and also by moving the charge forward so that the line connecting it to the FSP's center of geometry formed a 30° angle to the normal (Fig. 80). Some pairs of identical shots were made to reveal shot-to-shot variations.

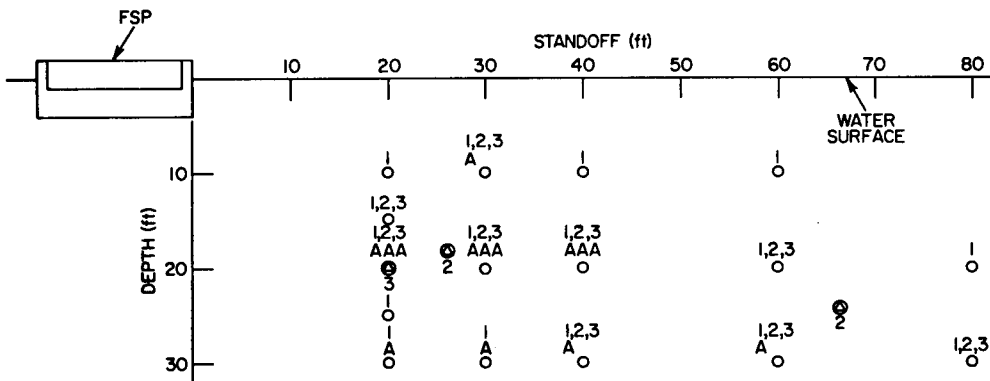
Test Procedure

The test load consisted of a damaged diesel engine and its shipboard foundation, together weighing 35,800 lb. When all removable parts had been stripped off, the weight was 18,400 lb. The lightest load, 9000 lb, consisted of two sections of 2-inch steel plate bolted to half of the engine foundation (Fig. 81). It was felt that since the reactance of



(a) The standard test series specified by MIL-S-901 requires five 60-lb charges to be exploded at a depth of 24 ft and distances of 60, 40, 30, 25, and 20 ft from the near side of the FSP.

- 60 lb CHARGE
- ⊙ 90 lb CHARGE
- 1 35,800 lb LOAD
- 2 18,400 lb LOAD
- 3 9,000 lb LOAD
- A 30° INCIDENCE



(b) The FSP calibration test series was more comprehensive. The schematic locates the shots in the depth-standoff plane. The load configurations for which shots were fired are indicated by the numbers above (60-lb charges) or below (90-lb charges) the shot indicator. In addition to the normal incidence shots, some were made with 30° incidence, where the normal array geometry was maintained but rotated 30° forward about the depth axis through the center of the FSP. These shots are indicated by the addition of an A below the load indicator for the corresponding normal shot. For example, the indicator at standoff 30 depth 10 reads that 60-lb charges were detonated at normal incidence with test loads of 35,800 lb, 18,400 lb, and 9,000 lb, and that a 60-lb charge was also detonated at 30° incidence with a test load of 35,800 lb. The indicator at standoff 20 depth 20 reads that 60-lb charges were detonated at normal incidence and at 30° incidence with all three test loads, and that a 90-lb charge was detonated at normal incidence with a test load of 9000 lb.

Fig. 80 — Schematic of the shot geometry for FSP tests

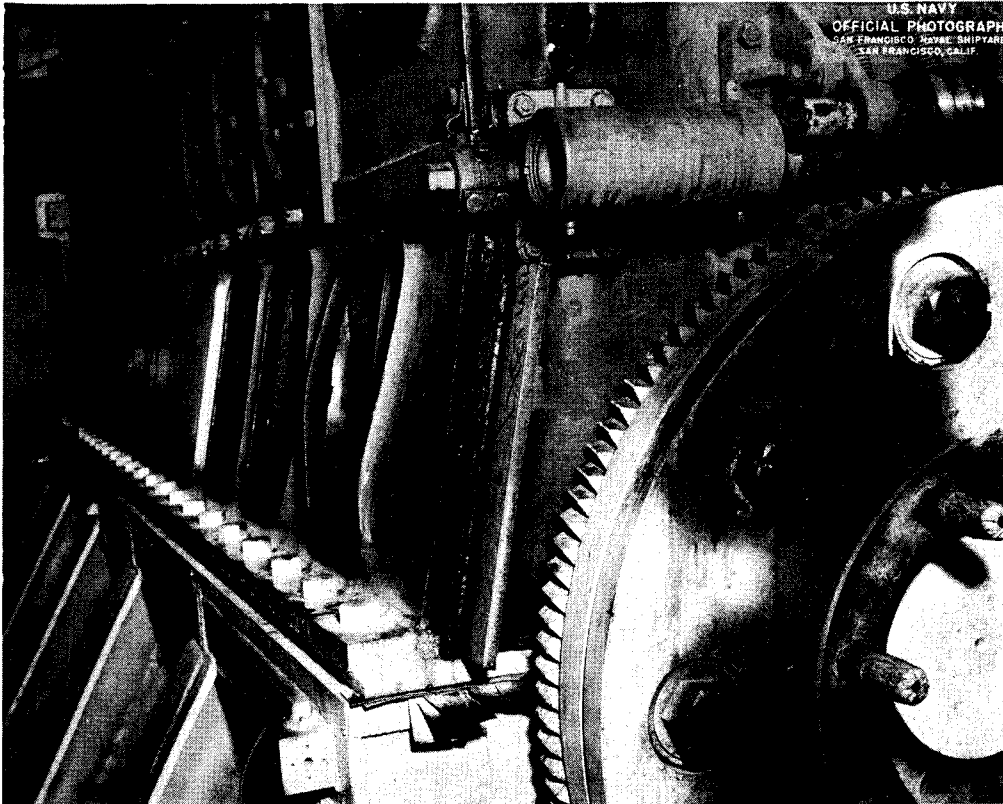


Fig. 81 — The test load for the FSP calibration series. This is an inoperable submarine diesel engine weighing 35,800 lb. After being stripped of all removable parts, its weight was 18,400 lb. The final test load of 9000 lb was attained by removing the engine, cutting its foundation in two, and attaching steel plates to one of the halves.

the load would have to be considered anyway, the convenience and economy of using an object at hand would outweigh the analytical conveniences of using specially designed load structures. It was realized that the diesel engine foundation had not been designed for shock resistance, except for the use of static multipliers ("shock design numbers"), which are intended to ensure that sufficient bolts are used to prevent flight. This procedure represents shock design at its crudest level, and foundation structures based on it may be expected to deform plastically and move about under shock since these factors are not considered at all. It was hoped that by starting with one of the more severe shocks and with maximum test load, the inadequacies of the design would be revealed immediately, and that when appropriate renovations had been made the new foundation structure would be suitable for the purpose.

Inadequacies did indeed become apparent immediately, but after renovation new ones continued to appear. After a time the information available on the spot indicated no further deterioration, and no new repairs were necessary. Later analysis of the recorded data revealed that in fact deformations were still occurring at a magnitude sufficient to cause the characteristics of the foundation structure to be constantly changing. It was only for the lightest load configuration that the test load structure could be considered the same for all shots.

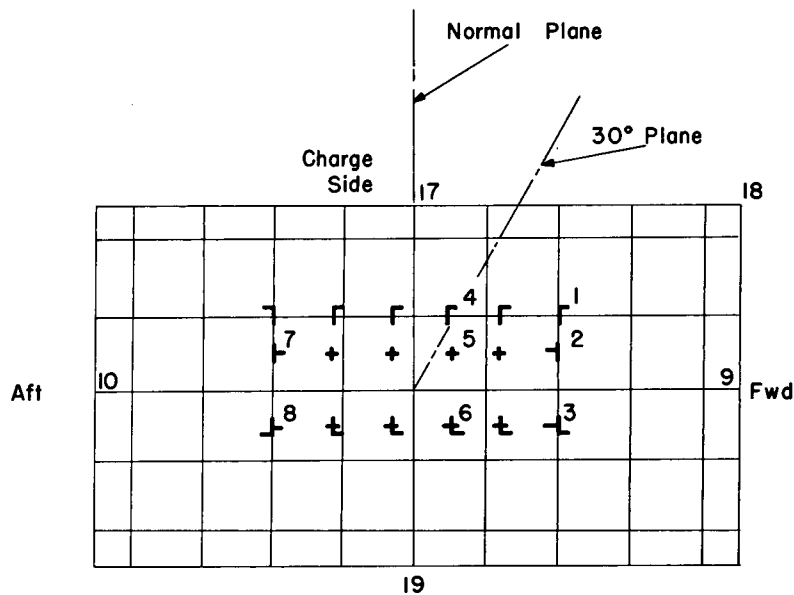


Fig. 82 — Schematic of the FSP structure and test load foundation showing the locations of input transducers. Note that locations 2, 3, 7, and 8 lie atop athwartship stringers, location 4 lies above a longitudinal stringer, and location 1 lies above an intersection. Locations 5 and 6 lie over the centers of cells. The line marked 30° indicates the axis of the test array for 30° incidence shots.

Measurement Instrumentation

The motion transducers used were seismic-magnet-type velocity meters (natural frequency 5 Hz, displacement capacity 5 inches) and an assortment of accelerometers, mostly of the strain gage type and mostly with natural frequencies of about 2 kHz. These were attached in various combinations to the base of the engine foundation at selected points or to the adjacent deck (Fig. 82). The arrangement of transducers attached at specific points to measure various shock motion components was varied from shot to shot. This technique allowed extrapolation of the values measured to give an estimate of those which were not. Considerable difficulty was experienced with the poor shock resistance of the transducers themselves. They are intended primarily for uniaxial shock, and the cross-axis shock proved highly deleterious. After appropriate signal conditioning, the outputs from the transducers were recorded on magnetic tape and later analyzed for peak velocities and accelerations. Shock spectra were then calculated by digital computer.

In a later series of standard specification tests, the rigid-body displacements (athwartship, vertical, and the coupled rotation) were evaluated from dockside high-speed movies. The test loads ranged from about 30,000 to 40,000 lb, the variation having little influence on the motion.

Output Shock Motion Waveforms (33,34)

Description

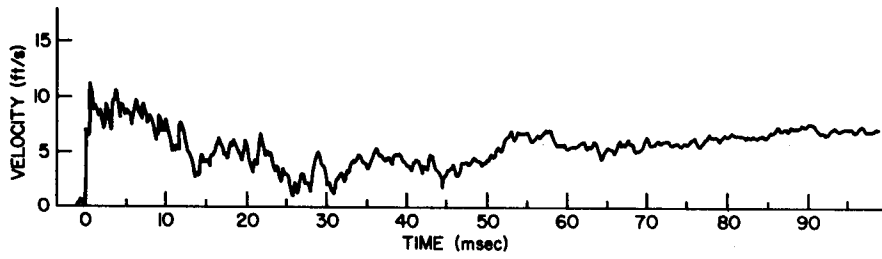
The most significant part of the FSP response to the primary shock wave occurs within about 50 ms after its arrival. By this time the rigid-body motion due to the surge of water displaced by the gas bubble is considerable, and this remains the most important feature until about 600 ms after the arrival of the primary shock wave. The rigid-body displacements (vertical and athwartship) have the basic form of a half-sine pulse of 600-ms duration. At about the time this displacement has returned to zero, the first bubble pulse arrives but is insignificant in shock effect compared to the primary shock wave. The motion tails off with undershoot from the rigid-body displacements, and finally the FSP rocks from the surface waves excited by venting of the gas bubble. The important epoch of the entire process occurs when the effects of the primary shock wave are in full force. There may, of course, be individual cases when other epochs will also be important.

The timing of the sequence outlined above is that for a 20-ft standoff and will be somewhat different for the less severe shots. The general features will remain the same.

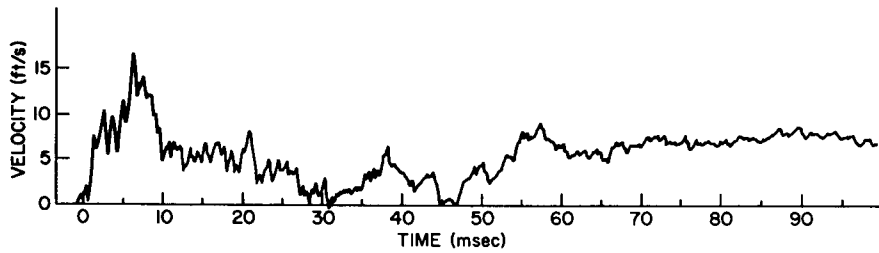
The character of the deck motion waveform is strongly affected by the structure of the FSP at the point of measurement, more strongly than by the test control parameters. Vertical velocities measured above the stiffeners feature a very sharp initial rise of about 1 ms or less, followed by a gradual decay with fairly strong sinusoidal components of 21, 47, 500, 1000, and 2000 Hz (Fig. 83a). Those measured at the center of the unsupported span show very nearly a damped $(1 - \cos)$ wave at 100 Hz carried on a basic 18 Hz and in turn carrying a 1000-Hz rider (Fig. 83b). Athwartship velocities are less distinctive. Both locations have sharp rise times and $(1 - \cos)$ -type waveform with a dominant frequency of about 200 Hz. This component is rapidly (2-3 cycles) damped to the same footing as the other major components, 100 Hz and 15 Hz. In addition, there is a component at 1000 Hz which is small and rapidly damped in the center of the span and strong and well sustained over the stiffeners (Figs. 83c and 83d).

Some estimates have been made of the natural frequencies which might be expected from the FSP. The rigid-body modes — heave, pitch, and roll — are around 1 Hz. The free-free beam frequencies calculate to 120 Hz (fore and aft) and 310 Hz (athwartship). No serious attempts have been made to calculate plate frequencies since the reliability of the answers would hardly justify the difficulty of the calculation, but the lowest plate mode may be somewhere in the range 50 to 100 Hz. The frequency associated with the unloaded deck plating between stiffeners might run from about 100 Hz to 140 Hz, depending on the loading condition of adjacent areas of the plating. The presence of a concentrated load in an unsupported space could reduce its membrane frequency to practically any value, however.

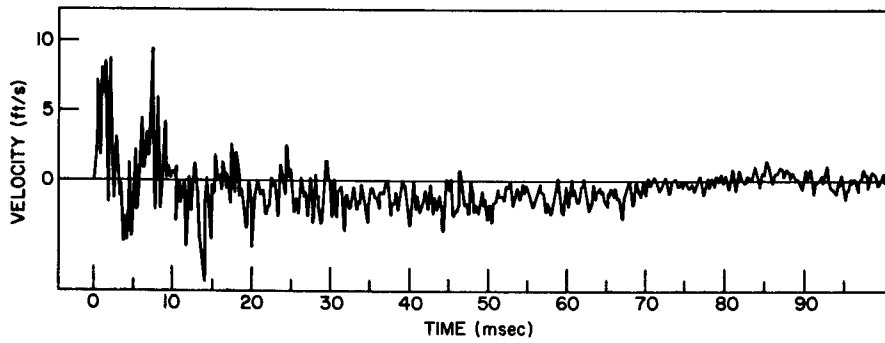
The effects of the test control parameters are largely to vary the amplitudes and fine structure of the velocity waveform, while its basic character remains primarily determined by the FSP deck structure. In this respect the FSP deck is very much like the LWSM mounting-plate/anvil-plate combination. The presence of the engine foundation itself has little influence except for the lower frequencies, as would be expected. As in the LWSM, the higher-frequency components are decidedly localized and in any event have little significance to shipboard equipments.



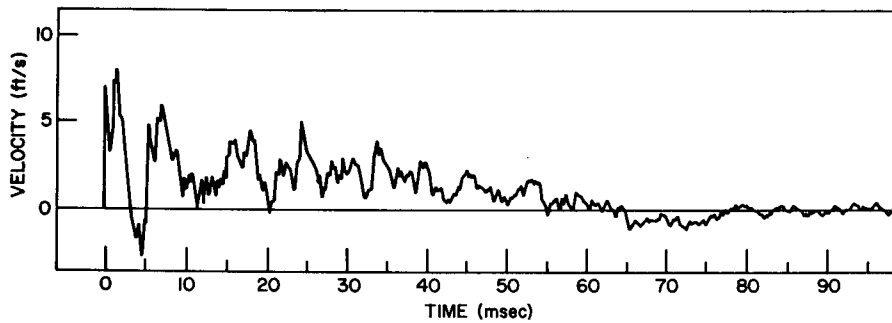
(a) Vertical velocity vs time measured above an athwartship stringer (location 3, load 18,400 lb)



(b) Vertical velocity vs time above a cell (location 5, load 18,400 lb)



(c) Athwartship velocity above an athwartship stringer (location 3, load 18,400 lb)



(d) Athwartship velocity above a cell (Location 5, load 35,800 lb)

Fig. 83 — Influence of FSP structure on velocity waveforms

The recorded transducer outputs were restricted to the significant range by filtration before peak accelerations and velocities were read. The cutoff frequency was set at the value which gave agreement between peaks read from filtered acceleration recordings and graphically determined slopes of velocity recordings. This value was 250 Hz, in reasonably good agreement with the traditional 300 Hz generally used for shipboard shock analysis. Both velocity and acceleration records were filtered with this cutoff before the peak values were read.

Effects of Measurement Location

The magnitudes and relative magnitudes of the peak velocities in the three component directions are influenced not only by the test geometry but also by the structure of the FSP at the point where the measurement is made and the structure of the test load. With so many variables, the pattern of FSP shock motions is somewhat confused. Some simplification can be made by averaging the values measured at the various locations to provide a measure of the overall shock input to the test load. This was done to the measured values of peak and spectral velocities to provide the values plotted in Figs. 84 through 86 and Figs. 91 through 93. Averaging is complicated by the variation of transducer locations from shot to shot. Of the input locations, only locations 3, 4, 5, and 6 were monitored consistently. Comparison of the averages found from this set alone with those found from the complete set of input locations (available for some shots) indicates that the overall averages lie quite consistently at 0.91 of the restricted averages. Accordingly, when a reasonably complete set of input values were not available, the averages from 3, 4, 5, and 6 were used after multiplication by 0.91.

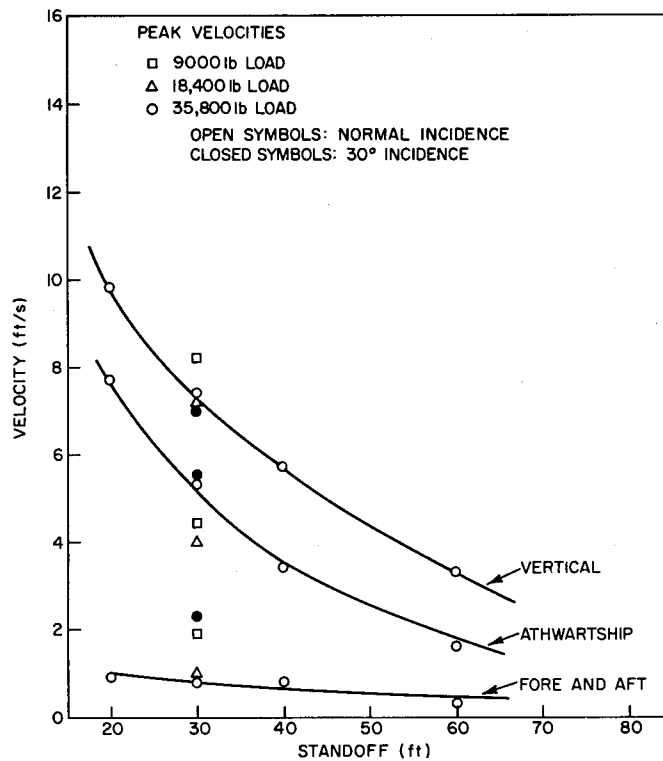


Fig. 84 — Peak velocity vs standoff for a 10-ft depth. The trend lines are given as a fiducial convenience and do not represent any particular formula for shock factor. They have been drawn to correspond roughly with the data for normal incidence tests with a 35,800-lb load.

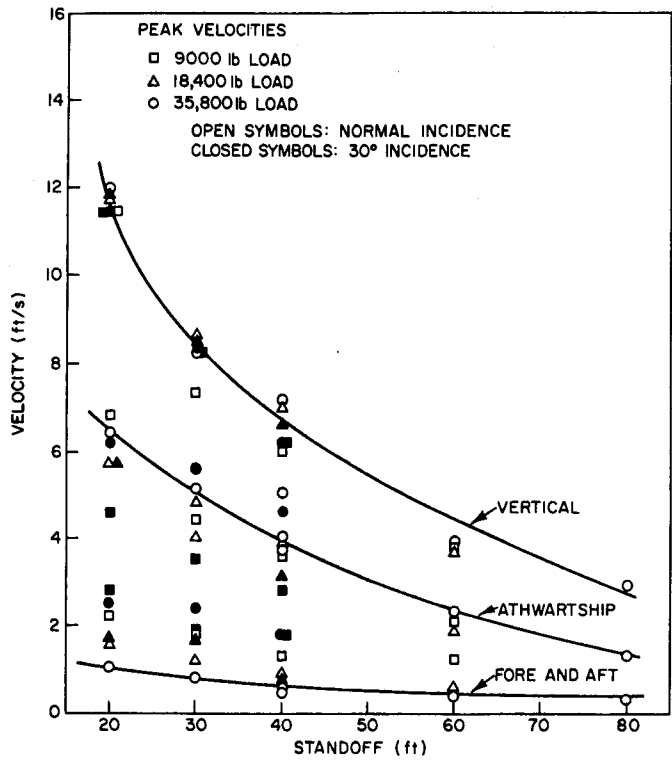


Fig. 85 — Peak velocity vs standoff for a 20-ft depth

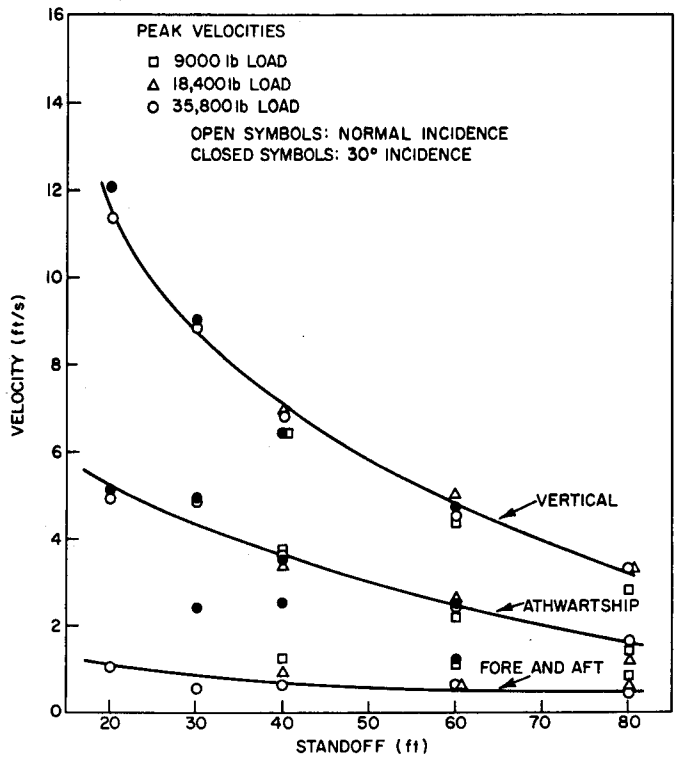


Fig. 86 — Peak velocity vs standoff for a 30-ft depth

The highest peak velocities are associated with the more flexible measurement locations because the stiffer locations have motions richer in high-frequency components and are more affected by the filtration. Since the vertical and athwartship stiffnesses at the stiffer locations are more nearly comparable, the shock motions are more nearly alike. This is reflected by the relative magnitudes of the peak athwartship velocities with respect to the peak vertical velocities being larger than at the softer locations. Moreover, the spread of peak vertical velocities is somewhat greater ($\pm 20\%$) than that of peak athwartship velocities ($\pm 15\%$) (Figs. 84 through 88). Evidently, then, the FSP is relatively stiff in the athwartship and fore-and-aft directions, of somewhat less stiffness in the vertical direction at the hard spots, and considerably less stiff in the vertical direction at the soft spots.

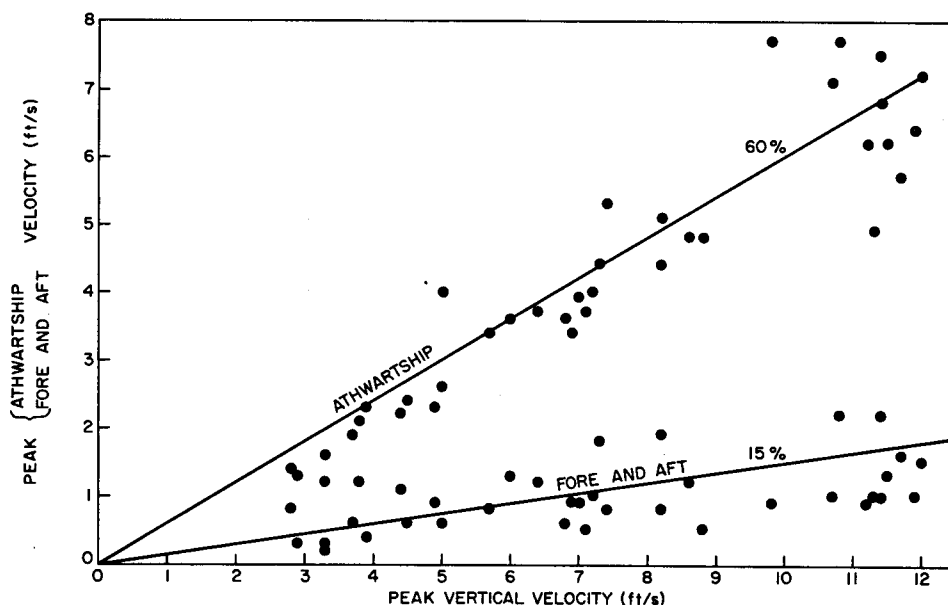


Fig. 87 — Peak athwartship and fore-and-aft velocities as functions of peak vertical velocity for normal incidence shots. Note that athwartship peaks cluster along the 60% line, and fore-and-aft peaks cluster along the 15% line.

Effects of Measurement Orientation

Peak velocities in the vertical direction are greatest, and those in the fore-and-aft direction are smallest, even for the angled shots. The latter are so small as to be negligible, but special cases may arise where the nature of the test equipment requires that they be considered. Peak athwartship velocities average about 60% of the vertical peaks, although the relationship between the magnitudes is not truly linear due to the changing geometry of the test setup (Fig. 87). The higher velocities occur with short standoffs, where the vertical component is more pronounced. The fore-and-aft peak velocities are about 15% of the vertical and are a more-or-less constant fraction. It is interesting that the peak accelerations in the athwartship direction are larger than those in the vertical direction for shallow, close-in shots with the 35,800-lb load (although not for the lighter loads), indicating the substantial high-frequency content of the athwartship motions.

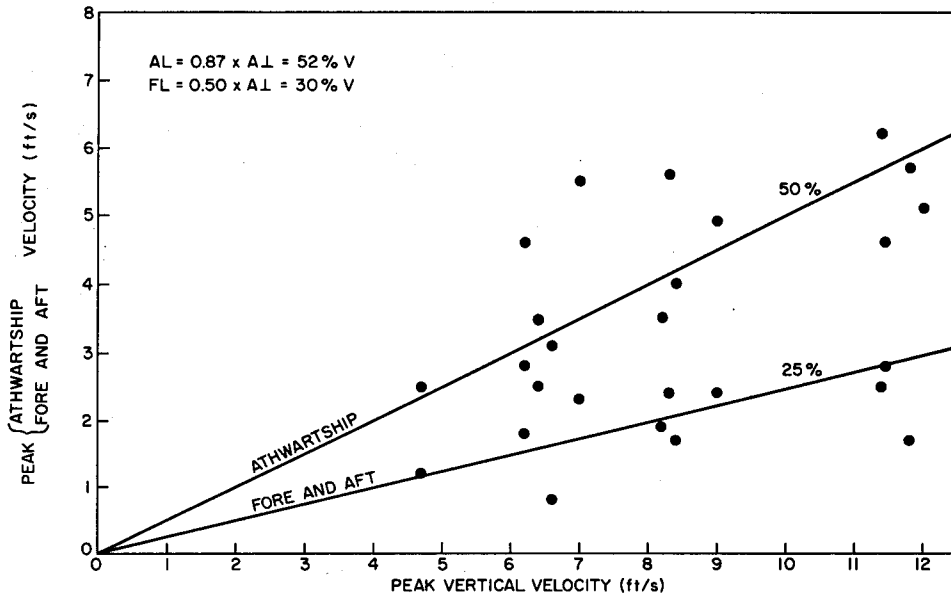


Fig. 88 — Peak athwartship and fore-and-aft velocities as functions of peak vertical velocity for 30° incidence shots. Here the athwartship and fore-and-aft peaks cluster around the 50% and 25% lines, respectively.

Effects of Load Weight

The variation of load weight in the calibration test series was only 24% of the average total. While load weight is thus not a dominating parameter, it does have some effect, and this may come from two conflicting actions. The first is simple presence of additional mass which tends to decrease the shock severity. The second is additional draft which tends to increase shock severity for shallow shots. The latter factor is presumably responsible for the excess of peak athwartship accelerations over peak vertical accelerations for the heaviest load weight with appropriate shot geometry. These two actions combine to the end that the shock is usually most severe with the 18,400-lb load, followed more often than not by that with the 9000-lb load. The overall variation of peak velocity with load weight runs about 10% (Figs. 84 and 86).

Effects of Charge Orientation

Placement of the charge along a line at 30° off the perpendicular to the FSP axis has no significant effect on the vertical motions and little on the athwartship motions, but it does about double those in the fore-and-aft direction (Fig. 88). Even so, they are considerably smaller than those in the two other directions, being about half as great as the athwartship motions. The peak athwartship velocities show the slight decrease to be expected from geometry, dropping to about 52% of the vertical. The fore-and-aft peak velocities rise to about 25% of the vertical, while the geometry would indicate a fraction of 30%. There is considerable scatter, however.

Effects of Charge Depth

The depth of the detonation is not a strong influence on the shock intensity, being more noticeable for its effect on the relative magnitudes of peak velocities in the component directions. Shots with the charge at a 10-ft depth yield somewhat lower peak velocities than the others, but little change is observable for depths of 15 ft and greater (Figs. 84 and 86).

The peak velocities in the vertical and athwartship directions are comparable for shallow shots (although the vertical peak is always the greater). As the depth is increased, the peak vertical velocity increases and the peak athwartship declines until the depth is about equal to the standoff, after which time their values remain essentially constant. The fore-and-aft peak velocities are totally indifferent to shot depth.

Effects of Standoff

Charge standoff is the control variable of the specification shock test and by far the most significant in its effect on the shock motions induced. The peak velocities for an 80-ft standoff are only about 30% of those for 20 ft (Figs. 84 through 86 and Table 4). The character of the motions remains essentially unchanged, and other than the decrease in magnitude the only effect is variation in relative magnitudes due to the change in geometry of the test arrangement.

Table 4
Multiplication Factors Relating Shock Inputs
by Charge Standoff

Standoff (ft)	Multiplier		
	Vertical	Athwartship	Fore and Aft
20	1.0	1.0	1.0
30	0.7	0.8	0.8
40	0.6	0.7	0.7
60	0.4	0.5	0.5
80	0.3	0.4	0.4

Effects of Charge Weight

Charges of 90 lb rather than the specified 60 lb produce greater shock severity, but the increase is slightly less than that predicted by the shock factor. Placement of 90-lb charges at standoffs calculated to provide the same shock factor also resulted in slightly lower peak velocities and accelerations than the specified 60-lb charges.

Reproducibility

Duplicate shots result in very similar peak velocities (Figs. 84 through 86). The spread is nil at some measurement locations, perhaps 20% at others, which is due to the mechanical details of the test load installation and the condition of the FSP. The FSP is not an elastic machine, as welds crack and plates bulge with use, but the normal maintenance procedures seem adequate to preserve predictability of shock output.

Rigid-Body Motions (35)

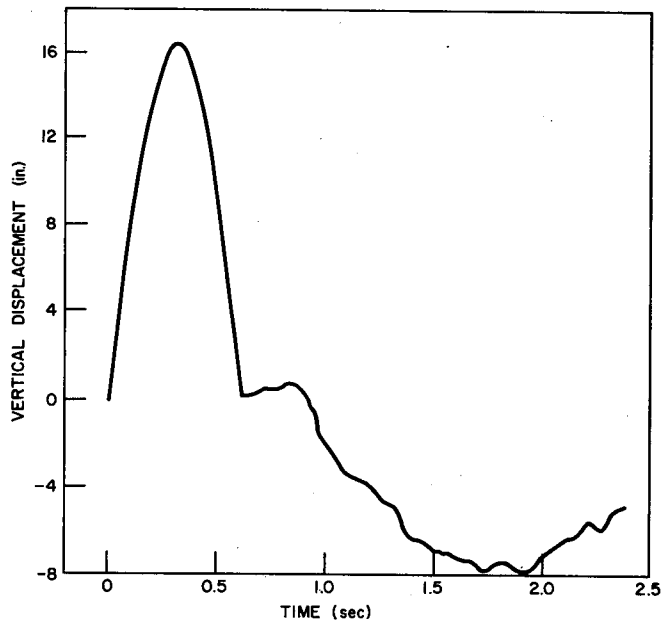
On a subsequent series of specification tests the FSP rigid-body motions were determined from high-speed movies. Test loads ranged from 29,300 lb to 41,100 lb but made little difference in the motions. Since the 20-ft standoff, 24-ft depth shot is the most severe, only the motions produced by it will be described. Because of the symmetry of the specification test arrangement, the rigid-body motions may be adequately described by the vertical and athwartship displacements of the center of gravity and the rotation about the roll axis through it.

The largest displacement occurs in the vertical direction (as the athwartship displacement is limited by the pressure buildup on the lee side), reaching a maximum of about 16.5 inches at 300 ms after the arrival of the shock wave (Fig. 89a). At about this same time the athwartship displacement reaches its maximum of 5 inches (Fig. 89b), and the rotation its maximum of 40 mrad (Fig. 89c). These motions are well described by a half-sine displacement pulse of 600-ms duration, implying a peak "bodily" velocity of 7.2 ft/sec. After this initial pulse has passed, there is some undershoot, amounting to 8 inches in the vertical direction (about 1.9 seconds after the arrival of the shock wave) and 5 inches in the athwartship (a little earlier than the vertical minimum). The rotational undershoot is small (6 mrad) and occurs somewhat earlier than those of the displacements, about 1.4 seconds after the shock wave arrives.

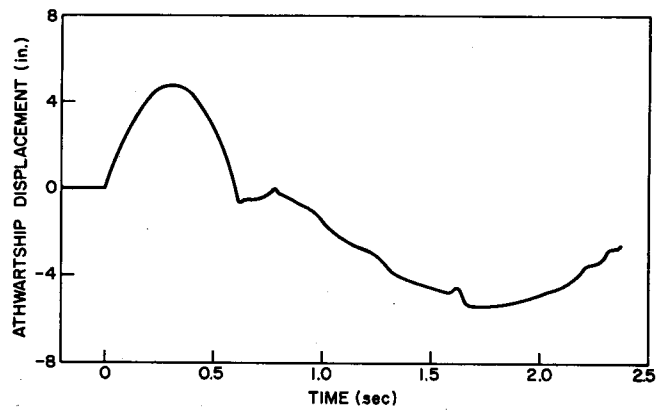
Output Shock Spectra (33,34)

Overall and residual shock spectra were calculated by digital computer for natural frequencies every 2 Hz from 0 to 150 Hz. The velocity recordings were used as inputs since this parameter is less influenced by the local properties of the measurement location, and a few acceleration records were processed to provide a cross check. Shock spectral values below about 20 Hz should be regarded with some reserve for two reasons. First, the nature of the velocity meter itself, with its 5-Hz natural frequency, seriously distorts the importance of motions in this region. Second, the spectra were calculated from the first 200 milliseconds of the velocity record, making it difficult to distinguish frequency components of a few hertz from each other or the dc bias of the magnetic tape recorder. A slight error in the estimate of this dc bias has a substantial effect on the shape of the shock spectrum at the low-frequency end.

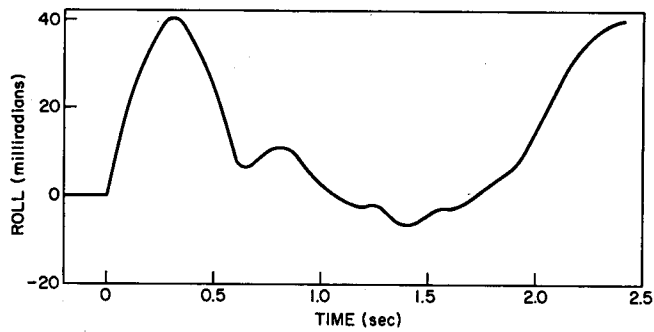
Even so, it is possible to extract some of the desired information, viz., the frequencies for which the residual spectrum has minima. The velocity level cannot be evaluated in this region but must be extrapolated from higher frequencies and the displacement limit set from other measurements. The ill-defined and changing characteristics of the load structure render these spectra considerably less useful than could be desired. Possibly due in part to the multiple-support nature of the foundation, the expected effect of load weight cannot be seen to any extent, and like the waveforms the shock spectra are largely characteristic of the measurement location. Averaging the spectral parameters measured at the several measurement locations provides an inkling of the behavior which may be expected with relatively nonreactive test loads. It is hoped that more data will be accumulated which will permit the influence of modal weight to be more apparent.



(a) Vertical displacement vs time



(b) Athwartship displacement vs time



(c) Roll vs time

Fig. 89 — Rigid-body motions of FSP: the center of mass displacements for a 20-ft standoff specification test shot

The shock spectra presented in the sections on the LWSM and MWSM were of the motions of dead-weight loads attached to rigid machines by flexible mountings. The shock spectra from the FSP are of motions measured at the interface of a load-foundation structure and a machine which are reactive and have comparable compliances. The shock spectra have highly individualistic shapes which are governed by the local peculiarities of the overall load-foundation-machine structural ensemble, and their most significant content lies in their values at the fixed-base natural frequencies of the load-foundation system. When the test load has been designed for a specific purpose, its modal frequencies and weights are (in principle) known. Therefore, enough spectral points can be extracted to define the design shock spectrum completely, although it may require several test load structures to provide an adequate range of modal weights and frequencies.

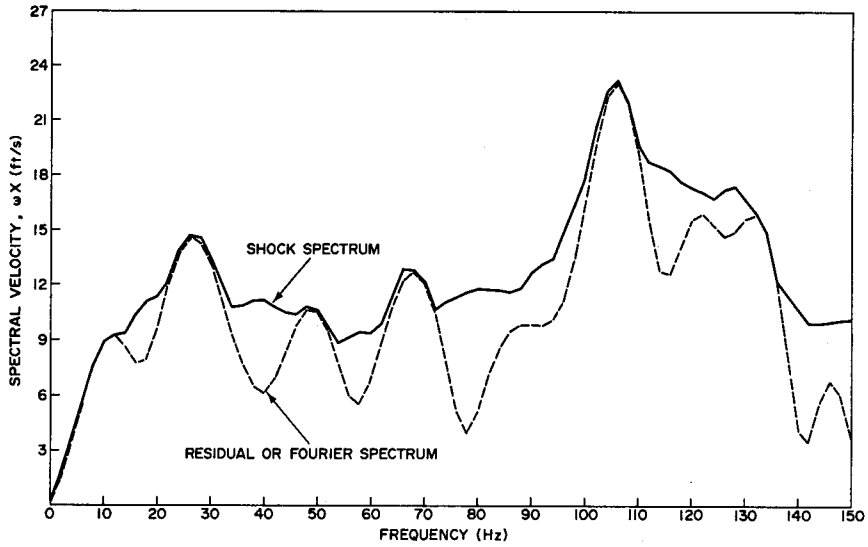
Unfortunately, this procedure cannot be applied to the shock spectra which have been obtained since the load structure is an unknown quantity. It is possible to make a fairly good guess at the frequencies of the first mode or two, as has been done, but the modal masses remain a mystery. The best estimate that can be made is based on the observation that for simple structures, where only translatory motions are involved, the modal mass of the first mode will be about 80% of the total mass.

Description

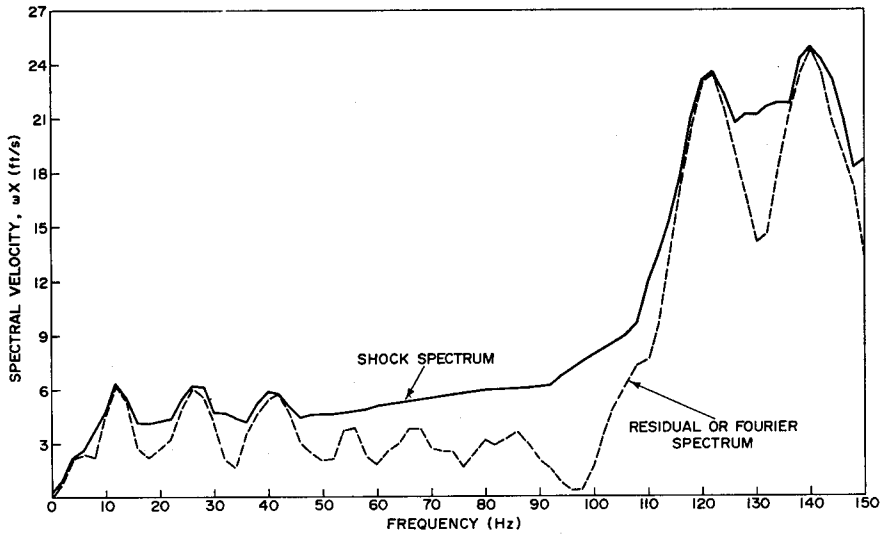
The basic character of the shock spectra is velocity shock. Interactions dominate above about 130 Hz, although some may occur at lower frequencies. The spectra probably become acceleration limited around 100 to 300 Hz, depending on the direction of the motion component and the measurement location. The residual shock spectrum shows its dips in the area of 20 Hz and multiples, indicating the natural frequencies of the test load-foundation structure. In this region the overall spectrum is substantially flat, and the shock spectrum value is taken as the average of the values of the overall spectrum at the frequencies of the first few well-defined residual dips (Fig. 90). This procedure essentially forces the shock spectrum of the FSP deck motion to a form similar to the MWSM anvillable motion — a low-frequency, displacement-limited region at the maximum displacement of the motion; a high-frequency, acceleration-limited region at the highest acceleration of the motion; and an intermediate velocity shock region where the equivalent velocity change is taken from the average of the values at the individual measurement locations. There is, naturally, a different shock spectrum applying to each component direction of motion.

The cutoff frequencies can be estimated by fitting the measured displacements, equivalent velocities, and peak accelerations to this pattern. The upper cutoff frequencies (the transition from velocity shock to acceleration limited) are 67 Hz, vertical; 220 Hz, athwartship; and 125 Hz, fore and aft. The lower cutoff (transition from displacement limit to velocity shock) is 1.15 Hz, from the displacements measured in the vertical and athwartship directions. This implies a peak fore-and-aft displacement of about 3 inches. Since the lower cutoff is so low, the usual design shock spectra assumed for dynamic analysis (which extend the velocity shock region to zero frequency) are valid for soft-mounted equipments as well as rigid mounted.

In general the shock spectrum velocity values so derived are fairly close to the peak velocities read from the waveforms. They tend to be somewhat higher, indicating that the filtration performed on the velocity waveforms before the peak values were read did in

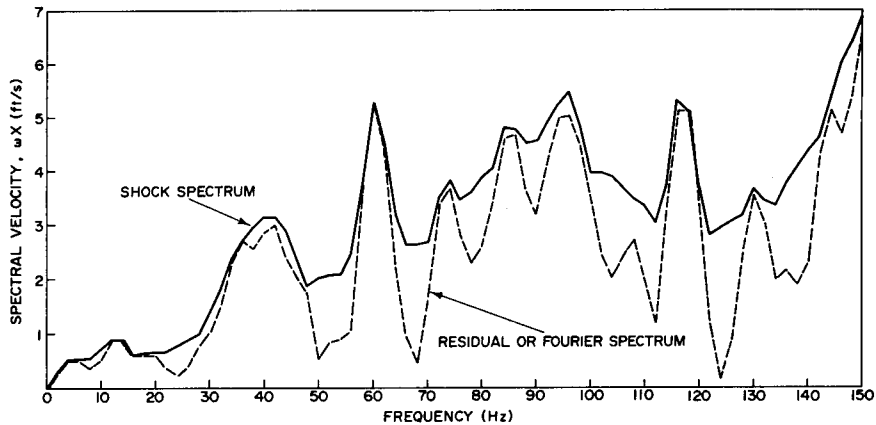


(a) Vertical, location 3



(b) Athwartship, location 5

Fig. 90 — Representative overall and residual shock spectra for shots at 20-ft standoff, 15-ft depth



(c) Fore and Aft, location 2

Fig. 90 (Continued) — Representative overall and residual shock spectra for shots at 20-ft standoff, 15-ft depth

fact remove some of the pertinent frequency components.* In view of this, it is hardly surprising that the shock spectrum values should exhibit the same reaction to variation in test parameters that the peak velocities do.

Effects of Measurement Location

The shock spectrum velocities show much the same pattern as the peak velocities but with some interesting variations of questionable importance. The first is that the scatter of athwartship and fore-and-aft shock spectrum velocities is generally less than the scatter of the peak velocities. The scatter of most of the locations' vertical shock spectrum velocities is also less than that of the peak velocities, but one or two locations will be far enough out of line with the rest to make the overall scatter comparable to that of the peak velocities.

Effects of Measurement Orientation

The vertical shock spectrum velocities are comparable to and slightly larger than the peak velocities. The athwartship shock spectrum velocities are considerably smaller than the peak velocities (about 35-50%), and the fore-and-aft shock spectrum velocities are larger than the peak velocities (about 50%). Therefore, the shock spectrum velocities of the athwartship and fore-and-aft motions are much more comparable than are the peak velocities. The athwartship shock spectrum velocities average about 35%, and fore-and-aft 20%, of the corresponding vertical shock spectrum velocities (Figs. 91 through 95). Since the athwartship direction seems to be the stiffest, more of the velocity waveform will be supplied by high-frequency components which will not be noticed by the load-foundation system and will not contribute to the shock spectrum. In the fore-and-aft direction the waveform does seem to contain a substantial component in the area of the load-foundation fixed-base fundamental.

*Even so, the agreement is far better than was shown by the reed gage values on the MWSM anvil table, demonstrating the improvements in measurement and analysis capabilities in the intervening years.

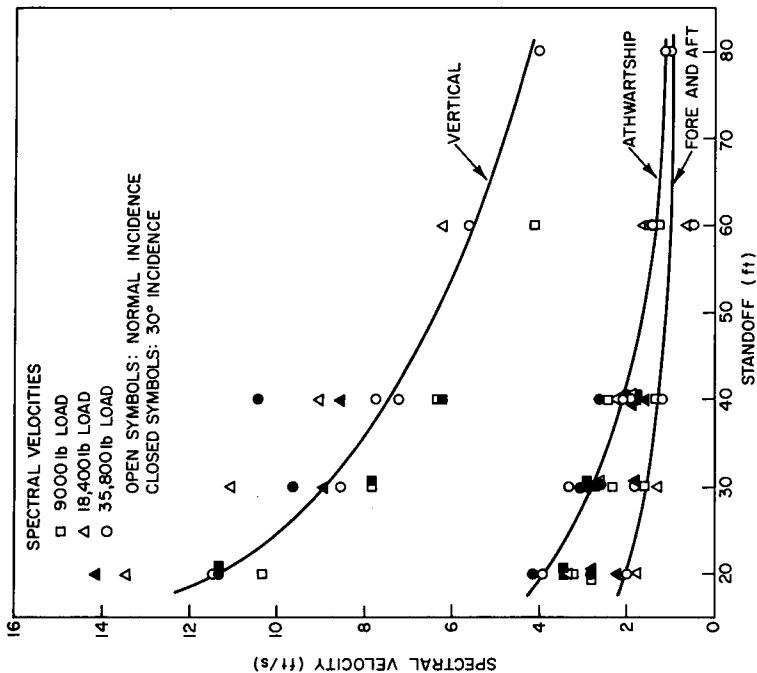


Fig. 92 — Spectral velocity vs standoff for 20-ft depth

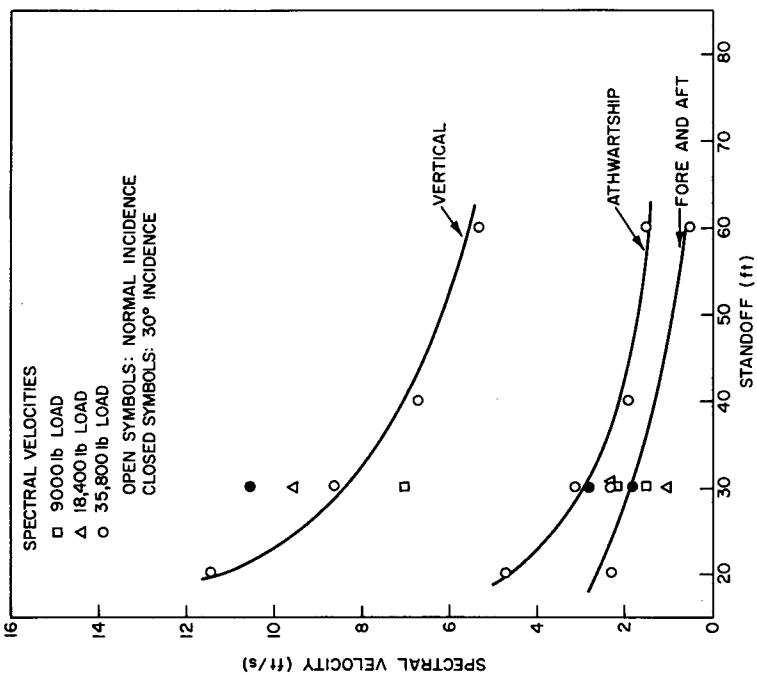


Fig. 91 — Spectral velocity vs standoff for 10-ft depth. As in Figs. 84 through 86, the trend lines of figs. 91 through 93 are of a fiducial character and roughly correspond to the behavior of the data for shots with a 35,800-lb load.

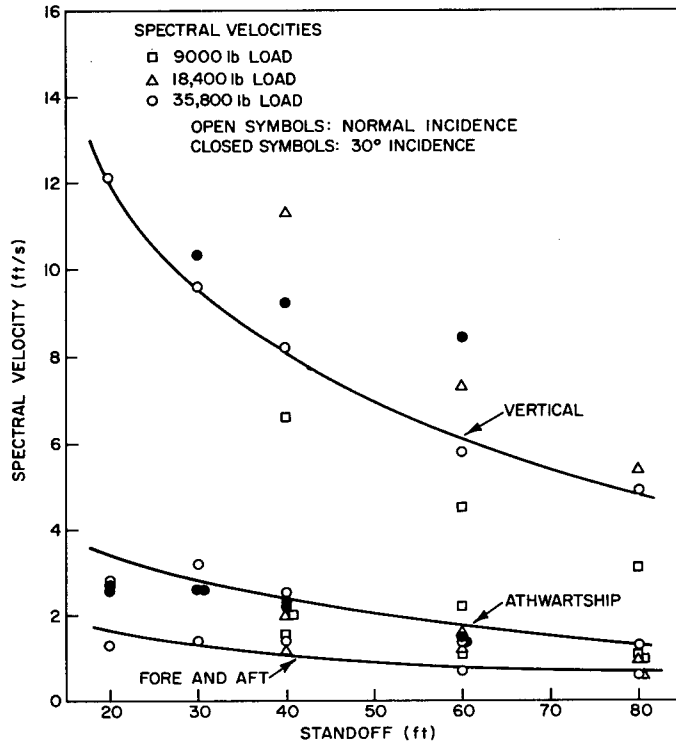


Fig. 93 — Spectral velocity vs standoff for 30-ft depth

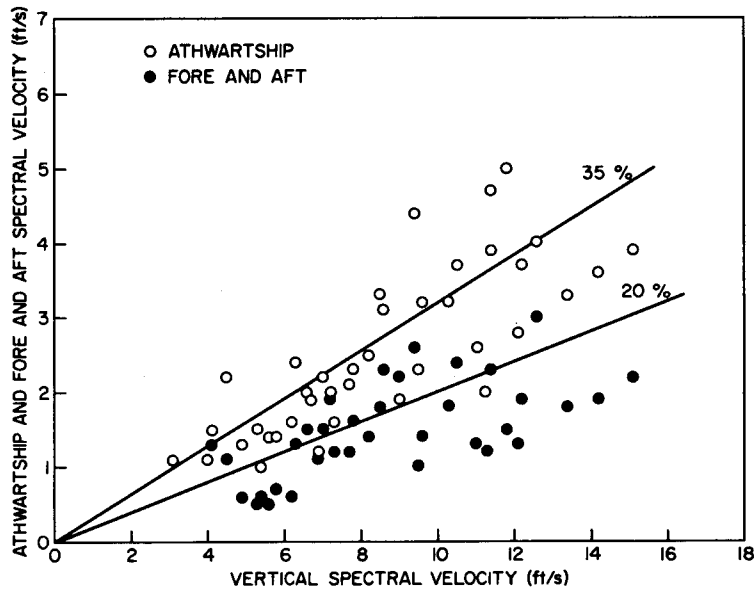


Fig. 94 — Athwartship and fore-and-aft spectral velocities as functions of vertical spectral velocity for normal incidence shots

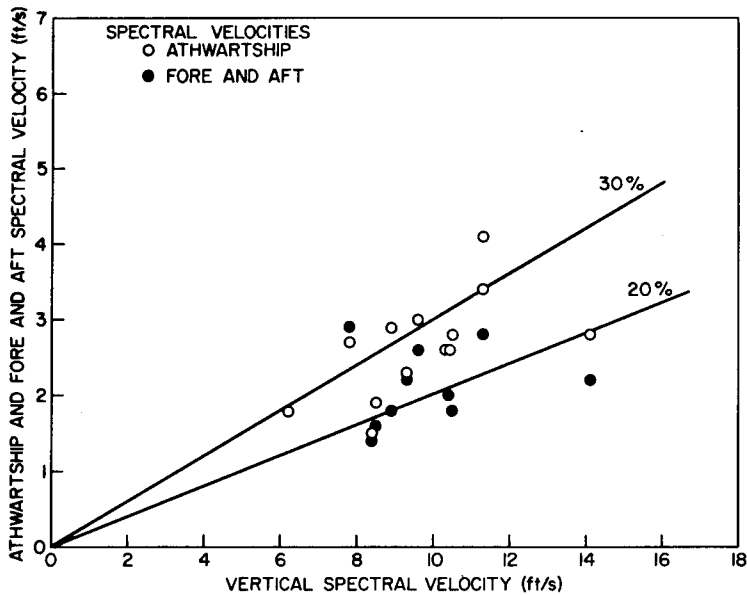


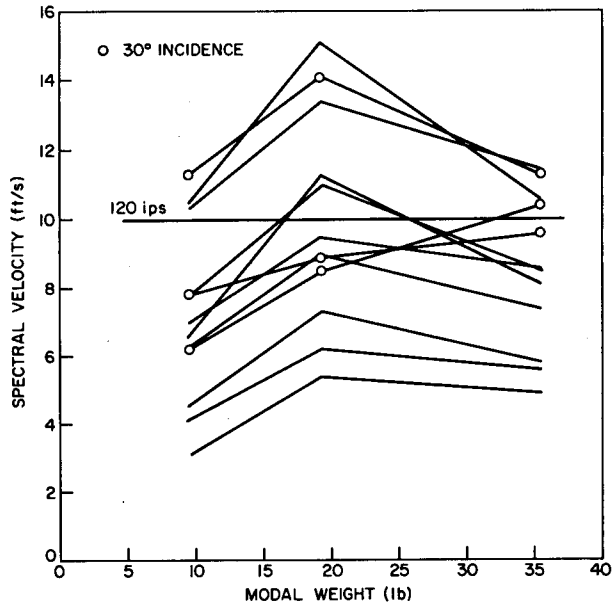
Fig. 95 — Athwartship and fore-and-aft spectral velocities as functions of vertical spectral velocity for 30° incidence shots

Effects of Load Weight

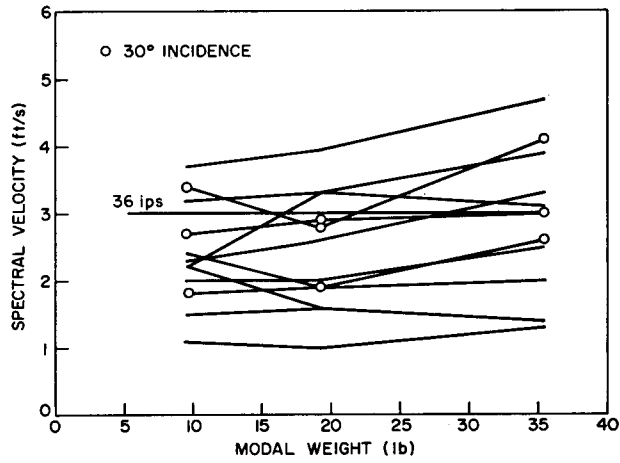
Dynamic analysis of structural shock response predicts that the shock spectrum velocity shock value should decrease smoothly as the modal mass increases. In the calibration tests, this did not occur (Figs. 91 through 93). If the modal mass associated with the first mode of each test load structure is taken as 80% of the total mass, the vertical shock spectrum velocity was found to peak at a modal weight of 14,720 lb and to decrease at 28,640 lb to a value which was still higher than that for 7200 lb. The athwartship shock spectrum velocity showed a similar action, though much less pronounced, and only the fore and aft exhibited the predicted uniform decline (Fig. 96).

Two possible contributing factors are that the shock input to the FSP is not entirely independent of load weight and that the load foundation deforms plastically for shots with the heavier loads. Investigations of a s.d.o.f. system with a yielding spring indicate that the shock spectrum value is higher than for a system of the same natural frequency with a linear spring. A similar effect may apply to more complicated structures. Other factors might include the imponderable action of multiple supports. The analysis of these factors involves enormous difficulties, and it is doubtful that a structure such as this test load will ever be feasible to model satisfactorily. A test series using loads designed specifically for the purpose would be more profitable.

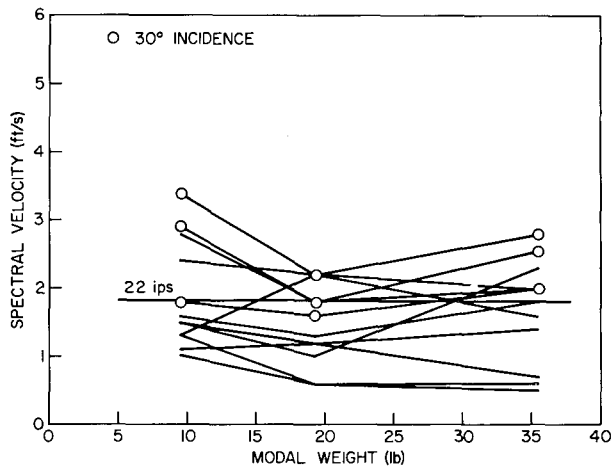
Since no clear trend for the influence of modal mass is discernible in the present data, the spectral parameters indicated in the design shock spectra for the most severe specification test shot (Fig. 97) represent the average values found over the range of calibration test loads. These spectra should be considered to apply to modes of any mass.



(a) Vertical



(b) Athwartship



(c) Fore and aft

Fig. 96 - Spectral velocities vs modal weight. The lines at 120 ips (vertical), 36 ips (athwartship), and 22 ips (fore and aft) represent the averages for the most severe shot of the specification test series.

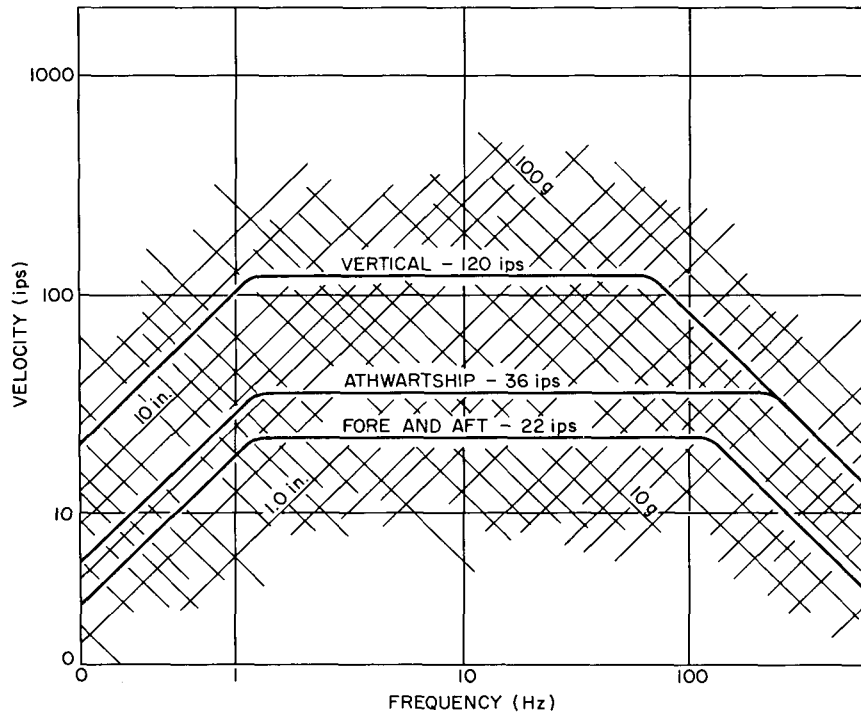


Fig. 97 - Design shock spectra for the FSP. The lower cutoff frequency for all directions is 1.15 Hz. The upper cutoffs are: vertical - 67 Hz, athwartship - 220 Hz, fore and aft - 125 Hz. These spectra should be used for all modal weights.

of 40,000 lb must rely largely on the calculated response as an indicator of shock resistance. Several methods for calculating these responses have been specified by the Navy at various times and have had various degrees of success.

Shock Design Numbers

One of the earlier methods of dynamic design required the use of "shock design numbers." These were presented as a set of three curves (for vertical, athwartship, and fore-and-aft shock) of static acceleration vs equipment weight. These curves seem to have been derived by starting at the average equivalent static acceleration found for loads on the LWSM, passing through values found for some ship tests, and proceeding to values considered to represent the feasible limit to construction of support structures for heavy propulsion components (Fig. 98).

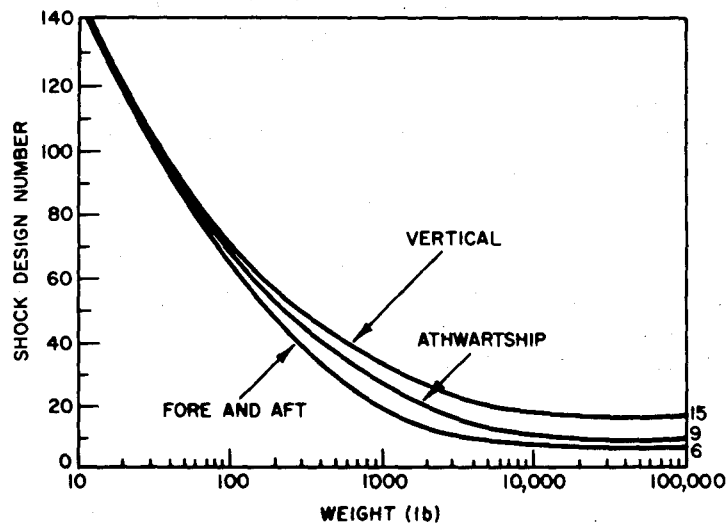


Fig. 98 — Shock design numbers. The numbers read from these curves were applied as weight multipliers at the equipment center of gravity to provide loading for a static analysis of hold-down bolts and supports.

In use, the static acceleration applying to a given equipment weight for each direction of shock was extracted from the appropriate curve and multiplied by the equipment weight to yield an equivalent force. This force was assumed to act at the center of gravity of the equipment, and a static analysis of the equipment mounting feet, hold-down bolts, and major structural members performed. Each shock direction was analyzed separately, and coupling between directions was not considered. This procedure could presumably be extended to include design of the foundation structure to which the equipment was attached, but this was not required and was not usually done.

Since this method ignores the interactions of equipment and ship, and the design curves were established on the basis of few data from outmoded vessels, the designs resulting were not realistic. Some equipments were undoubtedly overdesigned, and ship

shock tests revealed many to be underdesigned. Few, however, took leave of their mountings and traveled through the ship, which was what the method was originally intended to assure.

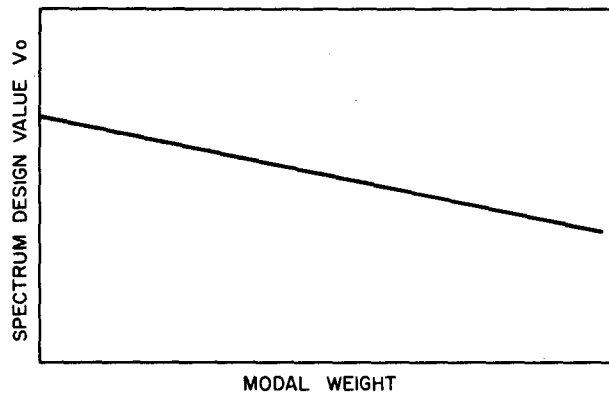
Dynamic Design Analysis Method (7)

Due to these inadequacies the shock design number procedure was supplanted by the Dynamic Design Analysis Method (DDAM). DDAM requires that the equipment be modeled and analyzed by a dynamic procedure using normal mode theory. Usually the models will be different for the three directions of shock input, but cross coupling is included by computing responses in all three directions to inputs in each direction. The inputs to be used for the shock analysis are presented as a design shock spectrum and curves of spectrum design value and of limiting acceleration vs modal weight. Since the primary application was intended to be to rigid-mounted equipments and few field data were available regarding ship displacements, the shock spectrum is represented as a velocity shock with an acceleration limit. In use, the input for each mode of the equipment model is determined by reading off the spectrum design value and limiting acceleration for the modal weight from the curves, then reading off the appropriate shock input at the modal frequency from the shock spectrum so defined (Fig. 99). Different curves and spectra are provided for each shock direction and for various locations on the several ship types. These were derived from measurements of ship tests by analysis of shock spectra and normal mode analysis of the equipments on which the measurements were made.

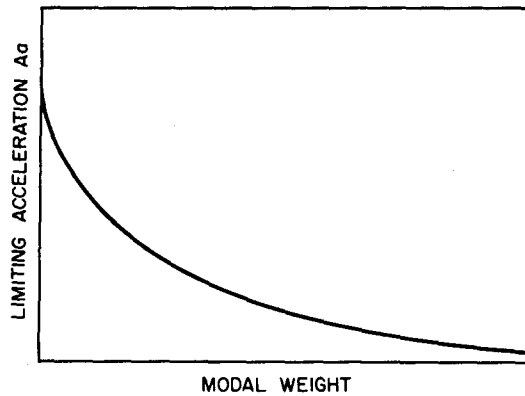
In general, this method has been very successful, but its users have not been uniformly proficient. The Navy has had to provide close guidance in the application of DDAM, and in some instances contractors have encountered difficulties in performing analyses which have contributed to extending ship lead times.

g Values

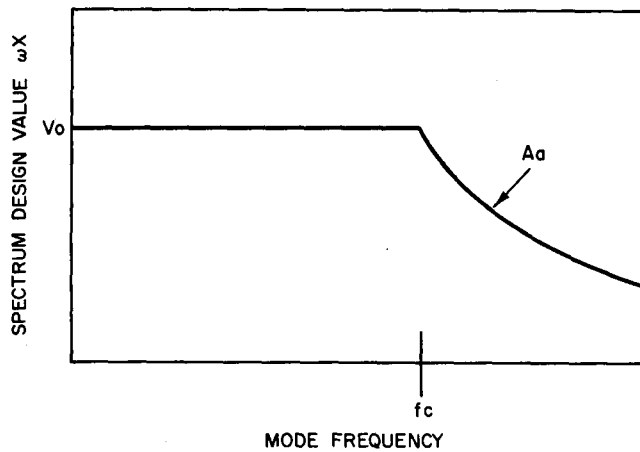
In view of the time required for dynamic analysis of some equipments, the present Navy approach to shock design separates items into two categories. The first consists of items whose dynamic analysis is expected (from past experience) to be straightforward and present little difficulty. For this category the shock design requirement is the application of the DDAM as outlined above. The second category consists of items for which detailed DDAM guidance cannot be provided, or for which production scheduling denies adequate time for dynamic analysis. For these items the Navy specifies a set of g values derived from previous analyses of similar equipments and from other appropriate sources. Like the earlier shock design numbers, the g values are to be used as center-of-gravity weight multipliers in a static analysis, the major difference being that the multipliers are provided for closely defined subsections of the equipment. In addition to designing to these static levels, the contractor is required to perform a concurrent dynamic analysis and identify any potentially unsatisfactory areas revealed by it. Dollar and time estimates of the cost of design fixes are to be furnished to the Navy and may be implemented at the option and expense of the Navy.



(a)



(b)



(c)

Fig. 99 — Examples of DDAM design curves. In part a the spectrum design value V_0 is read off corresponding to the modal weight. This is the value of the velocity shock region in part c, which shows how the spectrum design value ωX varies with frequency. Part b gives the limiting acceleration variation with modal weight.

SUMMARY

The Navy Shock testing devices for test items weighing up to 60,000 lb are the High-Impact Shock Machine for Lightweight Equipment, the High-Impact Shock Machine for Mediumweight Equipment, and the Floating Shock Platform. All provide about the same shock intensity to test loads, as shown by shock spectra and peak velocities. The major differences in the shock motions they generate are that the LWSM is rich in high-frequency components, that the motion of the FSP is triaxial, and that they have different displacement limits. The LWSM and MWSM are displacement limited at 1.5 inches and 3 inches respectively by mechanical stops. The FSP is displacement limited at 16.5, 5.1, and 3.0 inches in the vertical, athwartship, and fore-and-aft directions respectively by exhaustion of the driving energy. This large difference in displacement capability between the machines is of less consequence than it might seem. The bulk of shipboard items falling in the weight range of the LWSM and MWSM have mounting frequencies above the lower cutoff frequency of these machines (7-10 Hz), and the bulk of those items with mounting frequencies below this value are within the FSP weight range or heavier.

The anticipated addition of the large Floating Shock Platform to this family will extend the shock testing capability to 320,000 lb and perhaps higher in special cases. Over this entire range, the only gap in testing capability lies between 4800 and 6000 lb. The MWSM was designed for a maximum load of 4500 lb and can generate a shock environment of the full intensity with test loads of 4800 lb. For loads higher than this the test severity decreases. It would be advisable to consider ways in which the total load on the MWSM anvil table could be held to no more than 6000 lb, including transfer of shock testing to the FSP for items in the 5000- to 6000-lb range.

ACKNOWLEDGMENTS

The information presented here has been extracted principally from the publications of Conrad (20,23,24,28), Dick (21), Dick and Blake (29), Vigness (18), Belsheim (33), and unpublished material by Kaplan (34).

The publications given in the References span a period of approximately 25 years. During this period, the following people have figured prominently in NRL efforts toward the calibration of the Navy's shock testing devices by measurement and analysis of the motions they produce under standardized conditions. Most of these people did this work while at NRL; the others have their affiliations noted: J. L. Bachman, R. O. Belsheim, R. E. Blake, R. L. Bort, F. J. Bury, R. W. Conrad, R. C. Cowan, P. Cunniff, R. Daugherty (WCSF), A. F. Dick, H. M. Forkois, J. J. Harris, D. M. C. Hurt, E. Judd, R. E. Kaplan, C. L. Lamb, W. McDermott (WCSF), G. J. O'Hara, M. W. Oleson, L. P. Petak, R. J. Peters, P. Pida, G. Remmers, H. M. Schauer (UERD), C. Schrader (WCSF), R. Q. Tillman, I. Vigness, J. P. Walsh, J. W. Whyte, R. A. Willem, and S. E. Young.

Much of this work has been performed under the continuing sponsorship of the organization which is now the Ship Hardness Section, Code 6105G, of the Naval Ship Engineering Center: J. R. Sullivan and coworkers. A great deal of the research and development in the areas of shipboard shock and shock simulation has been rooted in the concern of this group with the combat effectiveness of Navy ships and its efforts to increase this effectiveness.